Doctoral Dissertation

Studies on Enantioselective Catalysis and Chiral Recognition Induced by C_3-Symmetric Chiral Cage-Shaped Phosphorus Compounds

LIU XIAO

July 2025

Graduate School of Engineering,
The University of Osaka

Preface and Acknowledgements

The study of this doctoral dissertation was carried out under the guidance of Prof. Dr. Makoto Yasuda at the Department of Applied Chemistry, Graduated School of Engineering, The University of Osaka from October 2020 to September 2025. The thesis describes the enantioselective catalysis and chiral recognition induced by C_3-symmetric chiral cage-shaped phosphorus compounds.

First and foremost, I would like to express my deepest appreciation to my supervisor Prof. Dr. Makoto Yasuda, for his insightful advice, continuous support, and hearty encouragements throughout my doctoral studies. I am deeply thankful for his thoughtful guidance, which has cultivated my insight and passion for becoming a better researcher.

I would also like to thank Professors Dr. Tadashi Mori and Dr. Hayato Tsurugi for their helpful advice and kind assistance. I would like to express my heartfelt gratitude to Professor Dr. Ikuya Shibata for his kind permission to study in his laboratory for a short period and for the valuable discussions we had during those days. I gratefully acknowledge Associate Prof. Dr. Yoshihiro Nishimoto for his always kind comments and encouragement. I really wish to make a grateful acknowledgement to Assistant Prof. Dr. Akihito Konishi for his helpful assistance, valuable discussion and kind encouragement. His insightful perspectives were invaluable in improving the quality of my research. I would also like to thank Associate Prof. Dr. Shuntaro Tsubaki for his kindness.

I am deeply thankful to Ms. Yoshimi Shinomiya and Ms. Tomoko Shimizu for giving me grateful support and heartwarming kindness.

I express my appreciation to all members of the Yasuda Group. I would like to express special thanks to my mentor Dr. Yuya Tsutsui for his kind encouragement and great suggestions.

I would like to thank Dr. Nobuko Kanehisa, Dr. Kyoko Inoue, Dr. Hiroaki Tanaka, Mr. Kunihiko Kamon, and Mr. Hiromi Ohi for giving me analytic assistance at the analytical instrumentation facility.

I wish to thank the Otsuka Toshimi Scholarship Foundation for financial support.

Finally, I would like to express my gratitude to my parents, Xiangdong Liu and Zhiping Xue, for their understanding of my work, constant assistance and financial support.

June, 2025

Xiao Liu

Department of Applied Chemistry
Graduate School of Engineering
The University of Osaka
2-1 Yamadaoka, Suita, Osaka 565-0871, JAPAN

Contents

General Introduction

Organophosphorus compounds play a central role in chemistry, finding widespread applications in fine chemicals and organic chemistry. In agriculture, they function effectively as herbicides; in materials science, they enhance polymer performance by imparting flame resistance and flexibility; and in medicine, they often appear as therapeutic agents[1] (Scheme 1). Additionally, organophosphorus reagents like phosphines[2] and ylides[3] are indispensable tools in constructing complex molecular architectures. Since the landmark introduction of BINAP-type chiral phosphine ligands[4] for asymmetric hydrogenation, chiral organophosphorus species have become fundamental in the realm of asymmetric synthesis[5], enabling high enantioselectivity in catalytic transformations.

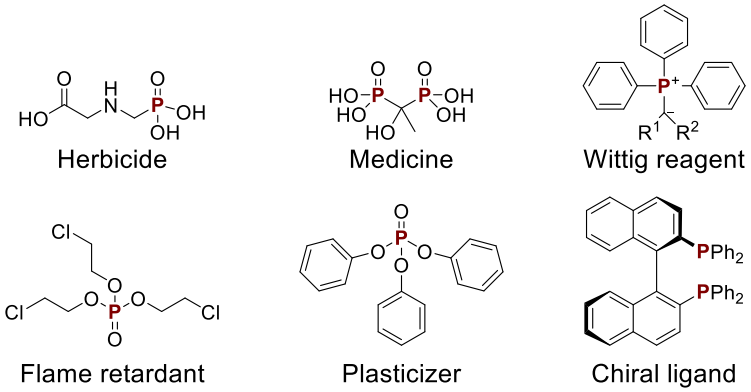

Scheme 1. Examples of widely used organophosphorus compounds in fine chemical industry and organic chemistry.

It is noteworthy that phosphorus(III) and phosphorus(V) compounds—although both pivotal in asymmetric catalysis—serve fundamentally distinct functions (Figure 1). Phosphorus(III) species, such as chiral phosphines[6] and phosphites,[7] predominantly act as chiral ligands coordinating to transition metals; they donate electron density via a lone pair and can engage in π-backbonding, thereby modulating both reactivity and enantioselectivity in metal-catalyzed transformations (Figure 1A). As an example, in 2008, Qi-Lin Zhou and co-workers reported the successful use of a chiral phosphite ligand in a Rh-catalyzed enantioselective conjugated addition[8] (Figure 1B). In this reaction, the C_2-symmetric phosphite ligand **1a** coordinates to the rhodium center, creating a chiral environment that guides the addition of the arylboronic acid to the *α*-ketoester. The method generates *α*-hydroxy-*α*-arylacetates with high enantioselectivity and highlights the utility of phosphite ligands as effective chiral inductors in asymmetric catalysis. In contrast, phosphorus(V) compounds—such as phosphates[9] and chiral phosphoric acids[10][11]—typically operate as Lewis bases or Brønsted acids, functioning independently of metals as organocatalysts (Figure 1C). Recently, Ishihara and co-workers reported the use of chiral triaryl phosphates in the asymmetric halocyclization of 1,1-disubstituted olefins, specifically in the iodolactonization of pent-4-enoic acids[12] (Figure 1d). In this transformation, the chiral phosphate functions as a Lewis base, while iodine (I_2) is activated cooperatively by *N*-chlorophthalimide (NCP), acting as a halogen-based Lewis acid. This catalytic system efficiently

converts benzyl-4-pentenoic acids into the corresponding iodolactones with high yield and enantioselectivity, though the substrate scope remains constrained to pent-4-enoic acid derivatives under the reported conditions.

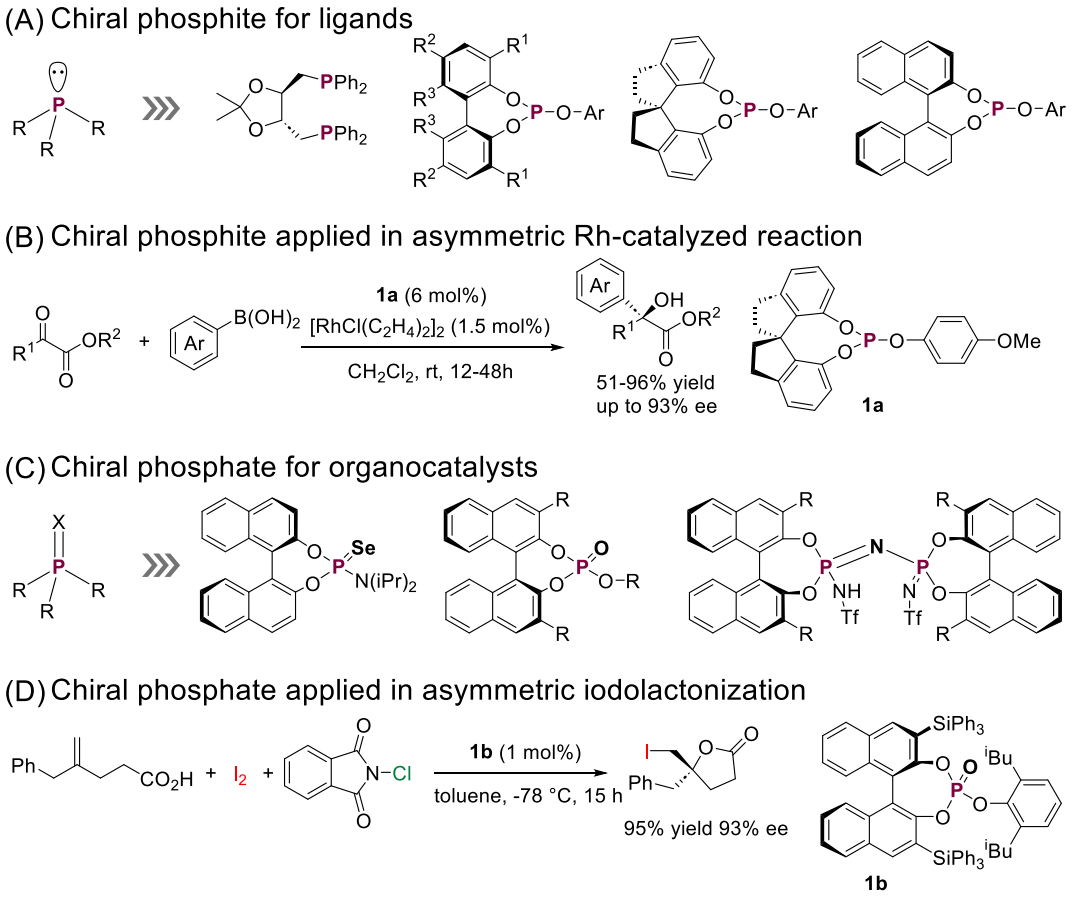

Figure 1. Chiral organophosphorus compounds in asymmetric catalysis.

However, it can be observed in Figure 1A and 1C that a large number of chiral phosphorus compounds possess C_2-symmetric[13] (Figure 2A) frameworks, and they are still widely employed in recent studies on asymmetric catalysis. This is mainly because the well-established research strategies have concentrated on modifying existing C_2-symmetric frameworks, whereas investigations into chiral phosphorus compounds with higher symmetry such as C_3-symmetric (Figure 2B) remain insufficient.[14]

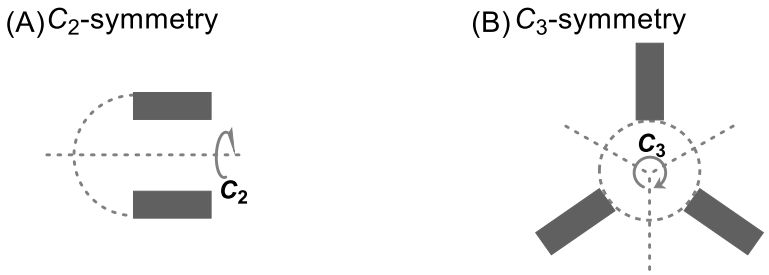

Figure 2. Symmetry in chiral phosphorus compounds

Although reports on C_3-symmetric chiral phosphorus compounds remain scarce, this should not be taken to indicate a lack of potential associated with C_3-symmetric chiral frameworks.[15] Indeed, the intrinsic merits of C_3-symmetry have been recognized in several studies, even though the compounds investigated

therein do not necessarily belong to the class of C_3-symmetric chiral phosphorus compounds. For instance, in Rh(I)-catalyzed hydrogenation of olefins (Figure 3A)[16], the enantioselective step typically proceeds via an octahedral transition state. When tridentate C_2-symmetric ligands are employed (Figure 3B), this can give rise to as many as eight possible diastereomeric transition states. In contrast, the introduction of tridentate C_3-symmetric ligands reduces this number to four (Figure 3C), potentially enhancing enantioselectivity. This mechanistic insight further reinforces our motivation to develop C_3-symmetric chiral phosphorus compounds.

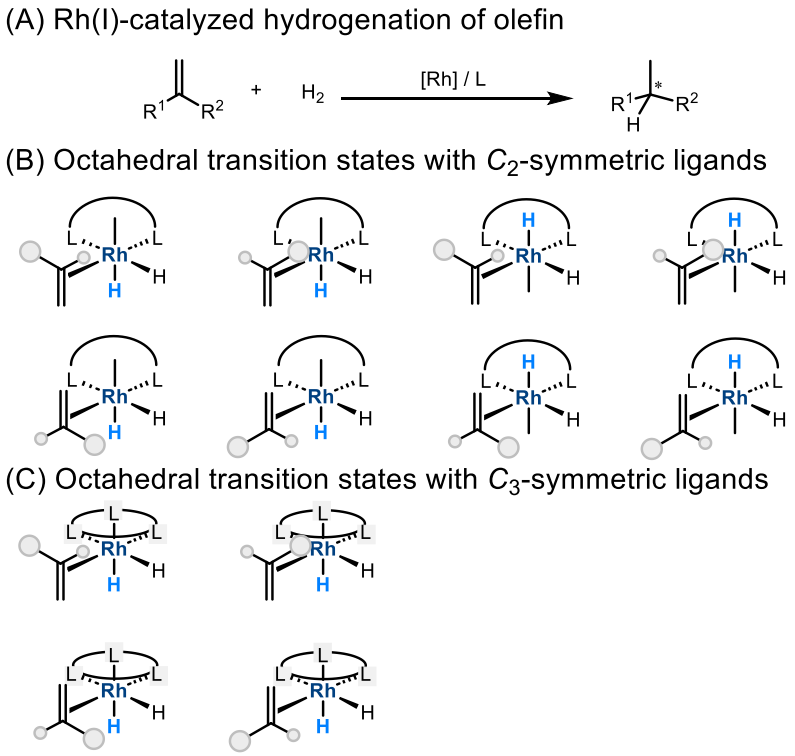

Figure 3. Comparison of C_2-symmteic and C_3-symmetric ligands in Rh(I)-catalyzed hydrogenation of olefin.

In the research group I belong to, a variety of cage-shaped Lewis acid compounds featuring C_3-symmetric frameworks have been established (Scheme 5). With the controllable C_3-symmetric cage-shaped skeleton, cage-shaped borate and aluminum complexes exhibit diverse functionalities on fields of chemoselectivity reaction and tuning the Lewis acidity.

A cage-shaped borate bearing a π-pocket that enables selective molecular recognition between aromatic and aliphatic aldehydes in Diels–Alder reactions was been developed .[17][18] By strategically modifying the tethered groups or substituents on the aromatic rings, the Lewis acidity of these borates could be precisely tuned to suit different reaction environments and substrate scopes.[19][20] In addition, a cage-shaped aluminum complex was found to function effectively as a Lewis acid catalyst for *β*-selective glycosylation, proceeding through a five-coordinate transition state.[21] Furthermore, the construction of a C_3-symmetric chiral cage-shaped borate opened new avenues for chiral molecular recognition, exhibiting promising capabilities in enantioselective transformations and highlighting the potential of higher-order symmetric frameworks in asymmetric catalysis.[22]

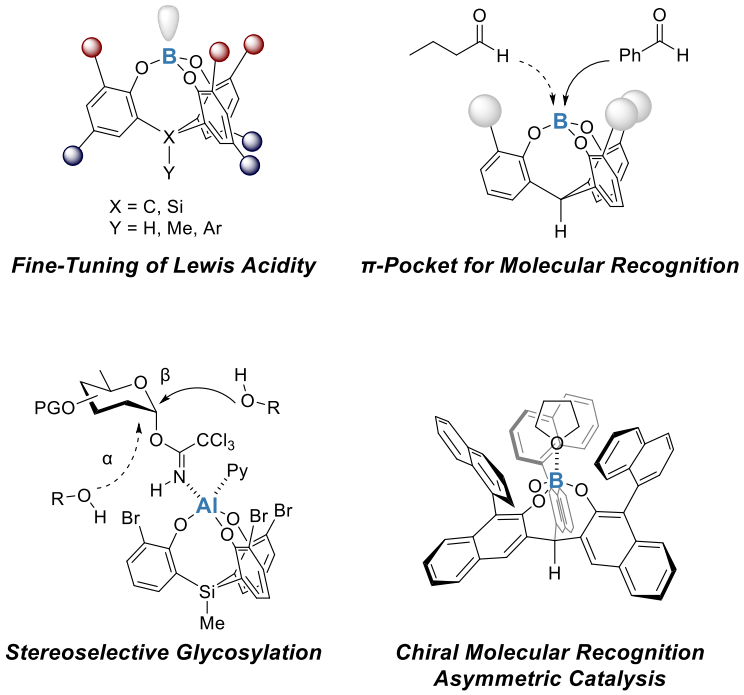

Figure 4. C_3-symmetric cage-shaped Lewis acid molecules.

Driven by the desire to overcome the structural uniformity typically found in conventional symmetric backbones of chiral phosphorus compounds, and inspired by the promising progress made in the development of C_3-symmetric Lewis acid compounds for catalytic applications, this study seeks to explore new structural paradigms in asymmetric catalysis. Specifically, the aim is to design and synthesize novel phosphorus-centered Lewis base architectures that incorporate C_3-symmetric chiral cage-shaped frameworks. These uniquely structured compounds are expected to exhibit enhanced steric and electronic control, enabling high enantioselectivity and reactivity in a range of asymmetric transformations. Furthermore, such C_3-symmetric cage-shaped scaffolds offer the potential to expand the structural diversity and functional versatility of chiral phosphorus chemistry beyond traditional C_3-symmetric systems.

In Chapter 1, two kinds of C_3-symmetric cage-shaped phosphites could be synthesized and characterized. Their Lewis basicity and chiral environment are precisely controlled by the tethered group. The cage-shaped phosphites successfully worked as chiral ligands in Rh-catalyzed asymmetric conjugate additions, realizing acceptable yields with excellent enantioselectivity, and were used to synthesize a pharmacologically important molecule.

In Chapter 2, C_3-symmetric chiral cage-shaped phosphates were successfully synthesized. Two cage-shaped phosphate derivatives containing either a C–H or Si–Me tethered group are air-stable and work as Lewis base catalysts in enantioselective iodolactonizations by I_2 activated with 1,3-dichloro-5,5-dimethylhydantoin (DCDMH). The C–H tethered phosphate demonstrated an efficient catalytic reactivity with good enantioselectivity for the iodolactonization of pent-4-enoic acids. In contrast, the Si–Me tethered phosphate was effective in the enantioselective iodolactonization of hex-5-enoic acid, yielding six-membered iodolactones.

In Chapter 3, C_3-symmetric cage-shaped phosphates serve as effective chiral shift reagents,

demonstrating clear NMR discrimination of chiral amino acids and carboxylic acids. The ^{1}H NMR measurements of a mixture of C_3-symmetric cage-shaped phosphates with chiral analytes in $CDCl_3$ at room temperature yielded effective chiral recognition. Mechanistic studies indicate that ring current effect, hydrogen bonding and π–π stacking interactions play a crucial role in this recognition process.

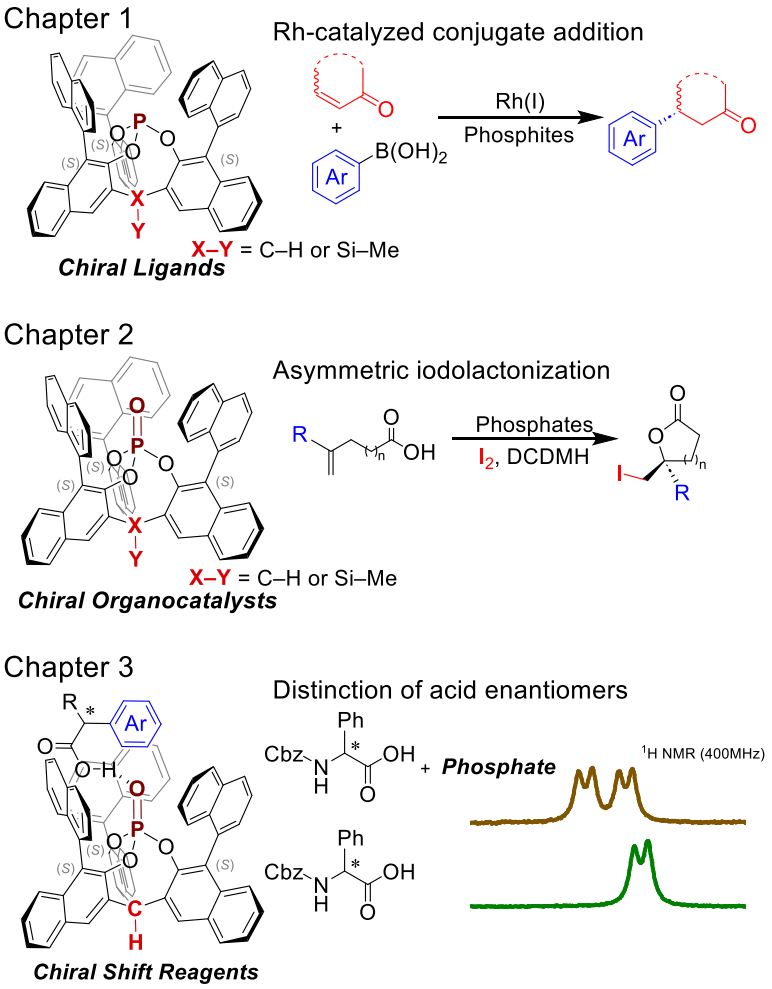

Figure 5. Cage-shaped phosphorus compounds for asymmetric catalytic reaction and chiral shift reagents.

References

[1] S. P.-M. Ung, C.-J. Li, *RSC Sustainability,* **2023**, *1*, 11–37.

[2] Y. Wei, M. Shi, *Chem. Asian. J.* **2014**, *9*, 2720–2734.

[3] Y. Xia, Y. Liang, Y. Chen, M. Wang, L. Jiao, F. Huang, S. Liu, Y. Li, Z.-X. Yu, *J. Am. Chem. Soc.* **2007**, *129*, 3470–3471.

[4] R. Noyori, H. Takaya, *Acc. Chem. Res.* **1990**, *23*, 345–350.

[5] E. Łastawiecka, S. Sowa, K. Szwaczko, K. Dziuba, M. Stankevič, A. Włodarczyk, in *Chiral Build. Blocks Asymmetric Synth.*, **2022**, pp. 389–440.

[6] P. Koschker, M. Kähny, B. Breit, *J. Am. Chem. Soc.* **2015**, *137*, 3131–3137.

[7] P. W. N. M. van Leeuwen, P. C. J. Kamer, C. Claver, O. Pàmies, M. Diéguez, *Chem. Rev.* **2011**, *111*, 2077–2118.

[8] H.-F. Duan, J.-H. Xie, X.-C. Qiao, L.-X. Wang, Q.-L. Zhou, *Angew. Chem. Int. Ed.* **2008**, *47*, 4351–4353.

[9] S. E. Denmark, H. M. Chi, *J. Am. Chem. Soc.* **2014**, *136*, 8915–8918.

[10] E. I. Jiménez, *Org. Biomol. Chem.* **2023**, *21*, 3477–3502.

[11] D. Parmar, E. Sugiono, S. Raja, M. Rueping, *Chem. Rev.* **2014**, *114*, 9047–9153.

[12] H. Nakatsuji, Y. Sawamura, A. Sakakura, K. Ishihara, *Angew. Chem. Int. Ed.* **2014**, *53*, 6974–6977.

[13] M. Rachwalski, *Symmetry (Basel).* **2023**, *15*, DOI 10.3390/sym15071363.

[14] C. Moberg, *Angew. Chemie - Int. Ed.* **2006**, *45*, 4721–4723.

[15] S. E. Gibson, M. P. Castaldi, *Chem. Commun.* **2006**, 3045–3062.

[16] C. Moberg, *Angew. Chem. Int. Ed.* **1998**, *37*, 248–268.

[17] H. Nakajima, M. Yasuda, R. Takeda, A. Baba, *Angew. Chem. Int. Ed.* **2012**, *51*, 3867–3870.

[18] D. Tanaka, Y. Tsutsui, A. Konishi, K. Nakaoka, H. Nakajima, A. Baba, K. Chiba, M. Yasuda, *Chem. - A Eur. J.* **2020**, *26*, 15023–15034.

[19] M. Yasuda, S. Yoshioka, H. Nakajima, K. Chiba, A. Baba, *Org. Lett.* **2008**, *10*, 929–932.

[20] A. Konishi, K. Nakaoka, H. Nakajima, K. Chiba, A. Baba, M. Yasuda, *Chem. Eur. J.* **2017**, *23*, 5219–5223.

[21] D. Tanaka, Y. Kadonaga, Y. Manabe, K. Fukase, S. Sasaya, H. Maruyama, S. Nishimura, M. Yanagihara, A. Konishi, M. Yasuda, *J. Am. Chem. Soc.* **2019**, *141*, 17466–17471.

[22] A. Konishi, K. Nakaoka, H. Maruyama, H. Nakajima, T. Eguchi, A. Baba, M. Yasuda, *Chem. Eur. J.* **2017**, *23*, 1273–1277.

Chapter 1: Cage-Shaped Phosphites Having *C*$_3$-Symmetric Chiral Environment: Steric Control of Lewis Basicity and Application as Chiral Ligands in Rhodium-Catalyzed Conjugate Additions

1-1. Introduction

The design and development of chiral ligands and catalysts are central issues in asymmetric synthesis.[1] One of the most powerful strategies is to focus on the rotational symmetry of the molecule.[2–4] The use of reagents with rotational symmetry can increase the selectivity of the reaction by decreasing the number of transition states and diastereomeric intermediates. As a result of these beneficial properties derived from rotational symmetry, many methodologies stand on chiral catalysts with rotational axes. C_2-symmetric catalysts have been widely used in asymmetric synthesis,[2,5–17] and many of the so-called privileged ligands[18] have two-fold symmetry. While two-fold rotational symmetry has been successfully employed in many chiral ligands and catalysts,[19–21] the efficiency of systems with higher rotational symmetry requires further improvement. For this reason, several C_3-symmetric molecules[22–25] have been developed for asymmetric catalysts,[26–29] molecular recognitions,[30,31] and material science.[32–34] Some C_3-symmetric ligands,[35–43] such as tridentate trisoxazolines[28,44,45] or monophosphites,[46] attained higher enantioselectivity in their use as chiral ligands compared to conventional ligands with C_2-symmetry.[47,48] These pioneering studies raise expectations of the usefulness of C_3-symmetric ligands as chiral ligands. The development and exploration of a diverse range of C_3-symmetric ligands is essential to realize high selectivity in asymmetric synthesis. Considering the development of C_3-symmetric ligands, I focused on a cage-shaped triphenolic framework.[49,50] Our recent studies have demonstrated its effectiveness in controlling the Lewis acidity of a boron[51,52] or aluminum atom.[53] The Lewis acidity of the cage-shaped borate **1a** can be tailored by changing the tethered group (X–Y),[54,55] the substituents (R),[52] and/or the π-conjugated system (π)[56–59] (Figure 1A). Furthermore, the cage-shaped borate **2a**B exhibits highly chiral recognition and behaves as a chiral Lewis acid catalyst owing to its inherent helicity.[60] Thanks to three rigid binaphthyl panels, the central boron atom has a robust chiral environment (Figure 1A). These results strongly indicate the usefulness of the cage-shaped triphenolic framework as the main structure for developing a C_3-symmetric chiral ligand.

Herein, I demonstrate the synthesis and application of cage-shaped phosphites **2a**P and **2b**P with a C_3-symmetric chiral environment (Figure 1B). Phosphite ligands are attractive for chiral catalysis because they are easily prepared from readily available alcohols.[61] Scott[62] and Kawashima[63] independently reported C_3-symmetric cage-shaped phosphites[64] based on triphenolic frameworks, but their Lewis basicity and performance as chiral metal ligands remain unexplored. The Lewis basicity and chiral environment of our chiral Lewis base 2P are controllable by the tethered group (X–Y = C–H (**2a**P) or Si–Me (**2b**P)). They work as chiral metal ligands in asymmetric Rh-catalyzed conjugate additions.

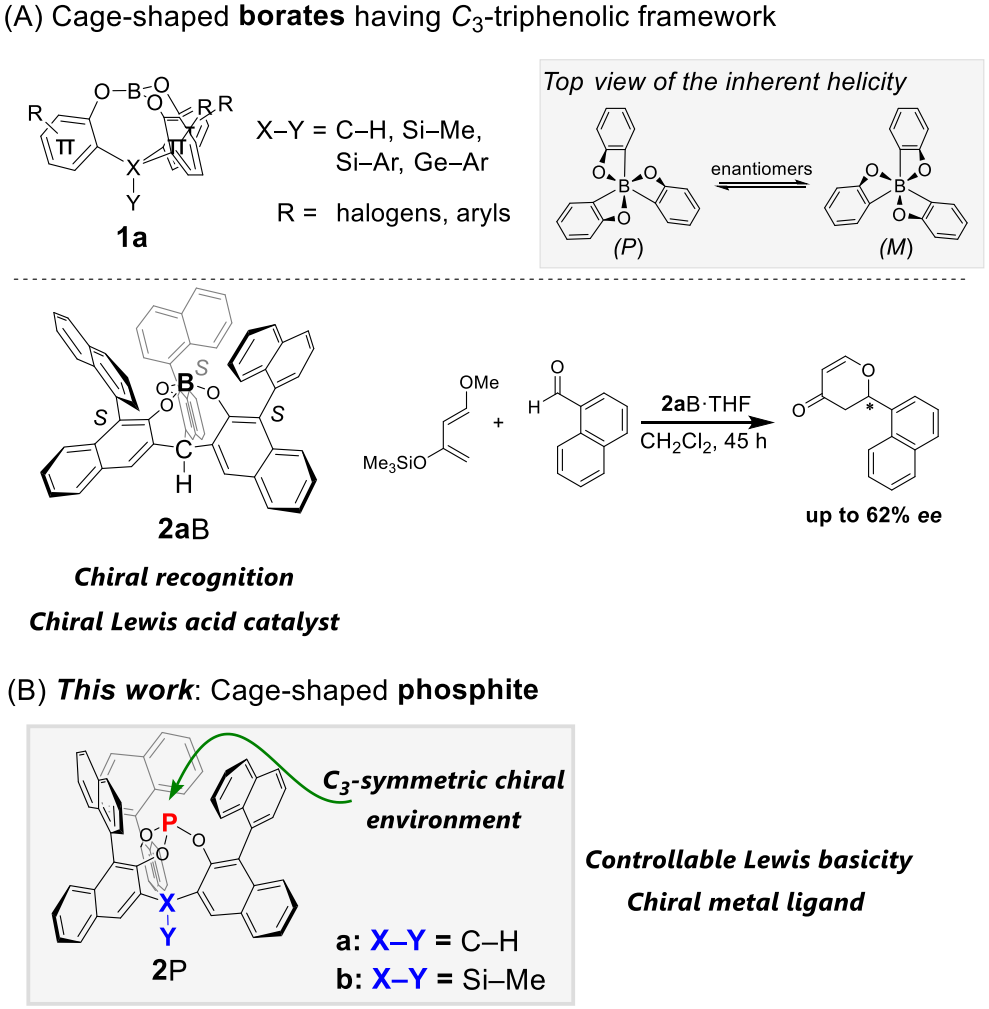

Figure 1. (a) Cage-shaped borate **1c** and its chiral Lewis acid **2a**B. (b) This work: Chiral phosphite **2**P with a C_3-symmetric chiral environment.

1-2. Results and Discussion

The synthetic routes of the chiral cage-shaped phosphites **2a**P and **2b**P are summarized in Scheme 1. The carbon tethered **2a**H_3 was synthesized according to our previous study.[60] The silicon tethered 2bH3 was also synthesized (Scheme 1A). Preparation of methoxymethyl (MOM)-protected **3**[65] from (*R*)-1,1'-bi-2-naphthol (BINOL) and its lithiation at the ortho-position, followed by treatment with methyltrichlorosilane, gave triarylmethylsilane derivative **2b**$(MOM)_3$. Treating **2b**$(MOM)_3$ with HBF_4 aq. effectively afforded **2b**H_3 without cleavage of Si–aryl bonds. Addition of phosphorus trichloride to a sufficiently dilute solution of **2**H_3 in toluene and triethylamine gave the desired cage-shaped phosphites **2**P as a colorless solid (Scheme 1B). The formation of the C_3-symmetric cage-shaped structure of **2**P was confirmed by ^{1}H and ^{31}P NMR spectroscopies, which showed the existence of a single isomer of two possible diastereomers in $CDCl_3$ solution at room temperature. Changing the temperature from 25 to 100 °C did not affect the NMR spectra, illustrating that the helical structure was not changed, and the equilibrium was overwhelmingly one-sided (Figures S4–S5). The obtained phosphite **2**P was sensitive to moisture, showing a gradual hydrolysis under ambient conditions.

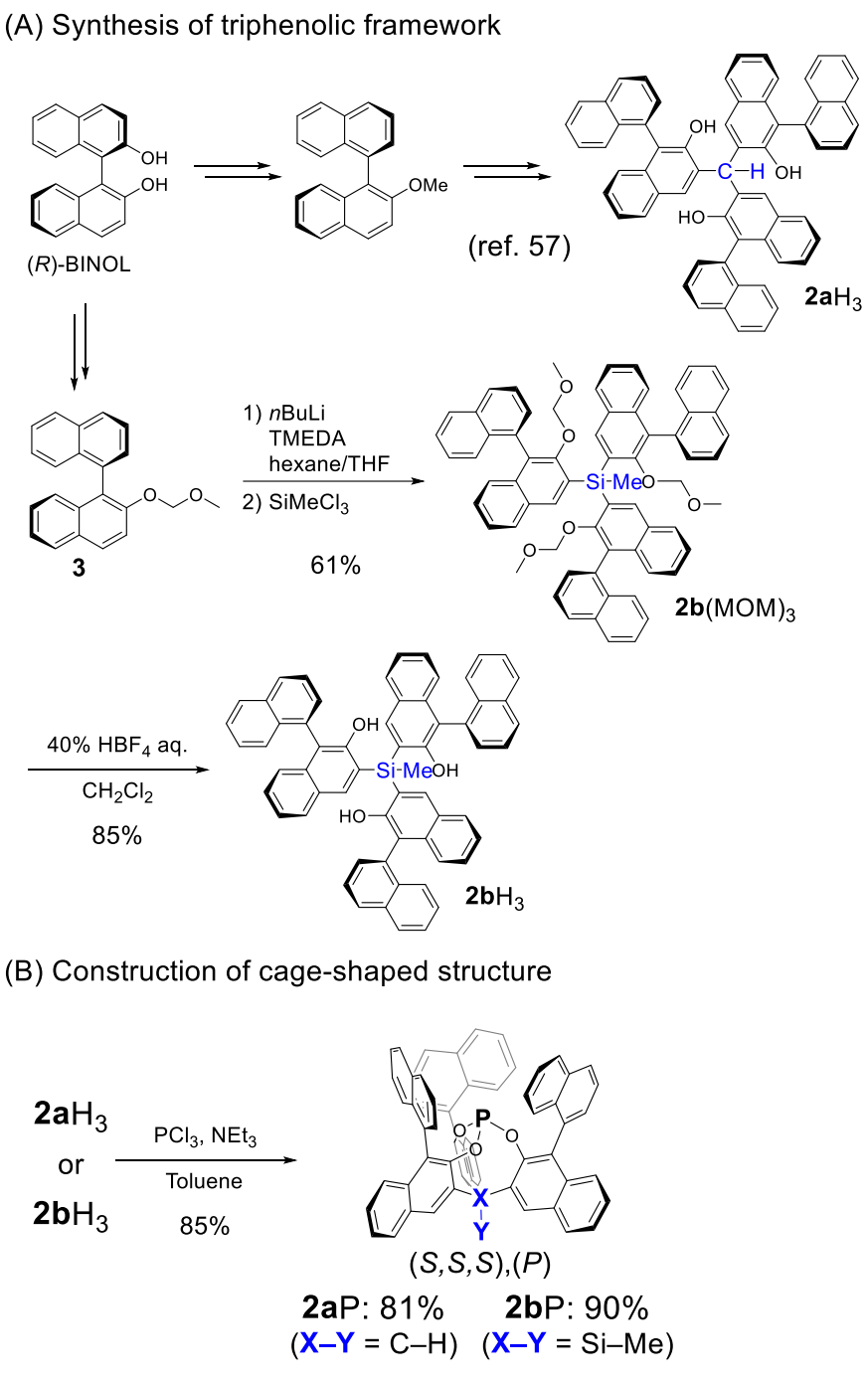

Scheme 1. Synthetic route for (A) triphenolic framework and (B) cage-shaped phosphites **2a**P and **2b**P.

Ortep drawings of **2a**P and **2b**P are shown in Figure 2A. Two crystallographically independent molecules of **2b**P were present in the asymmetric unit, one of which is shown in Figure 2A. No features distinguished the two molecules of **2b**P; therefore, the mean values of the two structures are reported in the following discussion. A robust C_3-symmetric structure is rendered by three naphthyl groups. All binaphthyl axes have (*S*)-forms and a helical structure around phosphorous showed a (*P*)-type. The selected geometric parameters are summarized in Table S1. The most significant geometrical difference between **2a**P and **2b**P is found in the dihedral angle of P–O–C_2–C_1. The angle of **2b**P (74.6°) is larger than that of **2a**P (64.4°) because the three binaphthyl panels are more twisted by embedding a larger Si–Me group than a C–H group

at the tethered position. The geometrical difference reflects in the steric crowding of the chiral C_3-symmetric environment. The percentage of buried volume ($\%V_{Bur}$)[66,67] indicates that 2bP (78.9) has a more shrunken spatial area around the P atom than **2a**P (77.4) (Figure 2B).

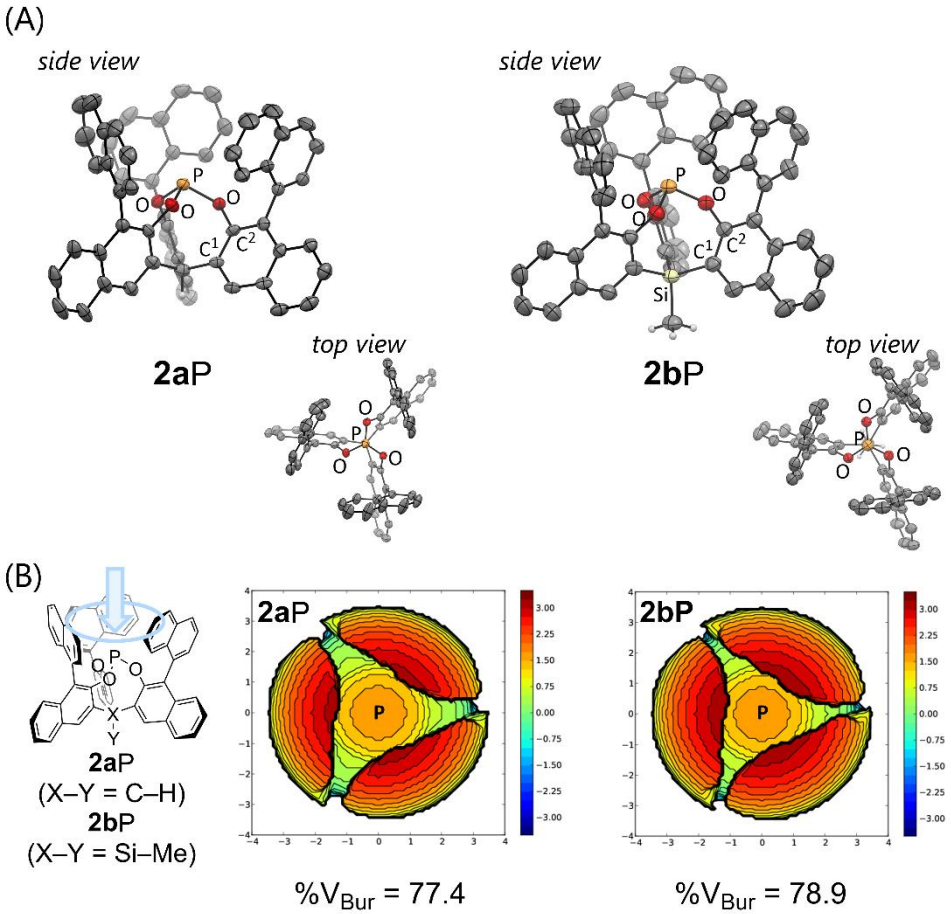

Figure 2. Proposed reaction mechanism of homologation of **1a** with **2a** catalyzed by InI_3/Me_3SiBr

The Lewis basicity of **2a**P and **2b**P was estimated from the ^{31}P NMR coupling constant $^1J(^{31}P–^{77}Se)$[68–70] of the prepared phosphite selenide **2**P=Se (Figures S6–S7). The larger the coupling constant indicates the larger *s* character of the central P atom, illustrating the lower σ-donating and Lewis basicity of the phosphite. The silicon-tethered selenide **2b**P=Se shows a smaller coupling constant ($^1J(^{31}P–^{77}Se)$ = 1102 Hz) than the carbon-tethered selenide **2a**P=Se ($^1J(^{31}P–^{77}Se)$ = 1107 Hz). This observation reveals that **2b**P has larger Lewis basicity than **2a**P, which is also supported by the order of the HOMO levels calculated at the B3PW91/6-311+G** level (Figure S11). The higher HOMO level in **2b**P might be caused by its largely twisted structure that effectively assists a spatial overlap of the lone paired electrons on the O atoms, resulting in the isolation and destabilization of the lone pair on the P atom.

Application of **2a**P and **2b**P as chiral ligands was investigated. The Rh-catalyzed conjugated addition of *α,β*-unsaturated carbonyl **4** with boronic acid **5** was chosen as a model transformation.[71] Our initial studies were focused on the development of reaction conditions. Using **2a**P as a chiral ligand for a Rh metal in the presence of Et_3N as a base, the asymmetric addition of phenylboronic acid **5a** to 2-cyclohexen-1-one

4a producing 3-phenylcyclohexanone **6aa** was performed (Table 1). When Rh(acac)$(C_2H_4)_2$ was employed as a metal source, I was pleased to find that the reaction in $CHCl_3$ at 50 °C afforded the desired product **6aa** in 74% yield with 95% enantiomeric excess (*ee*) of (*R*)-stereoisomer (entry 1). The choice of solvent was crucial; dioxane, THF, and acetone were not applicable (entries 2–4). The ^{31}P NMR measurements of the mixture of the ligand **2a**P and in $CDCl_3$ revealed that the phosphite **2a**P behaved as a monodentate ligand to the Rh center (Figure S8). The Rh center in the C_3-symmetric chiral environment might selectively recognize the *α-Re*-face[72] of the unsaturated carbonyl **4a** due to the steric repulsions between the three naphthyl panels and the substrates, which undergo migratory insertion to form a stereogenic carbon center with (*R*)-configuration (Figure S10). The Rh precursor is also important for reactivity and enantioselectivity (entries 5–6). Changing the Rh precursor from neutral Rh(acac)$(C_2H_4)_2$ to a dimeric $[RhCl(C_2H_4)_2]_2$, the yield of **6aa** decreased. A cationic Rh$(cod)_2BF_4$ gave **6aa** in a high yield but vanished its enantioselectivity. The ^{31}P NMR monitoring of a solution of the phosphite **2a**P and Rh$(cod)_2BF_4$ demonstrated no coordination of **2a**P to the Rh center, illustrating the reaction proceeded in the background. Reaction temperature affected the yield of the product (entries 7–9), but the high enantioselectivity was sustained even at higher temperatures (entries 7–8). For **2b**P, elevating the reaction temperature was required (entries 10–11). Although the trace amount of **6aa** (6%) was obtained at 60 °C, the appreciated yield (51%) with 98% *ee* was attained at 100 °C. The rate-limiting step of the Rh-catalyzed conjugate addition is reported as the transmetallation step,[73] whose activation barrier can be significantly influenced by the steric demand of the phosphorous ligand.[74] Therefore, it is reasonable that the bulkier **2b**P has a more considerable activation energy than that of **2a**P. According to Hayashi's mechanism study, the (acac)Rh catalyst is much less reactive towards transmetalation. That also causes the relatively low reactivity of our reaction system.[75] Replacing phenylboronic acid **5a** with 2,4,6-triphenylboroxin or phenylboronic acid pinacol ester was ineffective. Only trace amounts of **6aa** were obtained.

Table 3. Asymmetric Rh-catalyzed 1,4-addition using cage-shaped phosphite **2a**P or **2b**P.

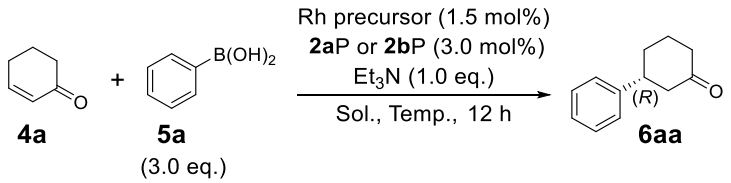

4a **5a** (3.0 eq.) **6aa**

entry	Rh precursor	Ligand	Sol.	Temp. /°C	yield/%[a] (*ee*/%)
1	Rh(acac)$(C_2H_4)_2$	**2a**P	$CHCl_3$	50	74 (95)
2	Rh(acac)$(C_2H_4)_2$	**2a**P	dioxane	50	12 (93)
3	Rh(acac)$(C_2H_4)_2$	**2a**P	THF	50	trace (n.d.)

4	$Rh(acac)(C_2H_4)_2$	**2a**P	acetone	50	trace (n.d.)
5	$[RhCl(C_2H_4)_2]_2$	**2a**P	$CHCl_3$	50	34 (92)
6	$Rh(cod)_2BF_4$	**2a**P	$CHCl_3$	50	99 (0)
7	$Rh(acac)(C_2H_4)_2$	**2a**P	$CHCl_3$	60	85 (94)
8	$Rh(acac)(C_2H_4)_2$	**2a**P	$CHCl_3$	70	49 (94)
9	$Rh(acac)(C_2H_4)_2$	**2a**P	$CHCl_3$	25	14 (90)
10	$Rh(acac)(C_2H_4)_2$	**2b**P	$CHCl_3$	60	6 (n.d)
11	$Rh(acac)(C_2H_4)_2$	**2b**P	$CHCl_3$	100	51 (97)

[a] Yields and ee were determined by ^1H NMR measurement and chiral HPLC analysis, respectively. The absolute configuration of 6aa was determined by comparison with literature data.

With the optimized conditions in hand, a variety of *α*,*β*-unsaturated ketones and boronic acids were applied in the reaction (Scheme 2). The reactions of various *α*,*β*-unsaturated ketones **4** with phenylboronic acid **5a** are summarized in Scheme 2A. The reaction of cyclic ketones **4a**–**4c** gave the corresponding products **6aa**–**6ca** in moderate yields. For 5- (**4b**) or 7-membered (**4c**) ketone, using **2b**P as a ligand afforded higher enantioselectivity of the products (**6ba**: 90% *ee*, **6ca**: 93% *ee*), compared to **2a**P (**6ba**: 69% *ee*, **6ca**: 89% *ee*). In the reaction of linear *α*,*β*-unsaturated ketones, enantioselectivity is generally difficult to control due to flexible conformational interconversions;[71] however, our phosphite system gave relatively high *ee* under appropriate conditions. For acrylophenone derivative **4d**, the yields of **6da** were high (~80%) regardless of the ligand, but its enantioselectivity was increased when **2a**P rather than **2b**P was employed. On the other hand, the products **6ea** and **6fa** from the *β*-aryl substituted ketones **4e** and **4f** were obtained in high enantioselectivity (**6ea**: 89% *ee*, **6fa**: 91% *ee*) only when using **2a**P as a ligand. Notably, the obtained *ee* of **6fa** is the highest among the reported literature.[76–79] Next, I examined the reaction of **4a** with various arylboronic acids **5a**–**i** (Scheme 2B). When **2a**P was used as a ligand, the boronic acids having electron-donating (**5b**, **5c**, **5d**) and electron-withdrawing (**5f**) groups and 1- or 2-naphthylboronic acid (**5h**, **5i**) were applicable to the reaction that afforded the products in moderate to high yields with approximately 90% *ee*. In the case of the boronic acids having a strong electron-donating (**5e**) or electron-withdrawing (**5g**) group at the 4-position, the yield of the product was dramatically suppressed (**6ae**: trace, **6ag**: 17%), although the high enantioselectivity of **6ag** was maintained (93% *ee*). Changing the chiral ligand from **2a**P to **2b**P generally decreased the yield of the product, presumably due to the larger steric hindrance of the chiral environment of **2b**P. In many cases (**6aa**, **6ab**, **6ad**, **6ae**, **6af**, **6ag**), however, the enantioselectivities of these products were improved with the use of **2b**P.

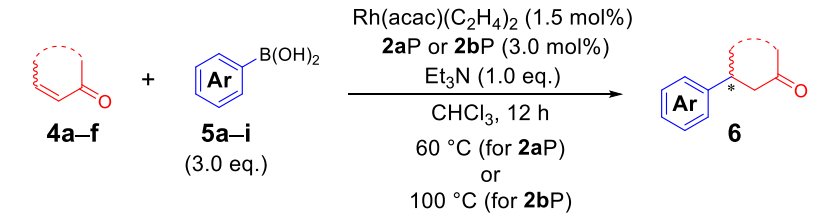

(A) Scope of *α,β*-unsaturated ketones

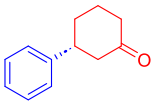

6aa
2aP 85% yield, 94% *ee*
2bP 51% yield, 97% *ee*

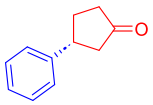

6ba
2aP 15% yield, 69% *ee*
2bP 53% yield, 90% *ee*

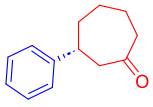

6ca
2aP 51% yield, 89% *ee*
2bP 56% yield, 93% *ee*

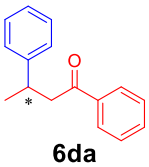

6da
2aP 80% yield, 76% *ee*
2bP 83% yield, 68% *ee*

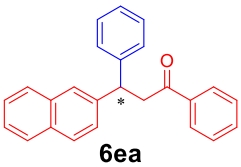

6ea
2aP 22% yield, 91% *ee*
2bP trace, n.d. *ee*

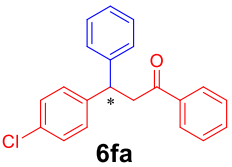

6fa
2aP 49% yield, 91% *ee*
2bP trace, n.d. *ee*

(B) Scope of arylboronic acids

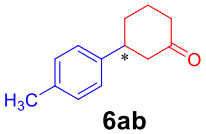

6ab
2aP 70% yield, 92% *ee*
2bP 38% yield, 99% *ee*

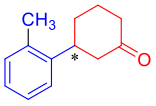

6ac
2aP 91% yield, 91% *ee*
2bP 33% yield, 84% *ee*

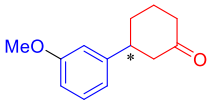

6ad
2aP 56% yield, 94% *ee*
2bP 61% yield, 98% *ee*

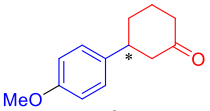

6ae
2aP trace, n.d. *ee*
2bP 34% yield, 98% *ee*

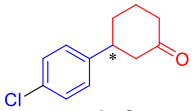

6af
2aP 24% yield, 87% *ee*
2bP 38% yield, 96% *ee*

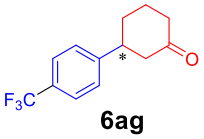

6ag
2aP 17% yield, 93% *ee*
2bP 13% yield, 97% *ee*

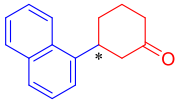

6ah
2aP 76% yield, 96% *ee*
2bP 26% yield, 86% *ee*

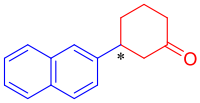

6ai
2aP 33% yield, 92% *ee*
2bP 10% yield, 89% *ee*

Scheme 4. (A) *α,β*-unsaturated ketones and (B) arylboronic acids. Yields and *ee* were determined by ^{1}H NMR measurement and chiral HPLC analysis, respectively.

Our chiral ligand **2a**P was applicable to the conjugated addition of arylboronic acid to *tert*-butoxycarbonyl (Boc)-protected unsaturated lactam. Under the optimized conditions for **2a**P, the reaction of lactam **7** and *p*-fluorophenyl boronic acid **5j** gave the 1,4-adduct **8** in 45% yield with 91% *ee* of (*R*)-configuration. Treating **8** with trifluoroacetic acid (TFA) followed by recrystallization allowed the isolation of the unprotected lactam **9** in an optically pure form (Figure 3). The (*R*)-configuration of **9** was determined

by the X-ray crystallographic analysis and the optical purity of **9** after recrystallization was confirmed by the chiral HPLC analysis. The obtained **9** is a crucial chiral intermediate for the synthesis of (3*S*, 4*R*)-paroxetine,[80–82] which is a selective serotonin reuptake inhibitor (SSRI). It should be noted that our phosphite is applied to synthesize a pharmacologically important molecule.

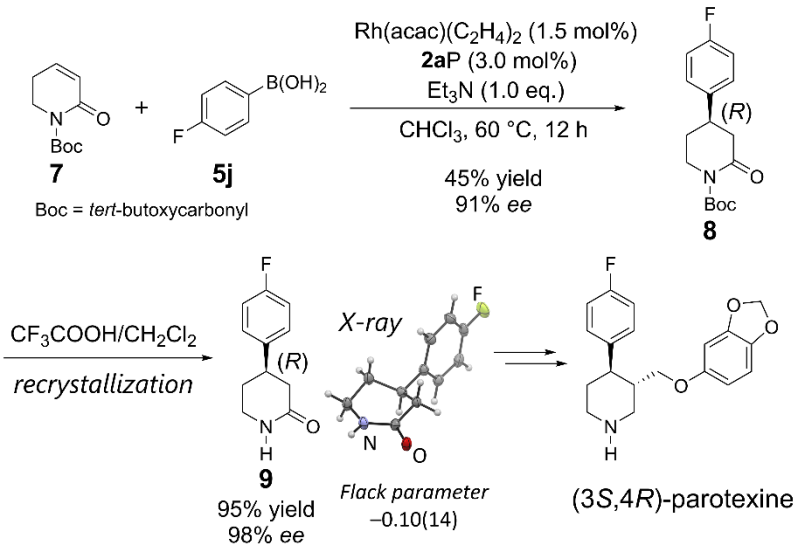

Figure 3. Conjugated addition of **5j** to Boc-protected unsaturated lactam **7** toward the synthesis of paroxetine.

1-3. Conclusion

In conclusion, I have synthesized the two chiral C_3-symmetric cage-shaped phosphites and applied them to the asymmetric Rh-catalyzed 1,4-addition of arylboronic acids to α,β-unsaturated ketones. The reaction was successfully expanded to synthesizing the chiral intermediate for (3*S*, 4*R*)-paroxetine. The Lewis basicity and chemical environment of **2**P were precisely controlled by replacing the tethered group, providing a potential chiral auxiliary governing the reactivity and selectivity in asymmetric reactions. This phosphite could be a basic template for chiral C_3-symmetric Lewis-base chemistry as a new type of chiral ligand.

1-4. Experimental Section

General

NMR spectra were recorded on JEOL-AL400, JEOL-ECS400 (400 MHz for ^{1}H, 100 MHz for ^{13}C, 78.7 MHz for ^{29}Si and 160 MHz for ^{31}P NMR) and Bruker AVANCE III spectrometers (600 MHz for ^{1}H, and 150 MHz for ^{13}C) with TMS as an internal standard. For ^{29}Si NMR spectra, Me_4Si in $CDCl_3$ was used as an external standard. For ^{31}P NMR spectra, H_3PO_4 in D_2O as an external standard was employed as an external standard. ^{1}H and ^{13}C NMR signals of compounds were assigned using HMQC, HSQC, HMBC, COSY, 1D ^{13}C NMR under conditions of proton off-resonance spin decoupling. Positive FAB/CI, EI, MALDI-TOF, ESI/DART mass spectra were recorded on a JEOL JMS-700, a Shimadzu GCMS-QP2010 Ultra, a JEOL JMS-S3000, and a JEOL JMS-T100LP respectively. IR spectra were recorded as thin films or as solids in KBr pellets on a JASCO FT/IR 6200 spectrophotometer. Data collection for X-ray crystal analysis was performed on

Rigaku/XtaLAB Synergy-S/Mo (MoK$_\alpha$ λ = 0.71075 Å) and Rigaku/XtaLAB Synergy-S/Cu (CuK$_\alpha$ λ = 1.54187 Å) diffractometers. All non-hydrogen atoms were refined with anisotropic displacement parameters and hydrogen atoms were placed at calculated positions and refined "riding" on their corresponding carbon atoms by Olex2[83] program.

Materials

Anhydrous dichloromethane, THF, acetonitrile, diethyl ether, toluene and hexane were purchased and used as obtained. All reagents were obtained from commercial suppliers and used as received. All reactions were carried out under nitrogen. In the synthesis of cage-shaped phosphites, loading reagents or purifying the reaction mixture were conducted in a nitrogen-filled glovebox. (*R*)-1,1'-bi-2-naphthol (BINOL) was from a commercial source and methoxymethyl (MOM)-protected binaphthyl **3** was prepared from (*R*)-BINOL according to a method found in the literature.[2] The carbon tethered **2a**H$_3$ was synthesized according to our previous study.[60]

Theoretical calculations

All calculations were conducted using the Gaussian 16 Rev. C.01 program.[84] The optimizations of **2a**P and **2b**P were performed with the CAM-B3LYP-D3(BJ)/def2-SVP level. The obtained optimized structures are local minimum structures with all positive vibrational frequencies at the CAM-B3LYP/Def2SVP level. Using these optimized structures, we estimated the HOMO energy level at the B3PW91/6-311+G** level and the percentage of buried volume (%V$_{Bur}$)[88] calculated by a SambVca 2.1 web server.[67]

Synthetic procedures

Tris{(*S*)-2-(methoxymethoxy)-(1,1'-binaphthalen)-3-yl}(methyl)silane 2b(MOM)$_3$

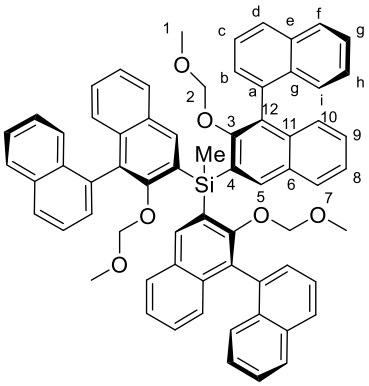

2b(MOM)$_3$

To a solution of (*S*)-2-(methoxymethoxy)-1,1'-binaphthyl **3**[65] (2.91 g, 9.30 mmol) and *N,N,N',N'*-tetramethyl ethylenediamine (0.330 g, 2.80 mmol) in THF (25.0 mL) was slowly added *n*BuLi in hexane (11.1 mmol, 7.00 mL, 1.6 M) via a dropping funnel at −78 ˚C, and the resulting mixture was stirred for 1 h at 0 °C, which yielded a black solution. The flask was cooled to −78 ˚C again and the dropping funnel was charged with trichloro methyl silane (0.610 g, 0.420 mmol), and then the solution was dropped to the flask

at −78 ˚C. After dropping the reaction mixture was allowed to warm to rt gradually and then heated to reflux for 48 h. After cooling to rt, H_2O (20 mL) was added to quench the reaction and the mixture was extracted with ethyl acetate (3 × 30 mL). The collected organic layers were washed with saturated NaCl aq. (2 × 30 mL) and then dried over $MgSO_4$ and evaporated to obtain a yellow solid. The solid was purified by column chromatography (hexane/ether acetate = 80:20, column length 17 cm, diameter 48 mm silica gel) to give **2b**$(MOM)_3$ as a yellow solid (1.70 g, 61%).

mp 159.0–159.6 ℃; IR (KBr) ν = 3050 (w), 2954 (w), 2899 (w), 1616 (w), 1573 (m), 1493 (w), 1437 (w), 1382 (s), 1363 (s), 1278 (m), 927 (s), 829 (w), cm^{-1}; ^1H NMR (400 MHz, $CDCl_3$) 8.38 (s, 3H, 5-H), 8.11 (d, J = 7.6 Hz, 3H), 8.07 (d, J = 8.4Hz, 3H), 8.02 (d, J = 8.4 Hz, 3H), 7.84–7.76 (m, 9H), 7.61 (t, J = 7.6 Hz, 3H), 7.55–7.52 (m, 6H), 7.48 (t, J = 7.6 Hz, 3H), 7.42 (t, J = 7.8 Hz, 3H), 4.59 (q, J = 4.7 Hz, 6H, 2-H), 2.62 (s, 9H, 1-H), 1.66 (s, 3H, Si–Me); ^{13}C NMR (100 MHz, $CDCl_3$) 157.4, 140.2, 135.8, 135.1, 134.0, 133.5, 131.9, 130.7, 129.8, 128.7, 128.6, 128.5, 127.3, 127.2, 126.8, 126.6, 126.25,126.20, 125.8, 125.0, 98.7 (t, C-2), 56.4 (q, C-1), 0.23 (q, Si–Me); ^{29}Si NMR (78.7 MHz, $CDCl_3$, Me_4Si in $CDCl_3$ as an external standard) −7.8; HRMS (MALDI-TOF MS) Calculated ($C_{67}H_{54}O_6NaSi$): 1005.3582 ($[M+Na]^+$), Found: 1005.3561.

(1'*S*,1'''*S*)-3,3''-[{(*S*)-2-hydroxy-(1,1'-binaphthalen)-3-yl}(methyl)silanediyl]bis[{(1,1'-binaphthalen)-2-ol}] 2bH_3

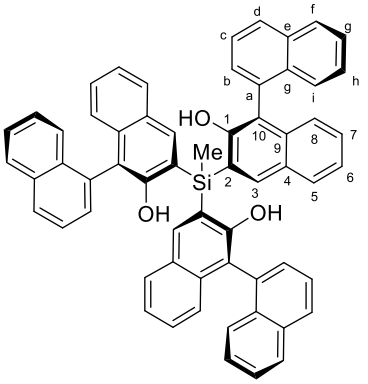

2bH_3

To a colorless solution of **2b**$(MOM)_3$ (0.940 mmol, 0.920 g) in CH_2Cl_2 (20 mL) was added HBF_4 aq. (42% in water, 9.4 mmol, 2.00 g) at room temperature. The mixture was heated at 40 ºC and stirred for 8 h. Cooling down to room temperature, saturated $NaHCO_3$ aq. (20 mL) was added to the mixture, which was extracted with CH_2Cl_2 (3 × 20 mL). The collected organic layers were washed with saturated NaCl aq. (2 × 20 mL) and then dried over $MgSO_4$ and concentrated in vacuo. The crude material was purified by column chromatography (hexane/ethyl acetate = 80:20, column length 20 cm, diameter 26 mm silica gel) to give the pure product **2b**H_3 as a yellow solid (0.760 g, 95%).

mp 219.2–220.0 ℃; IR (KBr) ν = 3530 (m), 3055 (w), 2926 (w), 1730 (w), 1498 (w), 1444 (w), 1365 (m), 1275 (w), 1192 (m), 1083 (w), 1004 (m), 865 (w), 779 (s), 702 (w), 683 (w) cm^{-1}; ^1H NMR (400 MHz, $CDCl_3$) 8.06 (s, 3H, 3-H), 7.98 (d, J = 8.0 Hz, 3H), 7.94 (d, J = 8.4Hz, 3H), 7.77 (d, J = 7.6 Hz, 3H), 7.63 (t, J = 7.6 Hz, 3H), 7.60– 7.55 (m, 6H), 7.51–7.47 (m, 3H), 7.33–7.23 (m, 9H), 7.16 (d, J = 8.4 Hz, 3H), 5.22 (s, 3H, OH), 1.20 (s, 3H, Si–Me); ^{13}C NMR (100 MHz, $CDCl_3$) 155.3, 139.1, 135.4, 134.3, 132.9, 131.8,

130.0, 129.2, 129.0, 128.7, 128.5, 127.2, 127.0, 126.6, 126.2, 125.7,125.0, 124.8, 123.3, 118.0, −1.48 (q, Si–Me); ^{29}Si NMR (78.7 MHz, $CDCl_3$, Me_4Si in $CDCl_3$ as an external standard) −9.0; HRMS (MALDI-TOF MS) Calculated ($C_{61}H_{42}O_3NaSi$): 873.2795 ([M+Na]$^+$), Found: 873.2795.

(5*S*)-5,9,25-Tri(naphthalen-1-yl)-15*H*-7,15-(epoxy[2,3]naphthaleno)dinaphtho[2,3-*d*:2',3'-*g*][1,3,2]dioxaphosphocine 2aP

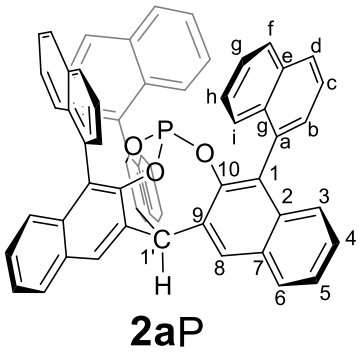

2aP

In a nitrogen-filled glovebox, to a solution of **2a**H_3 (0.180 mmol, 0.148 g) in toluene (50.0 mL) was added triethylamine (0.540 mmol, 0.0550 g) and phosphorus trichloride (0.180 mmol, 0.0250 g). The suspension was heated at 80 °C with stirring for 8 h in a sealed vessel. Evaporation of volatiles gave a colorless solid, which was washed by hexane to give the **2a**P as a colorless solid (0.138g, 90%). The pure product was given by recrystallization from a solution of dichloromethane/hexane. Single crystals suitable for the X-ray crystallographic analysis were obtained from an acetone solution.

^{1}H NMR (400 MHz, $CDCl_3$) 8.16 (s, 3H), 7.89 (d, J = 8.8 Hz, 3H), 7.82 (d, J = 8.4Hz, 3H), 7.76 (d, J = 8.0 Hz, 3H), 7.47 (t, J = 7.0 Hz, 3H), 7.41–7.37 (m, 3H), 7.28–7.21 (m, 12H), 7.04 (d, J = 8.4Hz, 3H), 6.69 (s, 3H), 6.31 (s, 1H); ^{13}C NMR (100 MHz, $CDCl_3$) 133.7, 133.5, 133.4, 132.6, 132.6, 132.4, 130.6, 129.9, 128.6, 128.0, 127.9, 127.7, 127.6, 126.3, 126.01, 125.96, 125.8, 125.7, 125.1, 125.0, 58.8; ^{31}P{^{1}H} NMR (160 MHz, $CDCl_3$, H_3PO_4 in D_2O as an external standard); 108.4.

(5*S*)-15-Methyl-5,9,25-tri(naphthalen-1-yl)-15*H*-7,15-{epoxy(2,3)naphthaleno}dinaphtho(2,3-*d*:2',3'-*g*)(1,3,2,6)dioxaphosphasilocine 2bP

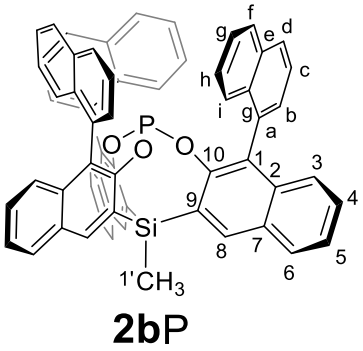

2bP

In a nitrogen-filled glovebox, to a solution of **2b**H_3 (0.015 mmol, 0.0076 g) in toluene (12 mL) was added triethylamine (0.075mmol, 0.055 g) and phosphorus trichloride (0.015 mmol, 0.0020 g). The suspension was

heated at 80 °C with stirring for 8 h in a sealed vessel. Evaporation of volatiles gave product, which was washed by hexane to give the **2b**P as a colorless solid (0.013g, 95%). The pure product was given by recrystallization from a solution of dichloromethane/hexane. Single crystals suitable for the X-ray crystallographic analysis were obtained from an THF/dichloromethane solution.

^{1}H NMR (400 MHz, $CDCl_3$) 8.24 (s, 3H), 7.92 (d, J = 8.4 Hz, 3H), 7.84 (d, J = 8.0Hz, 3H), 7.70 (d, J = 8.0 Hz, 3H), 7.49 (s, 3H), 7.40–7.36 (m, 3H), 7.29–7.23 (m, 9H), 7.05 (s, 3H), 6.90 (d, J = 8.8 Hz, 3H), 6.20 (s, 3H), 1.65 (s, 3H, Si–Me); ^{13}C NMR: (100 MHz, $CDCl_3$) 135.4, 135.3, 134.2, 133.5, 132.5, 130.5, 128.9, 128.8, 128.2, 127.8, 127.8. 127.7, 127.4, 127.1, 126.2, 126.1, 125.9, 125.7, 125.1, 124.9, −4.86 (Si-Me); ^{31}P{^{1}H} NMR (160MHz, $CDCl_3$, H_3PO_4 in D_2O as an external standard) 111.2; ^{29}Si{1H} NMR (78.7 MHz, $CDCl_3$, Me_4Si in $CDCl_3$ as an external standard) −16.8.

X-ray crystallographic data

Carbon-tethered cage-shaped phosphite **2a**P

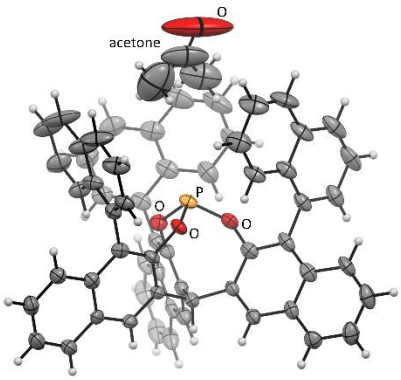

Figure S1. ORTEP drawing of **2a**P at the 50% probability level.

No. CCDC	2283100	Space Group	$P4_12_12$ (#92)
Empirical Formula	$C_{61}H_{37}O_3P + C_3H_6O$	Z value	8
Formula Weight	906.95	D_{calc}	1.283 g/cm^3
Crystal Color	translucent intense colourless	F_{000}	3792.0
Crystal Dimensions	0.161 × 0.091 × 0.085 mm	μ(CuK$_\alpha$)	0.927 mm^{-1}
Crystal System	tetragonal	Temperature	123 K
Lattice Parameters	a = 14.93390(10) Å	Data/restraints/parameters	9424/42/624
	b = 14.93390(10) Å	Residuals: R_1 ($I > 2.00\sigma(I)$)	0.0726
	c = 42.1028(4) Å	Residuals: wR_2 (all data)	0.1689
	α = 90 °	Goodness of Fit Indicator	1.183
	β = 90 °	Flack parameter	0.096(13)
	γ = 90 °	Recrystallization	From acetone/hexane
	V = 9389.82(15) Å^3		

Silicon-tethered cage-shaped phosphite **2b**P

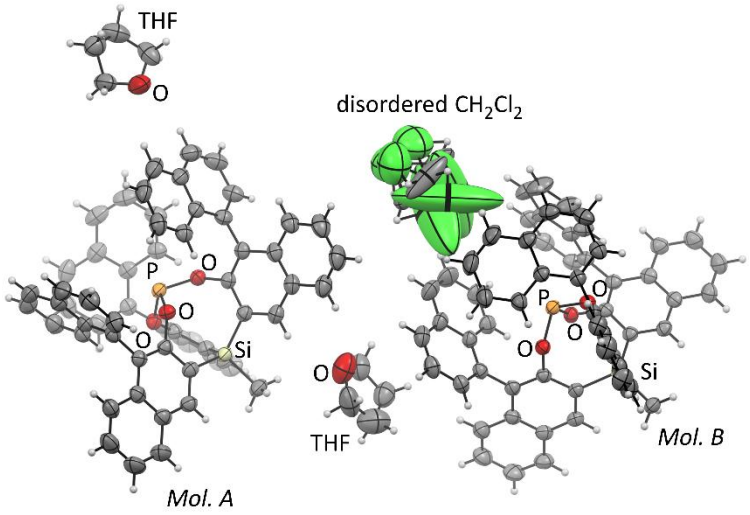

Figure S2. ORTEP drawings of **2b**P at the 50% probability level.

No. CCDC	2283101	Space Group	$R3$ (#146)
Empirical Formula	$2(C_{61}H_{39}O_3PSi) + 6(C_4H_8O) + (CH_2Cl_2)$	Z value	3
Formula Weight	2275.53	D_{calc}	1.256 g/cm^3
Crystal Color	translucent intense colourless	F_{000}	3594.0
Crystal Dimensions	0.189 × 0.115 × 0.06 mm	μ(CuK$_\alpha$)	1.434 mm^{-1}
Crystal System	trigonal	Temperature	190 K
Lattice Parameters	a = 18.1757(2) Å	Data/restraints/parameters	7016/22/516
	b = 18.1757(2) Å	Residuals: R_1 ($I > 2.00\sigma(I)$)	0.0438
	c = 31.5394(4) Å	Residuals: wR_2 (all data)	0.1248
	α = 90 °	Goodness of Fit Indicator	1.051
	β = 90 °	Flack parameter	−0.007(12)
	γ = 120 °	Recrystallization	From acetone/THF/CH_2Cl_2
	V = 9023.3(2) Å^3		

Lactam **9**

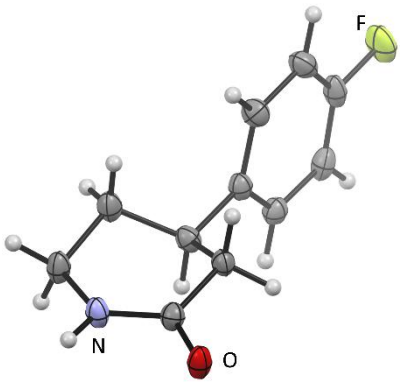

Figure S3. ORTEP drawing of **9** at the 50% probability level.

No. CCDC	2283102	Space Group	$P2_12_12_1$ (#19)
Empirical Formula	$C_{11}H_{12}FNO$	Z value	4
Formula Weight	193.22	D_{calc}	1.341 g/cm^3
Crystal Color	translucent intense colourless	F_{000}	408.0
Crystal Dimensions	0.28 × 0.27 × 0.19 mm	μ(CuK$_\alpha$)	0.824 mm^{-1}
Crystal System	orthorhombic	Temperature	123 K
Lattice Parameters	a = 5.8273(2) Å	Data/restraints/parameters	1678/0/127
	b = 7.6444(2) Å	Residuals: R_1 ($I > 2.00\sigma(I)$)	0.0339
	c = 21.4834(8) Å	Residuals: wR_2 (all data)	0.0875
	α = 90 °	Goodness of Fit Indicator	1.032
	β = 90 °	Flack parameter	−0.10(14)
	γ = 90 °	Recrystallization	From CH_2Cl_2/hexane
	V = 957.00(5) Å^3		

Summary for the geometries of **2a**P and **2b**P

Table S1. Selected geometric parameters for **2a**P and **2b**P

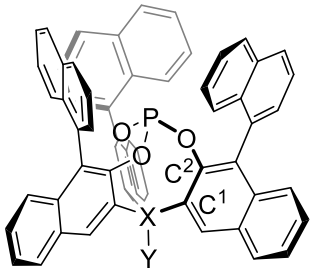

	2aP (X–Y = C–H)	**2b**P (X–Y = Si–CH$_3$) Mol. A	Mol. B
P–X / Å	3.351	3.566	3.564
∠O–P–O / °	100.36(19)	100.40(9)	99.61(8)
∠P–O–C^2–C^1 / °	64.36	73.27	75.70

Variable temperature NMR measurements

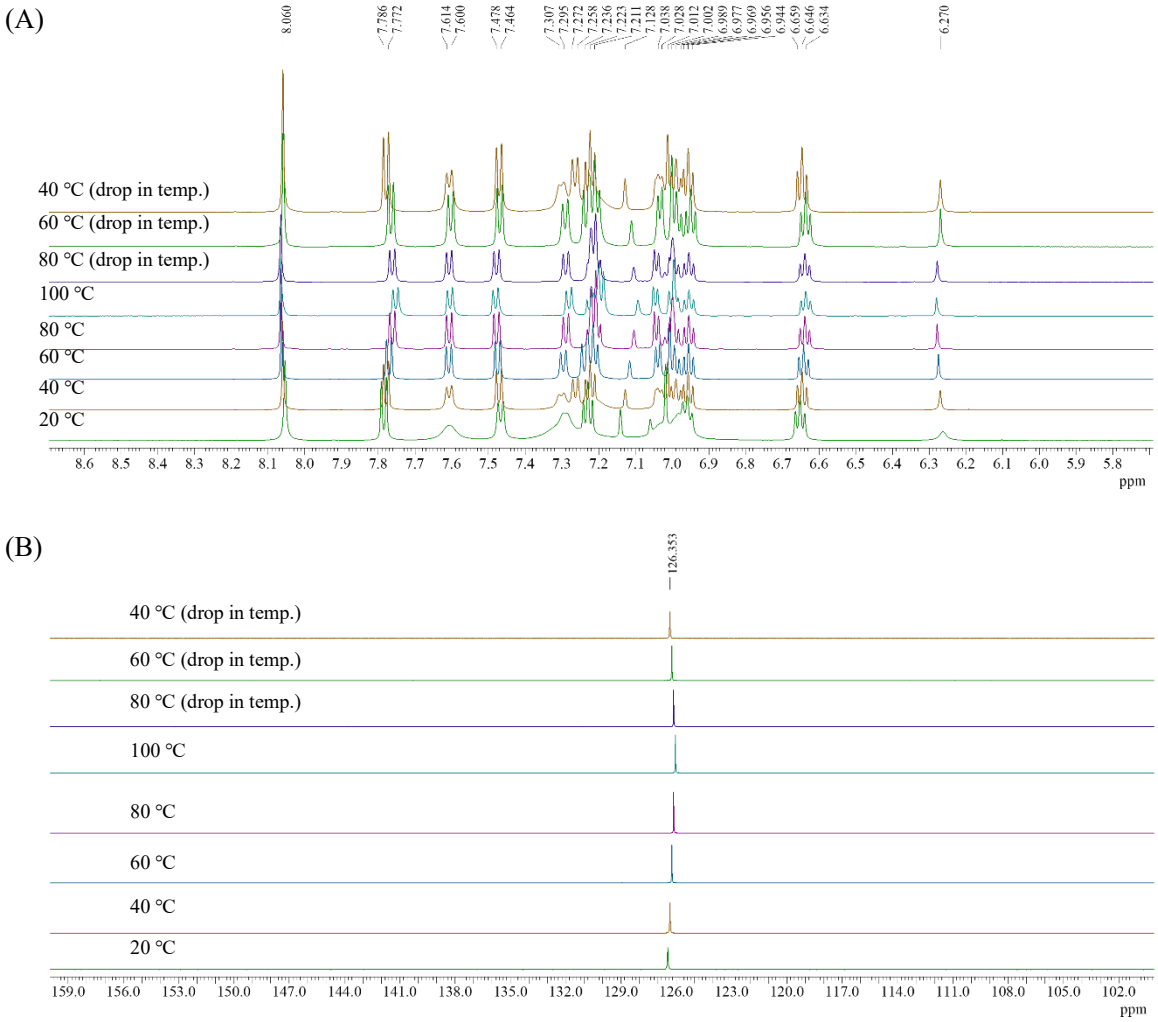

Figure S4. Variable temperature NMR spectra for **2a**P in toluene-d_8. (A) ^{1}H NMR spectrum of **2a**P recorded in the aromatic region (600 MHz). (B) ^{31}P{^{1}H} NMR spectrum of **2a**P (243 MHz, Triphenylphosphine in acetone-d_6 as an external standard.)

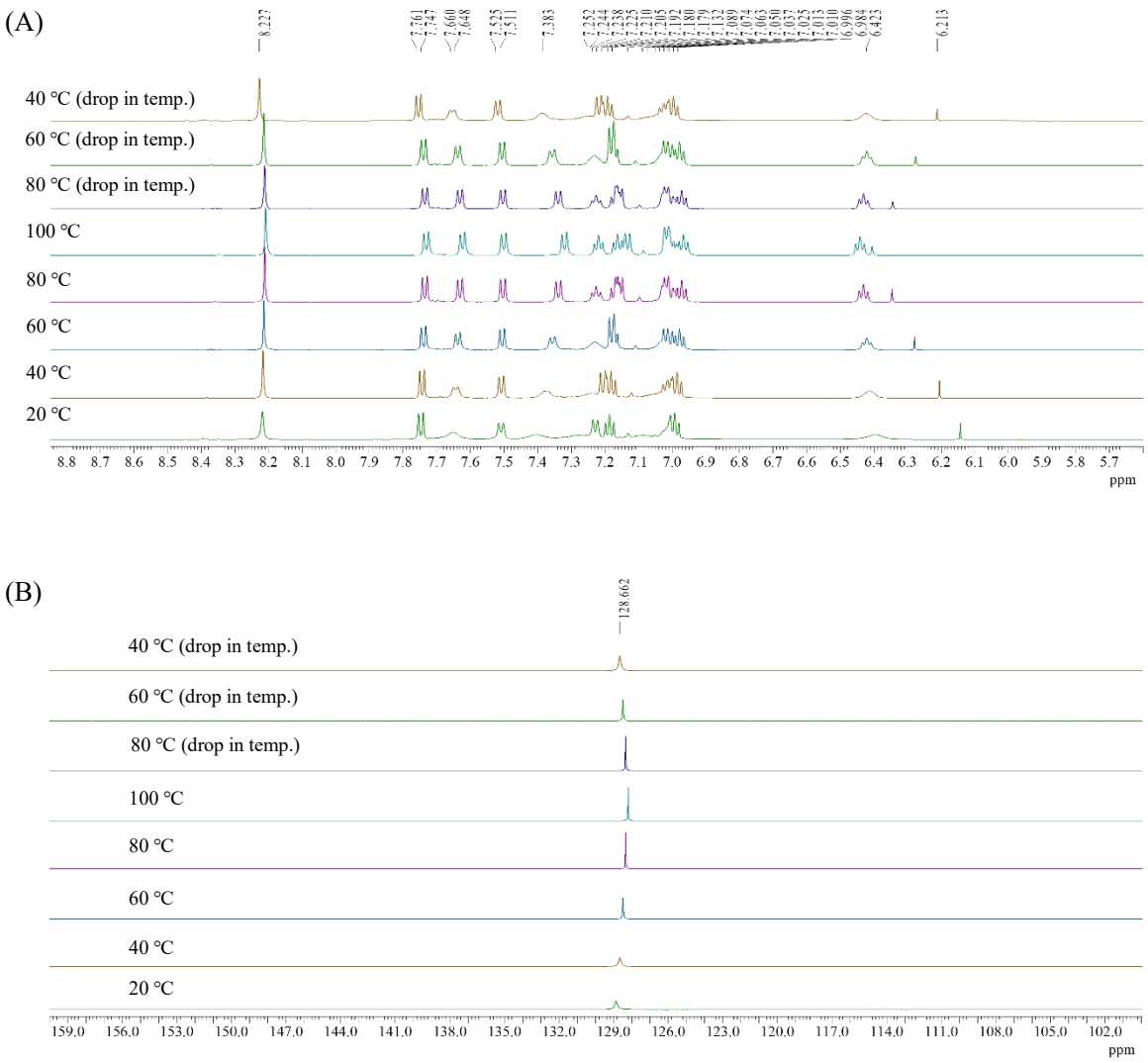

Figure S5. Variable temperature NMR spectra for **2b**P in toluene-d_8. (A) ^{1}H NMR spectrum of **2b**P recorded in the aromatic region (600 MHz). (B) ^{31}P{^{1}H} NMR spectrum of **2b**P (243 MHz, Triphenylphosphine in acetone-d_6 as an external standard.)

Preparation of phosphite selenide 2P=Se and evaluation of the Lewis basicity

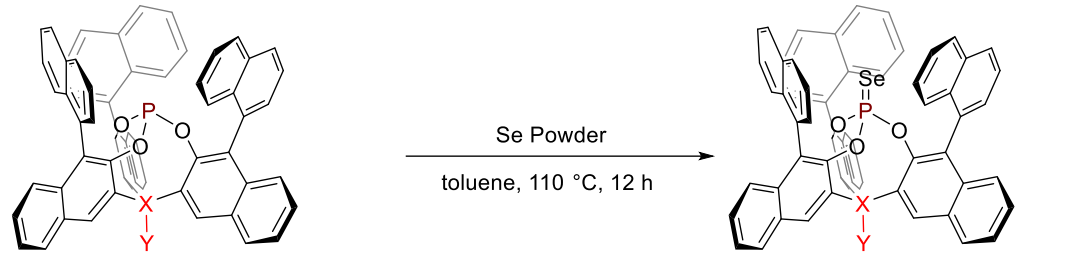

(*S*,*S*,*S*), (P) **2a**P: X–Y= C–H **2b**P: X–Y= Si–Me

2aP=Se: X–Y= C–H **2b**P=Se: X–Y= Si–Me

In a nitrogen-filled glove box, a mixture of the cage-shaped phosphite **2a**P or **2b**P (0.0120 mmol), selenium powder (3.8 mmol, 0.3 g, excess) in toluene (10ml), at a Schlenk flask under reflux for 12 h. After cooling to room temperature, the excess selenium was removed by filtration in the glove box, and the filtrate evaporated to give the compounds **2a**P=Se and **2b**P=Se in 99% yield.

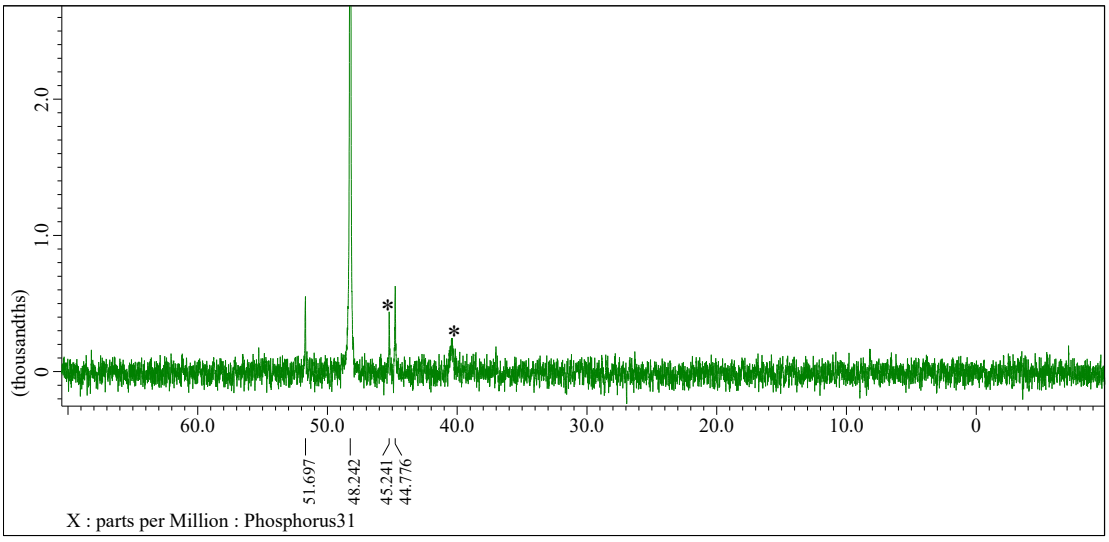

Figure S6. $^{31}P\{^{1}H\}$ NMR spectrum of **2a**P=Se in $CDCl_3$. (160MHz, H_3PO_4 in D_2O as an external standard.) Asterisks represent uncharacterized signals from some impurities or decomposed materials.

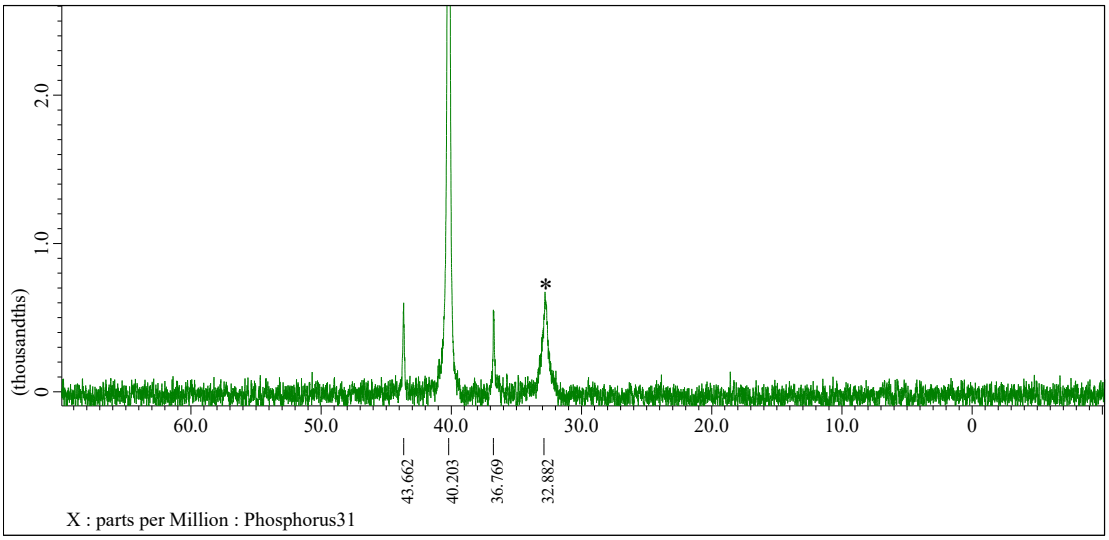

Figure S7. $^{31}P\{^{1}H\}$ NMR spectrum of **2b**P=Se in $CDCl_3$. (160MHz, H_3PO_4 in D_2O as an external standard.) Asterisk represents uncharacterized signals.

NMR examination of the coordination number of cage-shaped phosphite to Rh center

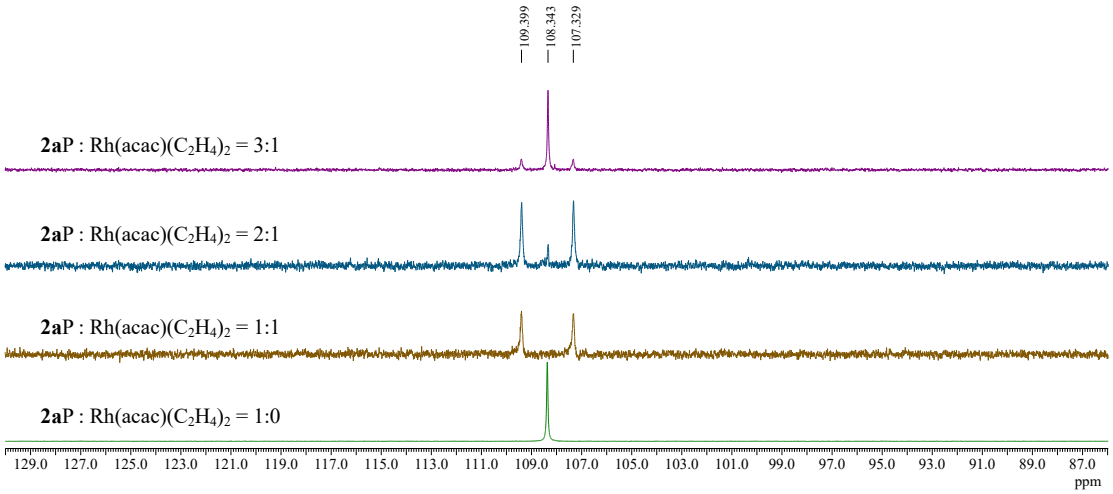

Figure S8. $^{31}P\{^{1}H\}$ NMR spectra of **2a**P in the presence of the various amounts of $Rh(acac)(C_2H_4)_2$ in $CDCl_3$. (160MHz, H_3PO_4 in D_2O as an external standard.)

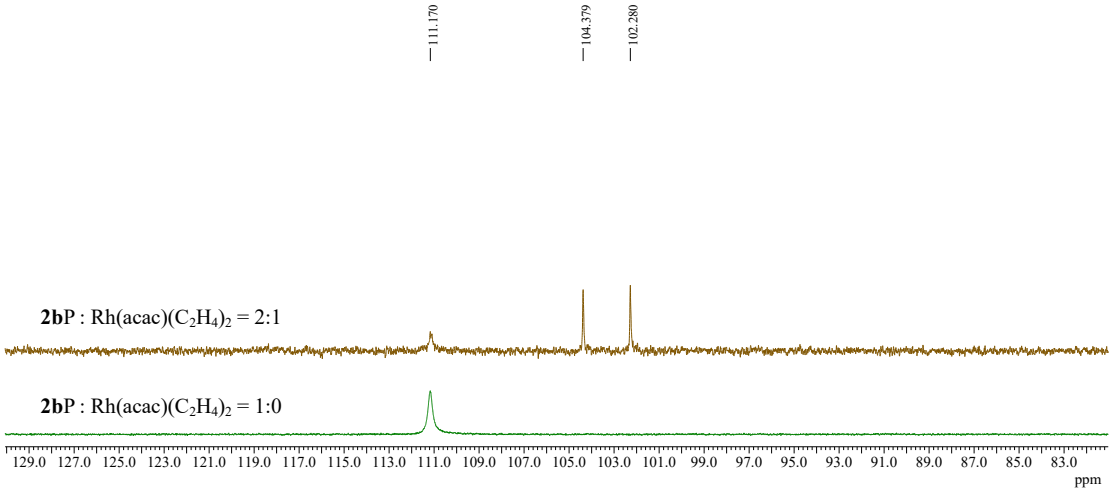

Figure S9. $^{31}P\{^{1}H\}$ NMR spectra of **2b**P in the presence of the various amounts of $Rh(acac)(C_2H_4)_2$ in $CDCl_3$. (160MHz, H_3PO_4 in D_2O as an external standard.)

Application of cage-shaped phosphites as chiral ligand in Rh-catalyzed conjugated addition

Plausible reaction mechanism to determine enantioselectivity

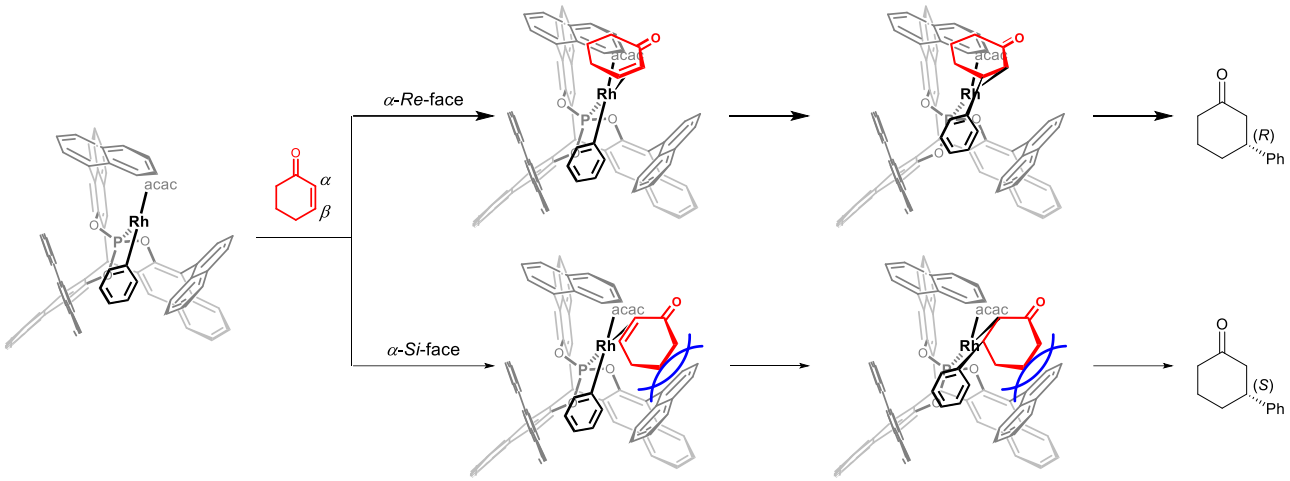

Figure S10. Proposed stereochemical pathway forming the product of (*R*)-configuration.

Typical procedure for the 1,4-addition of boronic acids to enones with 2aP or 2bP ligand

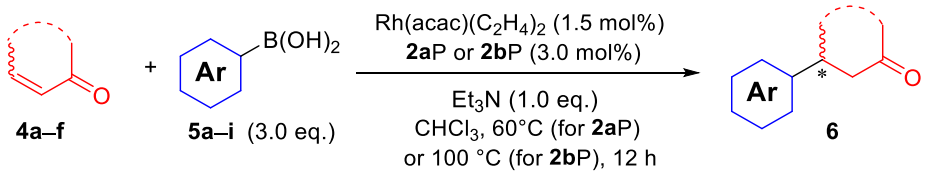

Optimized procedure when employing 2aP as a chiral ligand

In the nitrogen-filled glovebox, Rh(acac)(C_2H_4) (0.8 mg, 3.0 μmol) with **2a**P (5.1 mg, 6.0 μmol) were dissolved in CH_3Cl (1 mL, super dehydrated, amylene was added) in a mighty vial. The mixture was stirred for 1 hour. After stirred, boronic acid (0.6mmol), triethylamine (0.0203 g, 0.2 mmol) and enone (0.2 mmol) were added to the mixture. The reaction mixture was heated at 60 ℃ for 12 h. The reaction was quenched with saturated $NaHCO_3$ aq. The product was extracted with ethyl acetate (10 mL), the organic layer was washed with saturated $NaHCO_3$ aq. (2 × 5 mL) and brine (2 × 5 mL). The organic phase was dried by Na_2SO_4 and removed under vacuum. The obtained residue was purified by column chromatography on silica gel to afford corresponding product.

Application the optimized condition to the reaction in 1 mmol scale

In the nitrogen-filled glovebox, Rh(acac)(C_2H_4) (4.1 mg, 15.0 μmol) with **2a**P (25.7 mg, 30.0 μmol) were dissolved in CH_3Cl (5 mL, super dehydrated, amylene was added) in a mighty vial. The mixture was stirred for 1 hour. After stirred, phenylboronic acid (0.3655g, 3.0 mmol), triethylamine (0.1020 g, 1.0 mmol) and cyclohexenone (95.50 mg, 1.0 mmol) were added to the mixture. The reaction mixture was heated at 100 ℃ for 12 h. The reaction was quenched with saturated $NaHCO_3$ aq. The product was extracted with ethyl acetate

(20 mL), the organic layer was washed with saturated $NaHCO_3$ aq. (2 × 10 mL) and brine (2 × 10 mL). The organic phase was dried by Na_2SO_4 and removed under vacuum. The obtained residue was purified by column chromatography on silica gel to afford corresponding product **6aa** with 64% yield with 93% *ee*.

Optimized procedure when employing 2bP as a chiral ligand

In the nitrogen-filled glovebox, Rh(acac)(C_2H_4) (0.8 mg, 3.0 μmol) with **2b**P (5.3 mg, 6.0 μmol) were dissolved in CH_3Cl (1 mL, super dehydrated, amylene was added) in a mighty vial. The mixture was stirred for 1 hour. After stirred, boronic acid (0.6mmol), triethylamine (0.0203 g, 0.2 mmol) and enone (0.2 mmol) were added to the mixture. The reaction mixture was heated at 100 ℃ for 12 h. The reaction was quenched with saturated $NaHCO_3$ aq. The product was extracted with ethyl acetate (10 mL), the organic layer was washed with saturated $NaHCO_3$ aq. (2 × 5 mL) and brine (2 × 5 mL). The organic phase was dried by Na_2SO_4 and removed under vacuum. The obtained residue was purified by column chromatography on silica gel to afford corresponding product.

Procedure of 1,4-addition of Boc-protected lactam 7

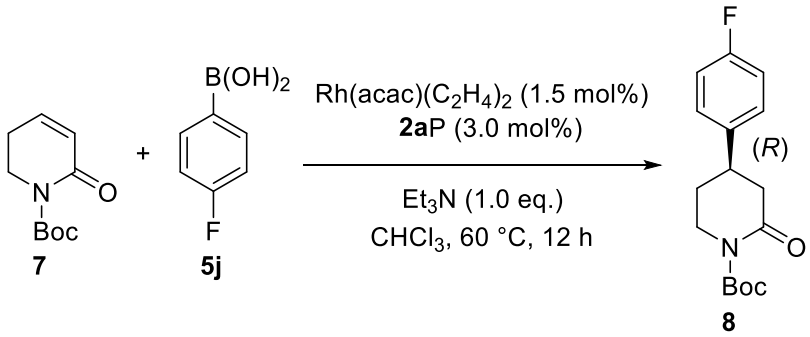

In the nitrogen-filled glovebox, Rh(acac)(C_2H_4) (0.8 mg, 3.0 μmol) with **2a**P (5.3 mg, 6.0 μmol) were dissolved in CH_3Cl (1 mL, super dehydrated, amylene was added) in a mighty vial. The mixture was stirred for 1 hour. After stirred, **5j** (0.0840g, 0.6 mmol), triethylamine (0.0203 g, 0.2 mmol) and **7** (39.4 mg, 0.2 mmol) were added to the mixture. The reaction mixture was heated at 100 ℃ for 12 h. The reaction was quenched with saturated $NaHCO_3$ aq. The product was extracted with ethyl acetate (20 mL), the organic layer was washed with saturated $NaHCO_3$ aq. (2 × 10 mL) and brine (2 × 10 mL). The organic phase was dried by Na_2SO_4 and removed under vacuum. The obtained residue was purified by column chromatography on silica gel to afford corresponding product **8** with 45% yield with 91% *ee*.

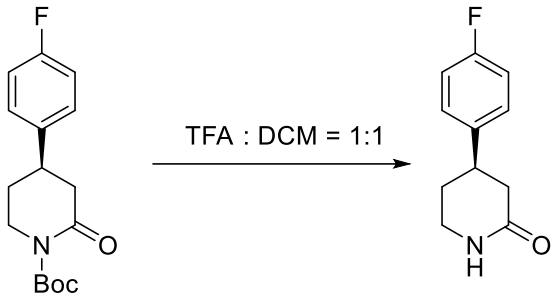

8 **9**

To a solution of **8** (0.02 g, 0.07 mmol) in 3 mL dichloromethane was added trifluoroacetic acid (3 ml, 39.2 mmol) and the mixture was stirred 12 h at rt. The reaction mixture was concentrated under reduced pressure and the residue was solved in CH_3Cl and washed with saturated $NaHCO_3$ aq. (2 × 10 mL) and brine (2 × 10 mL). The organic phase was dried by Na_2SO_4 and removed under vacuum. The obtained residue was purified by GPC to afford corresponding product **9** with 99% yield with 89% *ee*. For further purification, recrystallization from a dichloromethane/hexane solution afforded **9** in optically pure form (98% *ee*).

HPLC chromatograms and NMR spectra for the 1,4-adducts 6

3-Phenylcyclohexan-1-one (6aa)[89]

^{1}H NMR (400 MHz, $CDCl_3$) 7.34–7.32 (m, 2H), 7.24–7.22 (m, 3H), 3.05–2.99 (m, 1H), 2.62–2.36 (m, 4H), 2.18–2.08 (m, 2H), 1.88–1.76 (m, 2H); ^{13}C NMR (100 MHz, $CDCl_3$) 211.2, 144.3, 128.7, 126.7, 126.6, 49.0, 44.8, 41.2, 32.8, 25.6.

Chiralpak ID-3 (4.6 mm x 25 cm), hexane/2-propanol = 98/2, 1.0 mL min^{-1}, 35 °C, UV detection at 210.0 nm. For the racemic sample, based on the reported retention time of (*R*)- and (*S*)-3-phenylcyclohexan-1-one,[89] t_R = 11.7 min belongs to *S*-, t_R = 12.3 min belongs to *R*-enantiomer.

Racemate

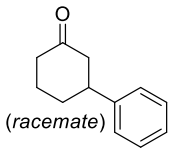

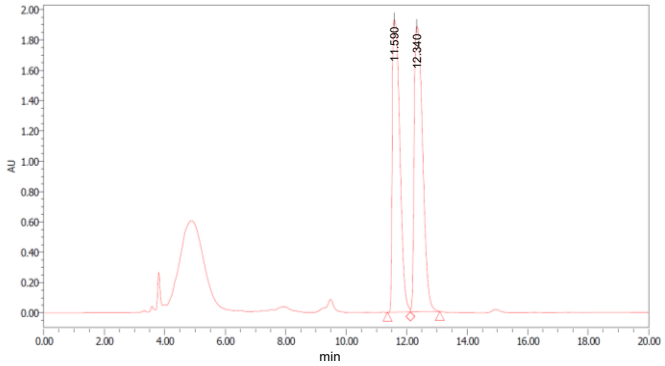

Peak No.	Ret. Time / min	area %
1(*S*)	11.590	47.78
2(*R*)	12.340	52.22

2aP as ligand:

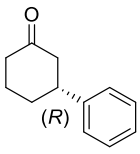

94% *ee* (85%)

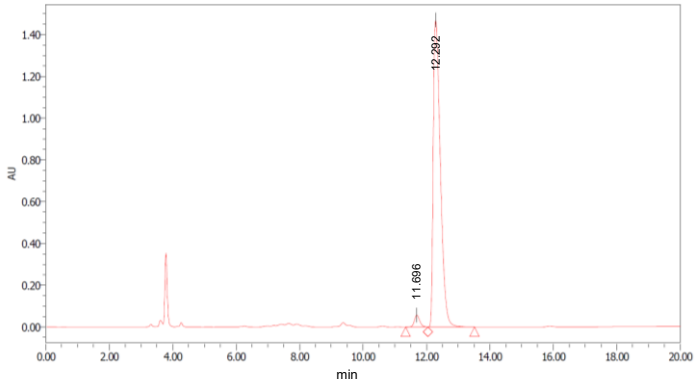

Peak No.	Ret. Time / min	area %
1(*S*)	11.696	2.96
2(*R*)	12.292	97.04

2bP as ligand:

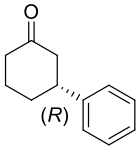

97% *ee* (51%)

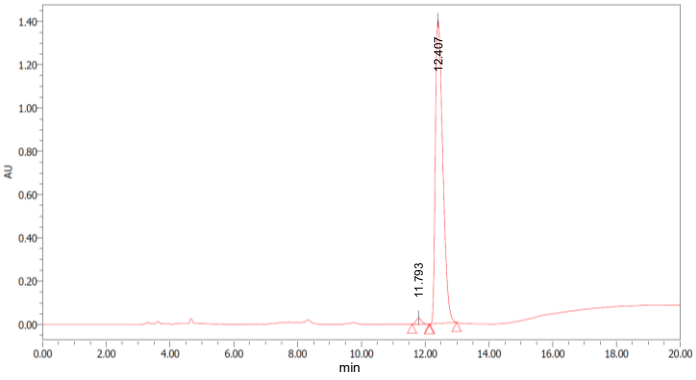

Peak No.	Ret. Time / min	area %
1(*S*)	11.793	1.44
2(*R*)	12.407	98.56

3-Phenylcyclopentan-1-one (6ba)[89,90]

^{1}H NMR (400 MHz, $CDCl_3$) 7.37–7.34 (m, 2H), 7.27–7.24 (m, 3H), 3.48–3.39 (m, 1H), 2.68 (dd, J = 18.4, 7.6 Hz, 1H), 2.52–2.42 (m, 2H), 2.39–2.27 (m, 2H), 2.06–1.95 (m, 1H); ^{13}C NMR (100 MHz, $CDCl_3$) 218.6, 143.0, 128.7, 126.7, 45.8, 42.2, 38.9, 31.2.

Chiralpak ID-3 (4.6 mm x 25 cm), hexane/2-propanol = 98/2, 1.0 mL min^{-1}, 35 °C, UV detection at 210.0 nm. For the racemic sample, based on the reported retention time of (*R*)- and (*S*)-3-phenylcyclohexan-1-one,[89,8] t_R = 10.8 min belongs to *S*-, t_R = 11.1 min belongs to *R*-enantiomer.

Racemate

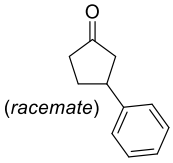

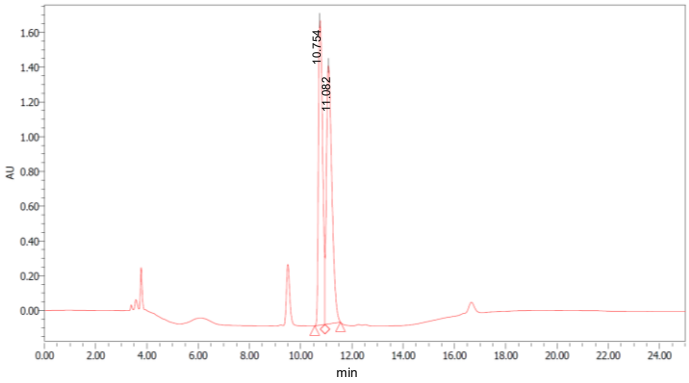

Peak No.	Ret. Time / min	area %
1(*S*)	10.754	47.60
2(*R*)	11.028	52.40

2aP as ligand

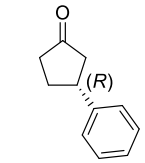

69% *ee* (15%)

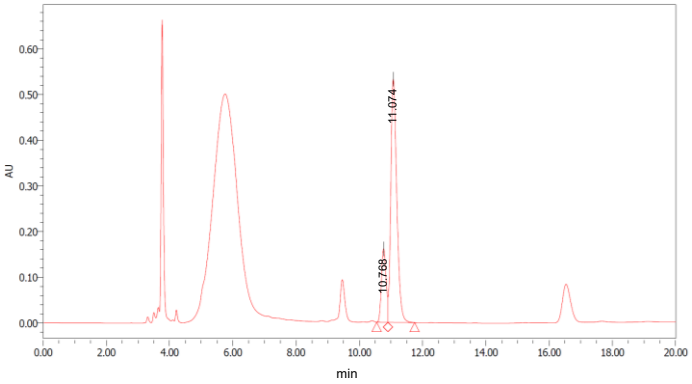

Peak No.	Ret. Time / min	area %
1(*S*)	10.768	19.16
2(*R*)	11.074	80.84

2bP as ligand

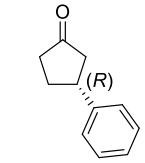

90% ee (53%)

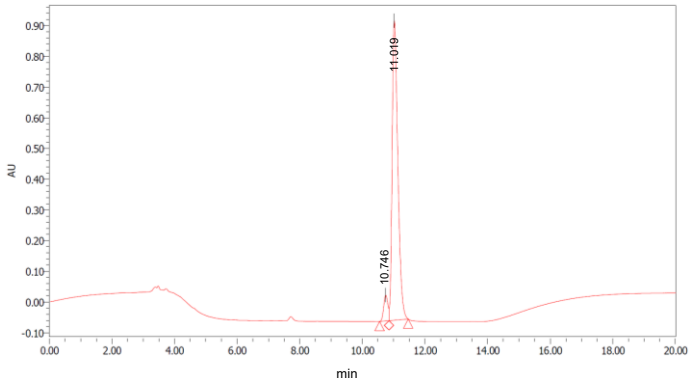

Peak No.	Ret. Time / min	area %
1(*S*)	10.746	5.7
2(*R*)	11.019	94.3

3-Phenylcycloheptan-1-one (6ca)[89]

^{1}H NMR (400 MHz, $CDCl_3$) 7.32–7.29 (m, 2H), 7.23–7.17 (m, 3H), 2.98–2.90 (m, 2H), 2.66–2.58 (m, 3H), 2.11–1.98 (m, 3H), 1.80–1.66 (m, 2H), 1.55–1.45 (m, 1H); ^{13}C NMR (100 MHz, $CDCl_3$) 213.8, 147.0, 128.7, 126.5, 126.4, 51.4, 44.1, 42.8, 39.3, 29.3, 24.3.

Chiralpak ID-3 (4.6 mm x 25 cm), hexane/2-propanol = 98/2, 1.0 mL min^{-1}, 35 °C, UV detection at 210.0 nm. For the racemic sample, based on the reported retention time of (*R*)- and (*S*)-3-phenylcycloheptan-1-one,[89] t_R = 12.8 min belongs to *S*-, t_R = 14.1 min belongs to *R*-enantiomer.

Racemate

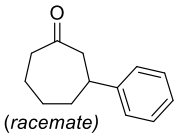

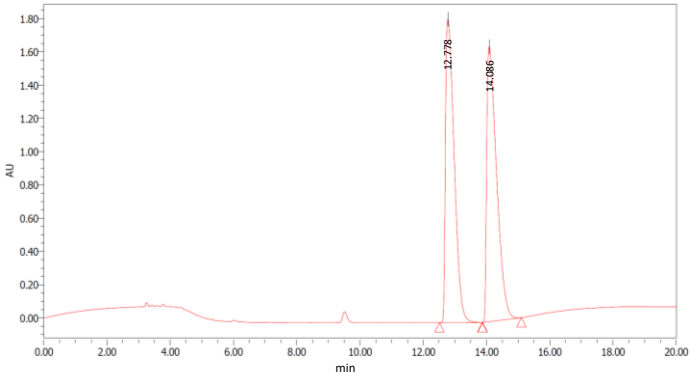

Peak No.	Ret. Time / min	area %
1(*S*)	12.778	49.46
2(*R*)	14.086	50.54

2aP as ligand

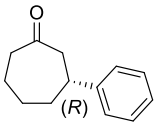

89% *ee* (51%)

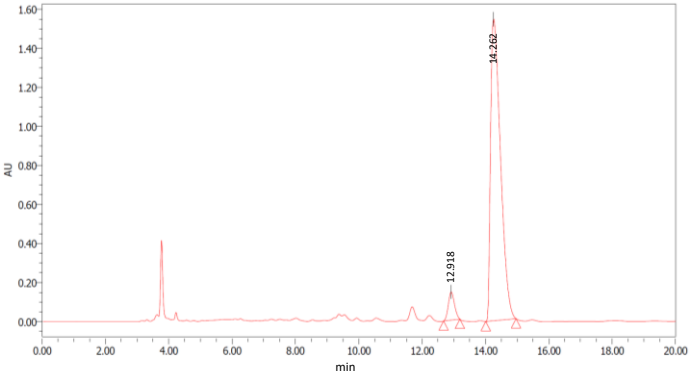

Peak No.	Ret. Time / min	area %
1(*S*)	12.918	5.46
2(*R*)	14.262	94.54

2bP as ligand

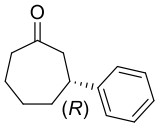

93% *ee* (56%)

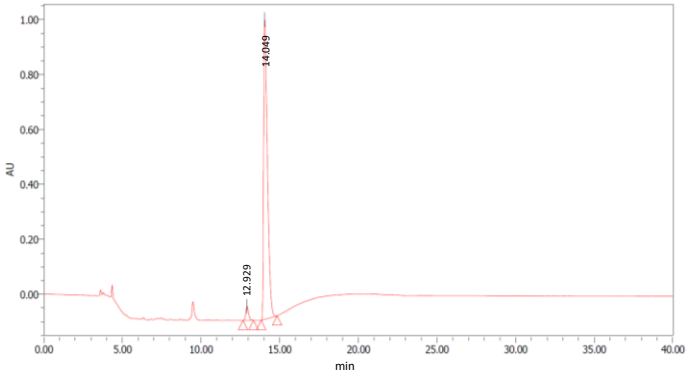

Peak No.	Ret. Time / min	area %
1(*S*)	12.929	3.39
2(*R*)	14.049	96.61

1,3-Diphenylbutane-1-one (6da)[91]

^{1}H NMR (400 MHz, $CDCl_3$) 7.95–7.92 (2H, m), 7.57–7.53 (1H, m), 7.47–7.43 (2H, m), 7.33–7.27 (4H, m), 7.22–7.18 (1H, m), 3.54–3.47 (1H, m), 3.33–3.16 (2H, m), 1.34 (3H, d, J = 7.2 Hz); ^{13}C NMR (100 MHz, $CDCl_3$) 199.1, 146.5, 137.1, 133.0, 128.6, 128.5, 128.1, 126.9, 126.3, 47.0, 35.5, 21.9.

Chiralpak ID-3 (4.6 mm x 25 cm), hexane/2-propanol = 98/2, 1.0 mL min-1, 35 °C, UV detection at 210.0 nm. The absolute configurations were not determined.

Racemate

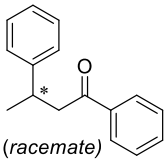

(*racemate*)

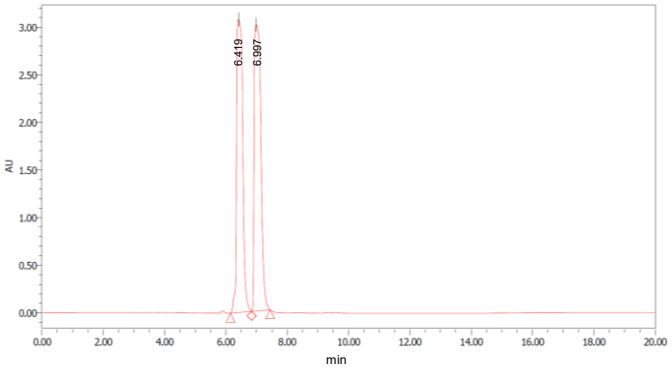

Peak No.	Ret. Time / min	area %
1	6.419	48.54
2	6.997	51.46

2aP as ligand:

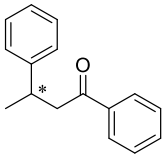

76% *ee* (80%)

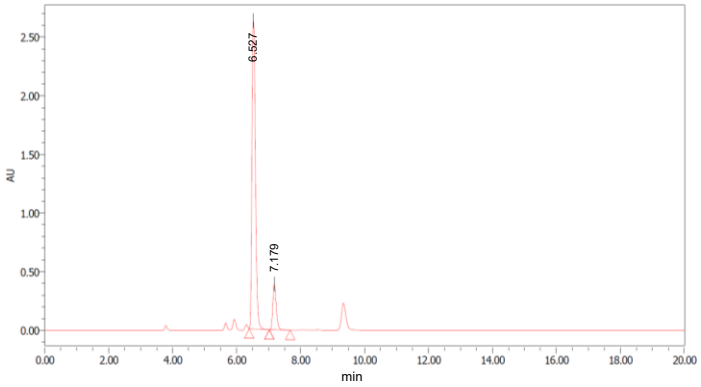

Peak No.	Ret. Time / min	area %
1	6.527	87.30
2	7.179	12.70

2bP as ligand:

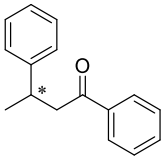

68% *ee* (83%)

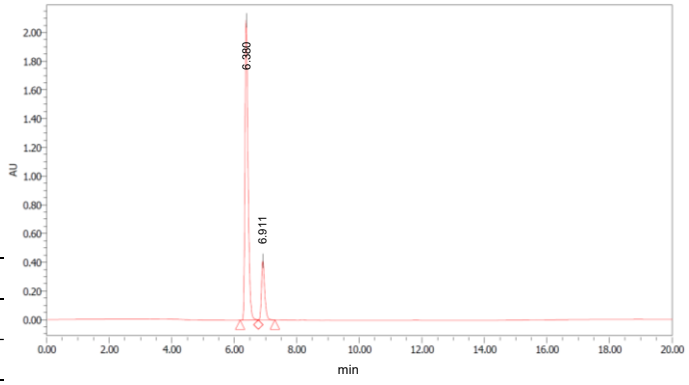

Peak No.	Ret. Time / min	area %
1	6.380	83.07
2	6.911	16.93

3-(Naphthalen-2-yl)-1,3-diphenylpropan-1-one (6ea)[92]

^{1}H NMR (400 MHz, $CDCl_3$) 7.95 – 7.93 (m, 2H), 7.76 – 7.71 (m, 4H), 7.55 – 7.51 (m, 1H), 7.44 – 7.36 (m, 5H), 7.32 – 7.24 (m, 4H), 7.19 – 7.15 (m, 1H), 5.00 (t, J = 7.2 Hz, 1H), 3.89 – 3.77 (m, 2H); ^{13}C NMR (100 MHz, $CDCl_3$) 198.1, 144.1, 141.6, 137.1, 133.6, 133.3, 132.3, 128.8, 128.7,128.4, 128.2, 128.1, 127.9, 127.7, 126.9, 126.6, 126.2, 125.9, 125.7, 125.6, 46.1, 44.7.

Chiralpak ID-3 (4.6 mm x 25 cm), hexane/2-propanol = 98/2, 1.0 mL min^{-1}, 35 °C, UV detection at 210.0 nm. The absolute configurations were not determined.

Racemate

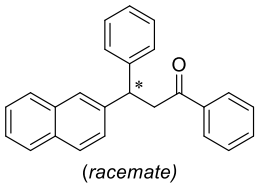

(*racemate*)

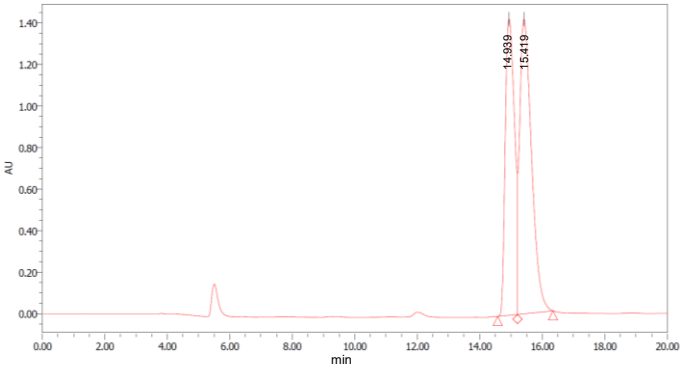

Peak No.	Ret. Time / min	area %
1	14.939	43.70
2	15.419	56.30

2aP as ligand:

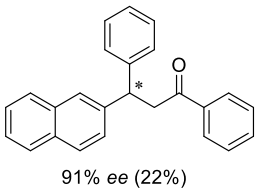

91% *ee* (22%)

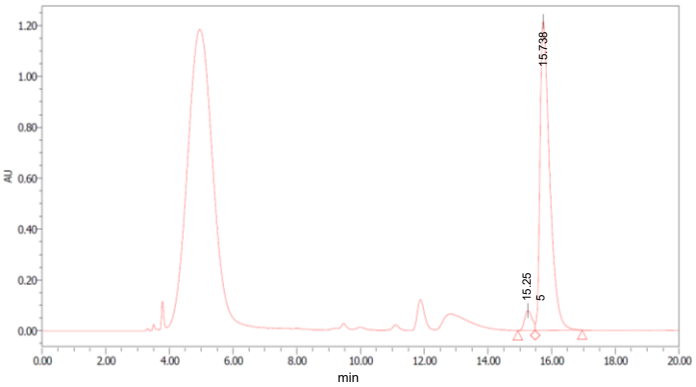

Peak No.	Ret. Time / min	area %
1	15.255	4.79
2	15.738	95.21

3-(4-Chlorophenyl)-1,3-diphenylpropan-1-one (6fa)[92]

^{1}H NMR (400 MHz, $CDCl_3$) 7.94–7.91 (m, 2H), 7.56–7.52 (m, 1H), 7.45–7.41 (m, 2H), 7.29–7.15 (m, 9H), 4.80 (t, J = 7.4 Hz, 1H), 3.72–3.66 (m, 2H); ^{13}C NMR (100 MHz, $CDCl_3$) 197.8, 143.8, 142.7, 137.0, 133.4, 132.2, 129.3, 129.2, 128.92, 128.8, 128.2, 128.0, 126.7, 45.4, 44.7.

Chiralpak ID-3 (4.6 mm x 25 cm), hexane/2-propanol = 98/2, 1.0 mL min-1, 35 °C, UV detection at 210.0 nm. The absolute configurations were not determined.

Racemate

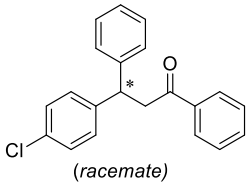

(*racemate*)

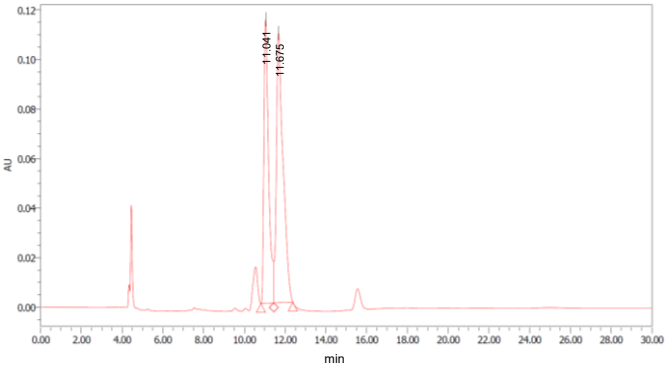

Peak No.	Ret. Time / min	area %
1	11.041	42.90
2	11.675	57.10

2aP as ligand:

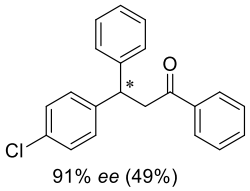

91% *ee* (49%)

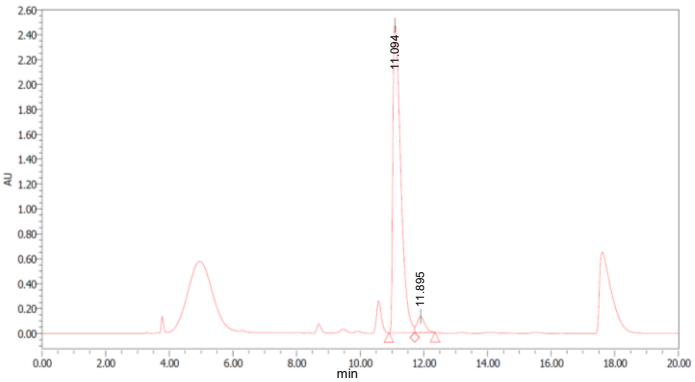

Peak No.	Ret. Time / min	area %
1	11.094	95.12
2	11.895	4.88

3-(*p*-Tolyl)cyclohexan-1-one (6ab)[93]

^{1}H NMR (400 MHz, $CDCl_3$) 7.15–7.10 (m, 4H), 3.01–2.95 (m, 1H), 2.59–2.36 (m, 4H), 2.33 (s, 3H), 2.16–2.04 (m, 2H), 1.88–1.71 (m, 2H); ^{13}C NMR (100 MHz, $CDCl_3$) 211.3, 141.4, 136.3, 129.3, 126.5, 49.1, 44.4, 41.2, 32.9, 25.6, 21.0.

Chiralpak ID-3 (4.6 mm x 25 cm), hexane/2-propanol = 98/2, 1.0 mL min-1, 35 °C, UV detection at 210.0 nm. The absolute configurations were not determined.

Racemate

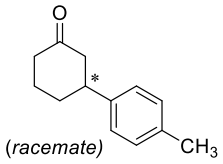

(*racemate*)

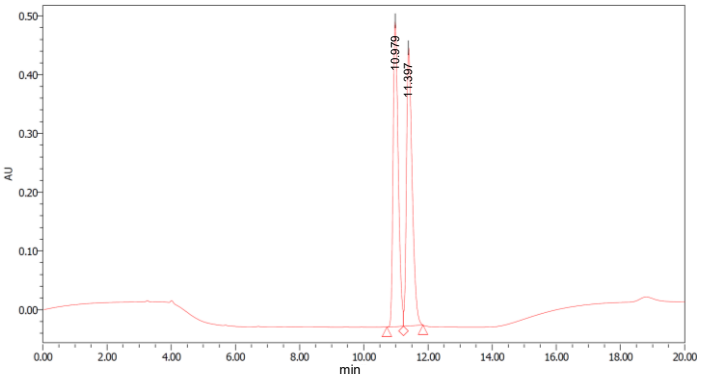

Peak No.	Ret. Time / min	area %
1	10.979	49.74
2	11.397	50.26

2aP as ligand

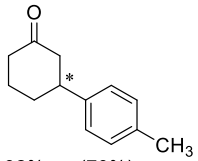

92% *ee* (70%)

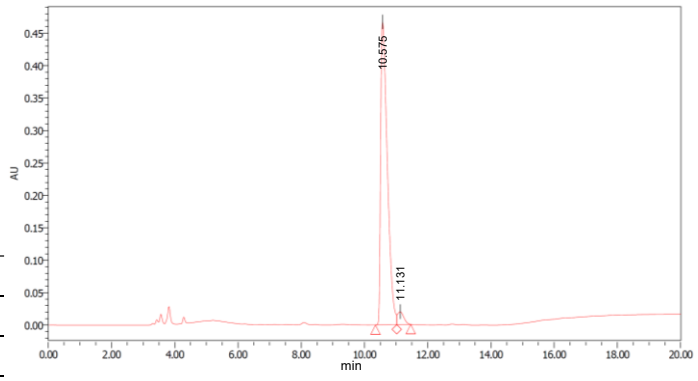

Peak No.	Ret. Time / min	area %
1	10.575	96.15
2	11.131	3.85

2bP as ligand

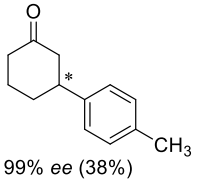

99% *ee* (38%)

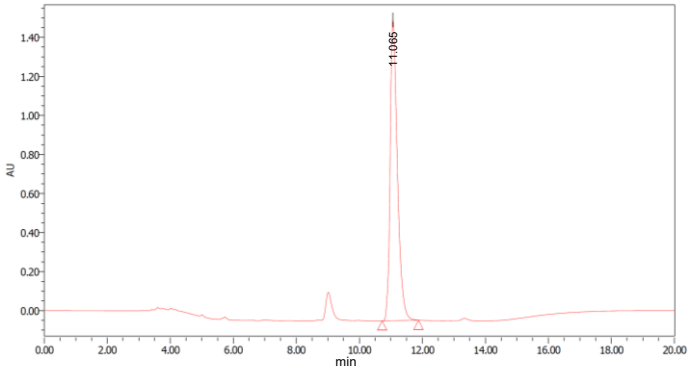

Peak No.	Ret. Time / min	area %
1	11.065	100.00
2	-	-

3-(*o*-Tolyl)cyclohexanone (6ac)[90]

^{1}H NMR (400 MHz, $CDCl_3$) 7.26–7.20 (m, 2H), 7.18–7.12 (m, 2H), 3.25–3.17 (m, 1H), 2.55–2.37 (m, 4H), 2.33 (s, 3H), 2.21–2.15 (m, 1H), 2.02–1.96 (m, 1H), 1.90–1.74 (m, 2H); ^{13}C NMR (100 MHz, $CDCl_3$): 211.51, 142.37, 135.21, 130.75, 126.52 (d, J = 4.0 Hz), 125.16, 48.44, 41.41, 40.38, 32.09, 25.91, 19.40. Chiralpak IA-3 (4.6 mm x 25 cm), hexane/2-propanol = 98/2, 1.0 mL min-1, 35 °C, UV detection at 210.0 nm. For the racemic sample, based on the reported retention time of (*R*)- and (*S*)-3-(o-tolyl)cyclohexanone,[90] t_R = 7.3 min belongs to *S*-, t_R = 8.6 min belongs to *R*-enantiomer.

Racemate

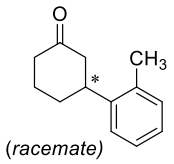

(*racemate*)

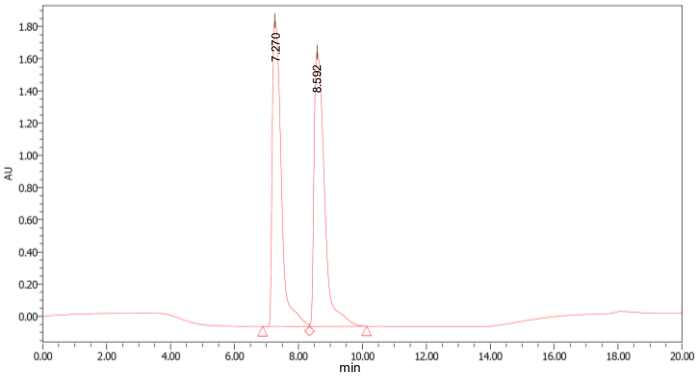

Peak No.	Ret. Time / min	area %
1(*S*)	7.270	49.09
2(*R*)	8.592	50.91

2aP as ligand

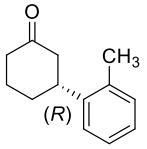

91% *ee* (91%)

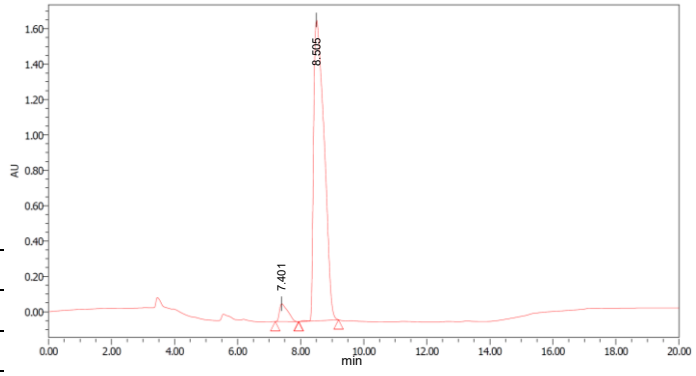

Peak No.	Ret. Time / min	area %
1(*S*)	7.401	4.48
2(*R*)	8.505	95.52

2bP as ligand

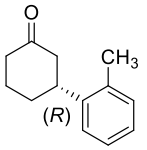

84% *ee* (33%)

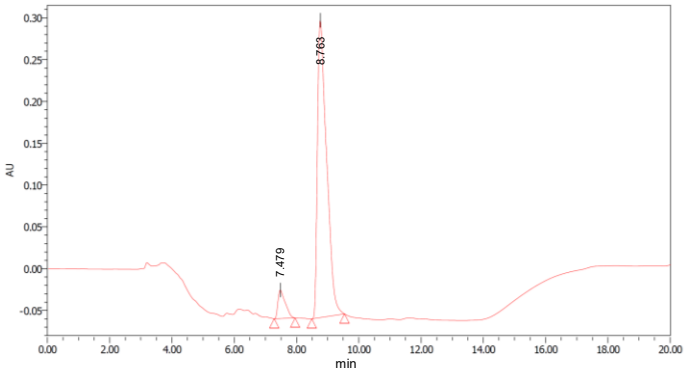

Peak No.	Ret. Time / min	area %
1(*S*)	7.479	7.09
2(*R*)	8.763	92.91

3-(3-Methoxyphenyl)cyclohexan-1-one (6ad)[90]

^{1}H NMR (400 MHz, $CDCl_3$) 7.26–7.22 (m, 2H), 6.83–6.77 (m, 2H), 3.81 (s, 3H), 3.02–2.95 (m, 1H), 2.63–2.34 (m, 4H), 2.19–2.06 (m, 2H), 1.90–1.72 (m, 1H); ^{13}C NMR (100 MHz, $CDCl_3$) 211.1, 159.8, 146.0, 129.7, 111.9, 112.7, 111.6, 55.2, 48.9, 44.8, 41.2, 32.7, 25.5.

Chiralpak ID-3 (4.6 mm x 25 cm), hexane/2-propanol = 98/2, 1.0 mL min-1, 35 °C, UV detection at 210.0 nm. The absolute configurations were not determined.

Racemate

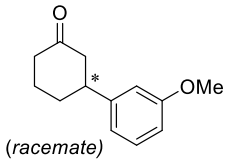

(*racemate*)

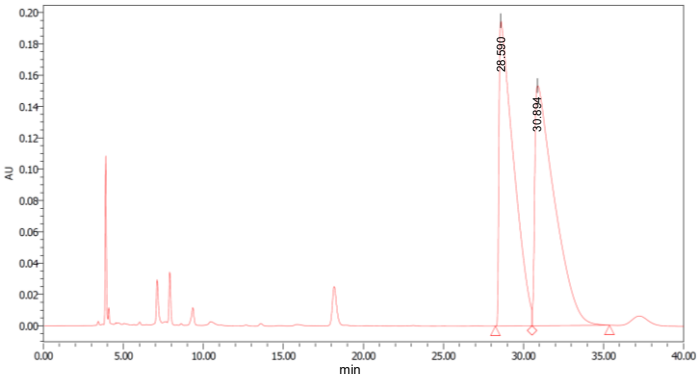

Peak No.	Ret. Time / min	area %
1	28.590	48.31
2	30.894	51.69

2aP as ligand

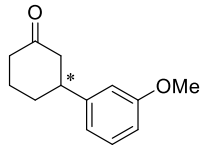

94% *ee* (56%)

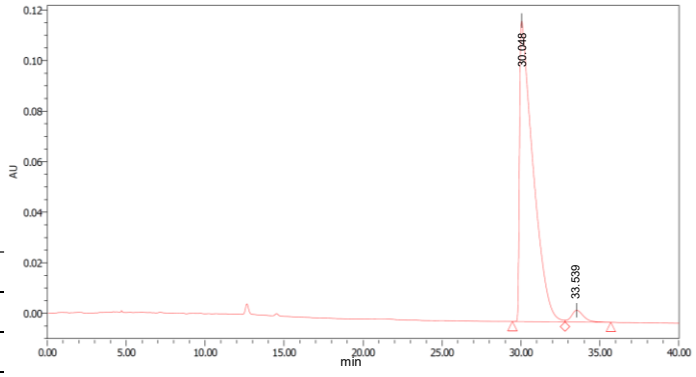

Peak No.	Ret. Time / min	area %
1	30.048	96.58
2	33.539	3.42

2bP as ligand

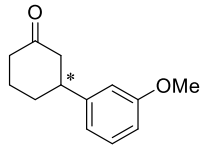

98% *ee* (61%)

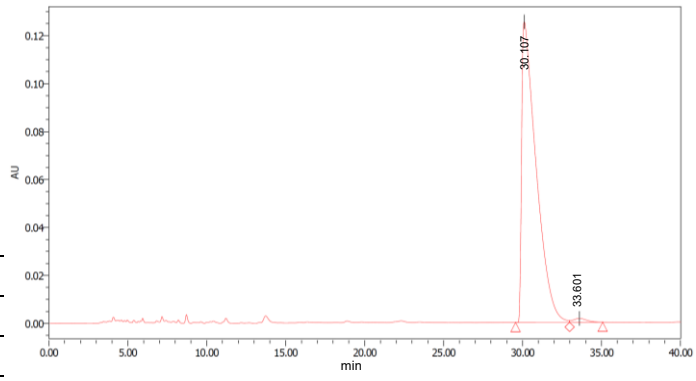

Peak No.	Ret. Time / min	area %
1	30.107	98.83
2	33.601	1.17

3-(4-Methoxyphenyl)cyclohexanone (6ae)[15]

^{1}H NMR (400 MHz, $CDCl_3$) 7.16–7.13 (m, 2H), 6.89–6.86 (m, 2H), 3.80 (s, 3H), 3.00–2.94 (m, 1H), 2.60–2.33 (m, 4H), 2.16–2.05 (m, 2H), 1.87–1.72 (m, 2H); ^{13}C NMR (100 MHz, $CDCl_3$): 211.4, 158.2, 136.6, 127.5, 114.0, 55.3, 49.3, 44.0, 41.2, 33.0, 25.5.

Chiralpak IC-3 (4.6 mm x 25 cm), hexane/2-propanol = 90/10, 1.0 mL min-1, 35 °C, UV detection at 210.0 nm. For the racemic sample, based on the reported retention time of (*R*)- and (*S*)-3-(4-methoxyphenyl)cyclohexanone,[15] t_R = 15.9 min belongs to *R*-, t_R = 17.3 min belongs to *S*-enantiomer.

Racemate

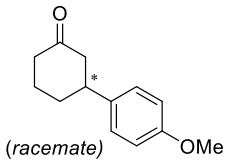

(*racemate*)

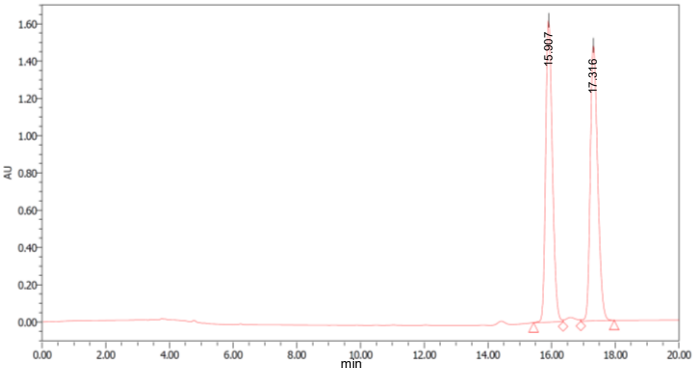

Peak No.	Ret. Time / min	area %
1(*R*)	15.907	49.81
2(*S*)	17.316	50.19

2bP as ligand

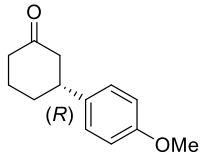

98% *ee* (34%)

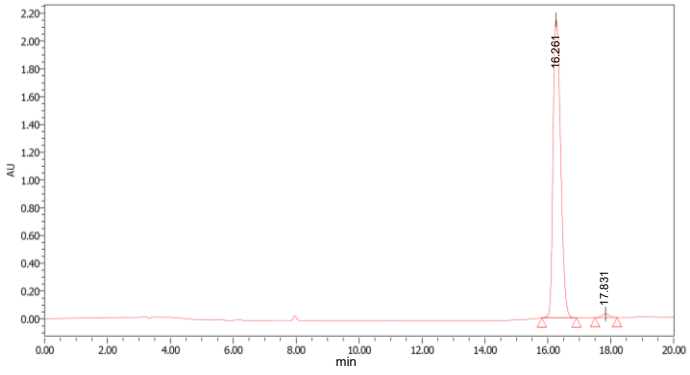

Peak No.	Ret. Time / min	area %
1(*R*)	16.261	98.88
2(*S*)	17.831	1.12

3-(4-Chlorophenyl)cyclohexanone (6af)[95]

^{1}H NMR (400 MHz, $CDCl_3$) 7.32–7.28 (m, 2H), 7.17–7.15 (m, 2H), 3.03–2.96 (m, 1H), 2.60–2.34 (m, 4H), 2.19–2.05 (m, 2H), 1.88–1.75 (m, 2H); ^{13}C NMR (100 MHz, $CDCl_3$) 210.7, 142.7, 132.3, 128.8, 127.9, 48.8, 44.1, 41.1, 32.7, 25.4.

Chiralpak IB N-3 (4.6 mm x 25 cm), hexane/2-propanol = 98/2, 1.0 mL min^{-1}, 35 °C, UV detection at 210.0 nm. The absolute configurations were not determined.

Racemate

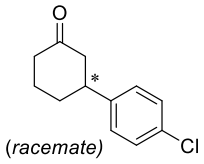

(*racemate*)

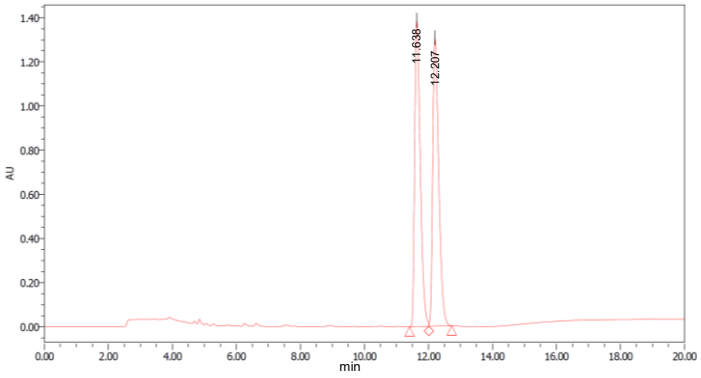

Peak No.	Ret. Time / min	area %
1	11.638	49.89
2	12.207	50.11

2aP as ligand

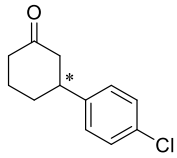

87% *ee* (24%)

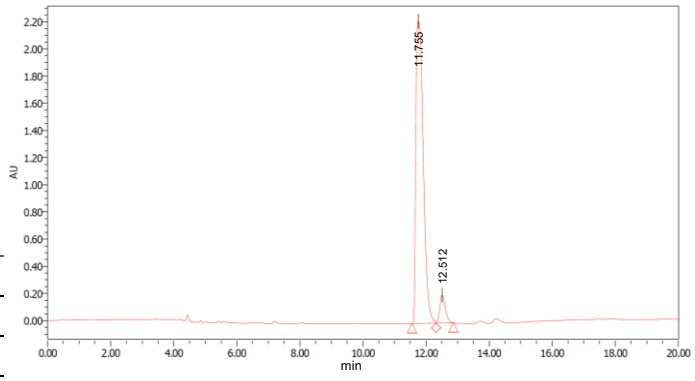

Peak No.	Ret. Time / min	area %
1	11.755	93.42
2	12.512	6.58

2bP as ligand

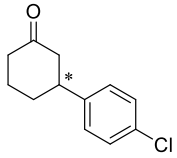

96% *ee* (38%)

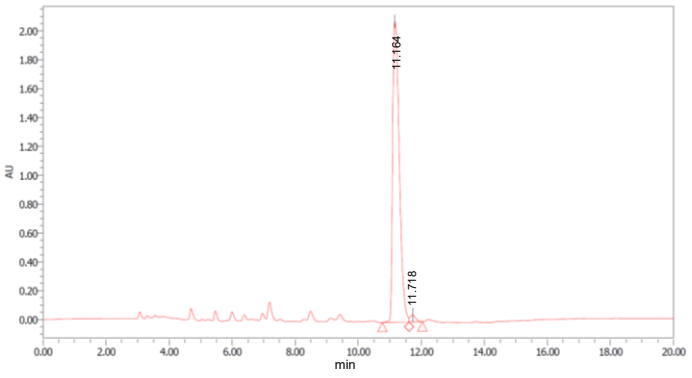

Peak No.	Ret. Time / min	area %
1	11.164	98.08
2	11.718	1.92

3-(4-(Trifluoromethyl)phenyl)cyclohexan-1-one (6ag)[89]

^{1}H NMR (400 MHz, $CDCl_3$) 7.60 (d, J = 8.4 Hz, 2 H), 7.34 (d, J = 8.0 Hz, 2 H), 3.09 (tt, J = 13.8, 4.0 Hz, 1 H), 2.63–2.33 (m, 4 H), 2.21–2.14 (m, 1 H), 2.12–2.08 (m, 1 H), 1.92–1.75 (m, 2 H); ^{13}C NMR (100 MHz, $CDCl_3$) 210.4, 148.3, 127.08, 125.8 (q, J = 3.9 Hz), 48.6, 44.6, 41.2, 32.6, 25.5.

Chiralpak ID-3 (4.6 mm x 25 cm), hexane/2-propanol = 98/2, 1.0 mL min-1, 35 °C, UV detection at 210.0 nm. For the racemic sample, based on the reported retention time of (*R*)- and (*S*)-3-(4-(trifluoromethyl)phenyl)cyclohexan-1-one,[89] t_R = 9.0 min belongs to *S*-, t_R = 11.0 min belongs to *R*-enantiomer.

Racemate

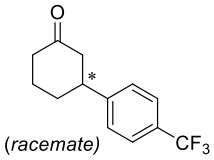

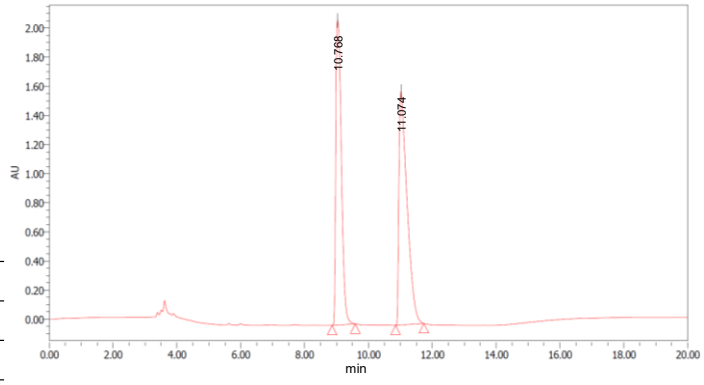

Peak No.	Ret. Time / min	area %
1(*R*)	9.034	47.29
2(*S*)	11.015	52.71

2aP as ligand

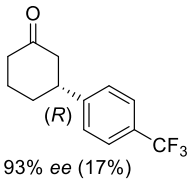

93% *ee* (17%)

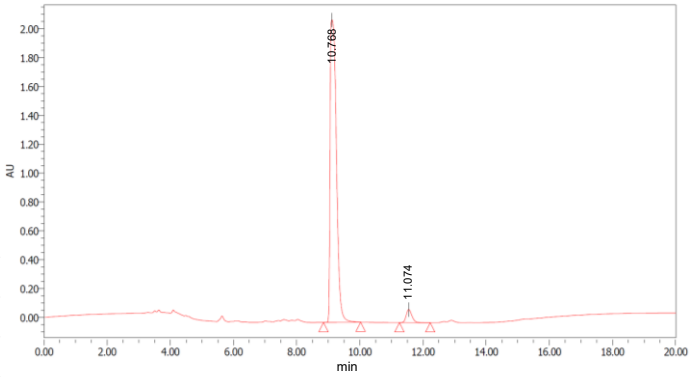

Peak No.	Ret. Time / min	area %
1(*R*)	9.115	96.17
2(*S*)	11.550	3.83

2bP as ligand

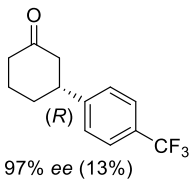

97% *ee* (13%)

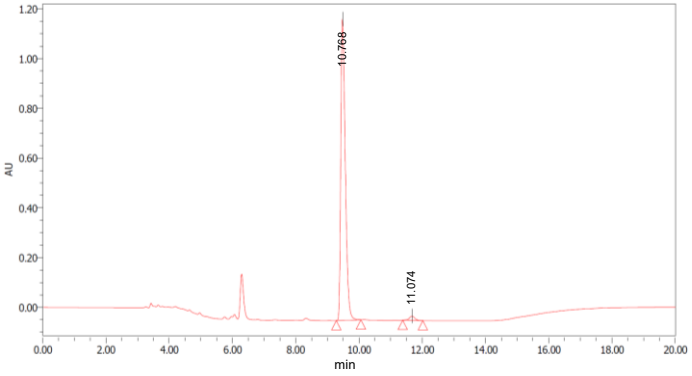

Peak No.	Ret. Time / min	area %
1(*R*)	9.478	98.22
2(*S*)	11.675	1.78

3-(Naphthalen-1-yl)cyclohexan-1-one (6ah)[90]

^{1}H NMR (400 MHz, $CDCl_3$) 8.04 (d, *J* = 8.4 Hz, 1H), 7.88 (d, *J* = 8.0 Hz, 1H), 7.76 (d, *J* = 8.0 Hz, 1H), 7.56–7.45 (m, 3H), 7.40 (d, *J* = 7.2 Hz, 1H) 3.86 (t, *J* = 11.2 Hz, 1H), 2.79–2.44 (m, 4H), 2.27–2.19 (m, 2H), 2.05–1.91 (m, 2H); ^{13}C NMR (100 MHz, $CDCl_3$) 211.4, 140.2, 134.1, 131.0, 129.2, 127.4, 126.4, 125.8, 125.7, 122.8, 122.6, 48.7, 41.6, 39.5, 32.4, 25.7.

Chiralpak ID-3 (4.6 mm x 25 cm), hexane/2-propanol = 98/2, 1.0 mL min-1, 35 °C, UV detection at 210.0 nm. The absolute configurations were not determined.

Racemate

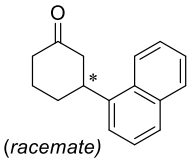

(*racemate*)

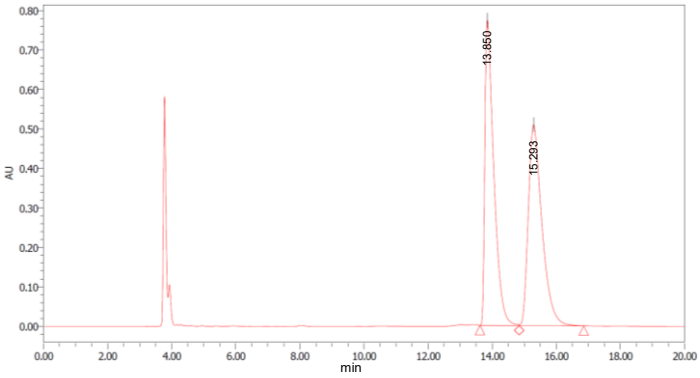

Peak No.	Ret. Time / min	area %
1	13.850	49.96
2	15.293	50.04

2aP as ligand

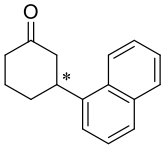

96% *ee* (76%)

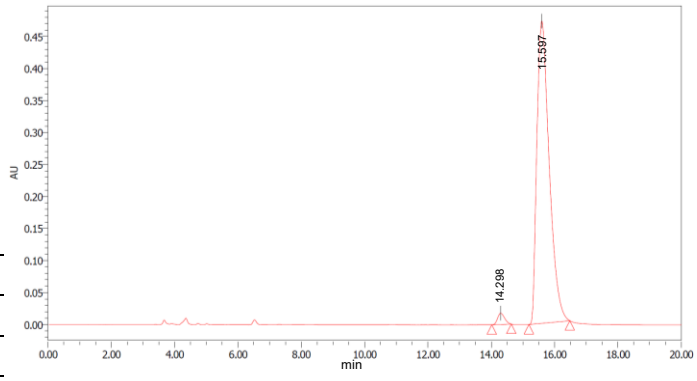

Peak No.	Ret. Time / min	area %
1	14.298	2.06
2	15.597	97.94

2bP as ligand

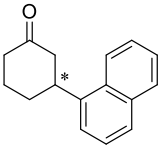

86% *ee* (26%)

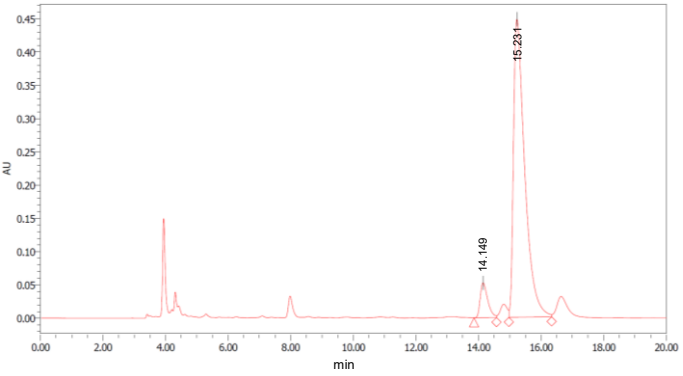

Peak No.	Ret. Time / min	area %
1	14.149	7.22
2	15.231	92.78

3-(2-Naphthyl)cyclohexan-1-one (6ai)[97]

^{1}H NMR (400 MHz, $CDCl_3$) 7.81 (t, J = 7.4 Hz, 1H), 7.65 (s, 1H), 7.50–7.43 (m, 2H), 7.38 (dd, J = 8.4, 2.0 Hz, 1H), 3.23–3.15 (m, 1H), 2.71–2.61 (m, 2H), 2.54–2.39 (m, 2H), 2.22–2.15 (m, 2H), 2.05–1.92 (m, 1H), 1.89–1.81 (m, 1H); ^{13}C NMR (100 MHz, $CDCl_3$) 211.1, 141.7, 133.5, 132.3, 128.3, 127.7, 127.6, 126.2, 125.6, 125.3, 124.7, 48.8, 44.8, 41.2, 32.6, 25.5.

Chiralpak IH-3 (4.6 mm x 25 cm), hexane/2-propanol = 98/2, 1.0 mL min-1, 35 °C, UV detection at 210.0 nm. For the racemic sample, based on the reported retention time of (*R*)- and (*S*)-3-(2-naphthyl)cyclohexan-1-one,[97] t_R = 19.7 min belongs to *S*-, t_R = 21.8 min belongs to *R*-enantiomer.

Racemate

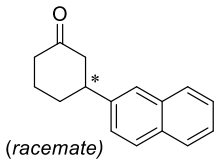

(*racemate*)

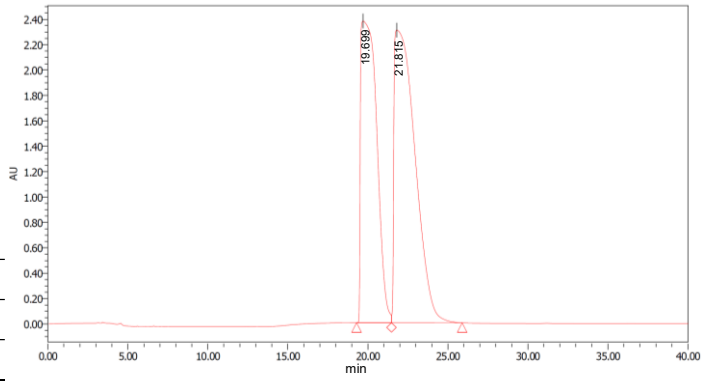

Peak No.	Ret. Time / min	area %
1(*S*)	19.699	44.20
2(*R*)	21.815	55.80

2aP as ligand

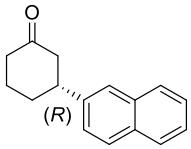

92% *ee* (33%)

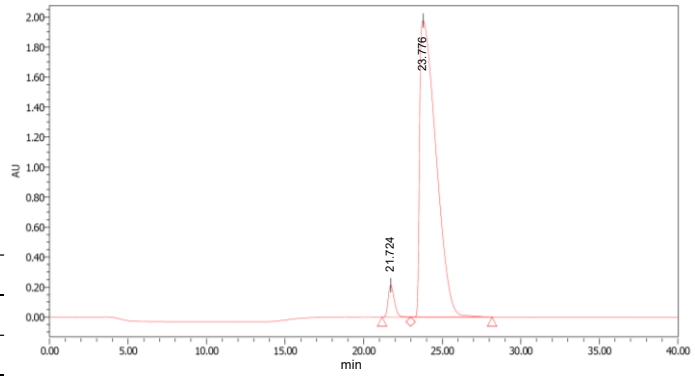

Peak No.	Ret. Time / min	area %
1(*S*)	21.724	3.87
2(*R*)	23.776	96.13

2bP as ligand

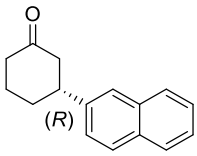

89% *ee* (10%)

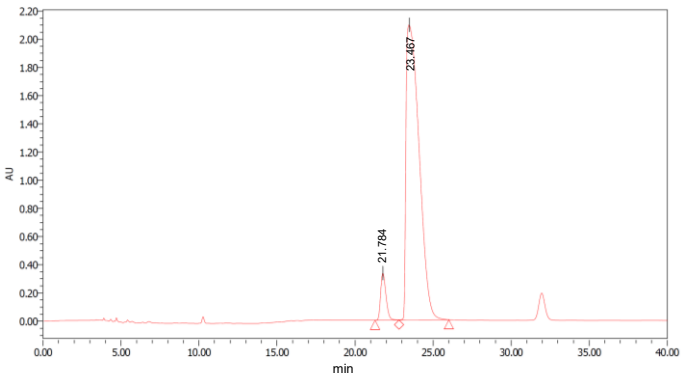

Peak No.	Ret. Time / min	area %
1(*S*)	21.784	6.08
2(*R*)	23.467	93.92

1-(*tert*-Butyloxycarbonyl)-4-(4-fluorophenyl)-2-piperidone (8)[98]

^{1}H NMR (400 MHz, $CDCl_3$) 7.16 (dd, J = 8.8, 5.2 Hz, 2H), 7.03 (t, J=8.8 Hz, 2H), 3.88 (dt, J = 12.4, 4.6 Hz, 1H), 3.61 (ddd, J =13.0, 10.2, 3.2 Hz, 1H), 3.15–3.08 (m, 1H), 2.83 (ddd, J = 17.2, 5.4, 2.2 Hz, 1H), 2.59 (dd, J =17.4, 11.4 Hz, 1H), 2.20–2.15 (m, 1H), 1.98–1.88 (m, 1H), 1.55 (s, 9H); ^{13}C NMR (100 MHz, $CDCl_3$) 170.3, 161.7 (d, $^{1}J_{CF}$ =246.3 Hz), 152.6, 138.8 (d, $^{4}J_{CF}$ = 2.9 Hz), 127.9 (d, $^{3}J_{CF}$ = 8.2 Hz), 115.7 (d, $^{2}J_{CF}$ = 21.6 Hz), 83.2, 45.6, 42.3, 37.8, 30.4, 28.0.

Chiralpak IC-3 (4.6 mm x 25 cm), hexane/2-propanol = 90/10, 1.0 mL min^{-1}, 35 °C, UV detection at 210.0 nm.

Racemate

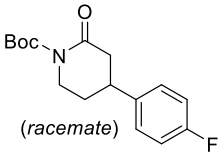

(*racemate*)

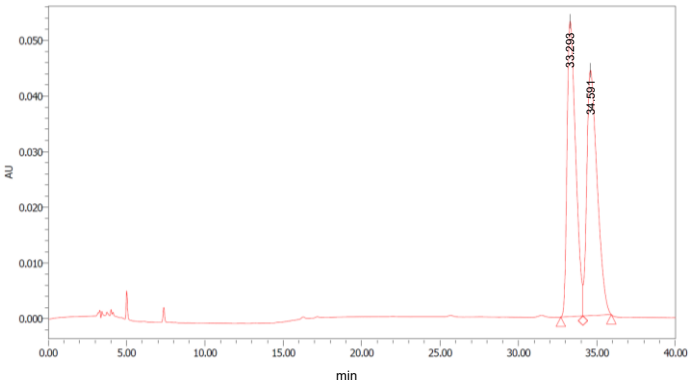

Peak No.	Ret. Time / min	area %
1	33.293	49.83
2	34.591	50.17

2aP as ligand

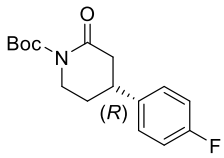

91% *ee* (45%)

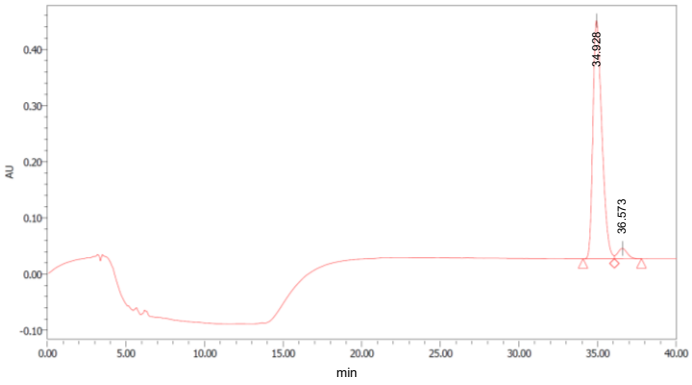

Peak No.	Ret. Time / min	area %
1	34.928	95.68
2	36.573	4.32

(*R*)-4-(4-fluorophenyl)piperidin-2-one (9)[99]

^{1}H NMR (400 MHz, $CDCl_3$) 7.21–7.16 (m, 2H), 7.07–7.00 (m, 2H), 6.27 (s, 1H), 3.43–3.40 (m, 2H), 3.14–3.06 (m, 1H), 2.71–2.65 (m, 1H), 2.49–2.42 (m, 1H), 2.09–2.06 (m, 1H), 1.96–1.73 (m, 1H); ^{13}C NMR (100 MHz, $CDCl_3$) 171.8, 161.7 (d, $^{1}J_{CF}$ =245.9 Hz), 139.2 (d, $^{4}J_{CF}$ = 3.3 Hz), 128.1 (d, $^{3}J_{CF}$ = 7.6 Hz), 115.7 (d, $^{2}J_{CF}$ = 21.1 Hz), 41.4, 39.0, 37.8, 29.7.

Chiralpak IG-3 (4.6 mm x 25 cm), hexane/ethanol = 90/10, 1.2 mL min^{-1}, 40 °C, UV detection at 210.0 nm.

Racemate

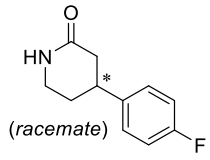

Peak No.	Ret. Time / min	area %
1(*R*)	26.557	50.05
2(*S*)	34.101	49.95

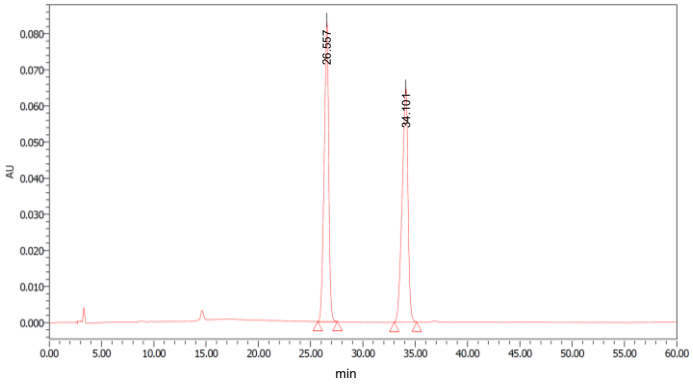

2aP as ligand

Before recrystallization

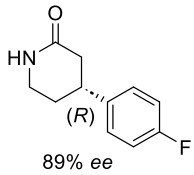

Peak No.	Ret. Time / min	area %
1(*R*)	26.110	94.37
2(*S*)	33.167	5.63

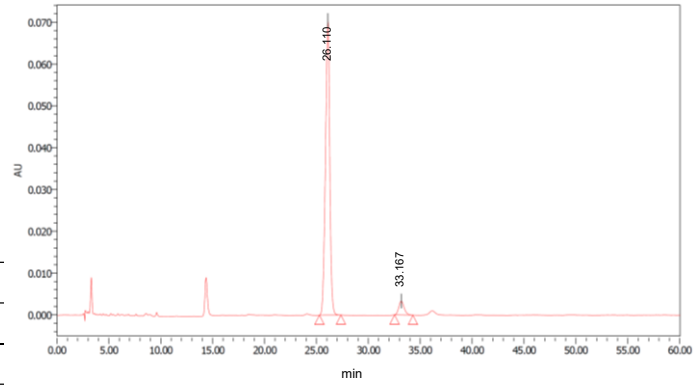

After recrystallization

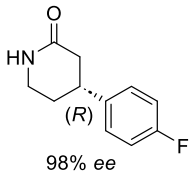

Peak No.	Ret. Time / min	area %
1(*R*)	26.728	98.20
2(*S*)	34.183	1.80

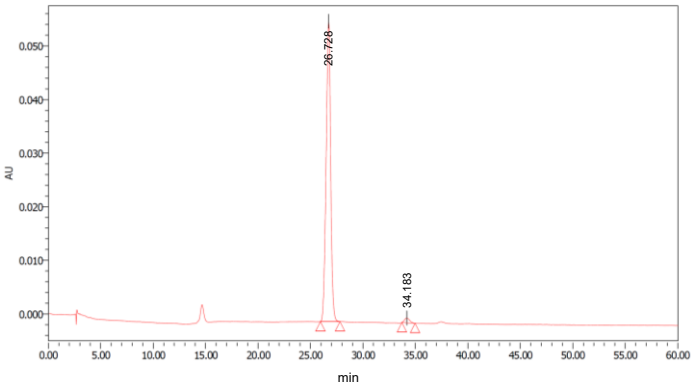

HOMO energy level and percentage of buried volume (%V_{Bur})

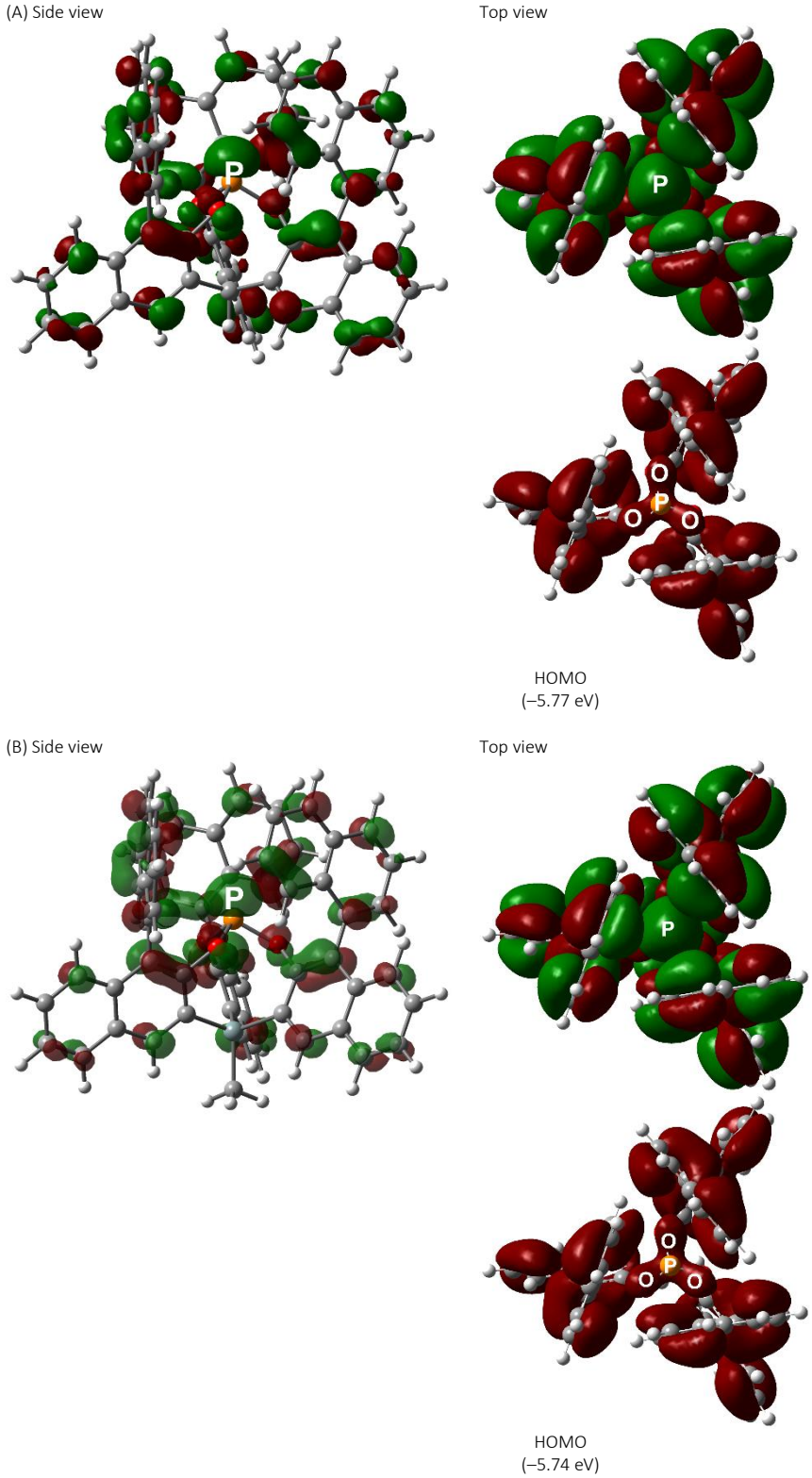

Figure S11. Unoccupied MOs concerning the Lewis acidity of (A) **2a**P and (B) **2b**P calculated at the B3PW91/6-311+G**//CAM-B3LYP-D3(BJ)/def2-SVP level. In the top view, extracted negative iso-surfaces are depicted to clarify the spatial interaction between the O and P atoms.

(A)

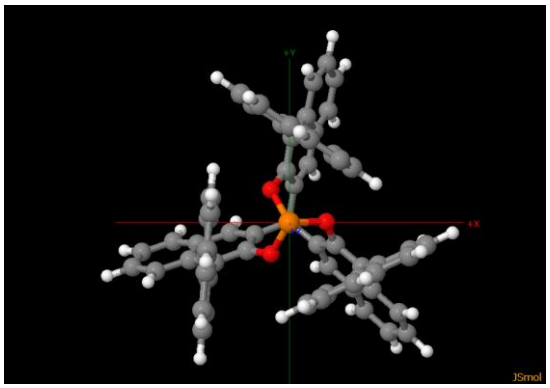

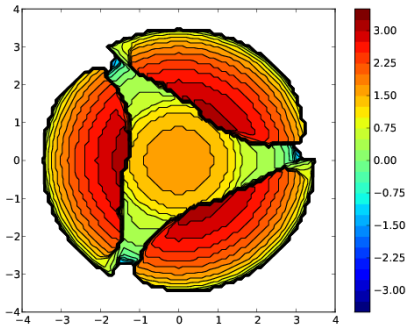

(B)

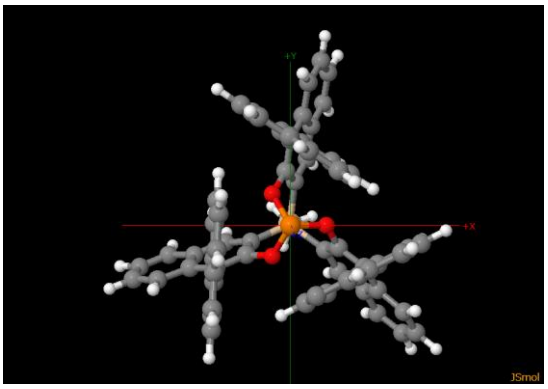

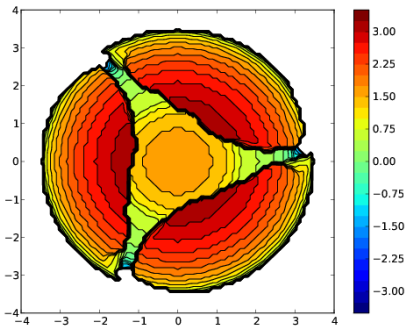

Figure S12. Percentage of buried volume (%V_{Bur}(3.5 Å))[88] of (A) **2a**P and **2b**P calculated by a SambVca 2.1 web server.[67] The DFT-optimized geometries were applied to the estimation.

Cartesian coordinates for optimized geometries

Table S13. Optimized geometry for **2a**P optimized at the CAM-B3LYP-D3(BJ)/def2-SVP level.

Atom	X	Y	Z
P	0.00000000	0.00000000	0.70131301
O	-0.75854074	1.23479329	-0.12380207
O	-0.69009199	-1.27431220	-0.12380207
C	-0.18829973	2.02464234	-1.08329561
O	1.44863273	0.03951890	-0.12380207
C	-1.65924183	-1.17539352	-1.08329561
C	0.00000000	3.35398517	-0.76549197
C	0.18235475	1.47272068	-2.33846747
C	1.84754157	-0.84924882	-1.08329561
C	-2.90463637	-1.67699258	-0.76549197
C	-1.36659089	-0.57843649	-2.33846747
C	0.56988573	4.23077192	-1.73310493
C	-0.38869841	3.79984273	0.60262847
C	0.00000000	0.00000000	-2.70202367
C	0.72887051	2.32574904	-3.26691299
C	2.90463637	-1.67699258	-0.76549197
C	1.18423615	-0.89428419	-2.33846747
C	-3.94889882	-1.62185044	-1.73310493
C	-3.09641112	-2.23654406	0.60262847
C	-2.37859301	-0.53165414	-3.26691299
C	0.93612546	3.70218377	-3.00341652
C	0.80963584	5.60697983	-1.47189749
C	-1.53649553	4.53031202	0.80179085
C	0.38120165	3.37208521	1.73221982
H	0.00000000	0.00000000	-3.79797162
H	1.02269539	1.93604240	-4.24501515
C	3.37901309	-2.60892147	-1.73310493
C	3.48510953	-1.56329866	0.60262847
C	1.64972249	-1.79409490	-3.26691299
C	-3.67424792	-1.04038345	-3.00341652
C	-5.26060491	-2.10232471	-1.47189749
C	-3.15511753	-3.59580017	0.80179085
C	-3.11091228	-1.35591229	1.73221982
H	-2.18800960	-0.08234101	-4.24501515
C	1.50881586	4.56718649	-3.97307645
C	1.36862402	6.41524087	-2.42847933
C	-3.08364738	0.05798825	1.59207878
C	-3.11312032	-1.90980999	3.04346152
C	1.71952815	5.89281899	-3.69590011
H	1.78305320	4.15333586	-4.94632721
H	1.54787990	7.47025610	-2.21130472
C	-1.28960147	4.40673373	3.20069374
H	-2.89967067	5.43032845	2.23145425
C	2.26164372	2.16239602	2.68980503
H	1.98133110	2.44163579	0.59440302
C	0.62358793	3.15085597	4.16015782
C	3.20089159	-3.59026611	-3.97307645
C	4.87144958	-4.39288362	-2.42847933
H	4.93372691	-3.47622936	-0.49460335
C	5.19130187	-0.70616916	2.10559256
H	5.25722230	-0.58055125	-0.06257274
C	1.49160440	-2.69951109	1.59207878
C	3.21050413	-1.74113628	3.04346152
C	-5.96309500	-1.45725444	-3.69590011
H	-4.48842097	-0.53249856	-4.94632721
H	-7.24337152	-2.39462474	-2.21130472
C	-3.17154262	-3.32019450	3.20069374
H	-3.25296707	-5.22635270	2.23145425
C	-3.00351174	0.87744290	2.68980503
H	-3.10518417	0.49506517	0.59440302
C	-3.04051528	-1.03538500	4.16015782
H	2.16244742	6.54801060	-4.44863133
H	-1.64408292	4.62597821	4.21063787
C	1.76680414	2.41257504	3.98988553
H	3.17138522	1.57371519	2.55673206
H	0.24228686	3.35896968	5.16276472
C	4.24356687	-4.43556455	-3.69590011
H	2.70536776	-3.62083730	-4.94632721
H	5.69549160	-5.07563138	-2.21130472
C	4.46114409	-1.08653922	3.20069374
H	6.15263772	-0.20397577	2.23145425
C	0.74186803	-3.03983892	2.68980503

H	0.54363948	6.01084753	-0.49460335
C	-1.98409050	4.84888388	2.10559256
H	-2.12583902	4.84316369	-0.06257274
C	1.59204299	2.64152285	1.59207878
C	-0.09738381	3.65094628	3.04346152
C	2.73812246	-2.66180031	-3.00341652
C	4.45096906	-3.50465513	-1.47189749
C	4.69161306	-0.93451184	0.80179085
C	2.72971063	-2.01617292	1.73221982
H	1.16531421	-1.85370139	-4.24501515
C	-4.70970745	-0.97692038	-3.97307645
C	-6.24007357	-2.02235728	-2.42847933
H	-5.47736638	-2.53461816	-0.49460335
C	-3.20721137	-4.14271472	2.10559256
H	-3.13138328	-4.26261244	-0.06257274
H	1.12385307	-2.93670096	0.59440302
C	2.41692735	-2.11547098	4.16015782
H	-6.75196720	-1.40127091	-4.44863133
H	-3.18417319	-3.73680669	4.21063787
C	-2.97275335	0.32380975	3.98988553
H	-2.94856994	1.95964257	2.55673206
H	-3.03009650	-1.46965826	5.16276472
H	2.30081352	2.01818086	4.85672454
H	4.58951982	-5.14673970	-4.44863133
H	4.82825611	-0.88917153	4.21063787
C	1.20594921	-2.73638479	3.98988553
H	-0.22281528	-3.53335776	2.55673206
H	2.78780964	-1.88931142	5.16276472
H	-2.89820266	0.98347253	4.85672454
H	0.59738914	-3.00165340	4.85672454

Table S14. Optimized geometry for **2b**P optimized at the CAM-B3LYP-D3(BJ)/def2-SVP level.

Atom	X	Y	Z
P	0.00000000	0.00000000	0.57857283
O	-0.85693223	1.17673539	-0.23862108
O	1.44754886	0.15375738	-0.23862108
C	-0.39692788	2.14772796	-1.09046634
O	-0.59061663	-1.33049277	-0.23862108
C	2.05845091	-0.73011435	-1.09046634
C	-0.37536772	3.44512943	-0.62223645
C	-0.00000000	1.78906030	-2.40730800
C	-1.66152304	-1.41761361	-1.09046634
C	3.17125346	-1.39748673	-0.62223645
C	1.54937167	-0.89453015	-2.40730800
C	0.05580313	4.48918854	-1.49526972
C	-0.79226533	3.71112104	0.78311030
Si	0.00000000	0.00000000	-3.00947172
C	0.40463859	2.80631448	-3.24301707
C	-2.79588574	-2.04764270	-0.62223645
C	-1.54937167	-0.89453015	-2.40730800
C	3.85984975	-2.29292120	-1.49526972
C	3.61005776	-1.16943862	0.78311030
C	2.22802033	-1.75358454	-3.24301707
C	0.44431476	4.16072897	-2.82490471
C	0.13286867	5.84692028	-1.08213787
C	-2.00155193	4.30930458	1.05307628
C	0.04119043	3.28608061	1.86648873
C	0.00000000	0.00000000	-4.88512529
H	0.71538616	2.58720913	-4.26746108
C	-3.91565289	-2.19626734	-1.49526972
C	-2.81779243	-2.54168242	0.78311030
C	-2.63265893	-1.05272994	-3.24301707
C	3.38113960	-2.46515235	-2.82490471
C	4.99714714	-3.03852777	-1.08213787
C	4.73274320	-0.42125747	1.05307628
C	2.82523407	-1.67871226	1.86648873
H	1.88289575	-1.91314715	-4.26746108
C	0.87355548	5.19449710	-3.69817786
C	0.55657251	6.82220882	-1.94875699
H	-0.14742147	6.10350552	-0.06039016
C	-2.44392921	4.49886415	2.38306130
H	-2.63628182	4.62574957	0.22288662
C	1.31725611	2.69777076	1.65530270
C	-0.42868954	3.43134412	3.20274492
H	-0.81231752	0.62789730	-5.27955224
H	-0.13761625	-1.01743625	-5.27955224
H	0.94993377	0.38953896	-5.27955224
C	-3.82545436	-1.69557662	-2.82490471
C	-5.13001581	-2.80839248	-1.08213787
C	-2.73119127	-3.88804711	1.05307628
C	-2.86642449	-1.60736834	1.86648873
H	-2.59828191	-0.67406198	-4.26746108
C	4.06178871	-3.35376979	-3.69817786
C	5.11809525	-0.13292729	2.38306130
H	5.32415756	-0.02978776	0.22288662
C	1.67770995	-2.48966263	1.65530270
C	5.62991987	-3.89311034	-1.94875699
H	5.35950157	-2.92408201	-0.06039016
C	3.18597595	-1.34441603	3.20274492
C	0.92766991	6.49682016	-3.27452069
H	1.16489620	4.92943548	-4.71736887
H	0.61156163	7.85970336	-1.61249533
C	-1.68120013	4.05898906	3.43312855
H	-3.40712291	4.97989053	2.56487001
C	2.06049692	2.22428617	2.70606829
H	1.70158024	2.60665837	0.63974543
C	0.36582362	2.93401871	4.26975181
C	-4.93534419	-1.84072732	-3.69817786
C	-6.18649242	-2.92909847	-1.94875699
H	-5.21208007	-3.17942349	-0.06039016
C	-2.67416603	-4.36593686	2.38306130
H	-2.68787573	-4.59596182	0.22288662
C	-2.99496606	-0.20810813	1.65530270
C	-2.75728641	-2.08692809	3.20274492
C	5.16257633	-4.05179577	-3.27452069
H	3.68656825	-3.47354744	-4.71736887
H	6.50092192	-4.45947958	-1.61249533
C	4.35578770	-0.57353251	3.43312855
H	6.01627314	0.46070973	2.56487001
C	0.89603988	-2.89658577	2.70606829
H	1.40664224	-2.77694090	0.63974543
C	2.35802292	-1.78382190	4.26975181
H	1.26107629	7.28382675	-3.95379913
H	-2.02772004	4.18007305	4.46222486
C	1.57405378	2.33219804	4.02852786
H	3.02346030	1.74778197	2.51897595
H	-0.01016136	3.03448445	5.29075523
C	-6.09024624	-2.44502436	-3.27452069
H	-4.85146445	-1.45588804	-4.71736887
H	-7.11248355	-3.40022376	-1.61249533
C	-2.67458758	-3.48545655	3.43312855
H	-2.60915025	-5.44060026	2.56487001
C	-2.95653679	0.67229959	2.70606829
H	-3.10822249	0.17028253	0.63974543
C	-2.72384654	-1.15019680	4.26975181
H	5.67744084	-4.73403747	-3.95379913
H	4.63390947	-0.33397946	4.46222486
C	1.23271585	-2.52926958	4.02852786
H	0.00189344	-3.49228442	2.51897595
H	2.63302130	-1.50844223	5.29075523
H	2.16780013	1.93738459	4.85537482
H	-6.93851711	-2.54978925	-3.95379913
H	-2.60618943	-3.84609358	4.46222486
C	-2.80676964	0.19707155	4.02852786
H	-3.02535374	1.74450244	2.51897595
H	-2.62285994	-1.52604222	5.29075523
H	0.59392421	-2.84606228	4.85537482
H	-2.76172434	0.90867769	4.85537482

1-5. Reference

[1] A. Boerner, Ed. , *Phosphorus Ligands in Asymmetric Catalysis: Synthesis and Applications*, Wiley-VCH, Weinheim, **2008**.

[2] J. K. Whitesell, *Chem. Rev.* **1989**, *89*, 1581–1590.

[3] C. Moberg, *Isr. J. Chem.* **2012**, *52*, 653–662.

[4] C. Moberg, *Bull. Chem. Soc. Jpn.* **2021**, *94*, 558–564.

[5] A. Pfaltz, W. J. Drury, *Proc. Natl. Acad. Sci* **2004**, *101*, 5723–5726.

[6] P. J. Pye, K. Rossen, R. A. Reamer, N. N. Tsou, R. P. Volante, P. J. Reider, *J. Am. Chem. Soc.* **1997**, *119*, 6207–6208.

[7] M. J. Burk, J. E. Feaster, W. A. Nugent, R. L. Harlow, *J. Am. Chem. Soc.* **1993**, *115*, 10125–10138.

[8] T. Hayashi, K. Ueyama, N. Tokunaga, K. Yoshida, *J. Am. Chem. Soc.* **2003**, *125*, 11508–11509.

[9] H. Nishiyama, H. Sakaguchi, T. Nakamura, M. Horihata, M. Kondo, K. Itoh, *Organometallics* **1989**, *8*, 846–848.

[10] G. Desimoni, G. Faita, K. A. Jørgensen, *Chem. Rev.* **2006**, *106*, 3561–3651.

[11] R. Rasappan, D. Laventine, O. Reiser, *Coord. Chem. Rev.* **2008**, *252*, 702–714.

[12] W. Tang, X. Zhang, *Chem. Rev.* **2003**, *103*, 3029–3070.

[13] R. Shintani, Y. Ichikawa, K. Takatsu, F.-X. Chen, T. Hayashi, *J. Org. Chem.* **2009**, *74*, 869–873.

[14] S. Anezaki, Y. Yamaguchi, M. Asami, *Chem. Lett.* **2010**, *39*, 398–399.

[15] X. Liu, L. Lin, X. Feng, *Acc. Chem. Res.* **2011**, *44*, 574–587.

[16] D. A. Evans, C. S. Burgey, M. C. Kozlowski, S. W. Tregay, *J. Am. Chem. Soc.* **1999**, *121*, 686–699.

[17] J.-X. Gao, T. Ikariya, R. Noyori, *Organometallics* **1996**, *15*, 1087–1089.

[18] T. P. Yoon, E. N. Jacobsen, *Science (80-.).* **2003**, *299*, 1691–1693.

[19] G. Yang, W. Zhang, *Chem. Soc. Rev.* **2018**, *47*, 1783–1810.

[20] Y. Nie, Q. Yuan, W. Zhang, *Chem. Rec.* **2023**, e202300133.

[21] F. Yang, J.-H. Xie, Q.-L. Zhou, *Acc. Chem. Res.* **2023**, *56*, 332–349.

[22] C. Moberg, *Angew. Chem. Int. Ed.* **1998**, *37*, 248–268.

[23] S. E. Gibson, M. P. Castaldi, *Chem. Commun.* **2006**, 3045.

[24] S. E. Gibson, M. P. Castaldi, *Angew. Chem. Int. Ed.* **2006**, *45*, 4718–4720.

[25] C. Moberg, *Angew. Chem. Int. Ed.* **2006**, *45*, 4721–4723.

[26] G. Bringmann, R.-M. Pfeifer, C. Rummey, K. Hartner, M. Breuning, *J. Org. Chem.* **2003**, *68*, 6859–6863.

[27] K. Murai, S. Fukushima, A. Nakamura, M. Shimura, H. Fujioka, *Tetrahedron* **2011**, *67*, 4862–4868.

[28] S. Bellemin-Laponnaz, L. H. Gade, *Angew. Chem. Int. Ed.* **2002**, *41*, 3473–3475.

[29] J. N. Moorthy, S. Saha, *Eur. J. Org. Chem.* **2010**, *2010*, 6359–6365.

[30] J. Chin, C. Walsdorff, B. Stranix, J. Oh, H. J. Chung, S. Park, K. Kim, *Angew. Chem. Int. Ed.* **1999**, *38*, 2756–2759.

[31] S.-G. Kim, K.-H. Kim, Y. K. Kim, S. K. Shin, K. H. Ahn, *J. Am. Chem. Soc.* **2003**, *125*, 13819–13824.

[32] J. van Gestel, A. R. A. Palmans, B. Titulaer, J. A. J. M. Vekemans, E. W. Meijer, *J. Am. Chem. Soc.* **2005**, *127*, 5490–5494.

[33] M. L. Bushey, T.-Q. Nguyen, W. Zhang, D. Horoszewski, C. Nuckolls, *Angew. Chem. Int. Ed.* **2004**, *43*, 5446–5453.

[34] T. Kubo, S. Miyazaki, T. Kodama, M. Aoba, Y. Hirao, H. Kurata, *Chem. Commun.* **2015**, *51*, 3801–3803.

[35] A. Ochida, K. Hara, H. Ito, M. Sawamura, *Org. Lett.* **2003**, *5*, 2671–2674.

[36] A. Ochida, S. Ito, T. Miyahara, H. Ito, M. Sawamura, *Chem. Lett.* **2006**, *35*, 294–295.

[37] S. Konishi, T. Iwai, M. Sawamura, *Organometallics* **2018**, *37*, 1876–1883.

[38] M. F. Cain, D. S. Glueck, J. A. Golen, A. L. Rheingold, *Organometallics* **2012**, *31*, 775–778.

[39] X. F. Wu, C. Min, E. Nyamzundui, H. B. Zhou, C. Dong, *Tetrahedron Asymmetry* **2011**, *22*, 1640–1643.

[40] Y. Pei, E. Brulé, C. Moberg, *Org. Biomol. Chem.* **2006**, *4*, 544.

[41] J. Lloret Fillol, A. Kruckenberg, P. Scherl, H. Wadepohl, L. H. Gade, *Chem. Eur. J.* **2011**, *17*, 14047–14062.

[42] S. Kawamorita, T. Miyazaki, T. Iwai, H. Ohmiya, M. Sawamura, *J. Am. Chem. Soc.* **2012**, *134*, 12924–12927.

[43] T. Iwai, Y. Goto, Z. You, M. Sawamura, *Chem. Lett.* **2021**, *50*, 1236–1239.

[44] K. Murai, T. Matsushita, A. Nakamura, S. Fukushima, M. Shimura, H. Fujioka, *Angew. Chem. Int. Ed.* **2010**, *49*, 9174–9177.

[45] C. Dro, S. Bellemin-Laponnaz, R. Welter, L. H. Gade, *Angew. Chem. Int. Ed.* **2004**, *43*, 4479–4482.

[46] M. T. Reetz, H. Guo, M. Jun-An, R. Goddard, R. J. Mynott, *J. Am. Chem. Soc.* **2009**, *131*, 4136–4142.

[47] C. Foltz, B. Stecker, G. Marconi, S. Bellemin-Laponnaz, H. Wadepohl, L. H. Gade, *Chem. Commun.* **2005**, 5115.

[48] C. Foltz, M. Enders, S. Bellemin-Laponnaz, H. Wadepohl, L. H. Gade, *Chem. Eur. J.* **2007**, *13*, 5994–6008.

[49] P. Axe, S. D. Bull, M. G. Davidson, M. D. Jones, D. E. J. E. Robinson, W. L. Mitchell, J. E. Warren, *Dalton Trans.* **2009**, 10169.

[50] M. Kol, M. Shamis, I. Goldberg, Z. Goldschmidt, S. Alfi, E. Hayut-Salant, *Inorg. Chem. Commun.* **2001**, *4*, 177–179.

[51] M. Yasuda, S. Yoshioka, S. Yamasaki, T. Somyo, K. Chiba, A. Baba, *Org. Lett.* **2006**, *8*, 761–764.

[52] M. Yasuda, H. Nakajima, R. Takeda, S. Yoshioka, S. Yamasaki, K. Chiba, A. Baba, *Chem. Eur. J.* **2011**, *17*, 3856–3867.

[53] D. Tanaka, Y. Kadonaga, Y. Manabe, K. Fukase, S. Sasaya, H. Maruyama, S. Nishimura, M. Yanagihara, A. Konishi, M. Yasuda, *J. Am. Chem. Soc.* **2019**, *141*, 17466–17471.

[54] M. Yasuda, S. Yoshioka, H. Nakajima, K. Chiba, A. Baba, *Org. Lett.* **2008**, *10*, 929–932.

[55] A. Konishi, K. Nakaoka, H. Nakajima, K. Chiba, A. Baba, M. Yasuda, *Chem. Eur. J.* **2017**, *23*, 5219–

5223.

[56] H. Nakajima, M. Yasuda, R. Takeda, A. Baba, *Angew. Chem. Int. Ed.* **2012**, *51*, 3867–3870.

[57] D. Tanaka, Y. Tsutsui, A. Konishi, K. Nakaoka, H. Nakajima, A. Baba, K. Chiba, M. Yasuda, *Chem. Eur. J.* **2020**, *26*, 15023–15034.

[58] A. Konishi, R. Yasunaga, K. Chiba, M. Yasuda, *Chem. Commun.* **2016**, *52*, 3348–3351.

[59] Y. Tsutsui, D. Tanaka, Y. Manabe, Y. Ikinaga, K. Yano, K. Fukase, A. Konishi, M. Yasuda, *Chem. – A Eur. J.* **2022**, *28*, e202202284.

[60] A. Konishi, K. Nakaoka, H. Maruyama, H. Nakajima, T. Eguchi, A. Baba, M. Yasuda, *Chem. Eur. J.* **2017**, *23*, 1273–1277.

[61] P. W. N. M. Van Leeuwen, P. C. J. Kamer, C. Claver, O. Pàmies, M. Diéguez, *Chem. Rev.* **2011**, *111*, 2077–2118.

[62] M. B. Dinger, M. J. Scott, *Inorg. Chem.* **2001**, *40*, 856–864.

[63] J. Kobayashi, Y. Domoto, T. Kawashima, *Chem. Lett.* **2010**, *39*, 134–135.

[64] P. Zhang, Z. Han, Z. Wang, K. Ding, *Angew. Chem. Int. Ed.* **2013**, *52*, 11054–11058.

[65] V. H. G. Rohde, M. F. Müller, M. Oestreich, *Organometallics* **2015**, *34*, 3358–3373.

[66] L. Falivene, Z. Cao, A. Petta, L. Serra, A. Poater, R. Oliva, V. Scarano, L. Cavallo, *Nat. Chem.* **2019**, *11*, 872–879.

[67] "SambVca 2.1 web server," can be found under https://www.molnac.unisa.it/OMtools/sambvca2.1/index.html, **n.d.**

[68] R. P. Pinnell, C. A. Megerle, S. L. Manatt, P. A. Kroon, *J. Am. Chem. Soc.* **1973**, *95*, 977–978.

[69] C. A. Tolman, *Chem. Rev.* **1977**, *77*, 313–348.

[70] D. W. Allen, B. F. Taylor, *J. Chem. Soc. Dalt. Trans.* **1982**, 51–54.

[71] T. Hayashi, K. Yamasaki, *Chem. Rev.* **2003**, *103*, 2829–2844.

[72] Y. Takaya, M. Ogasawara, T. Hayashi, M. Sakai, N. Miyaura, *J. Am. Chem. Soc.* **1998**, *120*, 5579–5580.

[73] A. Kina, H. Iwamura, T. Hayashi, *J. Am. Chem. Soc.* **2006**, *128*, 3904–3905.

[74] Y.-G. Li, G. He, H.-L. Qin, E. A. B. Kantchev, *Dalton Trans.* **2015**, *44*, 2737–2746.

[75] T. Hayashi, M. Takahashi, Y. Takaya, M. Ogasawara, *J. Am. Chem. Soc.* **2002**, *124*, 5052–5058.

[76] H. M. Turner, J. Patel, N. Niljianskul, J. M. Chong, *Org. Lett.* **2011**, *13*, 5796–5799.

[77] G. Chen, J. Xing, P. Cao, J. Liao, *Tetrahedron* **2012**, *68*, 5908–5911.

[78] J. Wong, K. Gan, H. J. Chen, S. A. Pullarkat, *Adv. Synth. Catal.* **2014**, *356*, 3391–3400.

[79] G. Casotti, V. Rositano, A. Iuliano, *Adv. Synth. Catal.* **2021**, *363*, 1126–1131.

[80] T. Senda, M. Ogasawara, T. Hayashi, *J. Org. Chem.* **2001**, *66*, 6852–6856.

[81] M. S. Yu, I. Lantos, Z.-Q. Peng, J. Yu, T. Cacchio, *Tetrahedron Lett.* **2000**, *41*, 5647–5651.

[82] D. Kong, M. Li, G. Zi, G. Hou, *Org. Biomol. Chem.* **2016**, *14*, 4046–4053.

[83] O. V Dolomanov, L. J. Bourhis, R. J. Gildea, J. A. K. Howard, H. Puschmann, *J. Appl. Crystallogr.* **2009**, *42*, 339–341.

[84] M. J. Frisch, G. W. Trucks, H. B. Schlegel, G. E. Scuseria, M. A. Robb, J. R. Cheeseman, G. Scalmani,

V. Barone, G. A. Petersson, H. Nakatsuji, X. Li, M. Caricato, A. V. Marenich, J. Bloino, B. G. Janesko, R. Gomperts, B. Mennucci, H. P. Hratchian, J. V. Ortiz, A. F. Izmaylov, J. L. Sonnenberg, D. Williams-Young, F. Ding, F. Lipparini, F. Egidi, J. Goings, B. Peng, A. Petrone, T. Henderson, D. Ranasinghe, V. G. Zakrzewski, J. Gao, N. Rega, G. Zheng, W. Liang, M. Hada, M. Ehara, K. Toyota, R. Fukuda, J. Hasegawa, M. Ishida, T. Nakajima, Y. Honda, O. Kitao, H. Nakai, T. Vreven, K. Throssell, J. J. A. Montgomery, J. E. Peralta, F. Ogliaro, M. J. Bearpark, J. J. Heyd, E. N. Brothers, K. N. Kudin, V. N. Staroverov, T. A. Keith, R. Kobayashi, J. Normand, K. Raghavachari, A. P. Rendell, J. C. Burant, S. S. Iyengar, J. Tomasi, M. Cossi, J. M. Millam, M. Klene, C. Adamo, R. Cammi, J. W. Ochterski, R. L. Martin, K. Morokuma, O. Farkas, J. B. Foresman, D. J. Fox, *Gaussian 16, Revision C.01*, Gaussian, Inc., Wallingford CT, **2016**.

[85] L. G. Borrego, R. Recio, E. Álvarez, A. Sánchez-Coronilla, N. Khiar, I. Fernández, *Org. Lett.* **2019**, *21*, 6513–6518.

[86] Z.-T. He, Y.-B. Wei, H.-J. Yu, C.-Y. Sun, C.-G. Feng, P. Tian, G.-Q. Lin, *Tetrahedron* **2012**, *68*, 9186–9191.

[87] M. Chen, F. Liu, G. Dong, *Angew. Chem. Int. Ed.* **2018**, *57*, 3815–3819.

[88] L. Falivene, Z. Cao, A. Petta, L. Serra, A. Poater, R. Oliva, V. Scarano, L. Cavallo, *Nat. Chem.* **2019**, *11*, 872–879.

[89] T. Nagano, S. Einaru, K. Shitamichi, K. Asano, S. Matsubara, *Eur. J. Org. Chem.* **2020**, *2020*, 7131–7133.

[90] T. Yasukawa, H. Miyamura, S. Kobayashi, *J. Am. Chem. Soc.* **2012**, *134*, 16963–16966.

[91] G.-P. Yang, N. Zhang, N.-N. Ma, B. Yu, C.-W. Hu, *Adv. Synth. Catalyis* **2017**, *359*, 926–932.

[92] J. Wong, K. Gan, H. J. Chen, S. A. Pullarkat, *Adv. Synth. Catalyis* **2014**, *356*, 3391–3400.

[93] A. Nikol, Z. Zhang, A. Chelouan, L. Falivene, L. Cavallo, A. Herrera, F. W. Heinemann, A. Escalona, S. Frieß, A. Grasruck, R. Dorta, *Organometallics* **2020**, *39*, 1348–1359.

[94] R. Rimkus, M. Jurgelėnas, S. Stončius, *Eur. J. Org. Chem.* **2015**, *2015*, 3017–3021.

[95] G.-Z. Zhao, D. Foster, G. Sipos, P. Gao, B. W. Skelton, A. N. Sobolev, R. Dorta, *J. Org. Chem.* **2018**, *83*, 9741–9755.

[96] Deposition numbers <url href="https://www.ccdc.cam.ac.uk/services/structures?id=doi:10.1002/chem.202301255"> 2283100 (**2a**P), 2283101 (**2b**P), and 2283102 (**9**) contain the supplementary crystallographic data for this paper. These data are provided free of charge by the joint Cambridge Crystallographic Data Centre and Fachinformationszentrum Karlsruhe <url href="http://www.ccdc.cam.ac.uk/structures">Access Structures service</url>.

[97] L. G. Borrego, R. Recio, E. Álvarez, A. Sánchez-Coronilla, N. Khiar, I. Fernández, *Org. Lett.* **2019**, *21*, 6513–6518.

[98] Z.-T. He, Y.-B. Wei, H.-J. Yu, C.-Y. Sun, C.-G. Feng, P. Tian, G.-Q. Lin, *Tetrahedron* **2012**, *68*, 9186–9191.

[99] M. Chen, F. Liu, G. Dong, *Angew. Chem. Int. Ed.* **2018**, *57*, 3815–3819.

Chapter 2: *C*$_3$-Symmetric Chiral Cage-Shaped Phosphates: Synthesis and Application to Organocatalysts in Asymmetric Iodolactonizations

2-1. Introduction

In organic chemistry, molecular symmetry is one of the most crucial factors for determining not only the chemical and physical properties of a molecule,[1,2] but also for controlling its reactivity and the selectivity of its reactions through a specific steric and/or electronic reaction field.[3,4] The design of the molecular skeletons of asymmetric catalysts that can achieve high enantioselectivity has been the subject of intense research efforts. As such, chiral ligands and catalysts possessing C_2 rotational symmetry have emerged as the most fundamental yet promising scaffolds and have been developed and applied to various asymmetric syntheses.[5–9] However, compared to the abundant number of chiral catalysts with C_2 symmetry, research on catalysts with higher rotational symmetry has lagged behind, even though C_3-symmetric molecules represent intriguing potential alternatives to C_2-symmetric chiral catalysts. Accordingly, the exploration of new chiral scaffolds with rotational symmetry higher than C_2 is in high demand.[10] Some C_3-symmetric molecules[11–14] have been developed as asymmetric catalysts,[15–18] for use in molecular recognition,[19,20] and in materials science.[21–23] The application of C_3-symmetric chiral molecules to organocatalysis[24–30] has been an important area of research for these molecules. For example, C_3-symmetric chiral trisimidazoline **1** has been used as an enantioselective catalyst in bromolactonization reactions (Figure 1a).[31,32]

Phosphate esters and amides are common structures found in organophosphorus(V) compounds. The P=O group acts as an n-type Lewis-basic moiety that can catalytically activate reactions by interacting with an electron-accepting atom in one of the reagents or substrates.[33] Moreover, introducing a chiral moiety into the phosphate group allows for the development of effective chiral Lewis-basic catalysts. Various phosphate derivatives have been used as catalysts, enabling enantioselective versions of reactions such as selenolactonization,[34] halocyclization,[35–41] and sulfenocyclization.[42–48]

In the research group I belong to, various C_3-symmetric cage-shaped Lewis acids that incorporate aluminum aryloxides,[49,50] borates,[50–55] and heavier group-14 elements[56] have been discovered. Recently, I have expanded this C_3-symmetric ligand design to include a Lewis base, resulting in C_3-symmetric cage-shaped phosphites **2a**P and **2b**P (Figure 1b).[57] The two cage-shaped phosphites **2a**P and **2b**P serve as chiral ligands in a Rh-catalyzed asymmetric conjugate addition, giving products in acceptable yield with excellent enantioselectivity. The Lewis basicity of **2a**P and **2b**P can be controlled by the differences in their steric bulk caused by the tethered C–H and Si–Me groups. These findings inspired us to replace the phosphite moiety of **2**P with a phosphate, and to explore the catalytic activity of the obtained **2**P=O molecules as chiral Lewis bases. Kawashima and co-workers have reported a related phosphate and, whilst they demonstrated its C_{60}-inclusion behavior, its catalytic activity remains unexplored.[58]

Herein, I describe the synthesis and catalytic activity of C_3-symmetric chiral cage-shaped phosphates **2a**P=O and **2b**P=O. Our chiral cage-shaped phosphates **2a**P=O and **2b**P=O catalyze asymmetric iodolactonizations[10] of pent-4-enoic acids and hex-5-enoic acids. The distinct steric environments of the two **2**P=O catalysts result in varying degrees of enantioselectivity depending on the substrates employed.

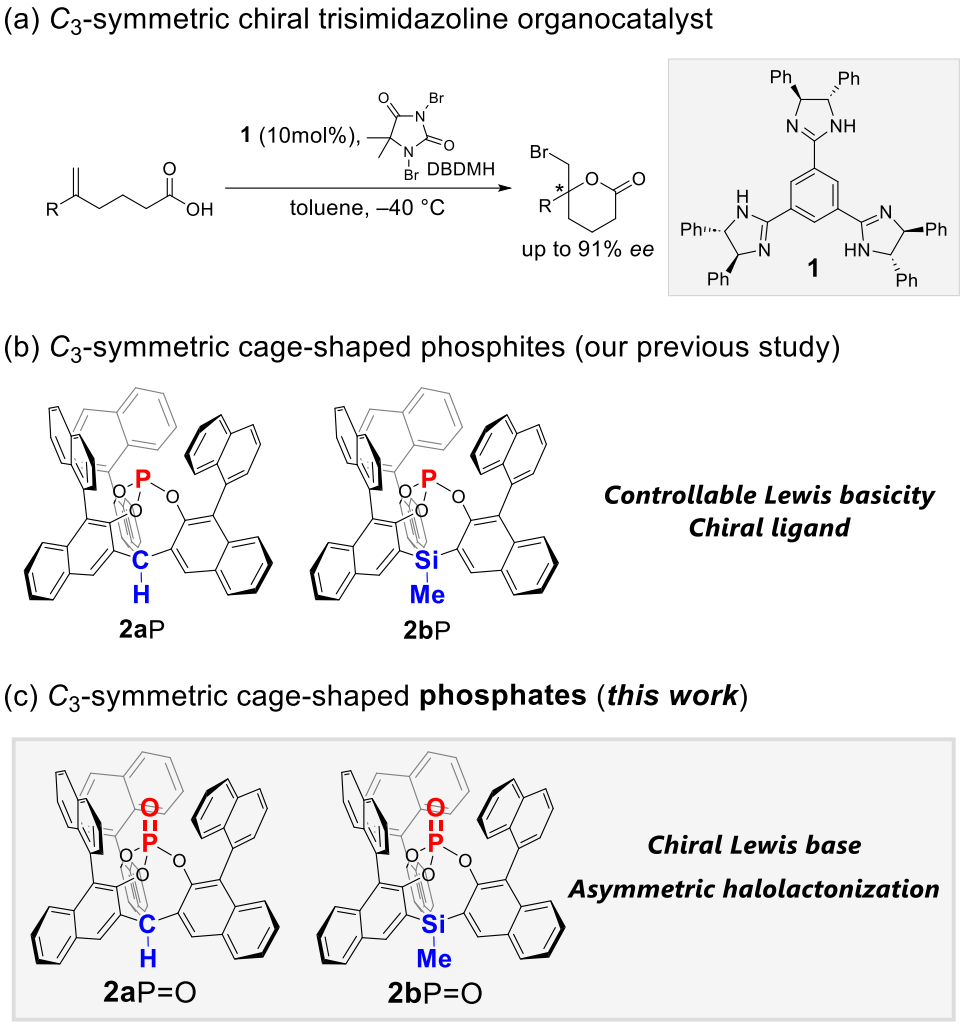

Figure 1. (a) C_3-symmetric chiral trisimidazoline **1** applied in an asymmetric bromolactonization. (b) Cage-shaped phosphites **2**P. (C) This work: cage-shaped phosphates **2**P=O.

2-2. Results and Discussion

The synthetic route to obtain the cage-shaped phosphates **2**P=O is depicted in Scheme 1. According to the protocol from our previous study, carbon-tethered **2a**H_3[53] and silicon-tethered **2b**H_3[57] were synthesized starting from (*R*)-BINOL. To construct the cage-shaped framework, the conditions reported by Kawashima[58] were employed. For that purpose, one equivalent of phosphoryl chloride was added to a dilute solution of **2a**H_3 in toluene (2 mM) in the presence of Et_3N (10 eq.). The reaction mixture was refluxed for 20 h to give carbon-tethered **2a**P=O in 30% yield. However, silicon-tethered **2b**P=O could not be obtained under the same reaction conditions. Thus, I modified the concentration of the reaction mixture and performed the reaction under harsher conditions. Specifically, a more concentrated reaction mixture containing **2b**H_3 (20 mM) and phosphoryl chloride in toluene was sealed in a Schlenk flask with a J-Young tap and was heated at 125 °C for 2 days, yielding silicon-tethered **2b**P=O in moderate yield (50%). Applying the new conditions to the synthesis of **2a**P=O improved the yield to 80%. The obtained cage-shaped phosphates **2a**P=O and

2bP=O are bench-stable colorless solids and can be purified using silica-gel-column chromatography. The stability of the **2**P=O molecules stands in contrast to that of the **2**P phosphites, which quickly decompose under ambient conditions.

A single-crystal X-ray diffraction analysis of carbon-tethered **2a**P=O confirmed the presence of the C_3-symmetric cage-shaped structure. Gradual evaporation of a solution of **2a**P=O in CH_3CN afforded single crystals suitable for a crystallographic analysis and the thermal-ellipsoid plots are shown in Figure 2. A robust C_3-symmetric structure is created by the three naphthyl groups. All binaphthyl axes have (*S*) configurations and the helical structure formed around the phosphate is of the (*P*)-type. Selected geometric parameters obtained from the crystal structure are summarized in Table S1. The P=O bond (1.448(3) Å) is comparable to that of triphenyl phosphate (1.432 Å).[59] Although determining the molecular structure of silicon-tethered **2b**P=O via a crystallographic analysis failed due to its poor crystallinity, spectroscopic analytical techniques, including ^{1}H, ^{13}C, ^{29}Si, and ^{31}P NMR spectroscopy and high-resolution mass spectrometry (HRMS) measurements, confirmed the successful formation of **2b**P=O. The ^{31}P NMR chemical shifts of **2a**P=O (−19.4 ppm) and **2b**P=O (−25.8 ppm) are up-field shifted compared to those of the corresponding phosphites **2a**P (108.4 ppm) and **2b**P (111.2 ppm). Moreover, the phosphorous center of **2**P=O should be magnetically shielded by the three surrounding naphthyl groups, resulting in an up-field shift compared to open-caged triphenyl phosphate (−17.0 ppm).

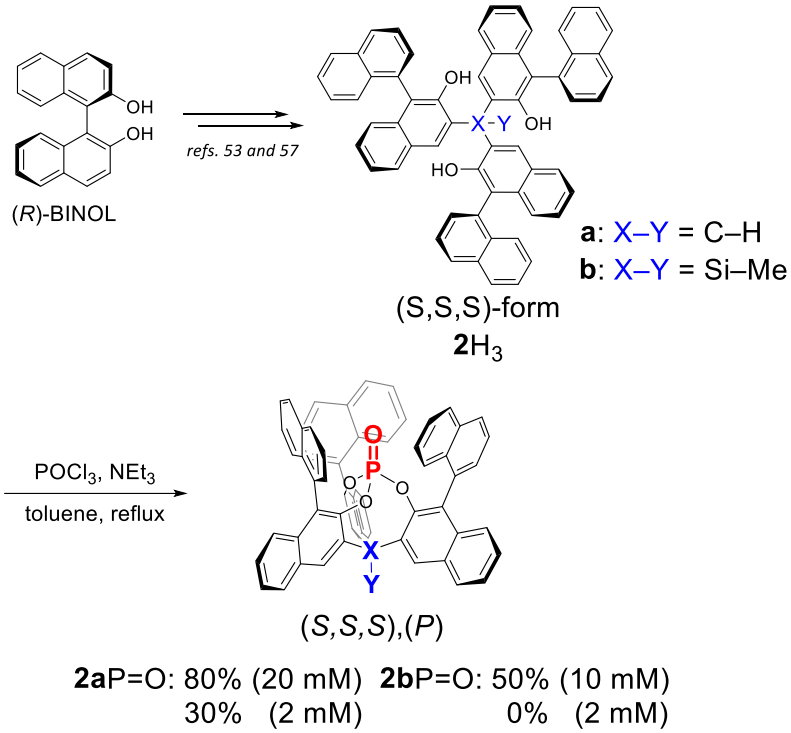

Scheme 1. Synthetic route to C_3-symmetric cage-shaped phosphates **2a**P=O and **2b**P=O.

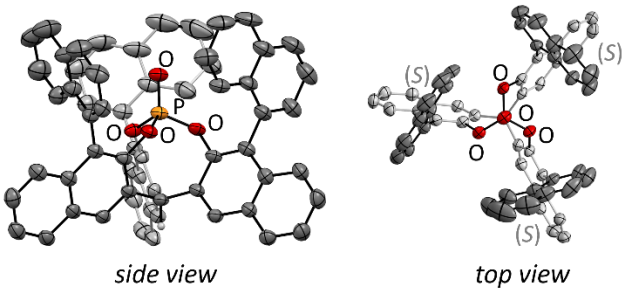

Figure 2. Molecular structure of cage-shaped phosphate **2a**P=O with thermal ellipsoids at 50% probability; some hydrogen atoms are omitted for clarity.

Then, I examined the ability of the chiral Lewis-basic phosphates **2**P=O to catalyze an asymmetric synthetic reaction. As a model transformation, I selected the iodolactonization of 4-benzylpent-4-enoic acid (**3a**) with I_2 in the presence of an *N*-chlorophthalimide (NCP) activator.[38,60,61] Using **2a**P=O as a chiral basic catalyst in the presence of NCP, the asymmetric addition of I_2 to **3a** to produce **4a** was performed (Table 1). The reaction in toluene at 25 °C smoothly afforded **4a** in 97% yield, albeit that the enantioselectivity was very poor (9% enantiomeric excess (*ee*) of the (*R*)-stereoisomer;[38] entry 1, Table 1). Lowering the reaction temperature from 25 °C to −78 °C effectively improved the enantioselectivity up to 65% *ee* (entries 2–6, Table 1). However, the yield of **4a** at −78 °C was significantly suppressed (3%). More polar solvents, such as CH_2Cl_2, Et_2O, and THF, yielded a lower *ee* or a racemic mixture in moderate to high yield (entries 7–9, Table 1). The reactivity and enantioselectivity of the reaction was found to dramatically depended on the solvent polarity. These features are consistent with Ishihara's finding that polar solvent systems impede the generation of active ionic species.[62]

Table 1. Enantioselective iodolactonization of **3a** with I_2 in the presence of NCP catalyzed by **2a**P=O.[a]

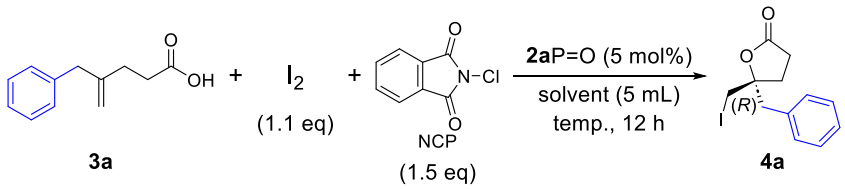

Entry	Temp. / °C	Solvent	Yield / %[b]	*ee* / %[b]
1	r.t.	toluene	97	9
2	0	toluene	84	17
3	-20	toluene	96	28
4	-40	toluene	62	43
5	-60	toluene	21	58
6	-78	toluene	3	65

7	-78	CH_2Cl_2	64	15
8	-78	Et_2O	52	0
9	-78	THF	100	0

[a] I_2, NCP, and **2a**P=O were stirred in toluene at −78 °C for 1 h prior to addition of **3a**. [b] Yield and *ee* values were determined via ^{1}H NMR measurements and chiral HPLC analyses, respectively.

Next, I screened the I_2 activator to achieve both a good yield and enantioselectivity for the iodolactonization of **3a** at low temperature (Table 2). First, *N*-iodosuccinimide (NIS) was utilized instead of NCP (entry 1, Table 2). Although the enantioselectivity was comparable to that of NCP (63% *ee*), the yield of **4a** remained poor (8%). Interestingly, *N*-bromosuccinimide (NBS), which is known to be a more reactive activator for halocyclization,[39] furnished **4a** quantitatively with a moderate enantioselectivity (entry 2, Table 2). According to a report by Ishihara, *N*-bromoimides can generate a more electrophilic ion pair with I_2 with the assistance of a Lewis-basic phosphonium catalyst.[39] Although this insight raised the expectation that *N*-bromoimides may serve as good activators, other related reagents, including 1,3-dibromo-5,5-dimethylhydantoin (DBDMH), *N*-bromophthalimide (NBP), and *N*-bromoacetamide (NBA), afforded **4a** in moderate yield with low enantioselectivity compared to NBS (entries 3–5, Table 2). Next, I shifted the focus on *N*-choloroimides. Despite the low yield of the reaction, *N*-chlorosuccinimide (NCS) improved the enantioselectivity to 75% *ee* (entry 6, Table 2). In this case, I presume that a slow release of a chiral iodoxyphosphonium ion active species is responsible for the enhanced enantioselectivity.[38]

Table 2. Optimization of the I_2 activator.[a]

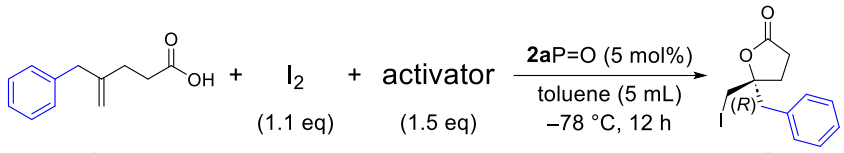

3a **4a**

Entry	Activator	Yield / %[b]	*ee* / %[b]
1	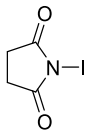 NIS	8	63
2	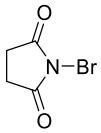 NBS	100	53
3	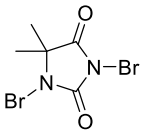 DBDMH	60	19
4	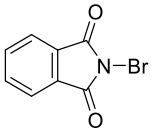 NBP	72	37
5	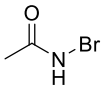 NBA	80	0
6	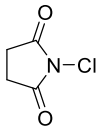 NCS	8	75
7	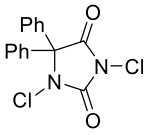 DCDPH	52	62
8	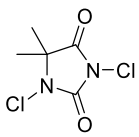 DCDMH	56	76
9	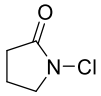	100	8

10	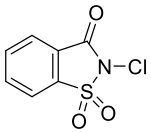	60	10
11	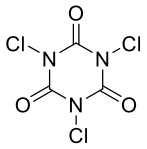	71	8
12	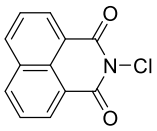	12	70

[a] I_2, activator, and **2a**P=O were stirred in toluene at −78 °C for 1 h prior to addition of **3a**. [b] Yield and *ee* values were determined via ^{1}H NMR measurements and chiral HPLC analyses, respectively.

Importantly, 1,3-dichloro-5,5-diphenylhydantoin (DCDPH; entry 7, Table 2) and 1,3-dichloro-5,5-dimethylhydantoin (DCDMH; entry 8, Table 2) improved both the yield and enantioselectivity of **4a** at −78 °C. *N*-chloro-2-pyrrolidone (entry 9, Table 2), *N*-chlorosaccharin (entry 10, Table 2), and trichloroisocyanuric acid (entry 11, Table 2) afforded **4a** in satisfactory yield but poor enantioselectivity. In contrast, *N*-chloro-1,8-naphthalimide (entry 12, Table 2) exhibited poor reactivity but high enantioselectivity. Of the tested activators, DCDMH (entry 8, Table 2) showed the best balance between reactivity and enantioselectivity.

Based on a report by Ishihara,[38] a plausible catalytic cycle is shown in Figure 3. Initially, the Lewis-acidic DCDMH might activate I_2 through halogen-bonding interactions to form the active iodinating species **A**. The cooperative activation of **A** with phosphate **2**P=O would then afford the chiral iodoxyphosphonium ion **B** as an active species. Finally, electrophilic iodination of the double bond of the substrate followed by cyclization would provide the desired iodolactones **4**/**7**/**8** and imide **C**.

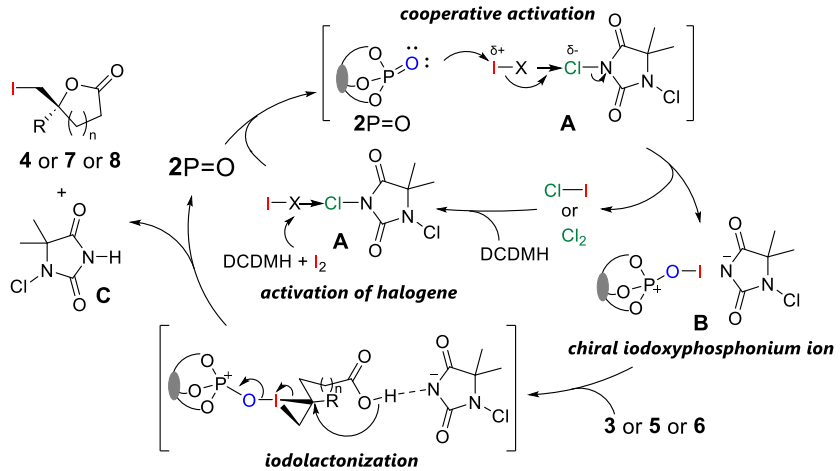

Figure 3. Proposed mechanism of the chiral iodolactonization catalyzed by **2**P=O.

With the optimized conditions in hand, pent-4-enoic acids (**3** and **5**) and hex-5-enoic acids (**6**) were examined (Scheme 2). The reactions of the pent-4-enoic acids with 4-methylbenzyl (**3b**) and 4-methoxybenzyl (**3c**) groups, catalyzed by **2a**P=O, furnished **4b** and **4c**, respectively, in moderate yield with

decreased enantioselectivity relative to **3a** (Scheme 2a). Using **2b**P=O as the Lewis-basic catalyst resulted in poor enantioselectivity, even though the yield of the products was improved. The same trends regarding reactivity and enantioselectivity were observed for the iodolactonization of **3d** and **3e** with 2- or 4-fluorobenzyl groups, respectively. A comparison of the two catalysts showed that the carbon-tethered cage-shaped phosphate **2a**P=O affords the products with better enantioselectivity (**4e**: 70% *ee*) than its silicon-tethered counterpart **2b**P=O (**4e**: 22% *ee*).

The iodolactonizations of 4-arylpent-4-enoic acid derivatives (**5**) catalyzed by **2a**P=O gave the corresponding products (**7**) in moderate enantioselectivity (46–68% *ee* of the (*R*)-stereoisomers;[38,63] Scheme 2b). Substrates with phenyl (**5a**), 4-chlorophenyl (**5b**), and 4-methylphenyl (**5c**) groups were tolerated under the applied conditions, yielding the corresponding products with moderate enantioselectivity. However, the pent-4-enoic acid with a 4-methoxyphenyl group (**5d**) afforded a racemic product probably because the electron-donating 4-methoxy group assists the generation of a cationic intermediate, leading to a competing background process. In comparison, the enantioselectivity of the corresponding reactions driven by **2b**P=O were inferior. According to a previous report, controlling the enantioselectivity of the iodolactonization of 4-aryllpent-4-enoic acid derivatives **5** using a phosphate-based Lewis-basic catalyst is challenging.[39] Highly reactive benzyl cations of these substrates are generated as intermediates of the iodolactonization, resulting in a direct iodolactonization. Chiral iodoxyphosphonium ion **B** (Figure 3) is not involved in the direct iodolactonization, and hence no enantioselectivity was observed. However, our carbon-tethered phosphate **2a**P=O attained respectable enantioselectivity.

Interestingly, the iodolactonization of hex-5-enoic acid derivatives (**6**) was smoothly catalyzed by silicon-tethered cage-shaped phosphate **2b**P=O instead of by carbon-tethered **2a**P=O (Scheme 2c). The reactions of the hex-5-enoic acids with phenyl (**6a**), 4-fuluorophenyl (**6b**), and 4-methylphenyl (**6c**) groups catalyzed by **2b**P=O furnished the corresponding six-membered lactones (**8a**–**8c**) in moderate yield (30–50%) and enantiomeric excesses (28–46% *ee* of the (*R*)-stereoisomer),[64] while the hex-5-enoic acid substrate containing a 4-methoxyphenyl group (**6d**) afforded a racemic product.

Based on our previous study of the cage-shaped phosphites **2**P,[57] the enantioselective formation of a product with a larger ring is more affected by steric demand. Therefore, it is reasonable to believe that bulkier **2b**P=O has a greater activation energy than **2a**P=O in reactions with substrate **6**.

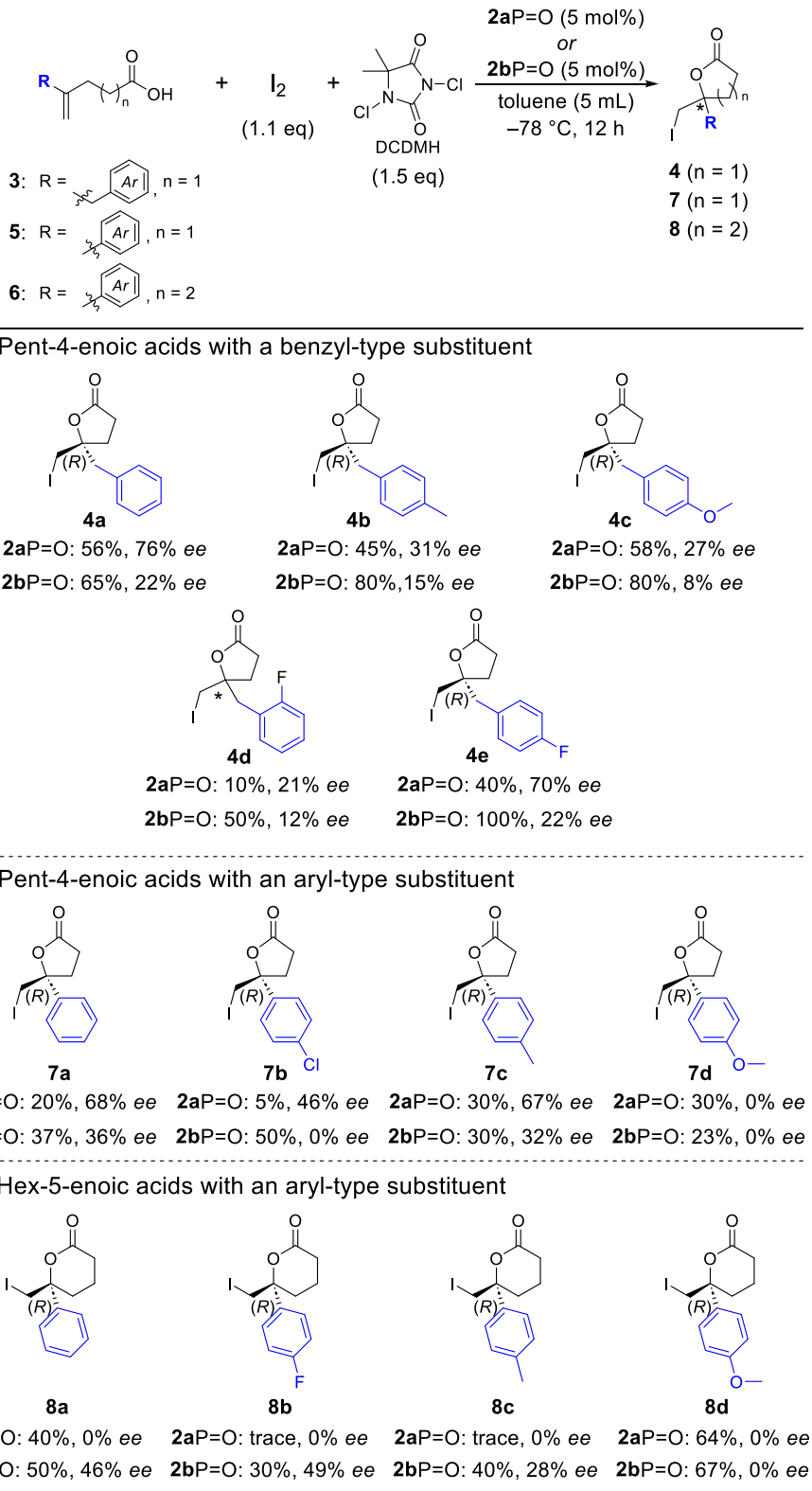

Scheme 2. Enantioselective iodolactonization of **3**, **5**, and **6** catalyzed by **2a**P=O and **2b**P=O. Yield and *ee* values of products were determined via ^{1}H NMR measurements and chiral HPLC analyses, respectively.

2-3. Conclusion

In conclusion, I have synthesized two chiral C_3-symmetric cage-shaped phosphates and applied them as catalysts in the asymmetric iodolactonization of pent-4-enoic acid and hex-5-enoic acid derivatives. The

I_2 activator 1,3-Dichloro-5,5-dimethylhydantoin (DCDMH) successfully balances the chemical reactivity and enantioselectivity of this catalytic reaction system. The Lewis basicity and chemical environment of the **2**P=O catalysts were precisely controlled by changing the tethered group of each catalyst. Cage-shaped phosphates **2a**P=O and **2b**P=O exhibit complementary catalytic activity, i.e., carbon-tethered **2a**P=O shows superior enantioselectivity for the formation of 5-membered ring products **4** and **7**, whereas silicon-tethered **2b**P=O was suitable for the enantioselective formation of 6-membered ring product **8**. The phosphates presented here can be expected to serve as a basic template for the creation of new chiral C_3-symmetric Lewis-basic catalysts.

2-4. Experimental Section

General

NMR spectra were recorded on JEOL-AL400, JEOL-ECS400 (400 MHz for ^{1}H, 100 MHz for ^{13}C, 78.7 MHz for ^{29}Si and 160 MHz for ^{31}P NMR) and Bruker AVANCE III spectrometers (600 MHz for ^{1}H, and 150 MHz for ^{13}C) with TMS as an internal standard. For ^{29}Si NMR spectra, Me_4Si in $CDCl_3$ was used as an external standard. For ^{31}P NMR spectra, H_3PO_4 in D_2O as an external standard was employed as an external standard. ^{1}H and ^{13}C NMR signals of compounds were assigned using HMQC, HSQC, HMBC, COSY, 1D ^{13}C NMR under conditions of proton off-resonance spin decoupling. Positive FAB/CI, EI, MALDI-TOF, ESI/DART mass spectra were recorded on a JEOL JMS-700, a Shimadzu GCMS-QP2010 Ultra, a JEOL JMS-S3000, and a JEOL JMS-T100LP respectively. IR spectra were recorded as thin films or as solids in KBr pellets on a JASCO FT/IR 6200 spectrophotometer or as solids in ATR-mode on a JASCO FT/IR-4X spectrophotometer. Data collection for X-ray crystal analysis was performed on Rigaku/XtaLAB Synergy-S/Mo (MoK_α λ = 0.71075 Å) and Rigaku/XtaLAB Synergy-S/Cu (CuK_α λ = 1.54187 Å) diffractometers. All non-hydrogen atoms were refined with anisotropic displacement parameters and hydrogen atoms were placed at calculated positions and refined “riding” on their corresponding carbon atoms by Olex2[65] program.

Materials

Anhydrous dichloromethane, THF, acetonitrile, diethyl ether, toluene and hexane were purchased and used as obtained. All reagents were obtained from commercial suppliers and used as received. All reactions were carried out under nitrogen. The carbon-tethered **2a**H_3 and silicon-tethered **2b**$H_3$was synthesized according to our previous study.[53]

Synthetic procedures

(5*S*)-7,9,25-Tri(naphthalen-1-yl)-9,25-di(naphthalen-1-yl)-15*H*-7,15-(epoxy[2,3]naphthaleno)dinaphtho[2,3-*d*:2',3'-*g*][1,3,2]dioxaphosphocine 7-oxide 2aP=O

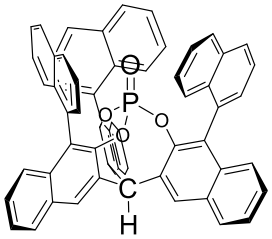

(*S,S,S*),(*P*)
2aP=O

In a Schlenk flask equipped with a J-Young bulb, triethylamine (1.00 mmol, 0.101 g) and phosphoryl chloride (0.100 mmol, 0.0153 g) were added to a solution of **2a**H_3 (0.100 mmol, 0.0821 g) in toluene (5 mL). After N_2 gas was purged, the shielded reaction mixture was heated at 125 °C for 2 days After cooling to room temperature, the reaction mixture was filtrated through a celite pad, and the obtained solution was evaporated under vacuum. The crude material was purified by column chromatography (hexane/ethyl acetate = 60:40, column length 20 cm, diameter 26 mm silica gel) to give the pure product **2a**P=O as a colorless solid (0.0689 g, 80%).

mp 273.2–274.0 ℃; IR (ATR) *v* = 3056 (w), 2956 (m), 2924 (s), 2857 (m), 1726 (w), 1503 (w), 1459 (w), 1372 (w), 1244 (w), 1105 (w), 875 (w) 989 (w), 797 (m), cm^{-1}; ^1H NMR (400 MHz, $CDCl_3$) 8.21 (s, 3H), 7.81 (d, *J* = 8.0 Hz, 3H), 7.77 (t, *J* = 4.8 Hz, 3H), 7.68 (d, *J* = 8.4 Hz, 3H), 7.36 (d, *J* = 7.2 Hz, 3H), 7.33 (t, *J* = 3.8 Hz, 3H), 7.26–7.23 (m, 6H), 7.20 (d, *J* = 6.8 Hz, 3H), 7.10 (d, *J* = 8.8 Hz, 3H), 7.07–7.02 (m, 6H), 6.66 (s, 1H); $^{13}C\{^1H\}$ NMR (100 MHz, $CDCl_3$) 146.7, 146.6, 133.4 (Two signals were overlapped,), 132.3, 131.7, 131.2, 131.0, 130.9, 129.0, 128.72, 128.65, 128.4, 128.3, 127.7, 126.9, 126.6, 125.9, 125.8, 125.4, 56.2; $^{31}P\{^1H\}$ NMR (160 MHz, $CDCl_3$, H_3PO_4 in D_2O as an external standard) −19.4; HRMS (MALDI-TOF MS) Calculated ($C_{61}H_{37}O_4P$): 864.2424 ($[M]^+$), Found: 864.2397.

15-methyl-(5*S*)-7, 9, 25-Tri(naphthalen-1-yl)-9,25-di(naphthalen-1-yl)-15*H*-7,15-(epoxy[2,3]naphthaleno)dinaphtho[2,3-d:2',3'-g][1,3,2,6]dioxaphosphasilocine 7-oxide 2bP=O

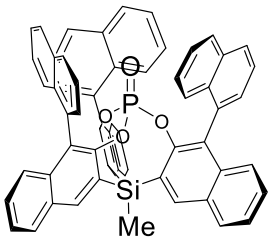

(*S,S,S*),(*P*)
2bP=O

In a Schlenk flask equipped with a J-Young bulb, triethylamine (1.60 mmol, 0.159 g) and phosphoryl chloride (0.157 mmol, 0.0241 g) were added to a solution of **2b**H_3 (0.160 mmol, 0.141 g) in toluene (5 mL).

After N_2 gas was purged, the shielded reaction mixture was heated at 125 °C for 2 days After cooling to room temperature, the reaction mixture was filtrated through a celite pad, and the obtained solution was evaporated under vacuum. The crude material was purified by column chromatography (hexane/ethyl acetate = 60:40, column length 20 cm, diameter 26 mm silica gel) to give the pure product **2b**P=O as a colorless solid (0.0698 g, 50%).

mp 243.0–243.5 °C; IR (KBr) ν = 3053 (m), 2963 (w), 1619 (m), 1495 (w), 1438 (w), 1393 (m), 1368 (s), 1174 (m), 1150 (m), 863 (m), 752 (s), 716 (w), cm^{-1}; ^1H NMR (400 MHz, $CDCl_3$) 8.30 (s, 3H), 7.94 (d, J = 8.4 Hz, 3H), 7.80 (d, J = 8.4 Hz, 6H), 7,43 (t, J = 7.2 Hz, 3H) 7.36 (t, J = 7.8 Hz, 3H), 7.25 (td, J = 7.6, 1.3 Hz, 3H), 7.15 (d, J = 8.4 Hz, 3H), 7.02 (s, 3H), 6.93 (d, J = 8.4 Hz, 3H), 6.86 (t, J = 7.4 Hz, 3H), 1.73 (s, 3H); $^{13}C\{^1H\}$ NMR (100 MHz, $CDCl_3$) 151.3, 151.2, 136.3, 135.2, 133.3, 132.2, 131.5, 130.7, 129.5, 128.3, 128.2, 128.0, 127.82, 127.76, 127.6, 126.7, 125.75, 125.66, 125.5, 125.2, −5.23; $^{31}P\{^1H\}$ NMR (160 MHz, $CDCl_3$, H_3PO_4 in D_2O as an external standard) −25.8; $^{29}Si\{^1H\}$ NMR (78.7 MHz, $CDCl_3$, Me_4Si in $CDCl_3$ as an external standard) −18.3; HRMS (MALDI-TOF MS) Calculated ($C_{61}H_{39}O_4PSiNa$) 917.2247 ($[M+Na]^+$), Found: 917.2279.

X-ray crystallographic data

Carbon-tethered cage-shaped phosphate 2aP=O

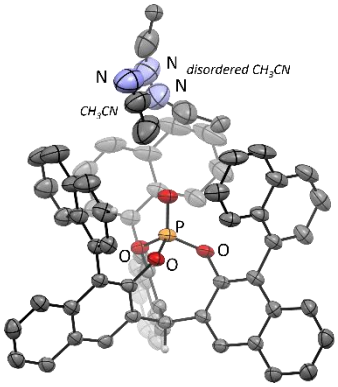

Figure S1. ORTEP drawing of **2a**P=O at the 50% probability level.

No. CCDC	2426798	Space Group	$P4_12_12$ (#92)
Empirical Formula	$2(C_{61}H_{37}O_4P) + 3(C_2H_3N)$	Z value	4
Formula Weight	1852.91	D_{calc}	1.269 g/cm^3
Crystal Color	translucent intense colourless	F_{000}	3864.0
Crystal Dimensions	0.18 × 0.12 × 0.09 mm	(CuK_α)	0.919 mm^{-1}
Crystal System	tetragonal	Temperature	123 K
Lattice Parameters	a = 14.9384(2) Å	Data/restraints/parameters	9661/0/651
	b = 14.9384(2) Å	Residuals: R_1 ($I > 2.00\sigma(I)$)	0.0701
	c = 43.4556(8) Å	Residuals: wR_2 (all data)	0.2097
	a = 90 °	Goodness of Fit Indicator	1.102
	= 90 °	Flack parameter	0.039(9)
	g = 90 °	Recrystallization	From CH_3CN
	V = 9697.4(3) Å^3		

Summary for the geometries of 2aP=O

Table S1. Selected geometric parameters for **2a**P=O

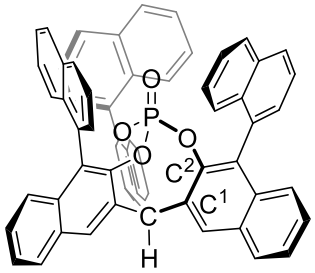

	2aP=O
P=O / Å	1.448(3)
∠O–P–O / °	104.29(10)
∠P–O–C²–C¹ / ° (mean value)	60.97

Typical procedure for iodolactonizations catalyzed by 2aP=O or 2bP=O

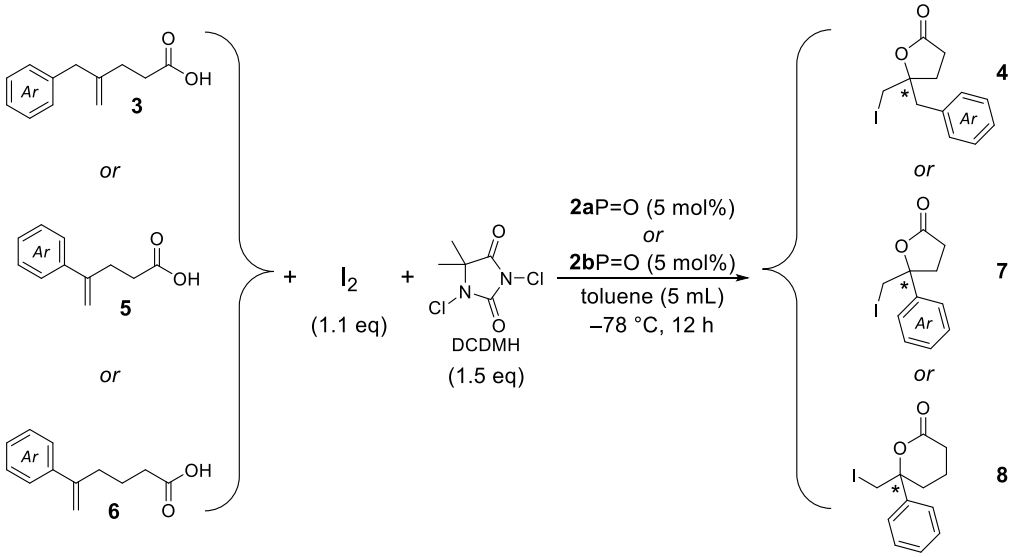

Optimized procedure

To a solution of **2a**P=O or **2b**P=O (4.3 mg, 5 μmol) in toluene (4 mL) were added DCDMH (29.6 mg, 0.15 mmol) and I_2 (27.9 mg, 0.11 mmol) successively at –78 °C under N_2 atmosphere. The mixture was stirred at –78 °C for 1 h. To the mixture was dropwisely added a solution of pent-4-enoic acids (**3**, **5**) or hex-5-enoic acids (**6**) (0.10 mmol) in toluene (1 mL) at –78 °C. The reaction mixture was further stirred at –78 °C for 12 h. The reaction mixture was quenched with saturated aqueous $Na_2S_2O_3$ (10 mL) at –78 °C and the organic layer was extracted with AcOEt (15.0 mL×3). The combined organic layer was washed with water and dried over Na_2SO_4. The filtrate was evaporated in vacuum. The obtained residue was purified by column chromatography on silica gel (hexane–AcOEt 4:1) to give **4**, **7** and **8**.

HPLC chromatograms and NMR spectra for iodolactones

5-benzyl-5-(iodomethyl)dihydrofuran-2(3*H*)-one (4a)[38]

^{1}H NMR (400 MHz, $CDCl_3$) 7.36–7.26 (m, 5H), 3.44 (d, J = 10.8 Hz, 1H), 3.37 (d, J = 10.8 Hz, 1H), 3.20 (d, J = 14.4 Hz 1H), 3.10 (d, J = 14.4 Hz 1H), 2.48 (m, 1H), 2.30–2.21 (m, 2H), 2.00 (m, 1H); ^{13}C{^{1}H} NMR (100 MHz, $CDCl_3$) 175.6, 134.7, 130.5, 128.8, 127.6, 85.4, 44.1, 30.9, 29.5, 14.3.HRMS (DART$^+$) Calculated ($C_{12}H_{14}O_2I$):317.0033 ([M+H]$^+$), Found: 317.0031.

Chiralpak IA-3 (4.6 mm x 25 cm), hexane/EtOH = 75/25, 1.0 mL min^{-1}, 30 °C, UV detection at 250.0 nm. For the racemic sample, based on the reported retention time of (*R*)- and (*S*)-**4a**, t_R = 7.093 min belongs to *R*-, t_R = 7.980 min belongs to *S*-enantiomer.

Racemate

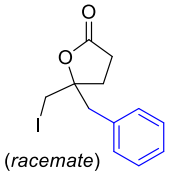

(*racemate*)

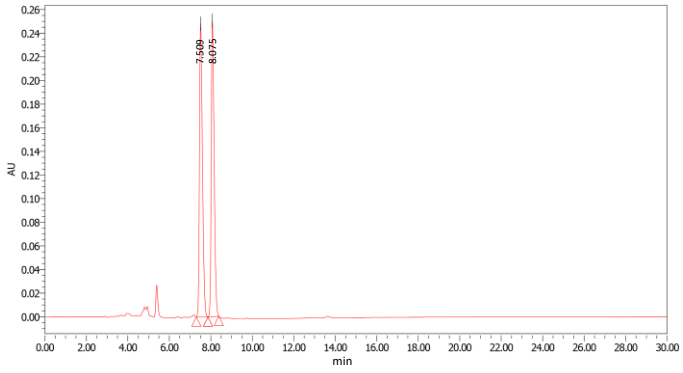

Peak No.	Ret. Time / min	area %
1(*R*)	7.509	50.60
2(*S*)	8.075	49.40

2aP=O as catalyst

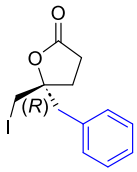

76% *ee* (56% yield)

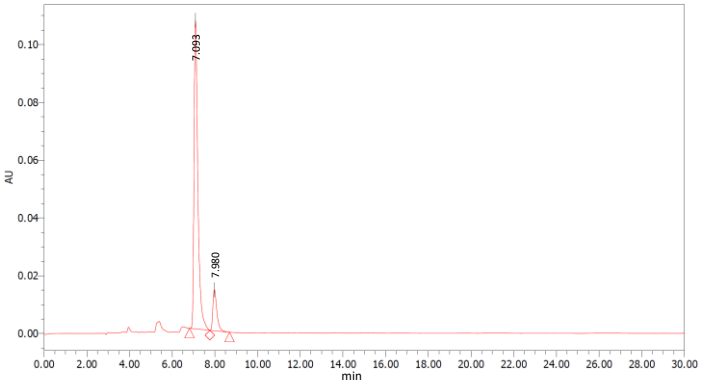

Peak No.	Ret. Time / min	area %
1(*R*)	7.093	87.90
2(*S*)	7.980	12.10

2bP=O as catalyst

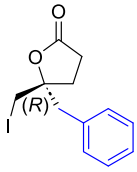

22% *ee* (65% yield)

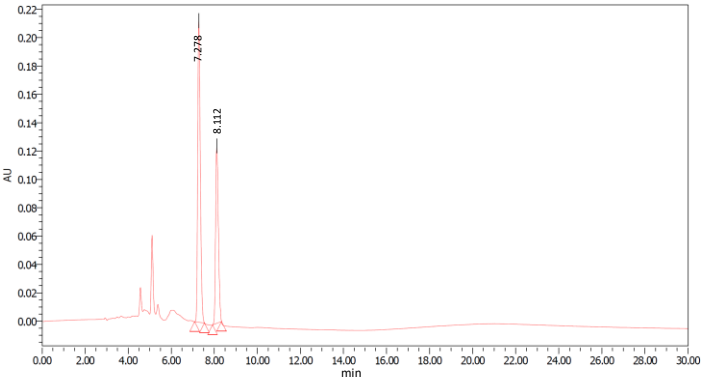

Peak No.	Ret. Time / min	area %
1(*R*)	7.278	61.68
2(*S*)	8.112	38.32

5-(iodomethyl)-5-(4-methylbenzyl)dihydrofuran-2(3*H*)-one (4b)[38]

^{1}H NMR (400 MHz, $CDCl_3$) 7.36–7.26 (m, 5H), 3.44 (d, J = 10.5 Hz, 1H), 3.37 (d, J = 10.8 Hz, 1H), 3.20 (d, J = 14.4 Hz, 1H), 3.10 (d, J = 14.4 Hz, 1H), 2.48 (m, 1H), 2.30–2.21 (m, 2H), 2.00 (m, 1H); ^{13}C{^{1}H} NMR (100 MHz, $CDCl_3$) 175.6, 134.7, 130.5, 128.8, 127.6, 85.4, 44.1, 30.9, 29.5, 14.3.HRMS (ESI$^+$) Calculated ($C_{13}H_{15}O_2INa$):353.0009 ([M+Na]$^+$), Found: 353.0005.

Chiralpak IA-3 (4.6 mm x 25 cm), hexane/*i*PrOH = 90/10, 1.0 mL min^{-1}, 30 °C, UV detection at 250.0 nm. For the racemic sample, based on the reported retention time of (*R*)- and (*S*)-**4b**, t_R = 12.411 min belongs to *S*-, t_R = 13.056 min belongs to *R*-enantiomer.

Racemate

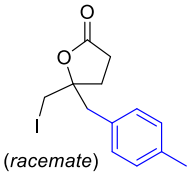

(*racemate*)

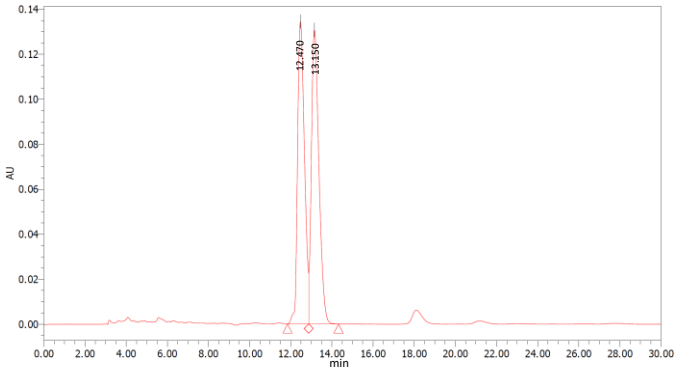

Peak No.	Ret. Time / min	area %
1(*S*)	12.470	48.50
2(*R*)	13.150	51.50

2aP=O as catalyst

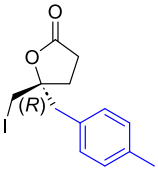

31% *ee* (45% yield)

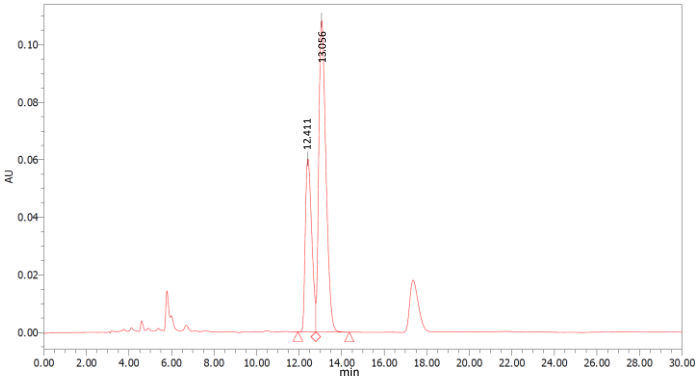

Peak No.	Ret. Time / min	area %
1(*S*)	12.411	33.23
2(*R*)	13.056	66.77

2bP=O as catalyst

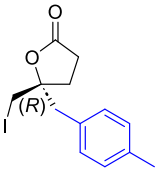

15% *ee* (80% yield)

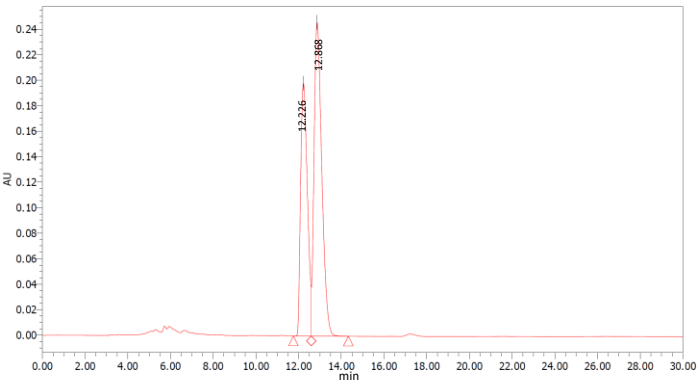

Peak No.	Ret. Time / min	area %
1(*S*)	12.226	41.29
2(*R*)	12.868	58.71

5-(iodomethyl)-5-(4-methoxybenzyl)dihydrofuran-2(3*H*)-one (4c)[38]

^{1}H NMR (400 MHz, $CDCl_3$) 7.20 (d, J = 8.8 Hz, 2H), 6.85 (d, J = 9.2 Hz, 2H), 3.80 (s, 3H), 3.39 (m, 2H), 3.08 (m, 2H), 2.29–2.43 (m, 1H), 2.25–2.21 (m, 2H), 2.05–1.98 (m, 1H); ^{13}C{^{1}H} NMR (100 MHz, $CDCl_3$) 176.1, 159.0, 131.45, 126.7, 114.1, 85.6, 55.3, 43.3, 30.9, 29.5, 14.3. HRMS (ESI$^+$) Calculated ($C_{13}H_{15}O_3INa$): 368.9958 ([M+Na]$^+$), Found: 368.9947.

Chiralpak IA-3 (4.6 mm x 25 cm), hexane/EtOH = 75/25, 1.0 mL min^{-1}, 30 °C, UV detection at 250.0 nm. For the racemic sample, based on the reported retention time of (*R*)- and (*S*)-**4c**, t_R = 9.223 min belongs to *R*-, t_R = 10.924 min belongs to *S*-enantiomer.

Racemate

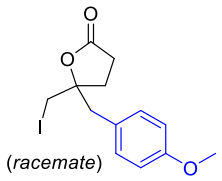

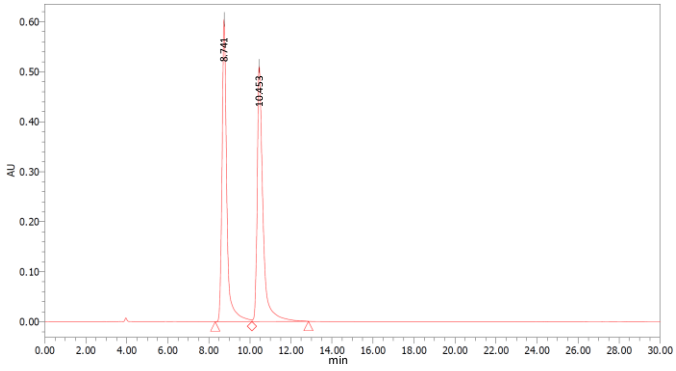

Peak No.	Ret. Time / min	area %
1(*R*)	8.741	49.76
2(*S*)	10.453	50.24

2aP=O as catalyst

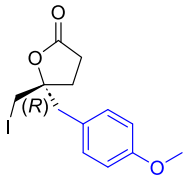

27% *ee* (58% yield)

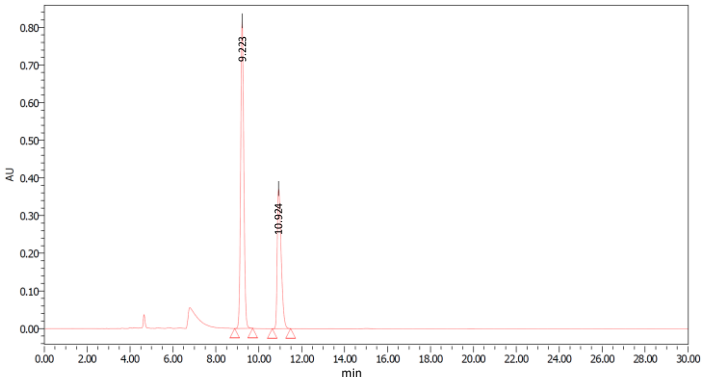

Peak No.	Ret. Time / min	area %
1(*R*)	9.223	63.68
2(*S*)	10.924	36.32

2bP=O as catalyst

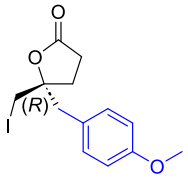

8% *ee* (80% yield)

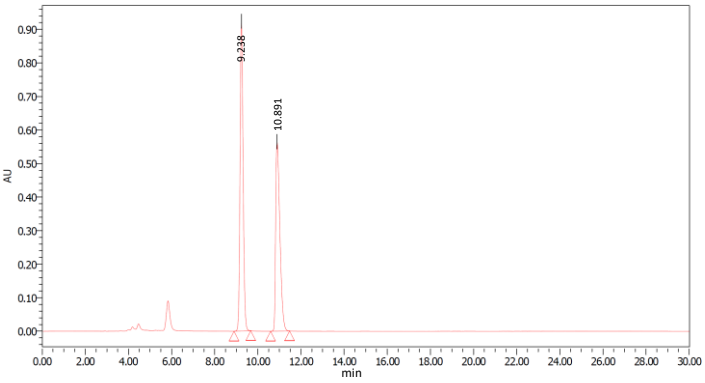

Peak No.	Ret. Time / min	area %
1(*R*)	9.238	54.04
2(*S*)	10.891	45.96

5-(2-fluorobenzyl)-5-(iodomethyl)dihydrofuran-2(3*H*)-one (4d)[38]

^{1}H NMR (400 MHz, $CDCl_3$) 7.35–7.26 (m , 2H), 7.14–7.05 (m, 2H), 3.46 (m, 2H), 3.32 (d, J = 14.4 Hz, 1H), 3.13 (d, J = 14.0 Hz, 1H), 2.54 (m, 1H), 2.33–2.20 (m, 2H), 2.13 (m, 1H); ^{13}C{^{1}H} NMR (100 MHz, $CDCl_3$) 175.8, 161.3 (d, $^{1}J_{C\text{-}F}$ = 246 Hz), 132.78 (d, $^{3}J_{C\text{-}F}$ = 4.8 Hz), 129.6 (d, $^{3}J_{C\text{-}F}$ = 8.1 Hz), 124.6 (d, $^{4}J_{C\text{-}F}$ = 3.8 Hz), 121.8 (d, $^{2}J_{C\text{-}F}$ = 15.3 Hz), 115.7 (d, $^{2}J_{C\text{-}F}$ = 23.1 Hz), 85.3, 36.5, 30.8, 29.5, 14.2. HRMS (ESI^{+}) Calculated ($C_{12}H_{12}O_2FINa$): 356.9758 ([M+Na]$^{+}$), Found: 356.9756.

Chiralpak IA-3 (4.6 mm x 25 cm), hexane/EtOH = 75/25, 1.0 mL min^{-1}, 30 °C, UV detection at 250.0 nm, t_R = 7.067 min and t_R = 7.430 min. The absolute configurations were not determined.

Racemate

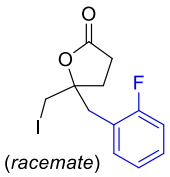

(*racemate*)

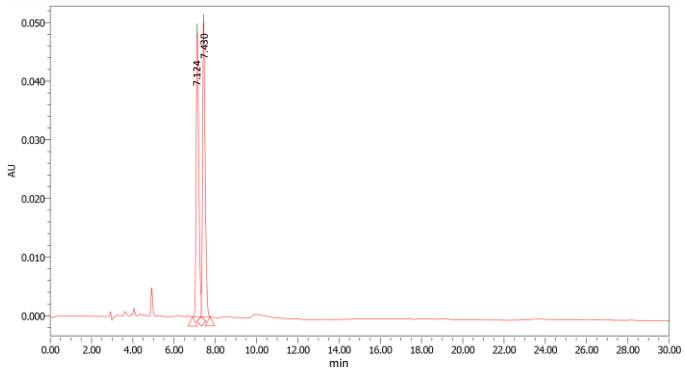

Peak No.	Ret. Time / min	area %
1	7.124	49.46
2	7.430	50.54

2aP=O as catalyst

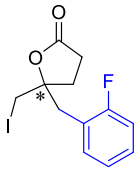

21% *ee* (10% yield)

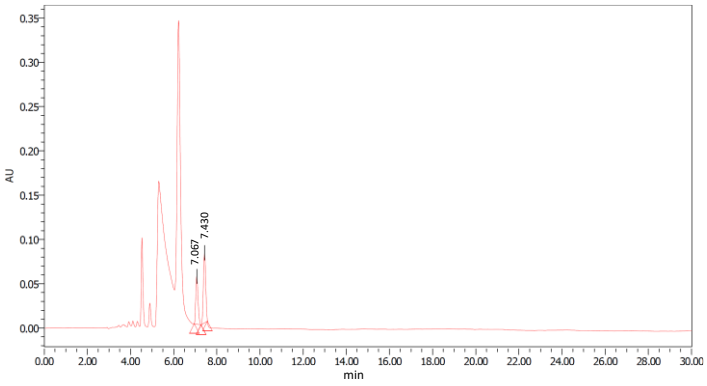

Peak No.	Ret. Time / min	area %
1	7.067	39.77
2	7.430	60.23

2bP=O as catalyst

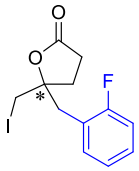

12% *ee* (50% yield)

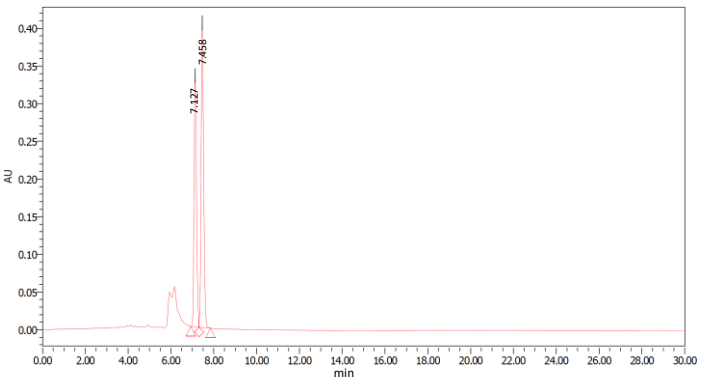

Peak No.	Ret. Time / min	area %
1	7.127	43.86
2	7.458	56.14

5-(4-fluorobenzyl)-5-(iodomethyl)dihydrofuran-2(3*H*)-one (4e)[38]

^{1}H NMR (400 MHz, $CDCl_3$) 7.27–7.25 (m , 2H), 7.00 (t, J = 8.4Hz, 2H), 3.38 (d, J = 10.4 Hz, 1H), 3.31 (d, J = 10.8 Hz, 1H), 3.17 (d, J = 14.4 Hz, 1H), 3.06 (d, J = 14.4 Hz, 1H), 2.54–2.46 (m, 1H), 2.30–2.16 (m, 2H), 2.05 (m, 1H); ^{13}C{^{1}H} NMR (100 MHz, $CDCl_3$) 175.8, 162.3 (d, $^1J_{C\text{-}F}$ = 248 Hz), 132.0 (d, $^3J_{C\text{-}F}$ = 8.2 Hz), 130.4 (d, $^4J_{C\text{-}F}$ = 3.4 Hz), 115.7 (d, $^2J_{C\text{-}F}$ = 21.1 Hz), 85.3, 43.3, 31.0, 29.4, 13.7. HRMS (ESI$^+$) Calculated ($C_{12}H_{12}O_2FINa$): 356.9758. ([M+Na]+), Found: 356.9754.

Chiralpak IA-3 (4.6 mm x 25 cm), hexane/EtOH = 75/25, 1.0 mL min^{-1}, 30 °C, UV detection at 250.0 nm. For the racemic sample, based on the reported retention time of (*R*)- and (*S*)-**4e**, t_R = 15.009 min belongs to *R*-, and t_R = 16.720 min belongs to *S*-enantiomer.

Racemate

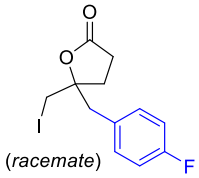

(*racemate*)

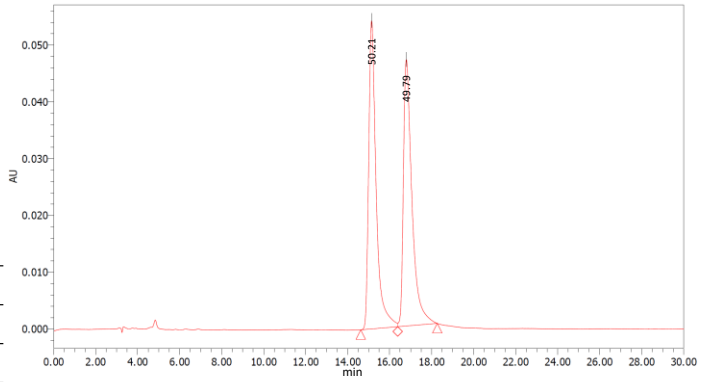

Peak No.	Ret. Time / min	area %
1(*R*)	15.139	50.21
2(*S*)	16.793	49.79

2aP=O as catalyst

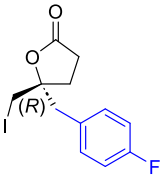

70% *ee* (40% yield)

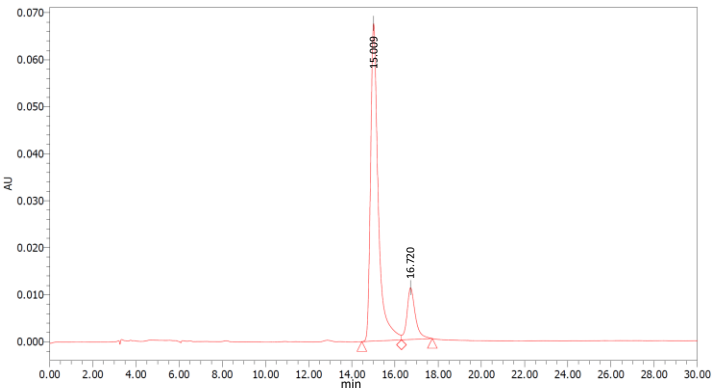

Peak No.	Ret. Time / min	area %
1(*R*)	15.009	85.07
2(*S*)	16.720	14.93

2bP=O as catalyst

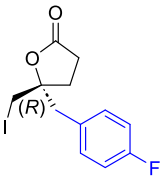

22% *ee* (100% yield)

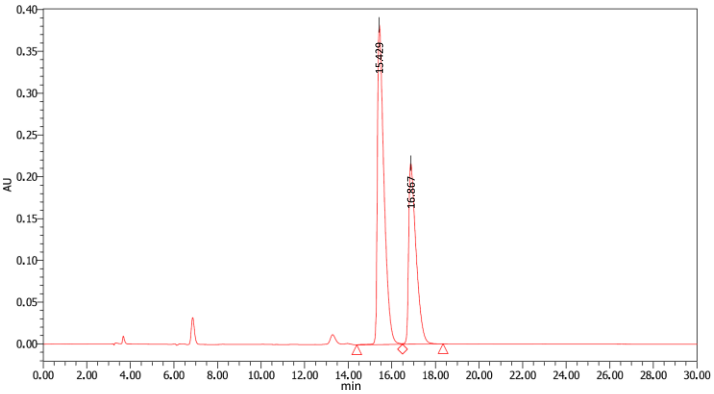

Peak No.	Ret. Time / min	area %
1(*R*)	15.429	61.01
2(*S*)	16.867	38.99

5-(Iodomethyl)-5-phenyldihydrofuran-2(3*H*)-one (7a)[66]

^{1}H NMR (400 MHz, $CDCl_3$) 7.41–7.27 (m, 5H), 3.63 (d, J = 0.9Hz, 2H), 2.82–2.49 (m, 4H); ^{13}C{^{1}H} NMR (100 MHz, $CDCl_3$) 175.5, 140.7, 128.9, 128.6, 124.9, 86.1, 34.0, 29.3, 16.4. HRMS (ESI^{+}) Calculated ($C_{11}H_{11}O_2INa$):324.9696 ([M+Na]$^{+}$), Found: 324.9688.

Chiralpak OD-3 (4.6 mm x 25 cm), hexane/*i*PrOH = 75/25, 1.0 mL min^{-1}, 30 °C, UV detection at 250.0 nm. For the racemic sample, based on the reported retention time of (*S*)- and (*R*)-**7a**, t_R = 7.123 min belongs to *S*-, t_R = 7.907 min belongs to *R*-enantiomer.

Racemate

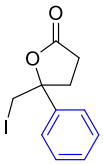

(*racemate*)

Peak No.	Ret. Time / min	area %
1(*S*)	6.885	49.54
2(*R*)	7.768	50.46

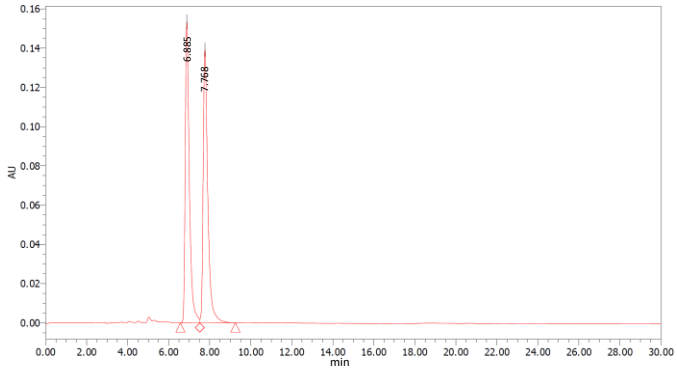

2aP=O as catalyst

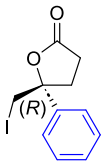

68% *ee* (20% yield)

Peak No.	Ret. Time / min	area %
1(*S*)	7.123	16.06
2(*R*)	7.907	83.94

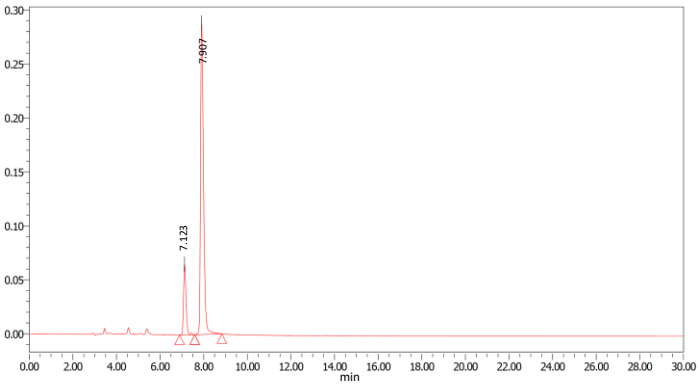

2bP=O as catalyst

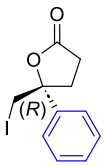

36% *ee* (37% yield)

Peak No.	Ret. Time / min	area %
1(*S*)	6.941	31.59
2(*R*)	7.903	68.41

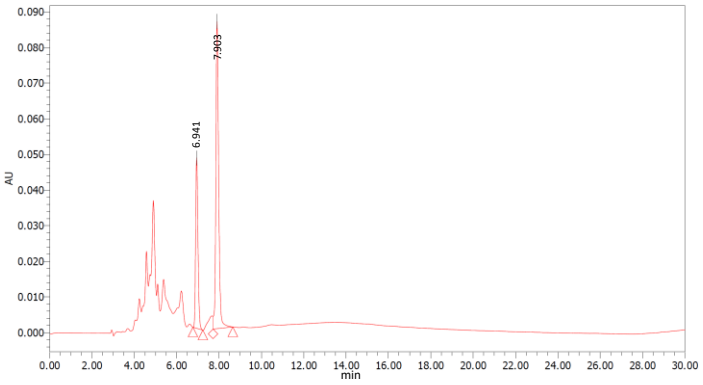

5-(4-chlorophenyl)-5-(iodomethyl) dihydrofuran-2(3*H*)-one (7b)[66]

^{1}H NMR (400 MHz, $CDCl_3$) 7.40–7.34 (m, 4H), 3.59 (q, J = 1.6, 11.2Hz, 2H), 2.84–2.68 (m, 2H), 2.64–2.48 (m, 2H); $^{13}C\{^1H\}$ NMR (100 MHz, $CDCl_3$) 175.1, 139.3, 134.7, 129.1, 126.5, 85.7, 34.0, 29.3, 15.8. HRMS (ESI$^+$) Calculated ($C_{11}H_{10}O_2INa$):358.9306 ([M+Na]$^+$), Found: 358.9299.

Chiralpak OD-3 (4.6 mm x 25 cm), hexane/*i*PrOH = 80/20, 1.0 mL min^{-1}, 30 °C, UV detection at 250.0 nm. For the racemic sample, based on the reported retention time of (*S*)- and (*R*)-**7b**, t_R = 13.148 min belongs to *S*-, t_R = 15.908 min belongs to *R*-enantiomer.

Racemate

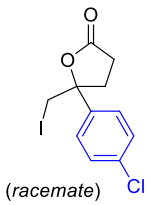

(*racemate*)

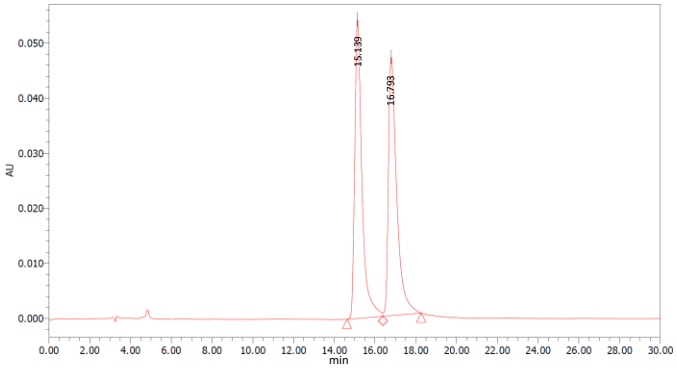

Peak No.	Ret. Time / min	area %
1(*S*)	15.139	50.21
2(*R*)	16.739	49.79

2aP=O as catalyst

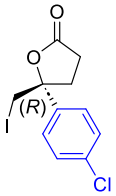

46% *ee* (5% yield)

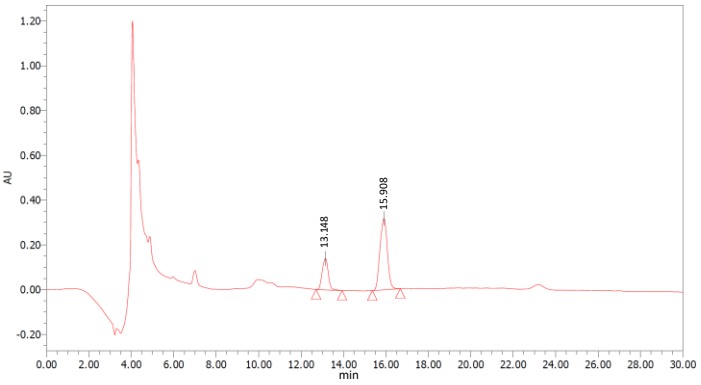

Peak No.	Ret. Time / min	area %
1(*S*)	13.148	26.68
2(*R*)	15.908	73.32

5-(iodomethyl)-5-(*p*-tolyl)dihydrofuran-2(3*H*)-one (7c)[66]

^{1}H NMR (400 MHz, $CDCl_3$) 7.29 (d, J = 8.4 Hz, 2H), 7.21 (d, J = 8.4 Hz, 2H), 3.63 (dd, J = 13.6, 11.2Hz, 2H), 2.80–2.48 (m, 4H), 2.36 (s, 3H); ^{13}C{^{1}H} NMR (100 MHz, $CDCl_3$) 175.6, 138.6, 137.6, 129.6, 124.9, 86.2, 34.0, 29.3, 21.2, 16.6.HRMS (ESI$^+$) Calculated ($C_{11}H_{13}O_2INa$): 338.9852 ([M+Na]$^+$), Found: 338.9848. Chiralpak OD-3 (4.6 mm x 25 cm), hexane/*i*PrOH = 80/20, 1.0 mL min^{-1}, 30 °C, UV detection at 250.0 nm. For the racemic sample, based on the reported retention time of (*S*)- and (*R*)-**7c**, t_R = 12.041 min belongs to *S*-, t_R = 13.810 min belongs to *R*-enantiomer.

Racemate

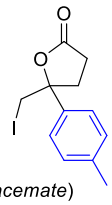

(*racemate*)

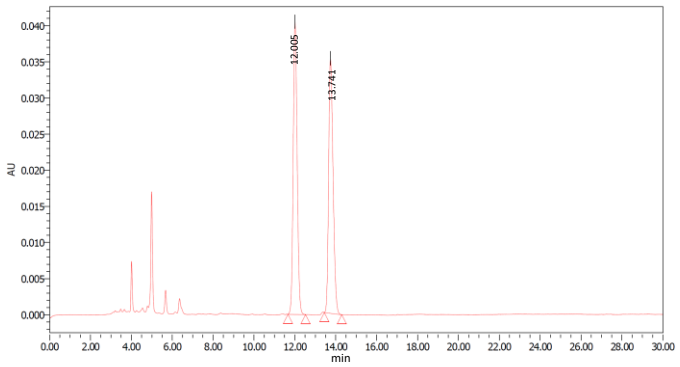

Peak No.	Ret. Time / min	area %
1(*S*)	12.005	50.50
2(*R*)	13.741	49.50

2aP=O as catalyst

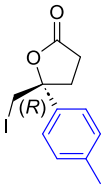

67%*ee* (30% yield)

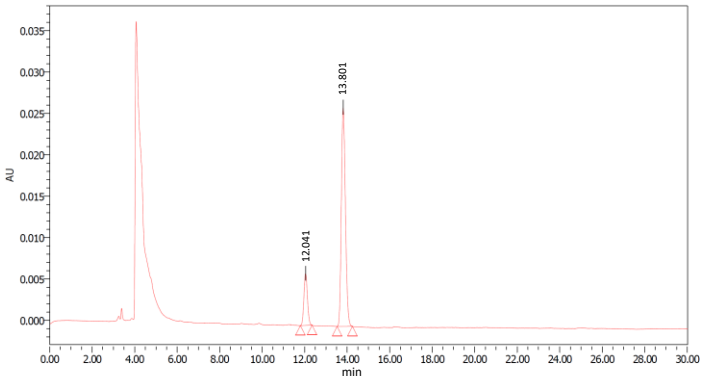

Peak No.	Ret. Time / min	area %
1(*S*)	12.041	16.91
2(*R*)	13.810	83.09

2bP=O as catalyst

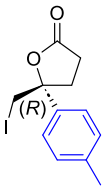

32%*ee* (30% yield)

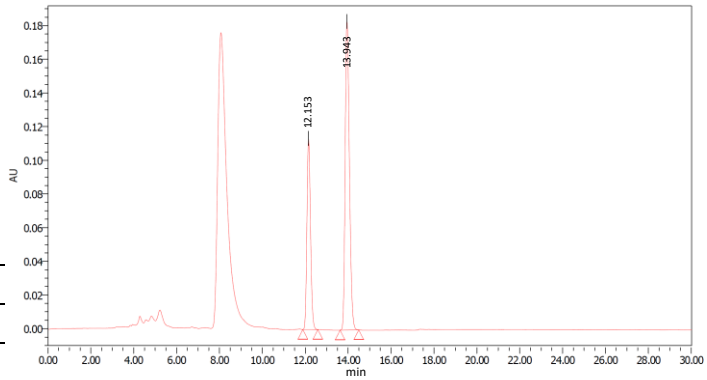

Peak No.	Ret. Time / min	area %
1(*S*)	12.041	34.50
2(*R*)	13.810	65.50

5-(iodomethyl)-5-(4-methoxyphenyl)dihydrofuran-2(3*H*)-one (7d)[66]

^{1}H NMR (400 MHz, $CDCl_3$) 7.31 (d, J = 8.8 Hz, 2H), 6.91 (d, J = 9.2 Hz, 2H), 3.81 (s, 1H), 3.59 (dd, J = 16.8, 11.2Hz, 2H), 2.71–2.54 (m, 4H); ^{13}C{^{1}H} NMR (100 MHz, $CDCl_3$) 175.6, 159.7, 132.4, 126.3, 114.2, 86.1, 55.5, 33.8, 29.4, 16.7. HRMS (ESI$^+$) Calculated ($C_{12}H_{13}O_3INa$): 357.9802 ([M+Na]$^+$), Found: 354.9813.

6-(iodomethyl)-6-phenyltetrahydro-2*H*-pyran-2-one (8a)[5]

^{1}H NMR (400 MHz, $CDCl_3$) 7.43–7.34 (m, 5H), 3.58 (t, J=11.4, 2H), 2.54–2.31 (m, 4H), 1.87–1.79 (m, 1H), 1.64–1.55 (m, 1H); ^{13}C{^{1}H} NMR (100 MHz, $CDCl_3$) 170.6, 140.3, 129.1, 128.5, 125.3, 84.5, 32.2, 29.1, 17.8, 16.6. HRMS (ESI$^+$) Calculated ($C_{12}H_{13}O_2INa$): 338.9852 ([M+Na]$^+$), Found: 338.9853.

Chiralpak IA-3 (4.6 mm x 25 cm), hexane/EtOH = 95/5, 1.0 mL min^{-1}, 30 °C, UV detection at 250.0 nm. For the racemic sample, based on the reported retention time of (*S*)- and (*R*)-**8a**, t_R = 16.614 min belongs to *S*-, t_R = 17.605 min belongs to *R*-enantiomer.

Racemate

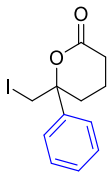

(*racemate*)

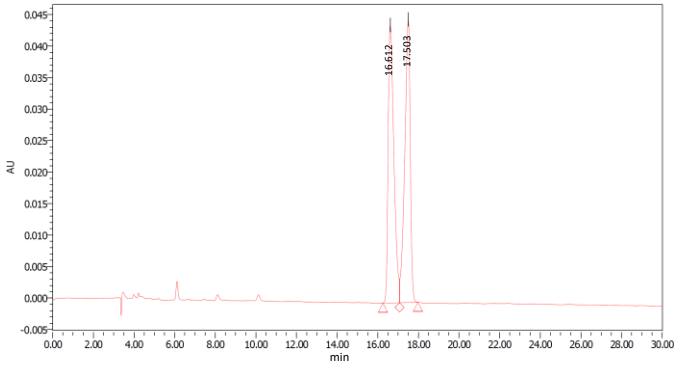

Peak No.	Ret. Time / min	area %
1(*S*)	16.612	50.72
2(*R*)	17.503	49.28

2bP=O as catalyst

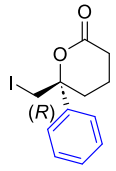

(*R*)

46% *ee* (50% yield)

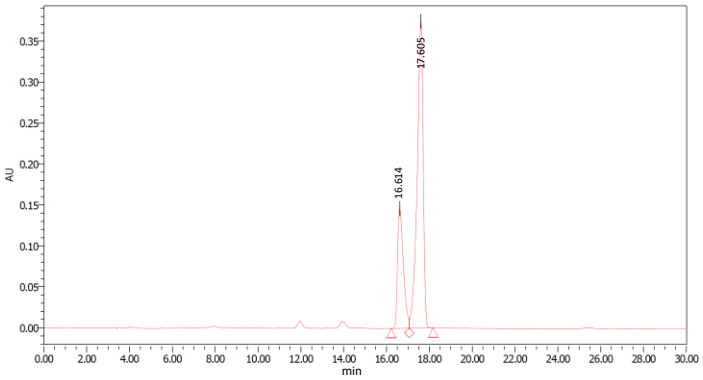

Peak No.	Ret. Time / min	area %
1(*S*)	16.614	27.59
2(*R*)	17.605	72.41

6-(4-fluorophenyl)-6-(iodomethyl)tetrahydro-2*H*-pyran-2-one (8b)[67]

^{1}H NMR (400 MHz, $CDCl_3$) 7.38–7.35 (m, 2H), 7.11–7.07 (m, 2H), 3.54 (dd, *J*=12.4, 11.2 Hz, 2H), 2.55–2.31 (m, 4H), 1.88–1.81 (m, 1H), 1.65–1.55 (m, 1H); ^{13}C{^{1}H} NMR (100 MHz, $CDCl_3$) 170.3, 162.6 (d, $^1J_{C\text{-}F}$=249.70 Hz), 136.1, 127.3 (d, $^3J_{C\text{-}F}$=8.1 Hz, 2C), 116.0 (d, $^2J_{C\text{-}F}$=21.6 Hz), 84.2, 32.0, 29.1, 17.6, 16.6. HRMS (ESI$^+$) Calculated ($C_{12}H_{12}O_2FINa$): 356.9758 ([M+Na]$^+$), Found: 356.9761.

Chiralpak IA-3 (4.6 mm x 25 cm), hexane/EtOH = 95/5, 1.0 mL min^{-1}, 30 °C, UV detection at 250.0 nm. For the racemic sample, based on the reported retention time of (*S*)- and (*R*)-**8b**, t_R = 15.188 min belongs to *S*-, t_R = 17.288 min belongs to *R*-enantiomer.

Racemate

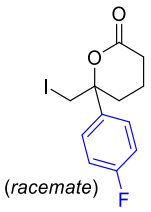

(*racemate*)

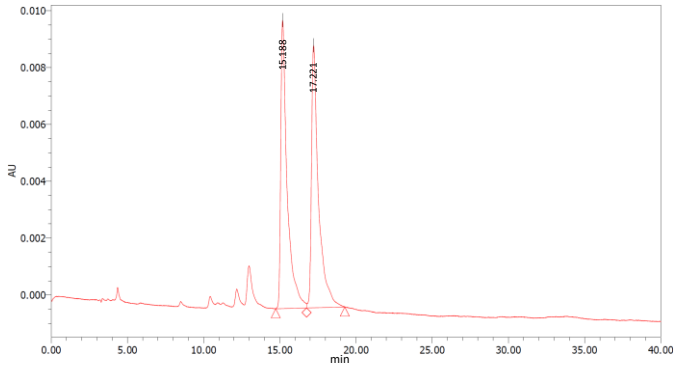

Peak No.	Ret. Time / min	area %
1(*S*)	15.188	50.08
2(*R*)	17.221	49.92

2bP=O as major enantiomer

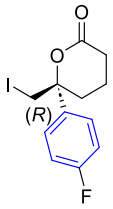

49% *ee* (30% yield)

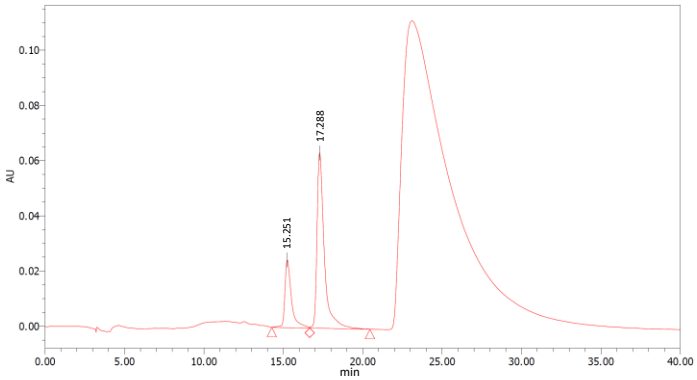

Peak No.	Ret. Time / min	area %
1(*S*)	15.251	25.80
2(*R*)	17.288	74.20

6-(iodomethyl)-6-(*p*-tolyl)tetrahydro-2*H*-pyran-2-one (8c)[67]

^{1}H NMR (400 MHz, $CDCl_3$) 7.25–7.18 (m, 4H), 3.54 (dd, J = 12.8, 11.2Hz, 2H), 2.50–2.31 (m, 7H), 1.83–1.77 (m, 1H), 1.62–1.53 (m, 1H); ^{13}C{^{1}H} NMR (100 MHz, $CDCl_3$) 170.7, 138.4, 137.2, 129.8, 125.2, 84.5, 32.0, 29.0, 21.1, 18.0, 16.6. HRMS (ESI$^+$) Calculated ($C_{13}H_{15}O_2INa$): 353.0009 ([M+Na]$^+$), Found: 353.0011.

Chiralpak OD-3 (4.6 mm x 25 cm), hexane/EtOH = 95/5, 1.0 mL min^{-1}, 30 °C, UV detection at 250.0 nm. For the racemic sample, based on the reported retention time of (*S*)- and (*R*)-**8c**, t_R = 9.674 min belongs to *S*-, t_R = 11.285 min belongs to *R*-enantiomer.

Racemate

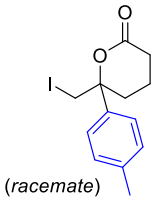

(*racemate*)

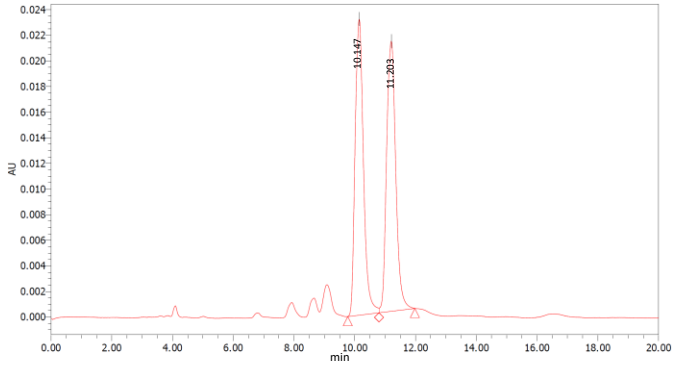

Peak No.	Ret. Time / min	area %
1(*S*)	10.147	50.02
2(*R*)	11.203	49.98

2bP=O as catalyst

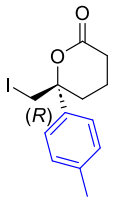

28% *ee* (40% yield)

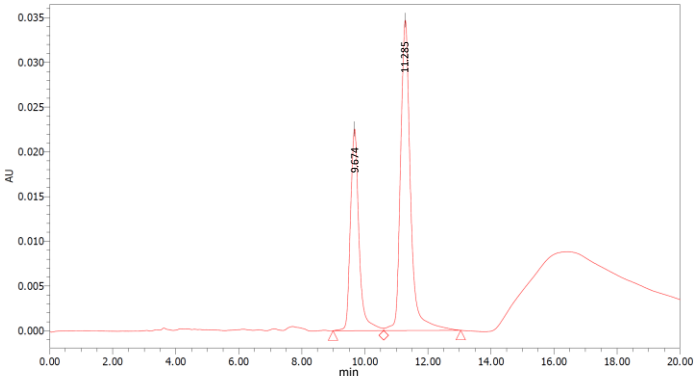

Peak No.	Ret. Time / min	area %
1(*S*)	9.674	35.97
2(*R*)	11.285	64.03

6-(iodomethyl)-6-(4-methoxyphenyl)tetrahydro-2*H*-pyran-2-one (8d)[5]

^{1}H NMR (400 MHz, $CDCl_3$) 7.30–7.27 (m, 2H), 6.92-6.90 (m, 2H) 3.82 (s, 3H), 3.58–3.51 (m, 2H), 2.48–2.33 (m, 4H), 1.86–1.78 (m, 1H), 1.67–1.55 (m, 1H); ^{13}C{^{1}H} NMR (100 MHz, $CDCl_3$) 170.7, 159.6, 132.0, 126.6, 114.4, 84.4, 55.4, 31.9, 29.0, 18.2, 16.6. HRMS (ESI$^+$) Calculated ($C_{13}H_{15}O_3INa$): 368.9958 ([M+Na]$^+$), Found: 368.9959.

2-5. Reference

[1] David J. Willock. The Point Groups Used with Molecules. *Mol. Symmetry*, John Wiley & Sons, Ltd, **2009**, pp. 45–74.

[2] David J. Willock. Symmetry in Chemical Bonding. *Mol. Symmetry*, John Wiley & Sons, Ltd, **2009**, pp. 219–297.

[3] C. Moberg, *Bull. Chem. Soc. Jpn.* **2021**, *94*, 558–564.

[4] C. Moberg, *Isr. J. Chem.* **2012**, *52*, 653–662.

[5] J. K. Whitesell, *Chem. Rev.* **1989**, *89*, 1581–1590.

[6] A. Pfaltz, W. J. Drury, *Proc. Natl. Acad. Sci.* **2004**, *101*, 5723–5726.

[7] J.-H. Xie, Q.-L. Zhou, *Acc. Chem. Res.* **2008**, *41*, 581–593.

[8] K. Ding, Z. Han, Z. Wang, *Chem. Asian J.* **2009**, *4*, 32–41.

[9] F. Yang, J.-H. Xie, Q.-L. Zhou, *Acc. Chem. Res.* **2023**, *56*, 332–349.

[10] G. E. Veitch, E. N. Jacobsen, *Angew. Chem. Int. Ed.* **2010**, *49*, 7332–7335.

[11] C. Moberg, *Angew. Chem. Int. Ed.* **1998**, *37*, 248–268.

[12] S. E. Gibson, M. P. Castaldi, *Chem. Commun.* **2006**, 3045.

[13] S. E. Gibson, M. P. Castaldi, *Angew. Chem. Int. Ed.* **2006**, *45*, 4718–4720.

[14] C. Moberg, *Angew. Chem. Int. Ed.* **2006**, *45*, 4721–4723.

[15] G. Bringmann, R.-M. Pfeifer, C. Rummey, K. Hartner, M. Breuning, *J. Org. Chem.* **2003**, *68*, 6859–6863.

[16] K. Murai, S. Fukushima, A. Nakamura, M. Shimura, H. Fujioka, *Tetrahedron* **2011**, *67*, 4862–4868.

[17] S. Bellemin-Laponnaz, L. H. Gade, *Angew. Chem. Int. Ed.* **2002**, *41*, 3473–3475.

[18] J. N. Moorthy, S. Saha, *Eur. J. Org. Chem.* **2010**, *2010*, 6359–6365.

[19] J. Chin, C. Walsdorff, B. Stranix, J. Oh, H. J. Chung, S. Park, K. Kim, *Angew. Chem. Int. Ed.* **1999**, *38*, 2756–2759.

[20] S.-G. Kim, K.-H. Kim, Y. K. Kim, S. K. Shin, K. H. Ahn, *J. Am. Chem. Soc.* **2003**, *125*, 13819–13824.

[21] J. van Gestel, A. R. A. Palmans, B. Titulaer, J. A. J. M. Vekemans, E. W. Meijer, *J. Am. Chem. Soc.* **2005**, *127*, 5490–5494.

[22] M. L. Bushey, T.-Q. Nguyen, W. Zhang, D. Horoszewski, C. Nuckolls, *Angew. Chem. Int. Ed.* **2004**, *43*, 5446–5453.

[23] T. Kubo, S. Miyazaki, T. Kodama, M. Aoba, Y. Hirao, H. Kurata, *Chem. Commun.* **2015**, *51*, 3801–3803.

[24] B. List, *Chem. Rev.* **2007**, *107*, 5413–5415.

[25] S. Mukherjee, J. W. Yang, S. Hoffmann, B. List, *Chem. Rev.* **2007**, *107*, 5471–5569.

[26] M. J. Gaunt, C. C. C. Johansson, *Chem. Rev.* **2007**, *107*, 5596–5605.

[27] T. Hashimoto, K. Maruoka, *Chem. Rev.* **2007**, *107*, 5656–5682.

[28] T. Akiyama, *Chem. Rev.* **2007**, *107*, 5744–5758.

[29] S.-H. Xiang, B. Tan, *Nat. Commun.* **2020**, *11*, 3786.

[30] O. García Mancheño, M. Waser, *Eur. J. Org. Chem.* **2023**, *26*, e202200950.
[31] K. Murai, T. Matsushita, A. Nakamura, S. Fukushima, M. Shimura, H. Fujioka, *Angew. Chem. Int. Ed.* **2010**, *49*, 9174–9177.
[32] K. Murai, A. Nakamura, T. Matsushita, M. Shimura, H. Fujioka, *Chem. Eur. J.* **2012**, *18*, 8448–8453.
[33] S. E. Denmark, G. L. Beutner, *Angew. Chem. Int. Ed.* **2008**, *47*, 1560–1638.
[34] S. E. Denmark, W. R. Collins, *Org. Lett.* **2007**, *9*, 3801–3804.
[35] A. Matviitsuk, S. E. Denmark, *Angew. Chem. Int. Ed.* **2019**, *58*, 12486–12490.
[36] S. E. Denmark, M. T. Burk, *Org. Lett.* **2012**, *14*, 256–259.
[37] S. E. Denmark, P. Ryabchuk, M. T. Burk, B. B. Gilbert, *J. Org. Chem.* **2016**, *81*, 10411–10423.
[38] H. Nakatsuji, Y. Sawamura, A. Sakakura, K. Ishihara, *Angew. Chem. Int. Ed.* **2014**, *53*, 6974–6977.
[39] Y. Lu, H. Nakatsuji, Y. Okumura, L. Yao, K. Ishihara, *J. Am. Chem. Soc.* **2018**, *140*, 6039–6043.
[40] Y. Tsuji, K. Kon, T. Horibe, K. Ishihara, *Chem. Asian. J.* **2023**, *18*, e202300019.
[41] R. C. Samanta, H. Yamamoto, *J. Am. Chem. Soc.* **2017**, *139*, 1460–1463.
[42] S. E. Denmark, A. Jaunet, *J. Am. Chem. Soc.* **2013**, *135*, 6419–6422.
[43] K. M. Hilby, S. E. Denmark, *J. Org. Chem.* **2021**, *86*, 14250–14289.
[44] T. Menard, A. Laverny, S. E. Denmark, *J. Org. Chem.* **2021**, *86*, 14290–14310.
[45] S. E. Denmark, E. Hartmann, D. J. P. Kornfilt, H. Wang, *Nat. Chem.* **2014**, *6*, 1056–1064.
[46] Z. Tao, K. A. Robb, K. Zhao, S. E. Denmark, *J. Am. Chem. Soc.* **2018**, *140*, 3569–3573.
[47] S. E. Denmark, D. J. P. Kornfilt, T. Vogler, *J. Am. Chem. Soc.* **2011**, *133*, 15308–15311.
[48] S. E. Denmark, H. M. Chi, *J. Am. Chem. Soc.* **2014**, *136*, 8915–8918.
[49] A. Konishi, H. Nakajima, H. Maruyama, S. Yoshioka, A. Baba, M. Yasuda, *Polyhedron* **2017**, *125*, 130–134.
[50] D. Tanaka, Y. Kadonaga, Y. Manabe, K. Fukase, S. Sasaya, H. Maruyama, S. Nishimura, M. Yanagihara, A. Konishi, M. Yasuda, *J. Am. Chem. Soc.* **2019**, *141*, 17466–17471.
[51] M. Yasuda, S. Yoshioka, S. Yamasaki, T. Somyo, K. Chiba, A. Baba, *Org. Lett.* **2006**, *8*, 761–764.
[52] H. Nakajima, M. Yasuda, R. Takeda, A. Baba, *Angew. Chem. Int. Ed.* **2012**, *51*, 3867–3870.
[53] A. Konishi, K. Nakaoka, H. Maruyama, H. Nakajima, T. Eguchi, A. Baba, M. Yasuda, *Chem. Eur. J.* **2017**, *23*, 1273–1277.
[54] D. Tanaka, Y. Tsutsui, A. Konishi, K. Nakaoka, H. Nakajima, A. Baba, K. Chiba, M. Yasuda, *Chem. Eur. J.* **2020**, *26*, 15023–15034.
[55] Y. Tsutsui, D. Tanaka, Y. Manabe, Y. Ikinaga, K. Yano, K. Fukase, A. Konishi, M. Yasuda, *Chem. – A Eur. J.* **2022**, *28*, e202202284.
[56] D. Tanaka, A. Konishi, M. Yasuda, *Chem. Asian J.* **2021**, *16*, 3118–3123.
[57] X. Liu, K. Tomita, A. Konishi, M. Yasuda, *Chem. Eur. J.* **2023**, *29*, e202302611.
[58] J. Kobayashi, Y. Domoto, T. Kawashima, *Chem. Lett.* **2010**, *39*, 134–135.
[59] G. W. Svetich, C. N. Caughlan, *Acta Crystallogr.* **1965**, *19*, 645–650.
[60] A. Sakakura, K. Ishihara, *Chem. Rec.* **2015**, *15*, 728–742.
[61] R. Kristianslund, J. E. Tungen, T. V. Hansen, *Org. Biomol. Chem.* **2019**, *17*, 3079–3092.

[62] A. Sakakura, A. Ukai, K. Ishihara, *Nature* **2007**, *445*, 900–903.

[63] R. Nishiyori, K. Okuno, B. Chan, S. Shirakawa, *Chem. Pharm. Bull.* **2022**, *70*, c22-00049.

[64] J. E. Tungen, J. M. J. Nolsøe, T. V. Hansen, *Org. Lett.* **2012**, *14*, 5884–5887.

[65] O. V. Dolomanov, L. J. Bourhis, R. J. Gildea, J. A. K. Howard, H. Puschmann, *J. Appl. Crystallogr.* **2009**, *42*, 339–341.

[66] J. Haas, S. Piguel, T. Wirth, *Org. Lett.* **2002**, *4*, 297–300.

[67] T. Arai, N. Sugiyama, H. Masu, S. Kado, S. Yab, M. Yamanaka, *Chem. Commun.* **2014**, *50*, 8287–8290.

Chapter 3: Chiral Recognition of Carboxylic Acids and Amino Acids Using *C*$_3$-Symmetric Cage-Shaped Phosphates as Chiral-Shift Reagents

3-1. Introduction

Chiral recognition, such as enantioselective interactions of enzymes with chiral substrates, is one of the most critical issues concerning biological activity. In the field of organic chemistry, developing catalytic asymmetric reactions has become a prominent topic because enantiomerically pure molecules exhibit identical physical properties but often distinct pharmacological activity.[1] Determining enantiomeric purity is also a vital step in asymmetric synthesis.[2] Among various methodologies, including chiral chromatographic analysis and measuring specific rotation, the use of chiral-shift reagents (CSRs) in NMR spectroscopy provides a direct method for the determination of optical purity.[3] The main advantages of CSRs are shorter measurement times, lower operational costs, and better compatibility with complex reaction mixtures.[4][5] Chiral lanthanide-based shift reagents represent a particularly interesting class of CSRs.[6] However, the paramagnetic properties of lanthanide ions can cause significant line broadening in NMR spectra, which results in reduced resolution and sensitivity in spectra recorded under routine or low-field conditions.[7–10]

To date, a wide variety of chiral compounds have been reported as suitable prospective CSRs, such as chiral amides,[11,12] chiral macrocyclic compounds,[13,14] and anionic octahedral metal complexes.[15,16] Despite significant advancements in this area, there is still a high demand for effective CSRs. For example, the chiral zwitterionic phosphorus-containing heterocycle **1** was synthesized and applied for the enantiodifferentiation of chiral carboxylic acids (Figure 1a). However, the narrow applicability, with only three examples, remains a problem.[17] Since chiral organophosphates have significantly contributed to the field of asymmetric organocatalysis,[18,19] researchers have also explored the enantiodifferentiation of chiral organophosphates.[20,21] While chiral amino acids have been investigated as CSRs for ^{31}P NMR measurements, some challenges remain due to the need for prolonged acquisition times and relatively high concentrations of the analytes (Figure 1b).[22,23]

In the research group I belong to, a series of cage-shaped compounds that contain a main-group-element center.[24–29] have been established. I have recently reported *C*$_3$-symmetric cage-shaped homochiral phosphates of the type **2**P=O for chiral Lewis-basic catalysts in asymmetric iodolactonization reactions.[29] Herein, I demonstrate the application of **2**P=O as CSRs for the enantiodifferentiation of chiral amino acids and carboxylic-acid derivatives (Figure 1c). Examples of chiral phosphate esters being used as CSRs are rare, and the structure–property relationship is investigated.

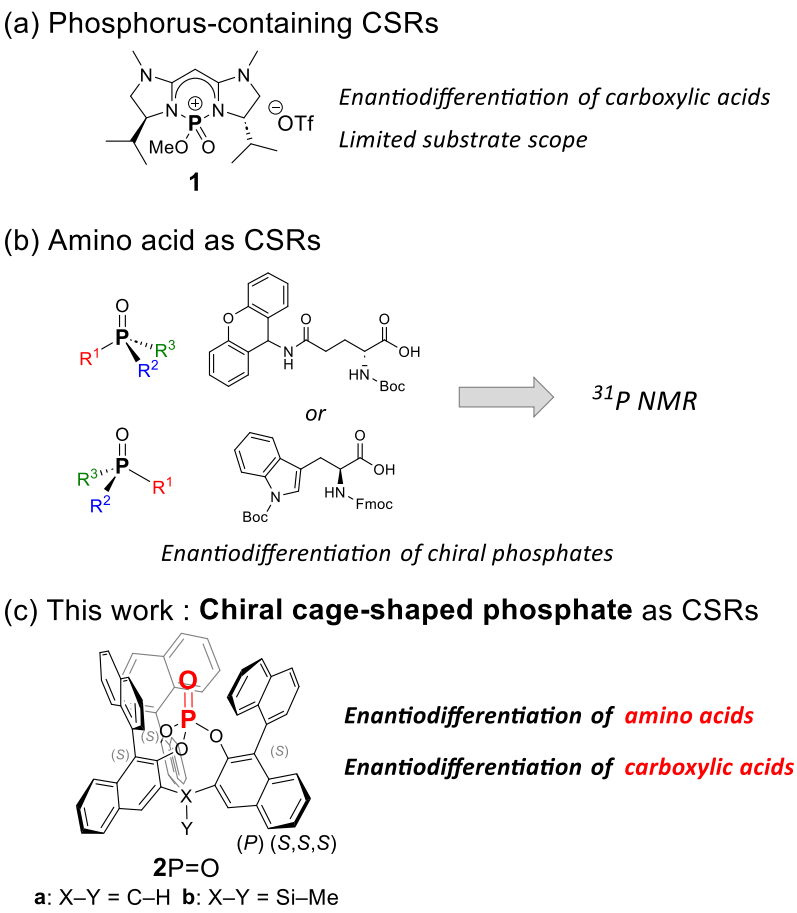

Figure 1. (a) Chiral phosphorus-containing heterocycle **1**. (b) Chiral amino acids for CSRs of chiral phosphates. (c) This work: Chiral cage-shaped phosphate **2**P=O as CSRs of chiral amino acids and carboxylic-acid derivatives.

3-2. Results and Discussion

As a model system, I first evaluated the applicability of **2a**P=O as a CSR toward *N*-carbobenzoxy-2-phenylglycine (**3a**). The NMR sample was prepared by mixing equimolar amounts of **2a**P=O and racemic **3a** in $CDCl_3$ (total concentration: 20 mM). The ^{1}H NMR measurement of the fresh sample was recorded on a 400 MHz spectrometer at room temperature. By adding **2a**P=O to racemic **3a** in $CDCl_3$, the doublet signal of the α-proton of **3a** was separated into two distinct doublet signals. The chemical shift non-equivalence ($\Delta\Delta\delta$ / ppm) was 0.052 ppm, which indicates the formation of diastereomeric complexes between **2a**P=O and **3a** (Figures 2a and 2b). To confirm the enantiodifferentiation of **3a**, each enantiomer of **3a** was mixed individually with **2a**P=O under optimized conditions. The obtained ^{1}H NMR spectra clearly showed that the signal in the high-field region corresponds to (*S*)-**3a**, while the signal in the low-field region corresponds to (*R*)-**3a** (Figures 2c and 2d). These results demonstrate that **2a**P=O forms diastereomeric complexes with the two enantiomers, thus enabling their effective discrimination by NMR spectroscopy. Although the clear signal separation was observed in the ^{1}H NMR measurements, the response of the ^{31}P NMR signal to the chiral recognition of **3a** was ineffective. No clear signal shift of the P center of **2a**P=O was observed in the ^{31}P NMR measurements.

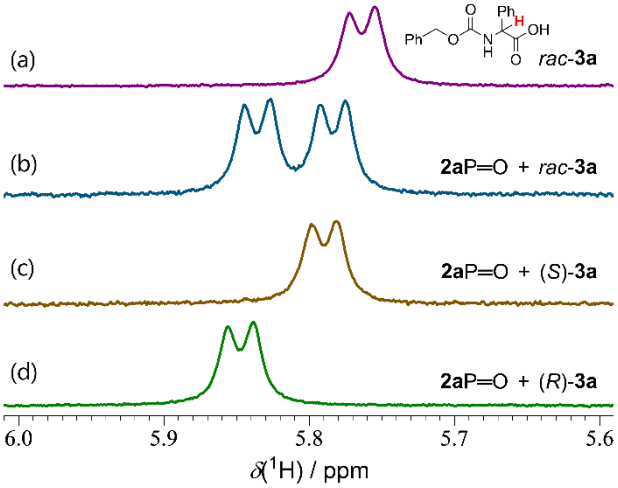

Figure 2. Partial ^{1}H NMR spectra ($CDCl_3$, 400 MHz, rt) of mixtures of **2a**P=O and **3a**: (a) Racemic **3a**; (b) 1:1 mixture of **2a**P=O and *rac*-**3a**; (c) 1:1 mixture of **2a**P=O and (*S*)-**3a**; (d) 1:1 mixture of **2a**P=O and (*R*)-**3a**.

I further investigated the ability of **2a**P=O to act as a CSR with various other amino acids (**3**) (Table 1). In addition to **3a** (entry 1), the *N*-Fmoc-protected analog **3b** was also effectively recognized by **2a**P=O (entry 2). The observed $\Delta\Delta\delta$ of the α-proton of **3b** (0.062 ppm) was larger than that of **3a**. Amino-acid derivative **3c**, which is known as MacMillan's chiral organocatalyst,[30] was also suitable when adding two equivalents of **2a**P=O (entry 3). Amino-acid derivative **3d** required four equivalents of **2a**P=O to achieve sufficient enantiodifferentiation in the signal splitting of the *tert*-butyl protons on the protecting group (entry 4). This result should most likely be interpreted in terms of the bulky substituents on **3d**, which can be expected to hinder interactions with **2a**P=O. In contrast, for phenylglycine derivatives **3e** and **3f**, which do not contain aromatic substituents on the terminal protecting groups, only minimal or no signal splitting was observed (entries 5–6). Replacing the α-phenyl group of **3b** with aliphatic substituents was ineffective. No enantiodifferentiation was observed for **3g** and **3h** (entries 7–8). These findings suggest that π–π stacking interactions between the aromatic moieties of the amino acids and the binaphthyl framework of **2a**P=O may stabilize the diastereomeric complexes and assist the observed enantiodifferentiation.

Table 1. Enantiomeric discrimination of amino acids (**3**) with **2a**P=O.[a]

entry	amino acid	partial ^{1}H NMR[b]	ΔΔδ /ppm
1	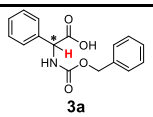 **3a**	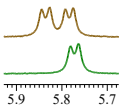	0.052
2	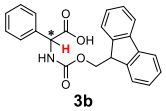 **3b**	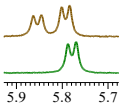	0.062
3	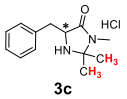 **3c**	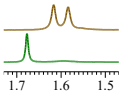	0.032[c]
4	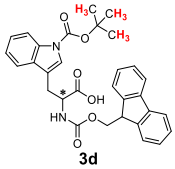 **3d**	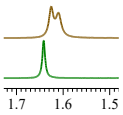	0.015[d]
5	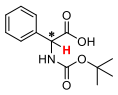 **3e**	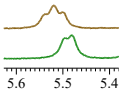	–
6	 **3f**	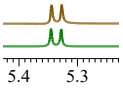	–[e]
7	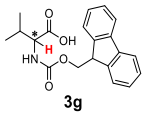 **3g**	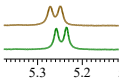	–
8	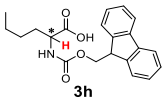 **3h**	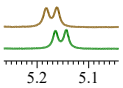	–

[a]Samples were prepared by mixing equimolar amounts of **2a**P=O and racemic **3** in $CDCl_3$ at a total concentration of 20 mM in NMR tubes. [b]Partial ^{1}H NMR spectrum ($CDCl_3$, 400 MHz) of the red proton; spectra correspond to the mixture of **3** with **2a**P=O (top) and **3** (bottom); scale: δ(^{1}H)/ppm. [c]2 equiv. of **2a**P=O. [d]4 equiv. of **2a**P=O. [e]CD_3CN was used.

Next, I explored the ability of **2a**P=O to act as a CSR with various chiral carboxylic acids (Figure 3). The ^{1}H NMR spectrum of the mixture of **2a**P=O with mandelic acid (**4a**) displayed a clear split of the singlet signal of the α-proton, resulting in two distinct signals (ΔΔδ = 0.024 ppm; Table S1). For other α-phenyl substituted carboxylic acids (**4b**–**4g**), enantiodifferentiation was also commonly observed. Carboxylic acids with electron-donating groups, such as a methyl (**4b**), methoxy (**4c**), or acetoxy (**4d**) groups, displayed smaller ΔΔδ values (0.005–0.010 ppm). In contrast, the presence of a halogen atom at the α-position resulted in increased ΔΔδ values (**4e**–**4g**). The ΔΔδ values increased in the order Br (**4e**, 0.025 ppm) < Cl (**4f**, 0.042 ppm) < F (**4g**, 0.043 ppm). This trend suggests a positive correlation between the electronegativity of the substituted halogen atom and the ΔΔδ values. When the phenyl group at the α-position of **4a** was replaced with an aliphatic group, e.g., an isopropyl (**4h**） or a *tert*-butyl (**4m**) group, the ΔΔδ values dramatically decreased. Notably, **4m** did not exhibit any signal splitting, most likely because the steric hindrance of the *tert*-butyl group prevents an efficient complexation with **2a**P=O. Mandelic-acid derivatives with a

substituted aryl group (**4i**–**4l**) were also evaluated. Although *ortho*-fluoro-substituted **4i** exhibited only weak signal separation, *para*-substituted derivatives **4j**–**4l** were subject to good signal separation with large $\Delta\Delta\delta$ values (0.017–0.032 ppm). In **4i**, an intramolecular hydrogen bonding between the *ortho*-fluorine atom and the carboxylic-acid group may hinder the intermolecular interactions with **2a**P=O.

The essential role of the carboxylic-acid group in the enantiodifferentiation was confirmed by comparisons between structurally related compound pairs. Compounds **4a**, **4b**, and **4e**, which all bear free carboxylic-acid groups, showed clear NMR signal separation in the presence of **2a**P=O. In contrast, analogs **5c**, **5a**, and **5b**, wherein the acid group was replaced by a hydroxyl or an ester group, showed no signal separation. These results demonstrate that the carboxylic-acid moiety is crucial for forming diastereomeric complexes with **2a**P=O via a certain type of hydrogen bonding. Another compound bearing an acidic functional group, such as (±)-10-camphorsulfonic acid, was inapplicable, as it showed no signal separation.

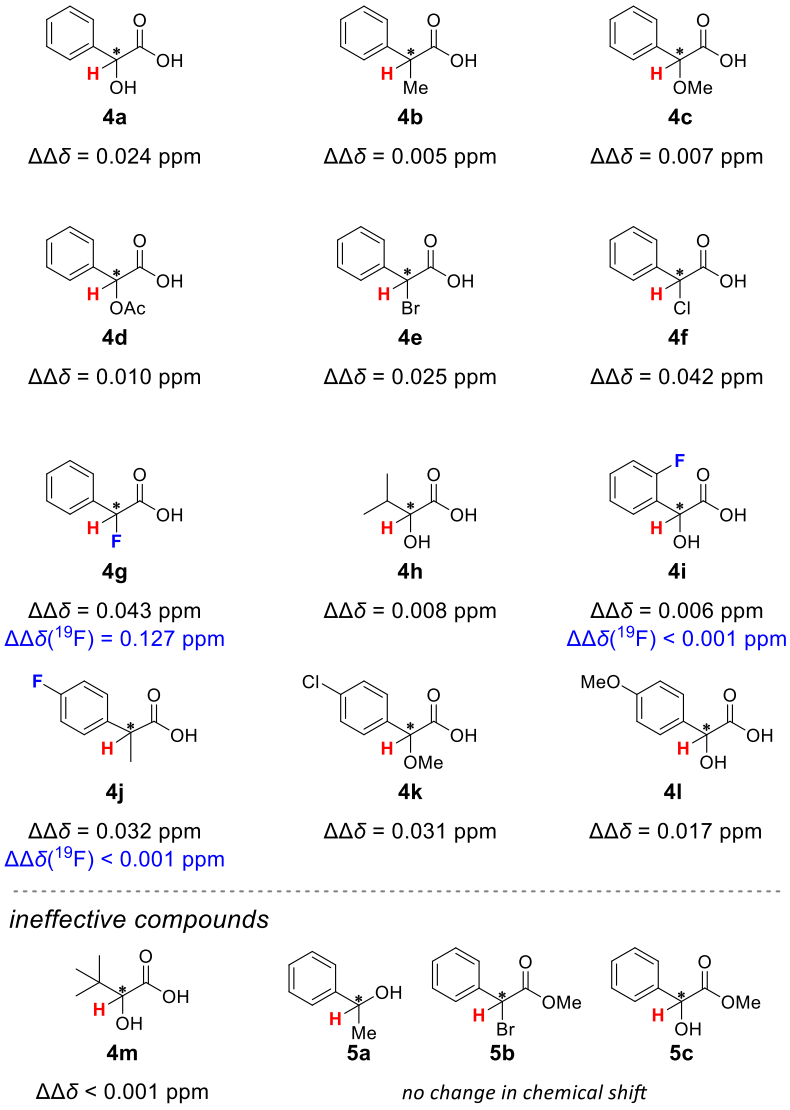

Figure 3. The ability of **2a**P=O to act as a CSR with various chiral carboxylic acids (**2a**P=O / carboxylic acid = 1:1; total concentration: 20 mM). Black $\Delta\Delta\delta$ values refer to ^{1}H NMR signals of the red protons, while blue $\Delta\Delta\delta$ values refer to ^{19}F NMR signals.

Interestingly, it is found that in the ^{19}F NMR spectra of **4g**, **4i**, and **4j**, an impact of the fluoro-substituted position on the $\Delta\Delta\delta$ value was clearly observed. When the fluorine atoms were attached to the phenyl rings of **4i** and **4j**, the $\Delta\Delta\delta$ values were negligible (Figure 4b and Table S1). In contrast, a significant $\Delta\Delta\delta$ value was observed for the ^{19}F NMR signal of **4g**, wherein the fluorine atom resides at the α-position (Figure 4a). This phenomenon should arise from the ring-current effect that originates from the chiral aromatic pocket of **2a**P=O, an interpretation consistent with our previous findings on chiral recognition using cage-shaped borates.[26]

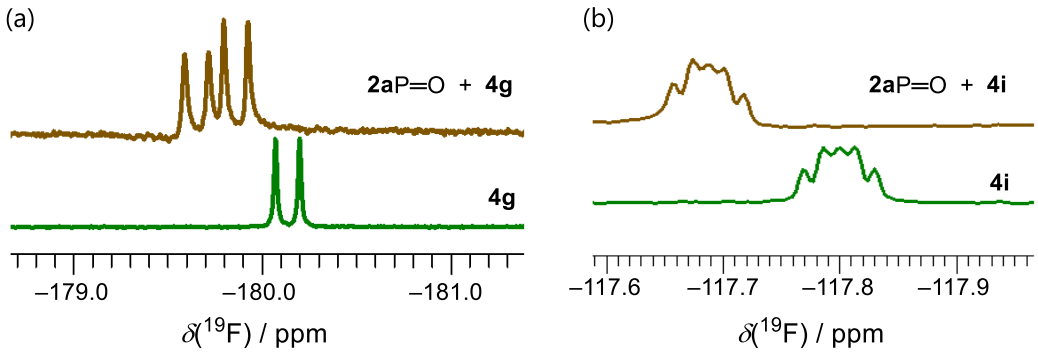

Figure 4. Signal separation in the ^{19}F NMR spectra (376 MHz, $CDCl_3$) of (a) **2a**P=O with **4g** and (b) **2a**P=O with **4i**.

To determine the factors by which **2a**P═O distinguishes chiral enantiomers, I investigated the ability of the phosphite analogue **2a**P to serve as a CSR (Figures 5a and 5b). In sharp contrast to the behavior of **2a**P═O, no enantiodifferentiation of **2a**P with **4a** was observed. The result highlights the critical role of the phosphoryl (P═O) group in **2a**P═O, which can interact with the carboxylic-acid moiety of **4a** via hydrogen bonding. Changing the tethered group (X–Y) from C–H (**2a**P=O) to Si–Me (**2b**P=O) also impacts the enantiomeric discrimination (Figure 5c). The silicon-tethered cage-shaped phosphate **2b**P=O contains a smaller chiral environment.[31][29] Although this structural feature of **2b**P=O caused a larger signal shift compared to that of **2aP**=**O**, the signal separation remained minimal, suggesting limited practical utility for enantiodifferentiation. Furthermore, (*R*)-BINOL-based phosphate **6**P═O, an open-shaped phosphate, did not induce any signal separation (Figure 5d). These results indicate that the cage-shaped scaffold of **2**P═O enhances the enantiomeric discrimination, which is induced by ring-current effects from the rigid binaphthyl moiety.

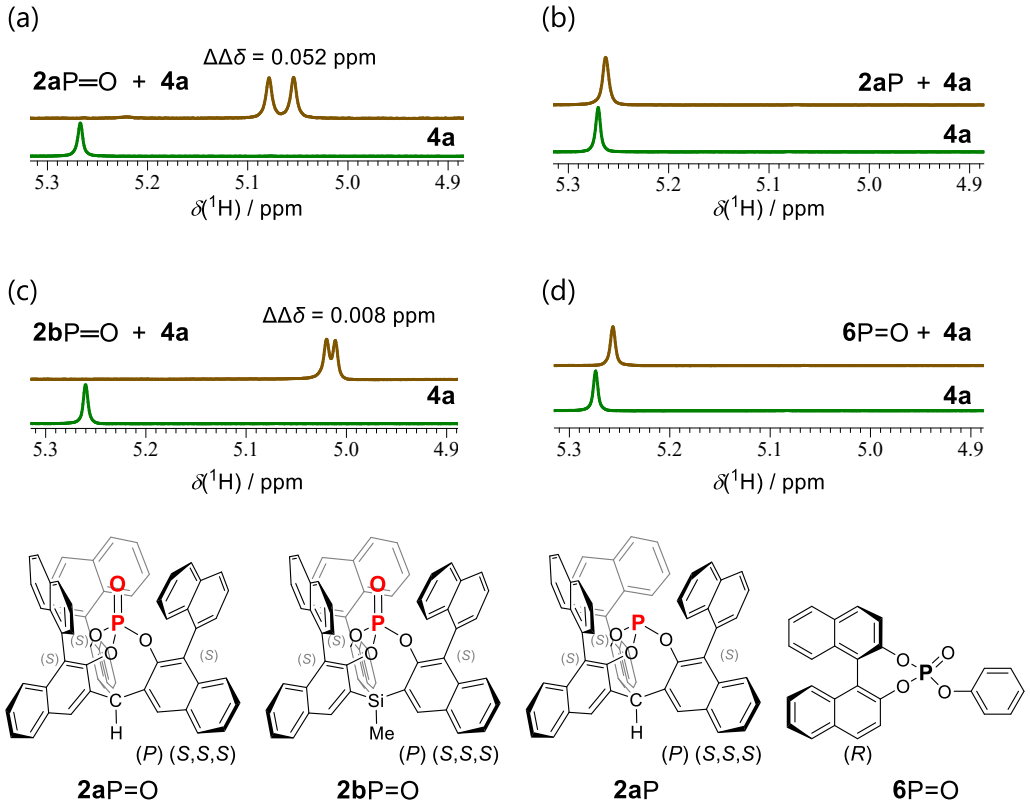

Figure 5. Partial ^{1}H NMR spectra of mixtures of phosphorus compounds **2a**P=O, **2b**P=O, **2a**P, or **6**P=O with **4a** (1:1; total concentration: 20 mM; in $CDCl_3$; 400 MHz; room temperature): (a) **2a**P=O + **4a**; (b) **2a**P + **4a**; (c) **2b**P=O + **4a**; (d) **6**P=O with **4a**; spectra correspond to mixtures of **4a** with the specified phosphorus compound (top) and **4a** (bottom).

Subsequently, the binding behavior between **2a**P=O and **3a** or **4a** was analyzed using Job plots (Figure 6). The chemical-shift differences ($\Delta\delta$) of the α-proton of **3a** or **4a** was recorded at varying molar ratios (X), where X = [**2a**P=O]/([**2a**P=O] + [**3a** or **4a**]). Both curves showed a clear maximum near X = 0.5, indicating a 1:1 binding stoichiometry of each diastereomeric complex formed between **2a**P=O and **3a** or **4a**. Moreover, it was confirmed that the intensity ratio of the separated signals correlates well with the enantiomeric excess (ee) of the analyzed solution of 4a (Figure 7 and Table S2).

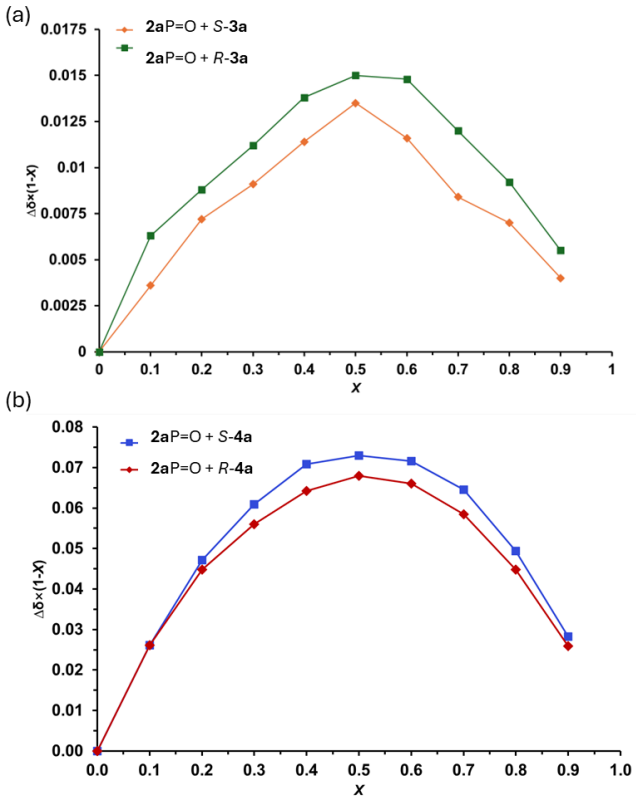

Figure 6. Job plots of **2a**P=O with (a) enantiopure (*S*)/(*R*)-**3a** with a total concentration of 10 mM. (b) enantiopure (*S*)/(*R*)-**4a** with a total concentration of 20 mM. $\Delta\delta$ stands for the chemical shift change of the a-H proton of (*S*)/(*R*)-**4a** in the presence of **2a**P=O. X stands for the molar fraction of the **2a**P=O (X = [**2a**P=O]/([**2a**P=O]+[**3a** or **4a**])).

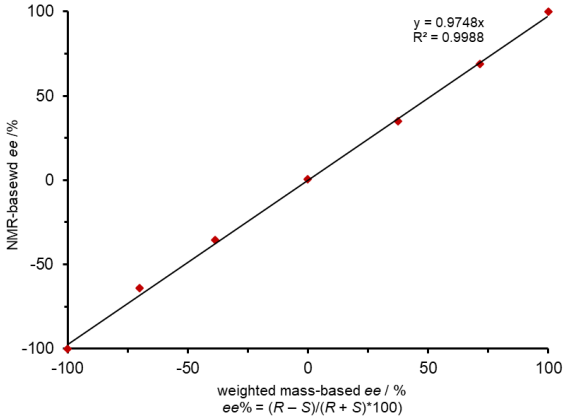

Figure 7. Linear correlation between the optical purities of **4a** and the signal intensity of its separated NMR signal when analyzed with **2a**P=O.

3-3. Conclusion

In conclusion, I have demonstrated that the chiral cage-shaped phosphate **2a**P=O is an effective chiral-shift reagent (CSR) for amino acids and carboxylic acids. The mechanism by which **2a**P=O recognizes chirality as a CSR depends on a combination of directional and conformational effects that are determined

by the P=O moiety and the rigid aromatic wall. Hydrogen bonding and π–π stacking interactions between **2a**P=O and the substrates play a crucial role in achieving enantiodifferentiation. Furthermore, the rigid *C*$_3$-symmetric three-binaphthyl scaffold produces a pronounced ring-current effect, which significantly enhances the differences in chemical shifts and facilitates clear discrimination between enantiomers in the NMR spectra. Importantly, the phosphates discussed here, especially **2a**P=O, are expected to serve as a foundational template for the development of effective NMR shift reagents, thereby opening new avenues for chiral recognition in the fields of chemistry and materials science.

3-4. Experimental Section

General Information

NMR spectra were recorded on JEOL-AL400, JEOL-ECS400 (400 MHz for ^{1}H, 100 MHz for ^{13}C, 78.7 MHz for ^{29}Si, 160 MHz for ^{31}P NMR and 376 MHz for ^{19}F NMR). For ^{31}P NMR spectra, H_3PO_4 in D_2O as an external standard was employed as an external standard. For ^{19}F NMR spectra, $BF_3{\cdot}OEt_2$ in $CDCl_3$ was employed as an external standard (–153.0 ppm). ^{1}H and ^{13}C NMR signals of compounds were assigned using HMQC, HSQC, HMBC, COSY, 1D ^{13}C NMR under conditions of proton off-resonance spin decoupling. Positive FAB/CI, EI, MALDI-TOF, ESI/DART mass spectra were recorded on a JEOL JMS-700, a Shimadzu GCMS-QP2010 Ultra, a JEOL JMS-S3000, and a JEOL JMS-T100LP respectively. IR spectra were recorded as thin films or as solids in KBr pellets on a JASCO FT/IR 6200 spectrophotometer or as solids in ATR-mode on a JASCO FT/IR-4X spectrophotometer. Data collection for X-ray crystal analysis was performed on Rigaku/XtaLAB Synergy-S/Mo (MoK$_\alpha$ λ = 0.71075 Å) and Rigaku/XtaLAB Synergy-S/Cu (CuK$_\alpha$ λ = 1.54187 Å) diffractometers. All non-hydrogen atoms were refined with anisotropic displacement parameters and hydrogen atoms were placed at calculated positions and refined “riding” on their corresponding carbon atoms by Olex2[32] program.

Materials

Anhydrous dichloromethane, THF, acetonitrile, diethyl ether, toluene and hexane were purchased and used as obtained. All reagents were obtained from commercial suppliers and used as received. All reactions were carried out under nitrogen. The CSRs **2a**P=O, **2b**P=O and **2a**P was synthesized according to our previous study.[29,31]

Synthetic procedures

(11b*R*)-4-phenoxydinaphtho[2,1-*d*:1',2'-*f*][1,3,2]dioxaphosphepine 4-oxide[33]

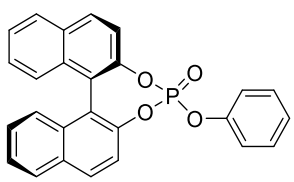

6P=O

In a Schlenk flask equipped with a J-Young bulb, triethylamine (1.00 mmol, 0.101 g) and phosphoryl

chloride (0.100 mmol, 0.0153 g) were added to a solution of (*R*)-BINOL (0.100 mmol, 0.0280 g) in toluene (5 mL). After N_2 gas was purged, the shielded reaction mixture was heated at 125 °C for 2 days. After cooling to room temperature, the reaction mixture was filtrated through a celite pad, and the obtained solution was evaporated under vacuum. The crude material was purified by column chromatography (hexane/ethyl acetate = 60:40, column length 20 cm, diameter 26 mm silica gel) to give the pure product **6**P=O as a colorless solid (0.0400 g, 94%).

^{1}H NMR (400 MHz, $CDCl_3$) 8.01 (d, *J* = 9.2 Hz, 1H), 7.95 (d, *J* = 8.8 Hz, 1H), 7.90–7.88 (m, 2H), 7.63(d, *J* = 8.8 Hz, 1H), 7.44–7.29 (m, 9H), 7.25–7.20 (m, 2H), 7.18–7.15 (m, 1H); ^{13}C{^{1}H} NMR (100 MHz, $CDCl_3$) 150.4 (d, *J* = 6.2 Hz), 147.5 (d, *J* = 11.5 Hz), 146.2 (d, *J* = 8.2 Hz), 132.4 (s), 132.1 (s), 131.9 (s), 131.5 (s), 130.1 (s, two signals were overlapped), 128.8 (s), 128.7 (s), 127.3 (s), 127.14 (s), 127.11 (s), 127.09 (s), 126.15 (s, two signals were overlapped), 125.9 (s), 121.6 (d, *J* = 2.4 Hz), 121.3 (d, *J* = 2.4 Hz), 120.7 (d, *J* = 2.9 Hz), 120.2 (d, *J* = 3.8 Hz), 120.2 (s, two signals were overlapped), 120.1 (s, two signals were overlapped); ^{31}P{^{1}H} NMR (160 MHz, $CDCl_3$) −2.54 (s).

Typical procedure for NMR analysis of chiral acids 3 and 4 with CSRs.

Chiral acids **3** and **4** are commercially available compounds and used without further purification or drying. In a NMR tube, 0.005 mmol of CSR_S (**2**P=O, **2a**P or **6**P=O) and 0.005 mmol of chiral acid analyte (**3** or **4)** were dissolved in 0.5 mL of a deuterated solvent (total concertation was 20 mM.). The ^{1}H and ^{19}F NMR spectra were recorded on a JEOL-AL400, JEOL-ECS400 spectrometer (400 MHz for ^{1}H and 376 MHz for ^{19}F NMR) with 8-time accumulations at room temperature. For the determination of *R*/*S* configuration, enantiopure or enantioenriched samples can be analyzed.

Table of investigation 2aP=O as CSR with chiral carboxylic acids.

Table S1. 2aP=O as chiral shift reagent for chiral carboxylic acids[a]

Substrates	Partial ^{1}H NMR[b]	Partial ^{19}F NMR	ΔΔδ(ppm)
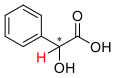 **4a**	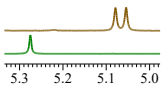		0.024
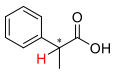 **4b**	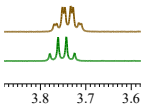		0.005
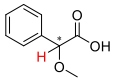 **4c**	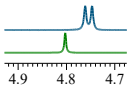		0.014[c]
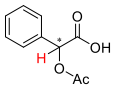 **4d**	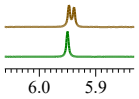		0.010
 **4e**	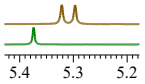		0.025
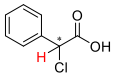 **4f**	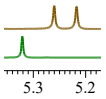		0.042
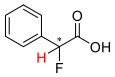 **4g**	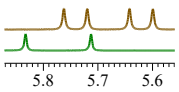	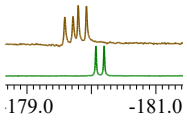	0.043 (0.127[d])
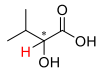 **4h**	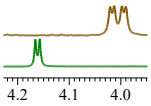		0.008
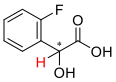 **4i**	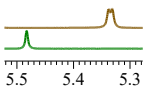	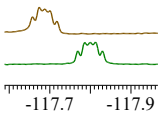	0.006 (< 0.001[d])
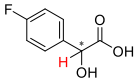 **4j**	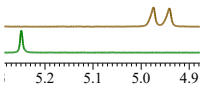	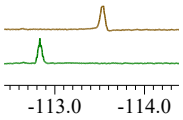	0.032 (< 0.001[d])
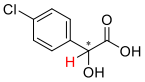 **4k**	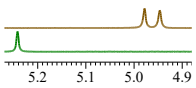		0.031
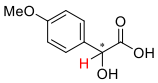 **4l**	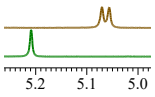		0.017
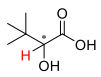 **4m**	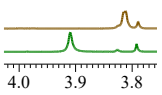		-

[a]Samples were prepared by mixing 1 equiv of **2a**P=O (10 M in $CDCl_3$) and 1 equiv of **4** (10 mM in $CDCl_3$) in NMR tubes. [b]Partial ^{1}H NMR of selected proton in red color. [c]Using 2 equiv. of **2a**P=O. [d]ΔΔδ values were from ^{19}F NMR signals.

Table S2. Correlation between the optical purities of **4a** and the signal intensity of its separated NMR signal in the when analyzed with **2a**P=O

enantiomeric excess based on the weighted mass			enantiomeric excess based on the NMR signal		
(*R*)-**4a** / mg	(*S*)-**4a** / mg	ee / %	Intensity for (*R*)-**4a**	Intensity for (*S*)-**4a**	ratio / %
1.50	0.00	100	1.34	–	100
12.9	2.13	72	1.41	0.26	69
10.9	4.95	38	1.30	0.63	35
7.58	7.59	0.0	1.00	0.99	0.0
4.87	11.0	−39	0.59	1.24	-36
2.28	13.0	−70	0.33	1.51	-64
0.00	1.50	−100	–	1.00	-100

NMR Spectra of chiral analysis of chiral acids 3 and 4 with CSRs.

^{1}H NMR (400 MHz, $CDCl_3$)

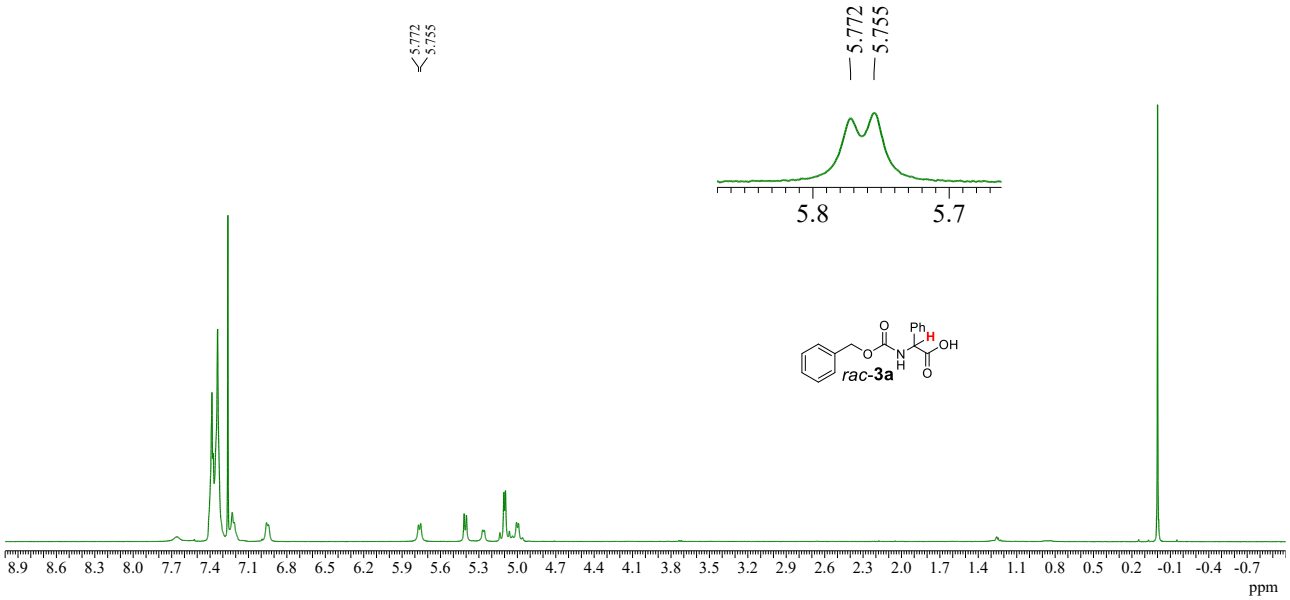

^{1}H NMR (400 MHz, $CDCl_3$)

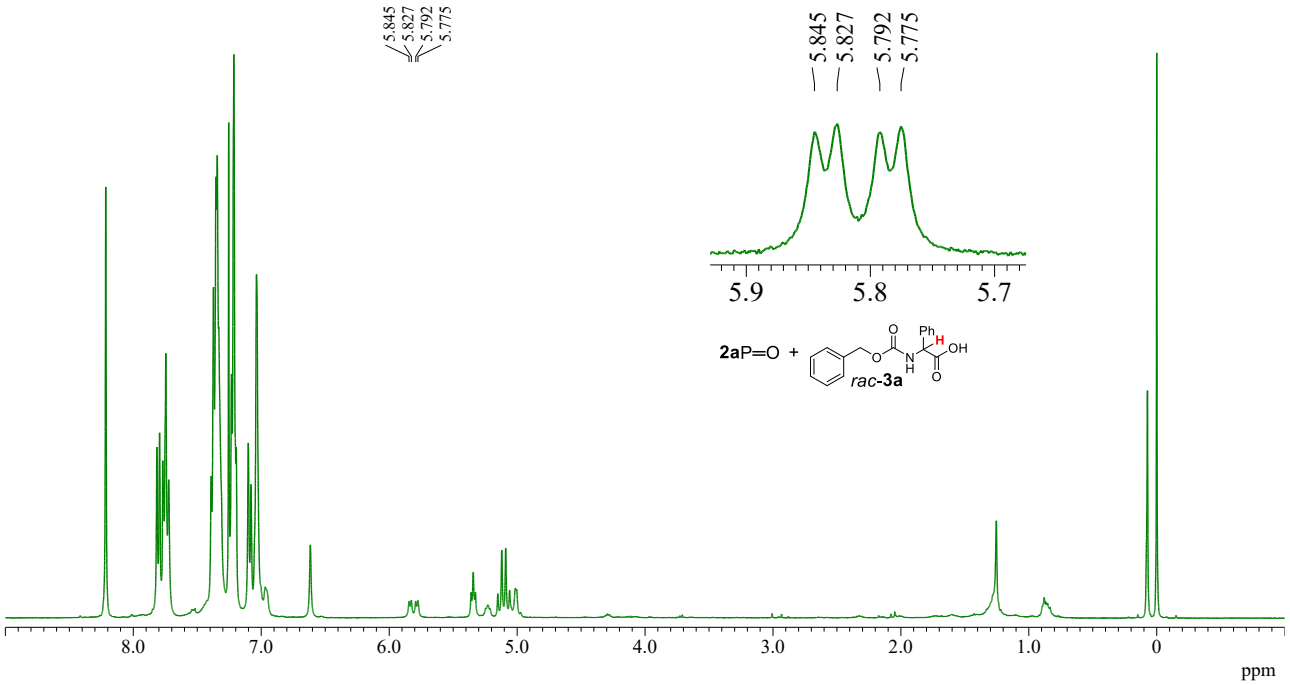

^{1}H NMR (400 MHz, $CDCl_3$)

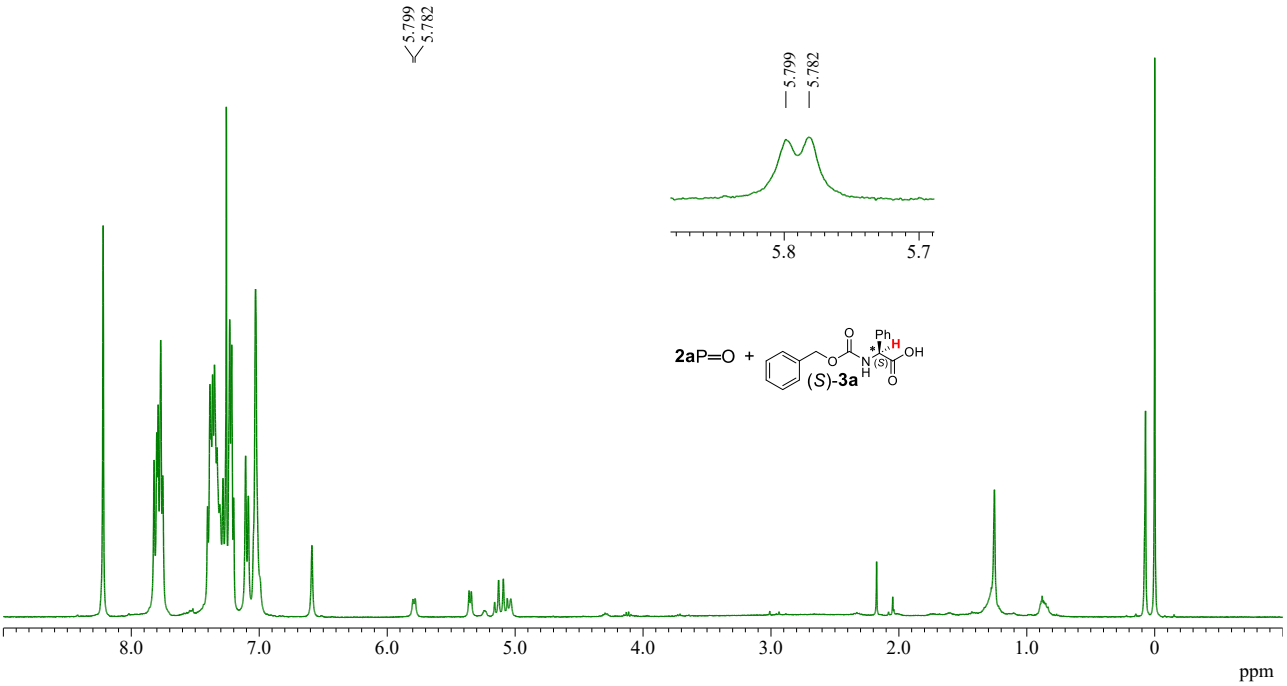

^{1}H NMR (400 MHz, $CDCl_3$)

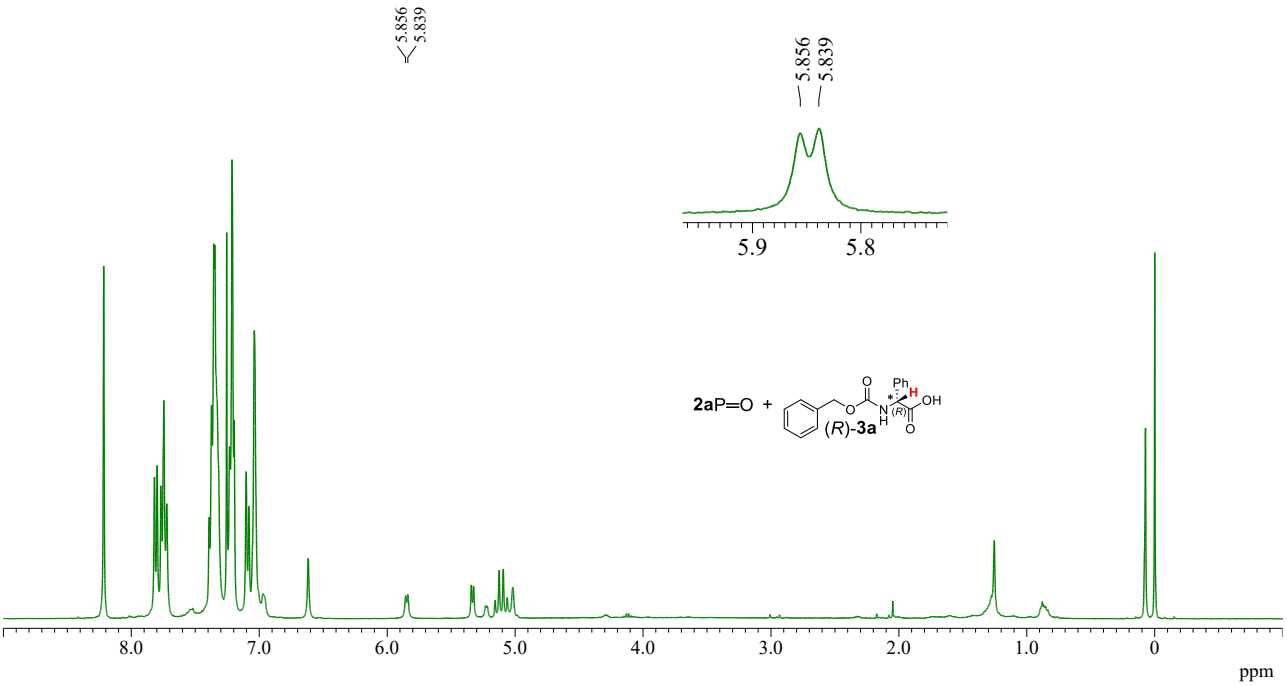

^{1}H NMR (400 MHz, $CDCl_3$)

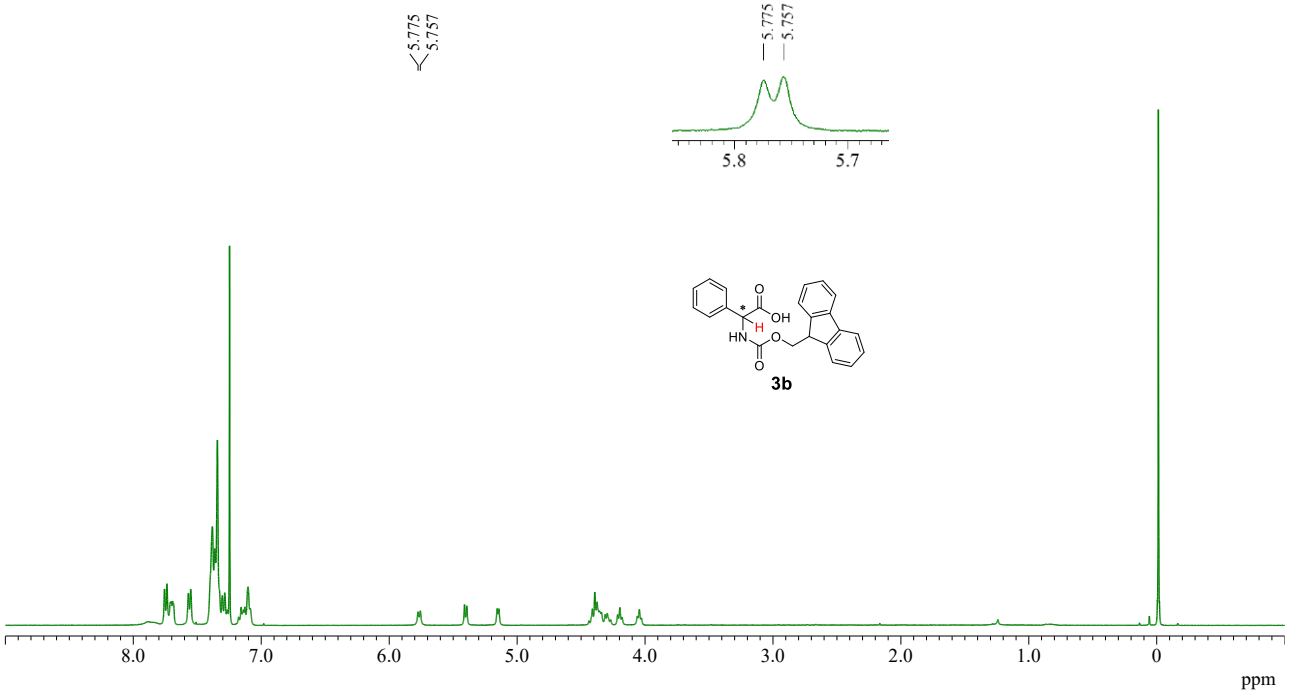

^{1}H NMR (400 MHz, $CDCl_3$)

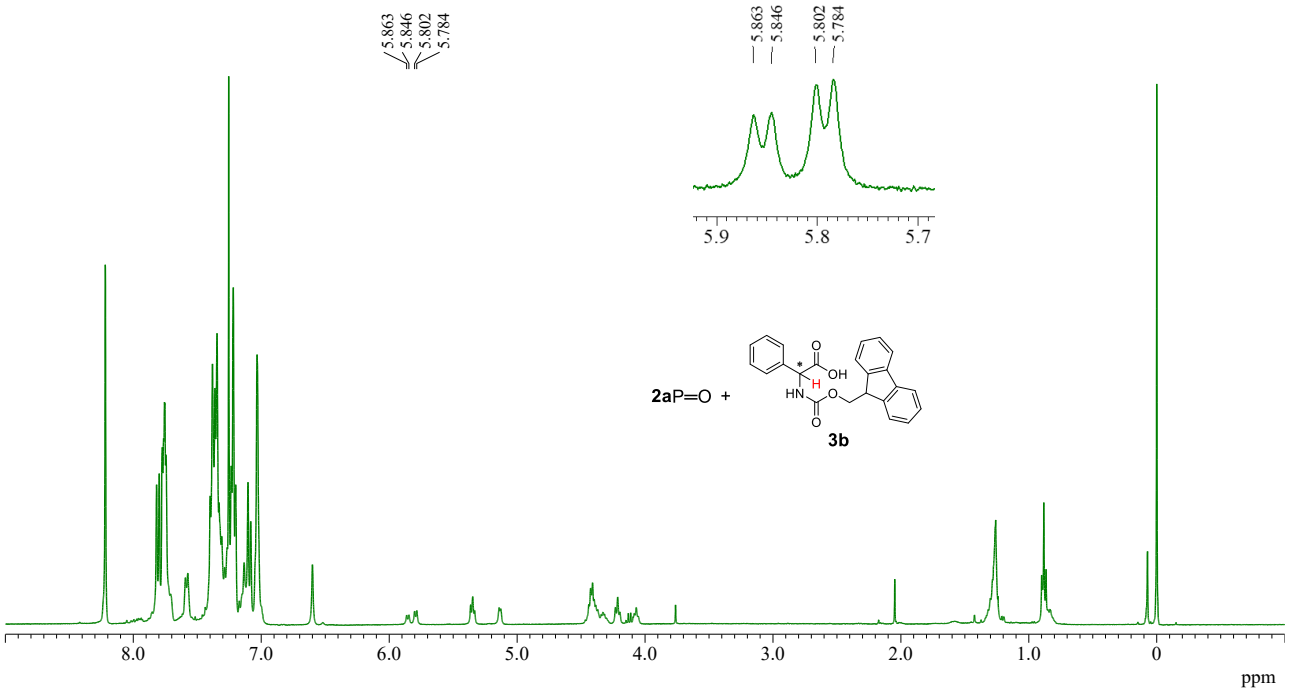

^{1}H NMR (400 MHz, $CDCl_3$)

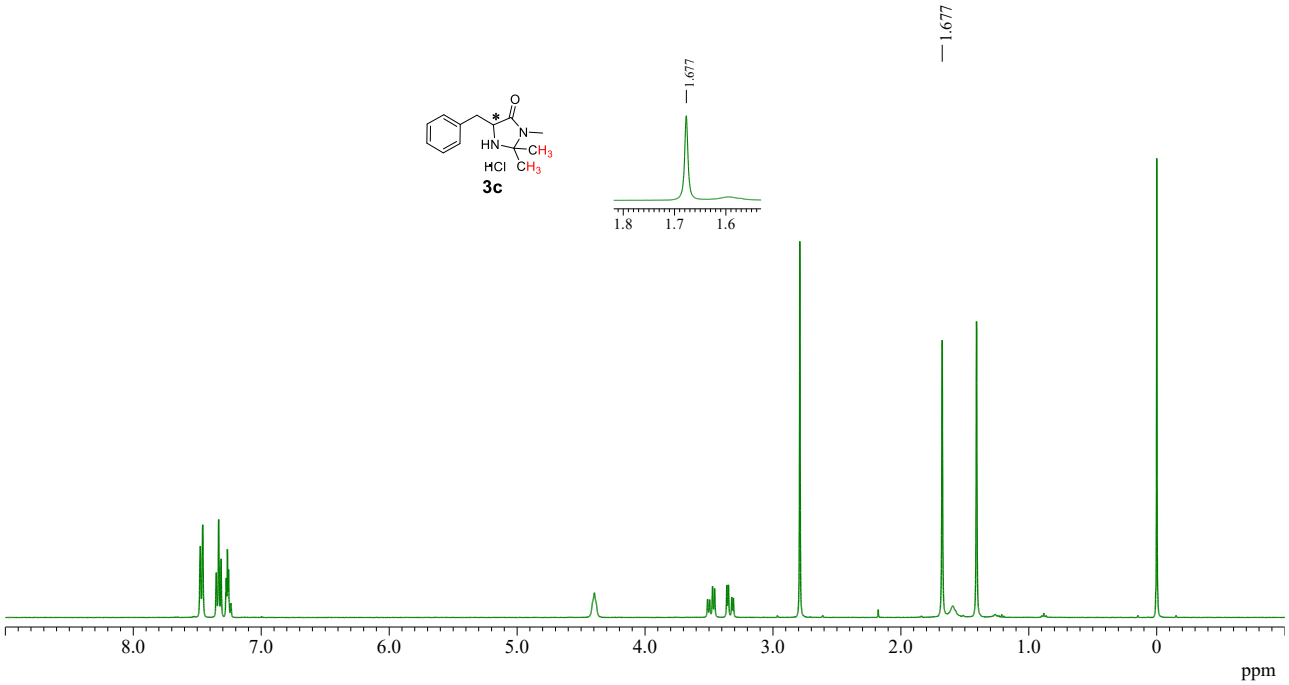

^{1}H NMR (400 MHz, $CDCl_3$)

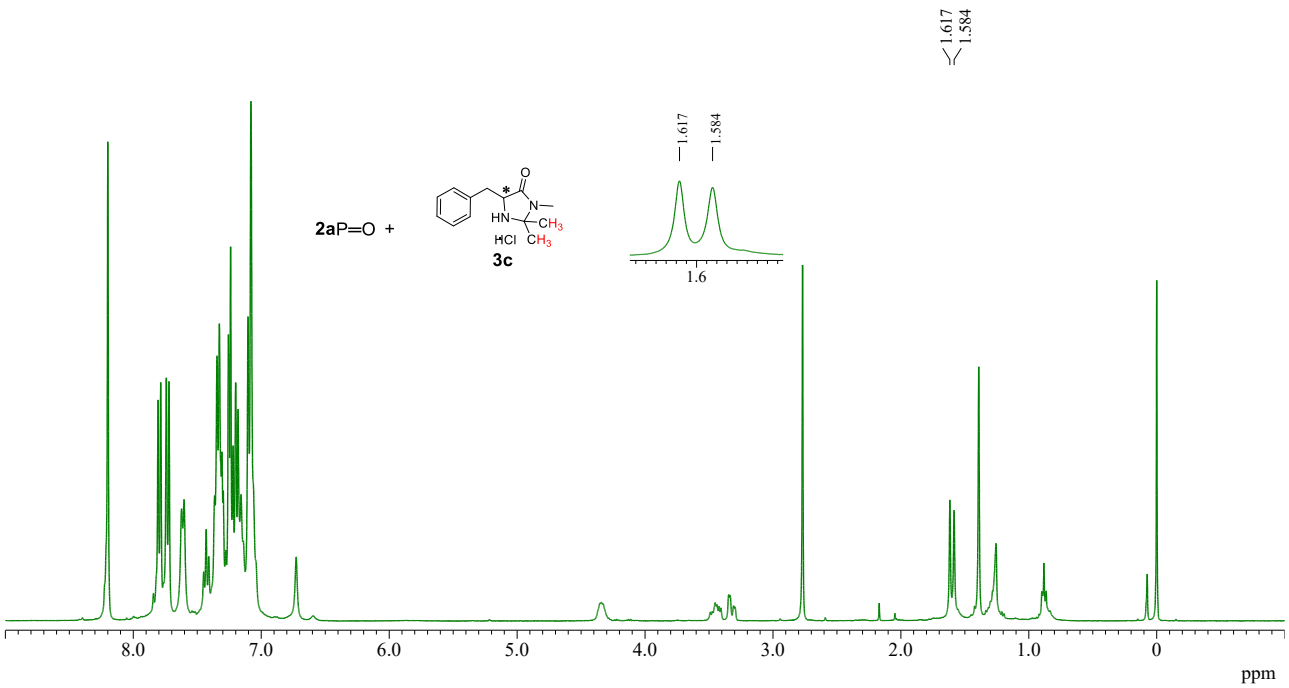

^{1}H NMR (400 MHz, $CDCl_3$)

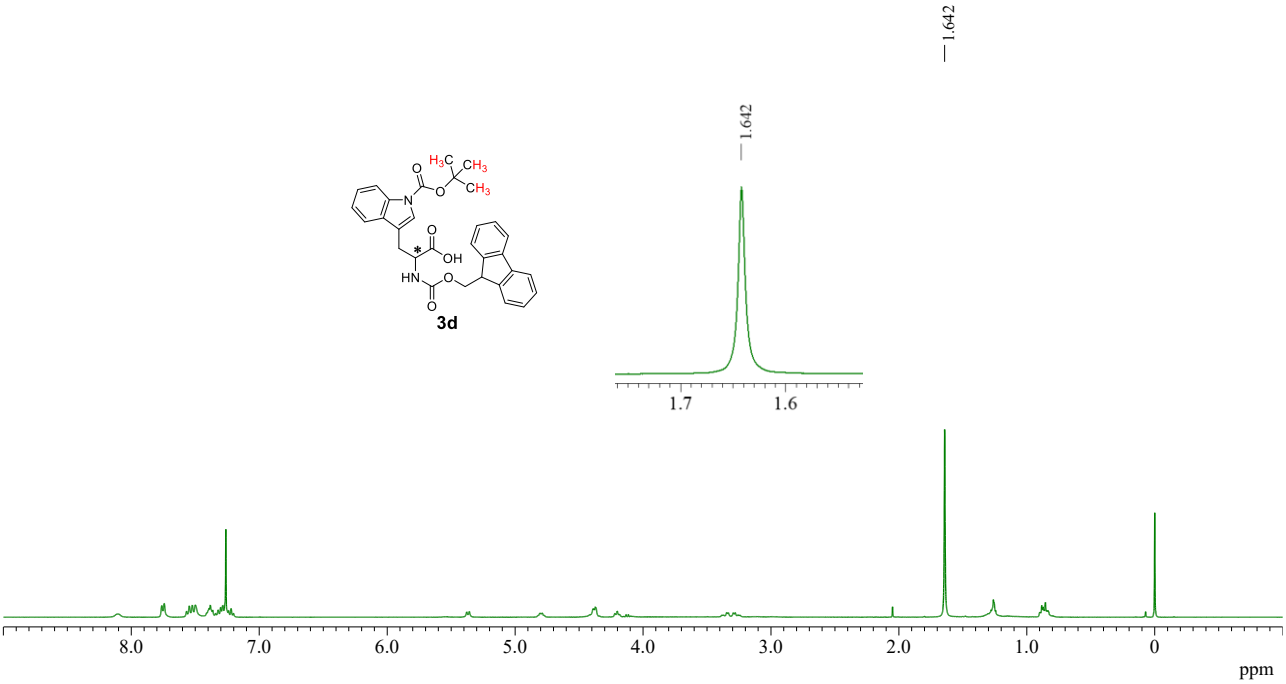

^{1}H NMR (400 MHz, $CDCl_3$)

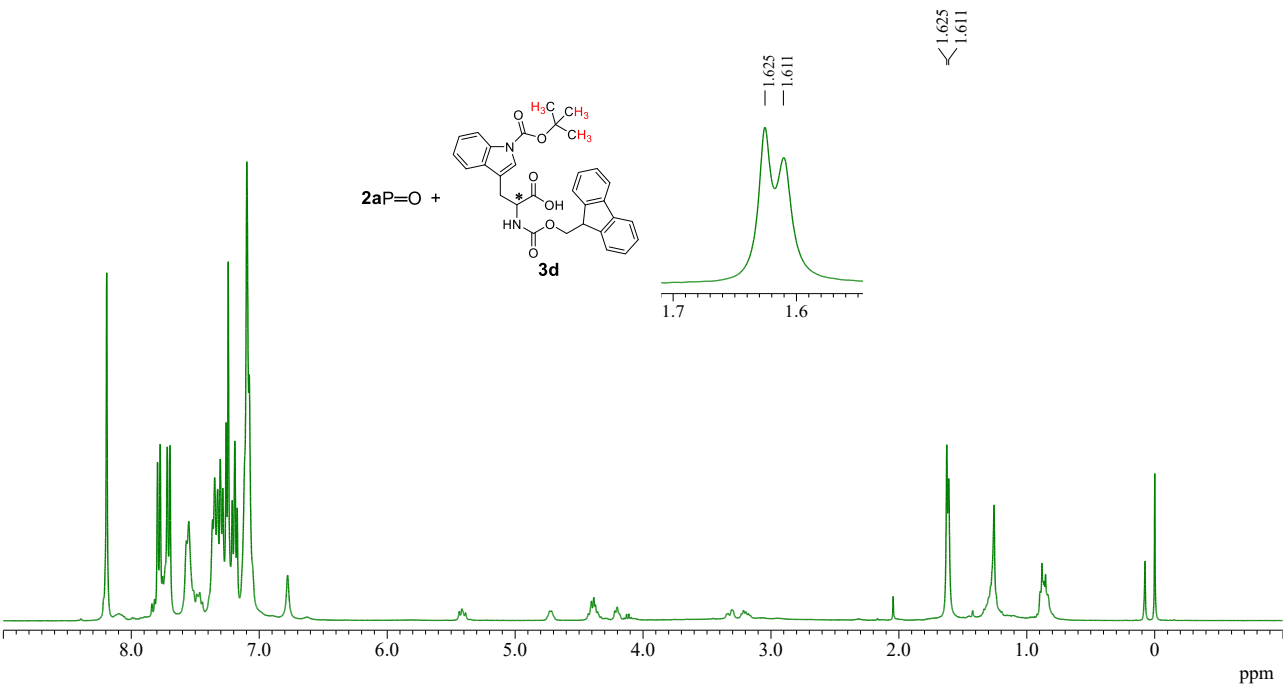

^{1}H NMR (400 MHz, $CDCl_3$)

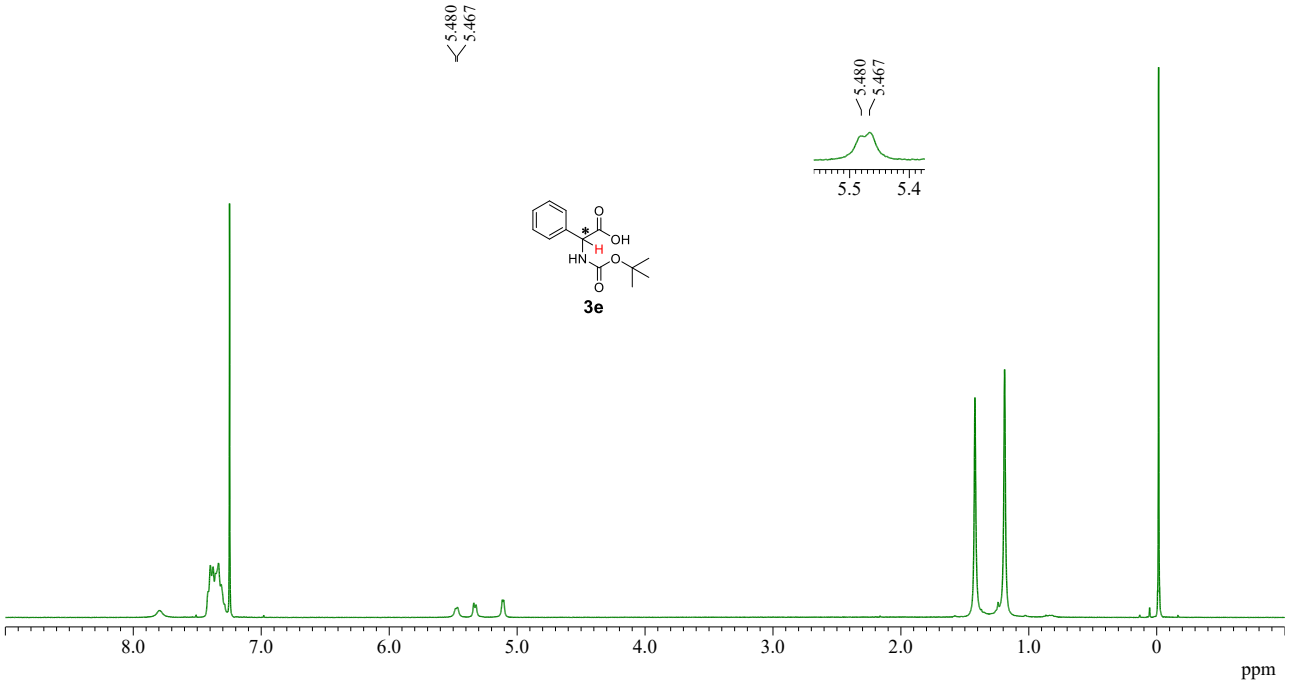

^{1}H NMR (400 MHz, $CDCl_3$)

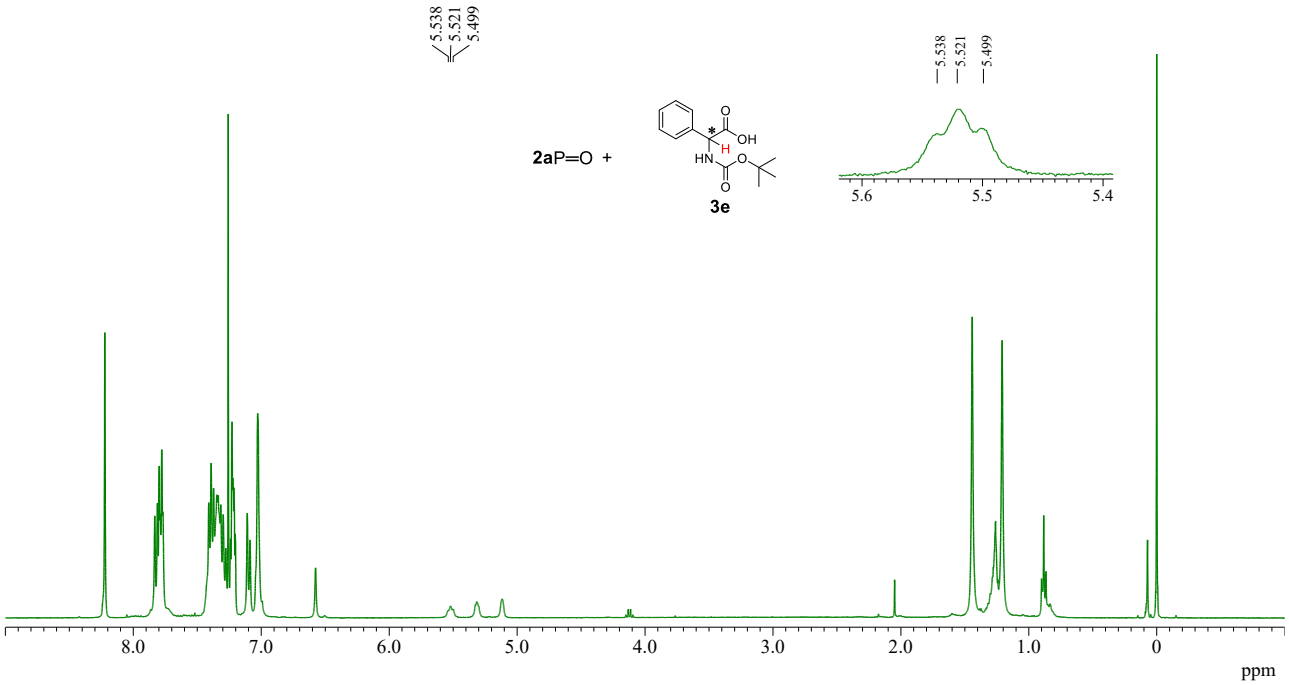

^{1}H NMR (400 MHz, CD_3CN)

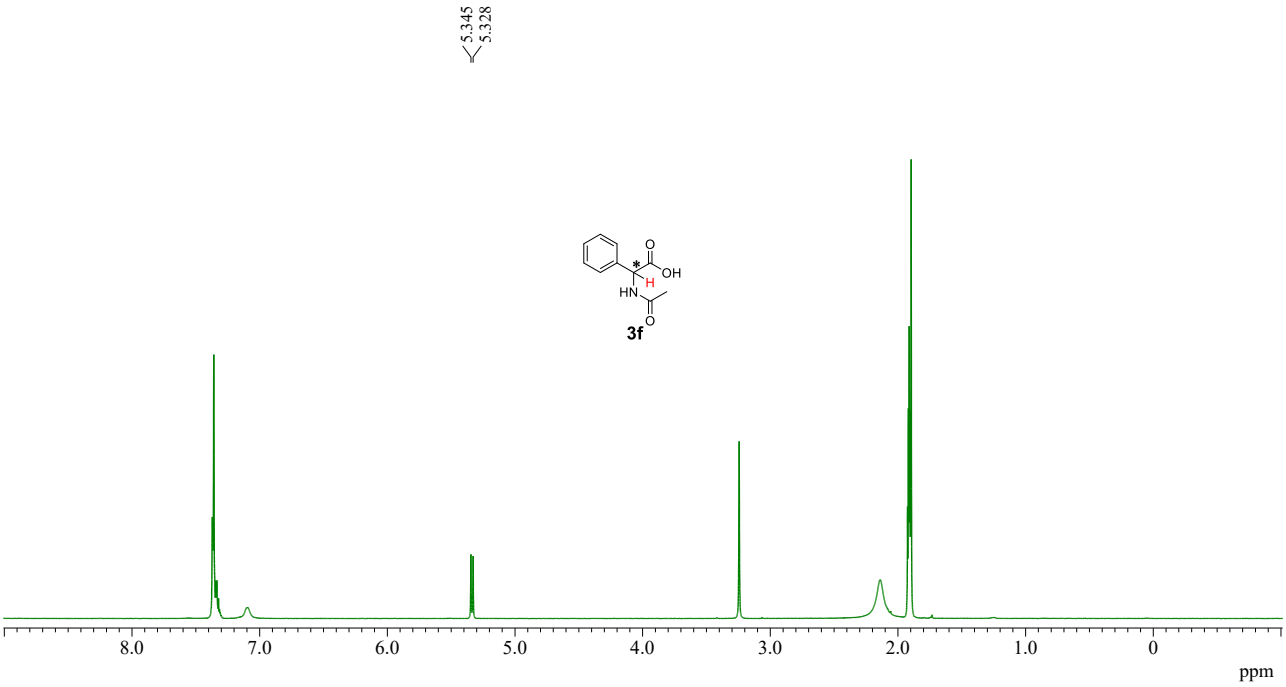

^{1}H NMR (400 MHz, CD_3CN)

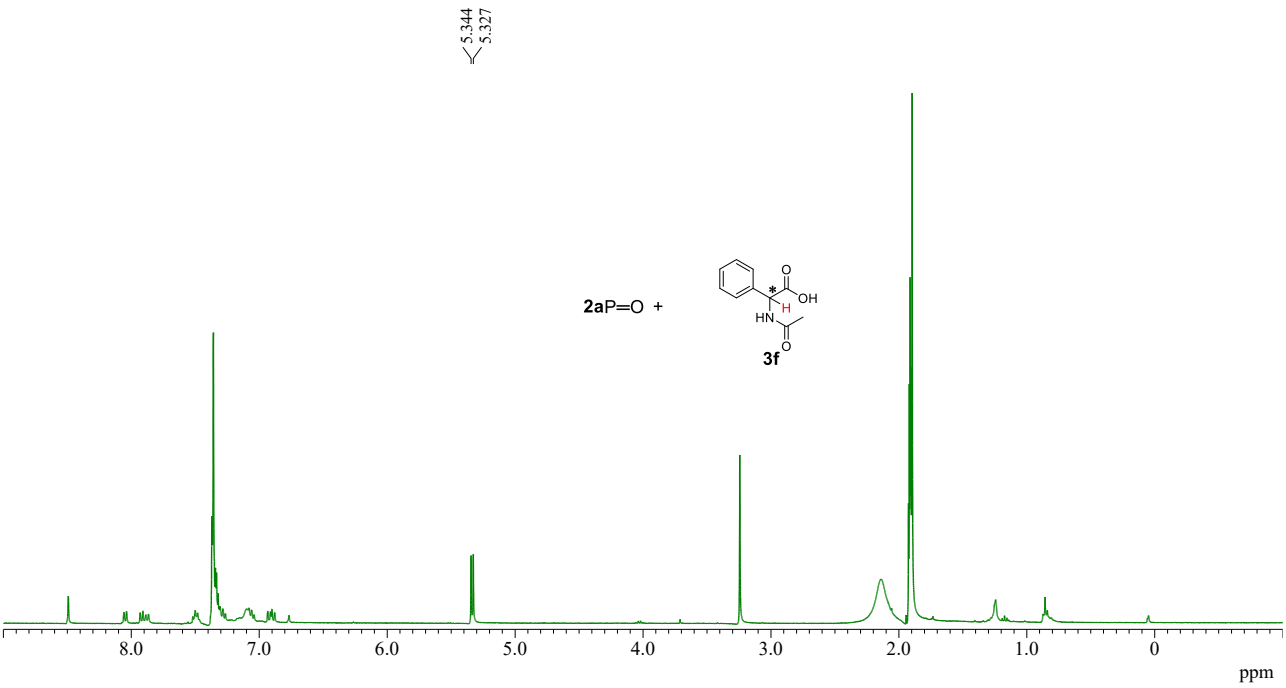

^{1}H NMR (400 MHz, $CDCl_3$)

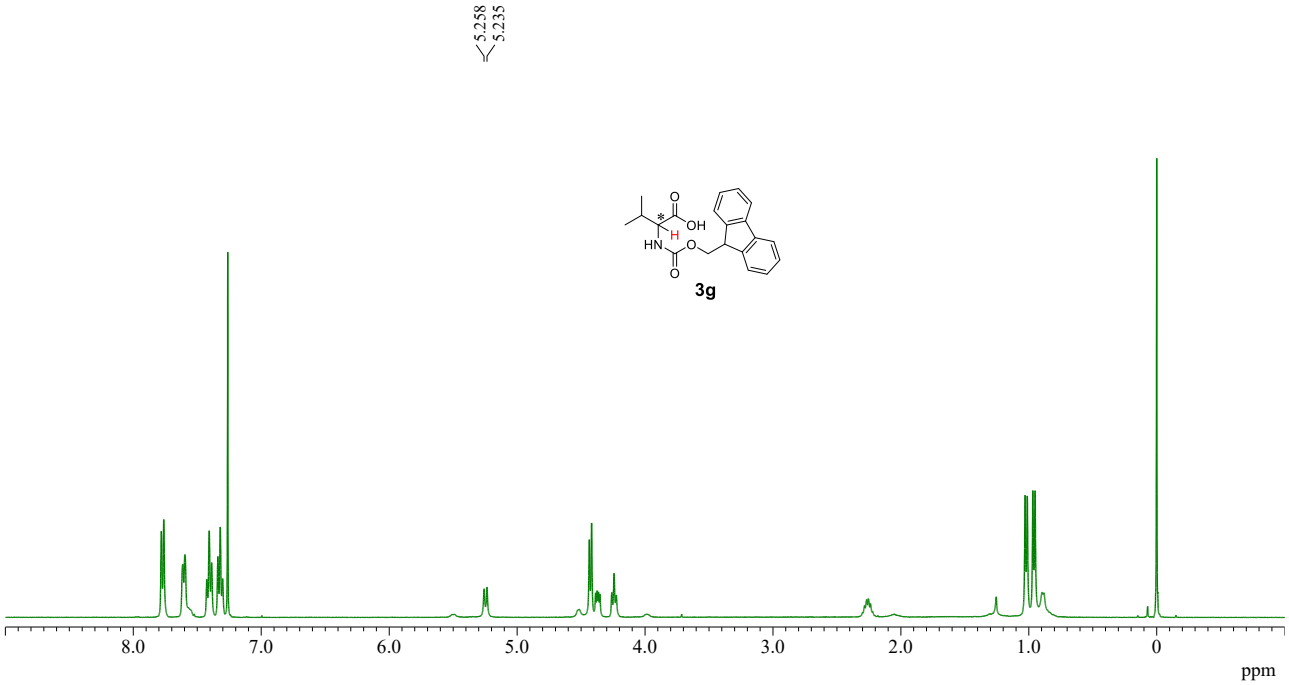

^{1}H NMR (400 MHz, $CDCl_3$)

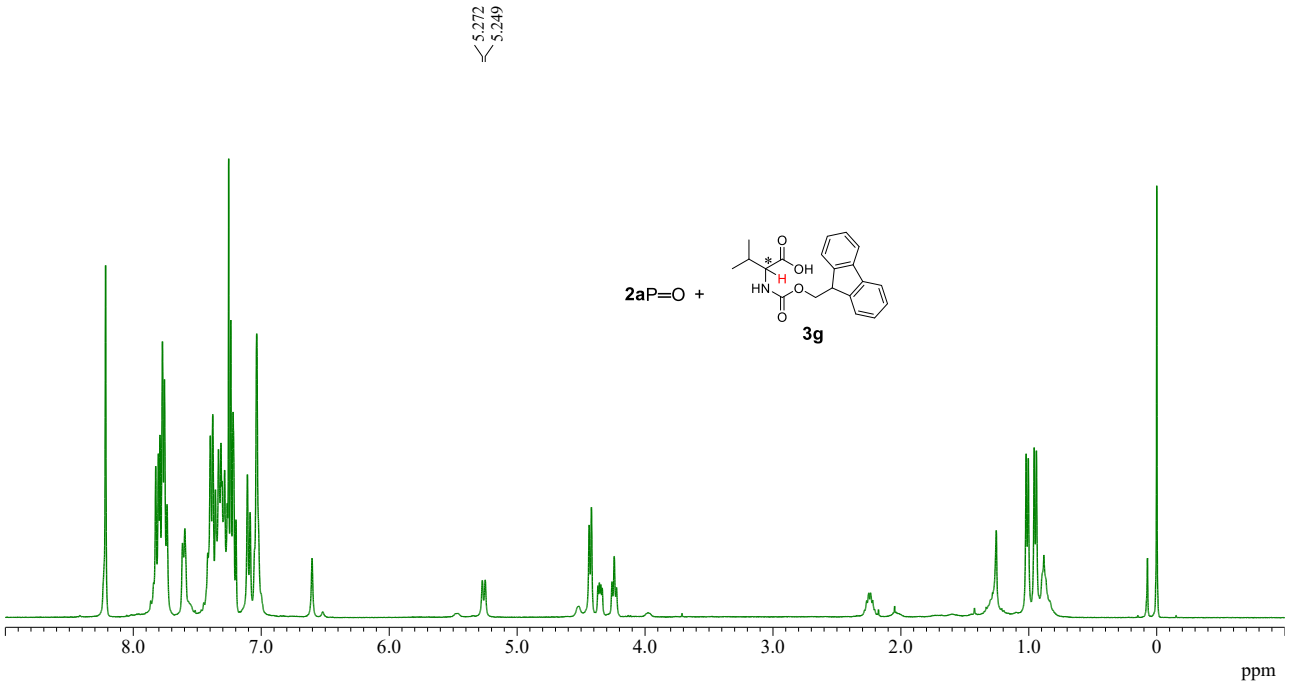

^{1}H NMR (400 MHz, $CDCl_3$)

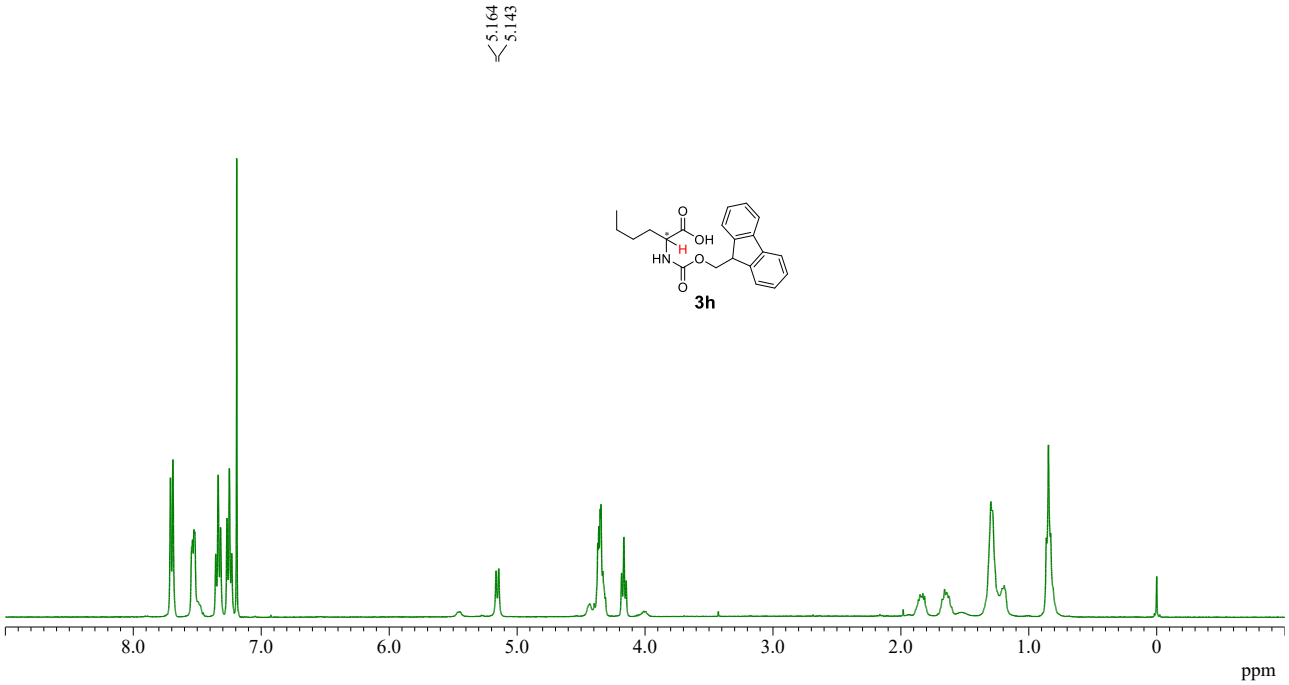

^{1}H NMR (400 MHz, $CDCl_3$)

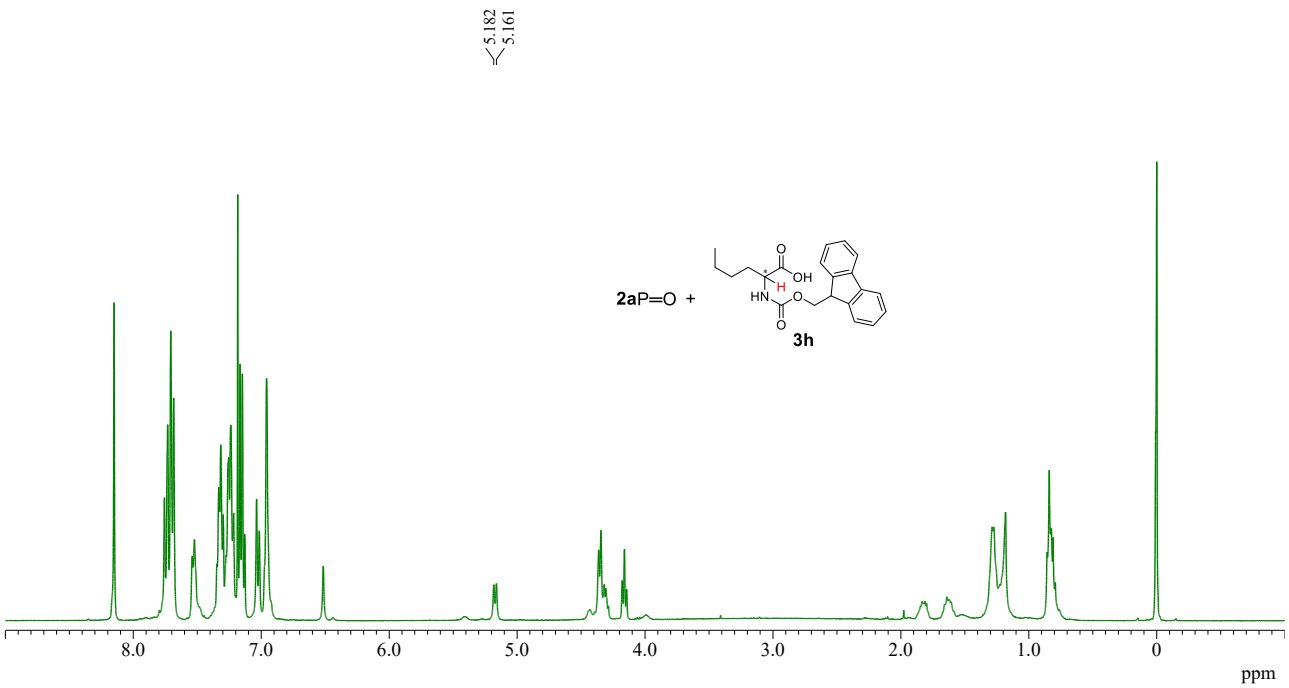

^{1}H NMR (400 MHz, $CDCl_3$)

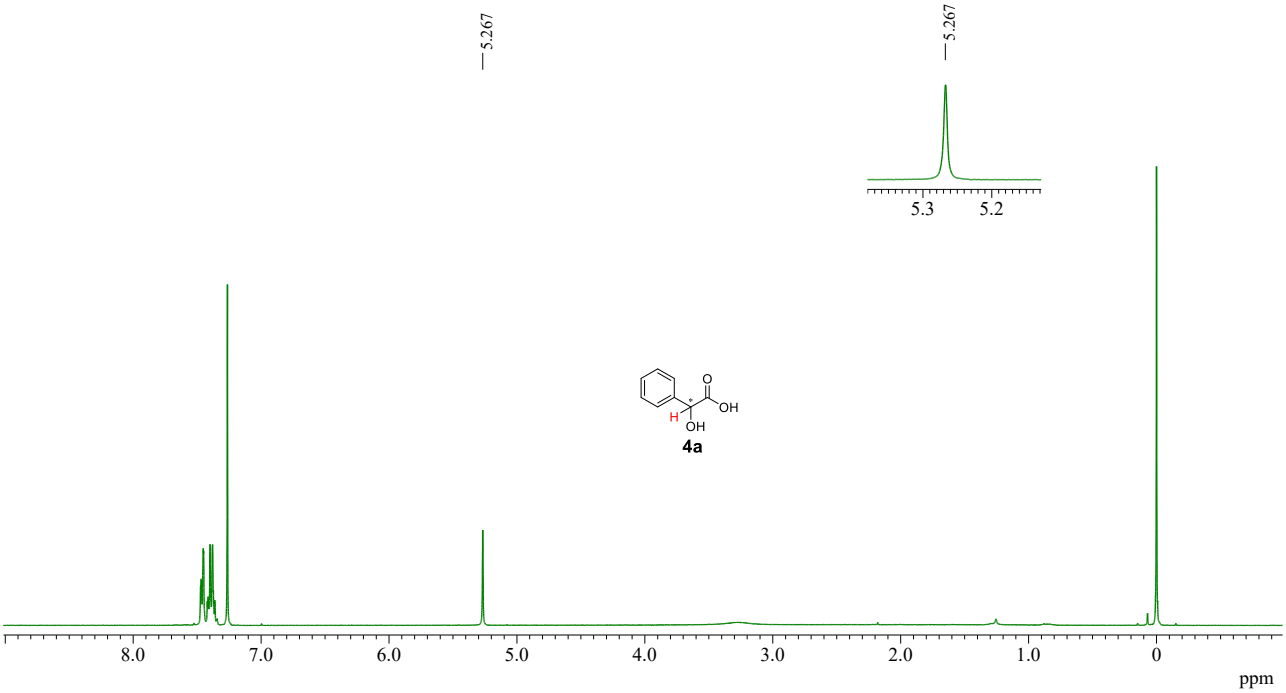

^{1}H NMR (400 MHz, $CDCl_3$)

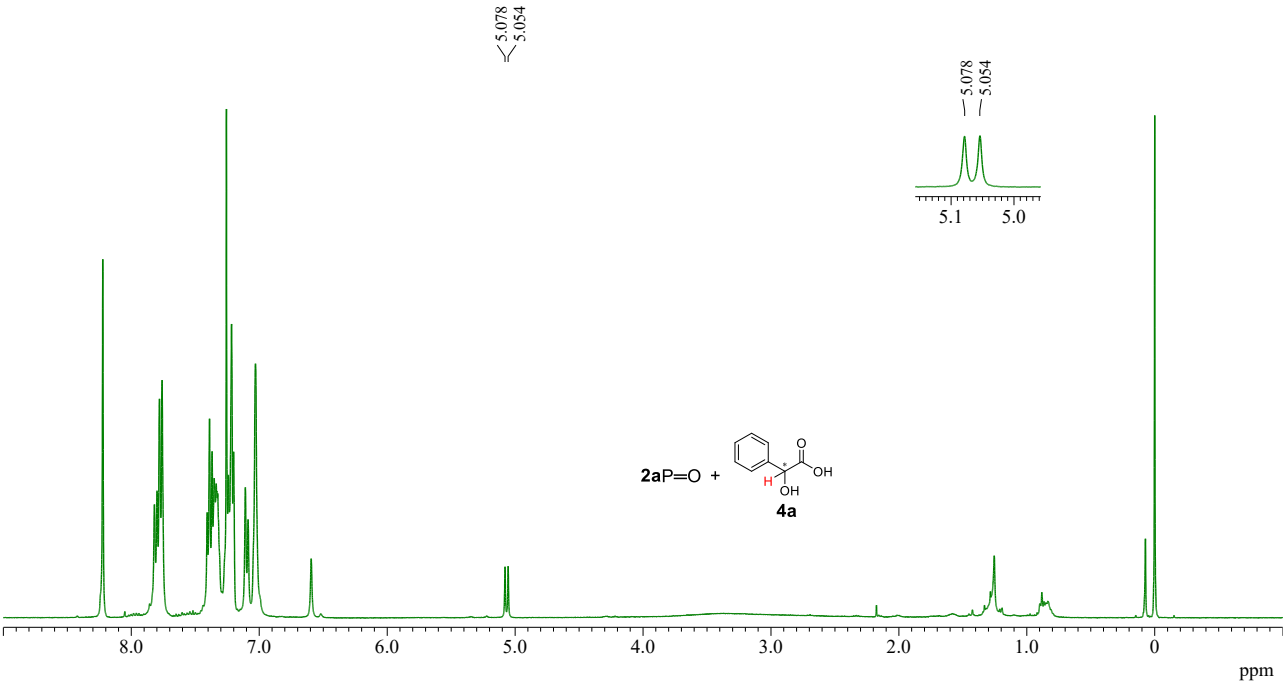

^{1}H NMR (400 MHz, $CDCl_3$)

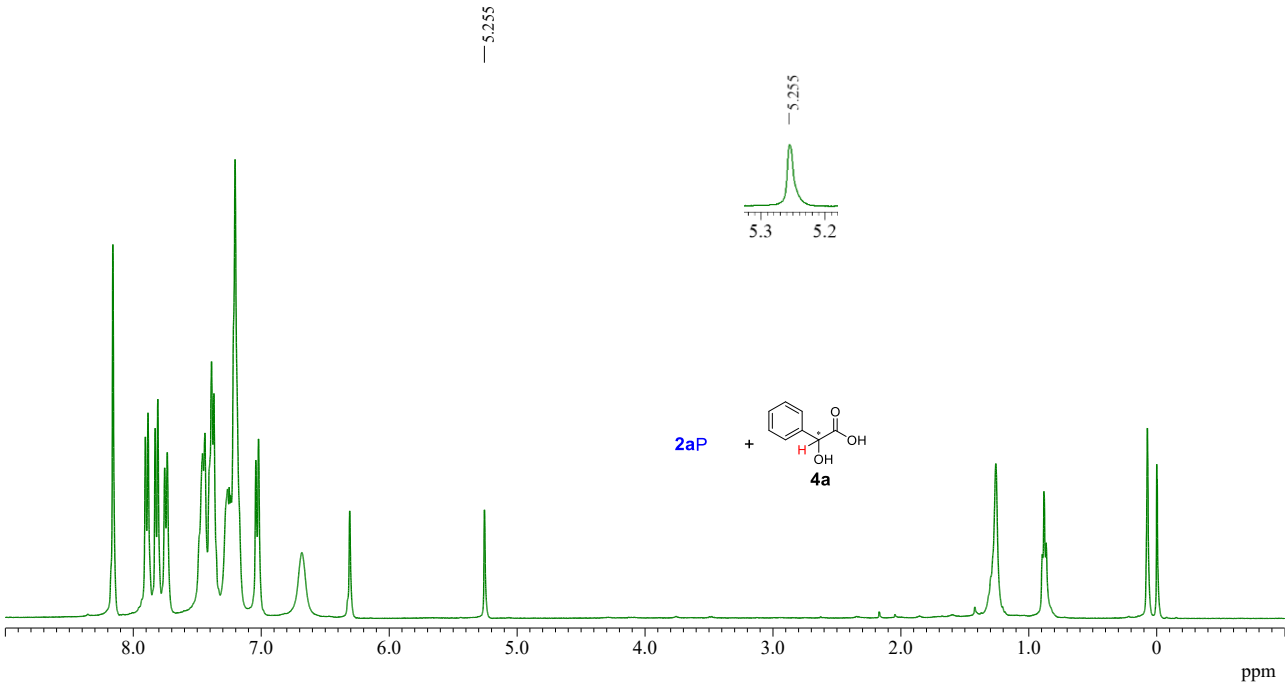

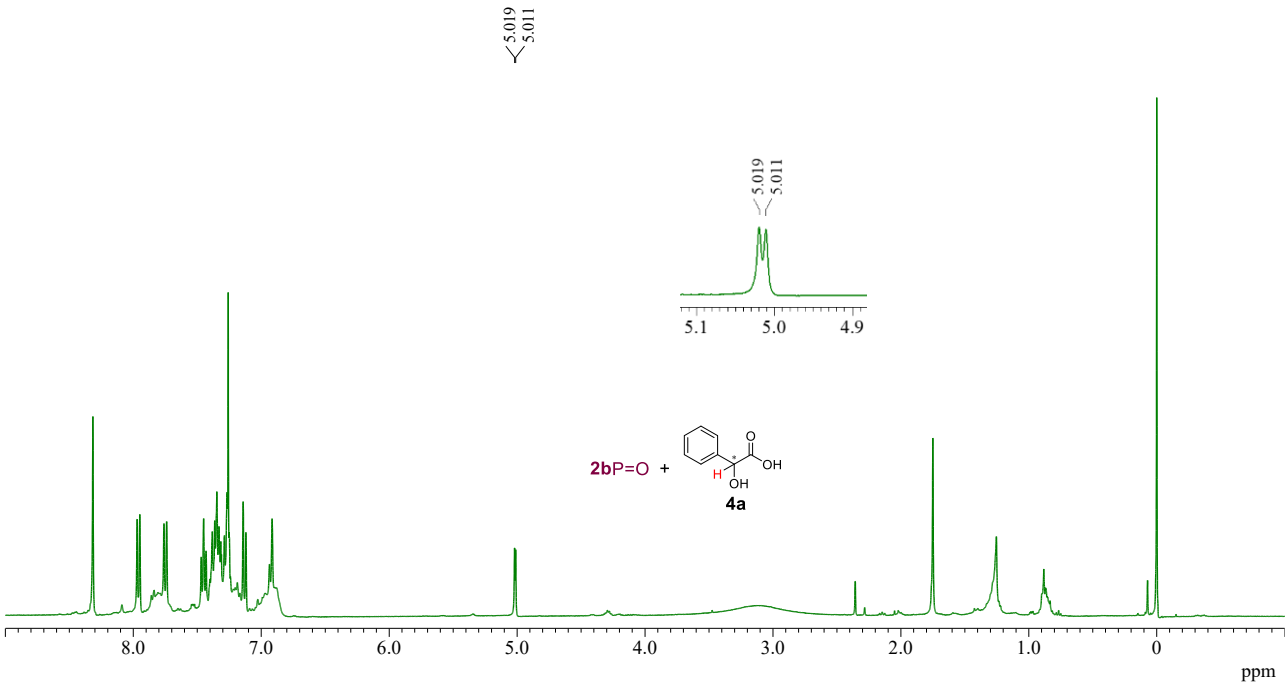

^{1}H NMR (400 MHz, $CDCl_3$)

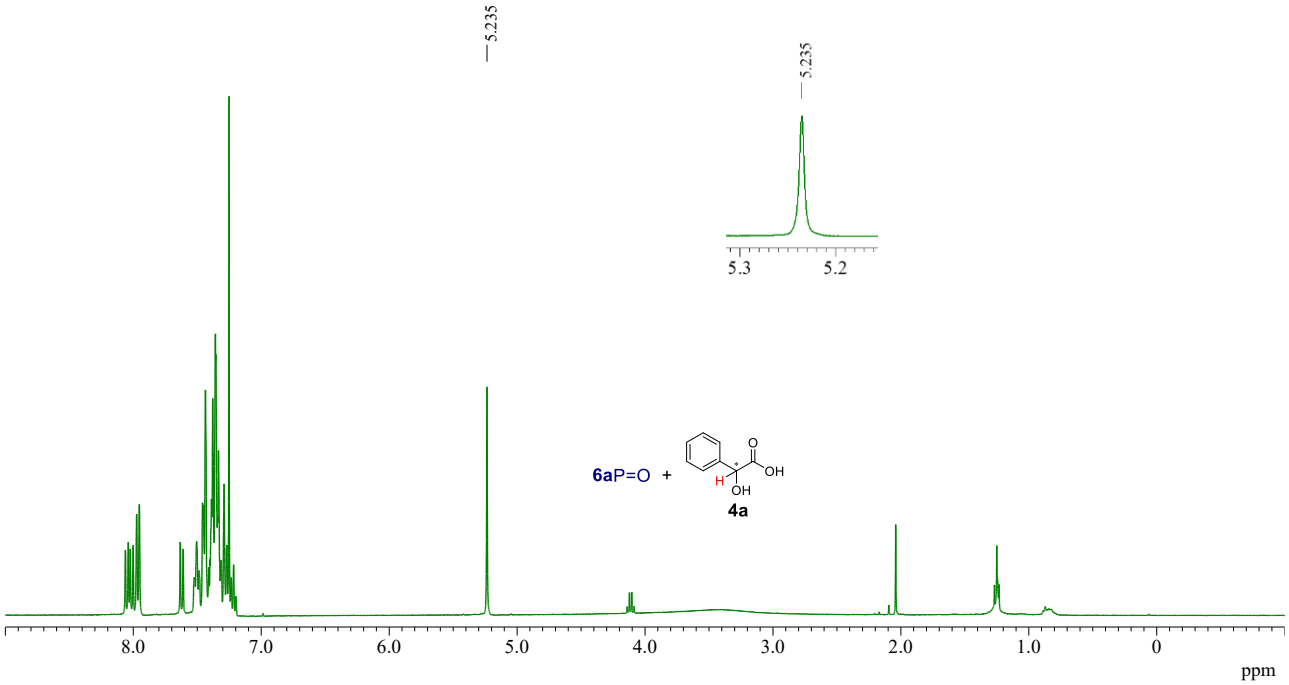

^{1}H NMR (400 MHz, $CDCl_3$)

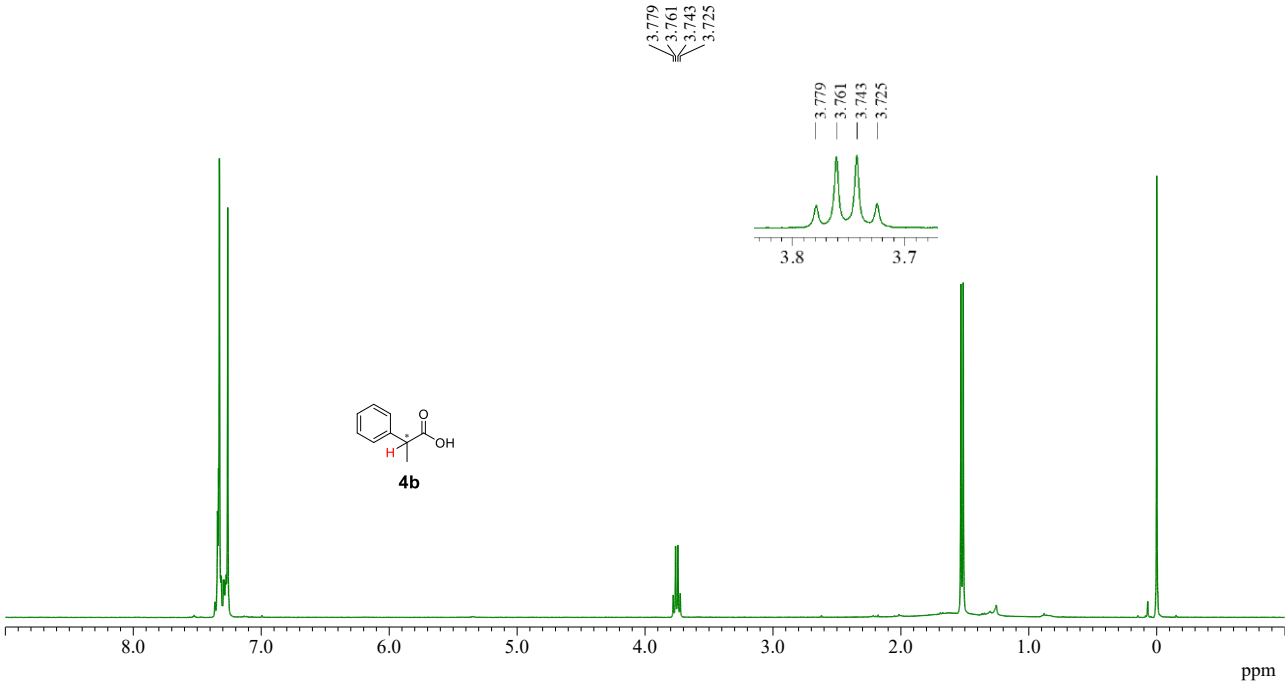

^{1}H NMR (400 MHz, $CDCl_3$)

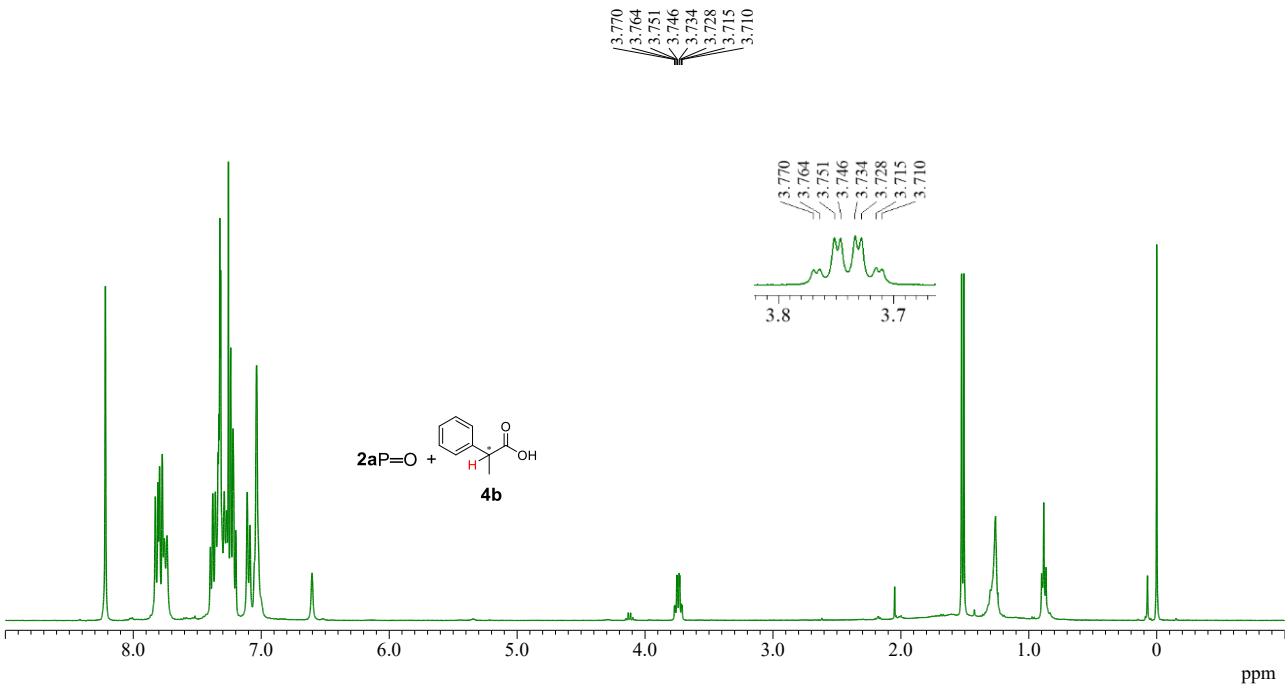

^{1}H NMR (400 MHz, $CDCl_3$)

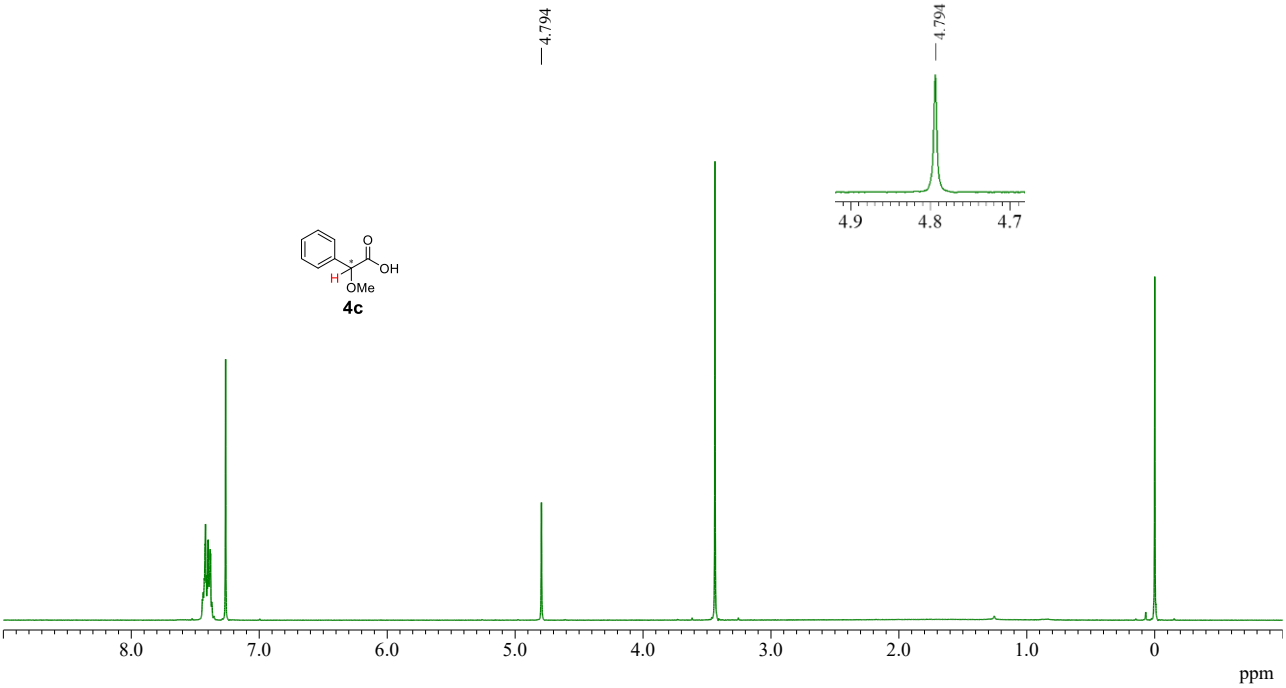

^{1}H NMR (400 MHz, $CDCl_3$)

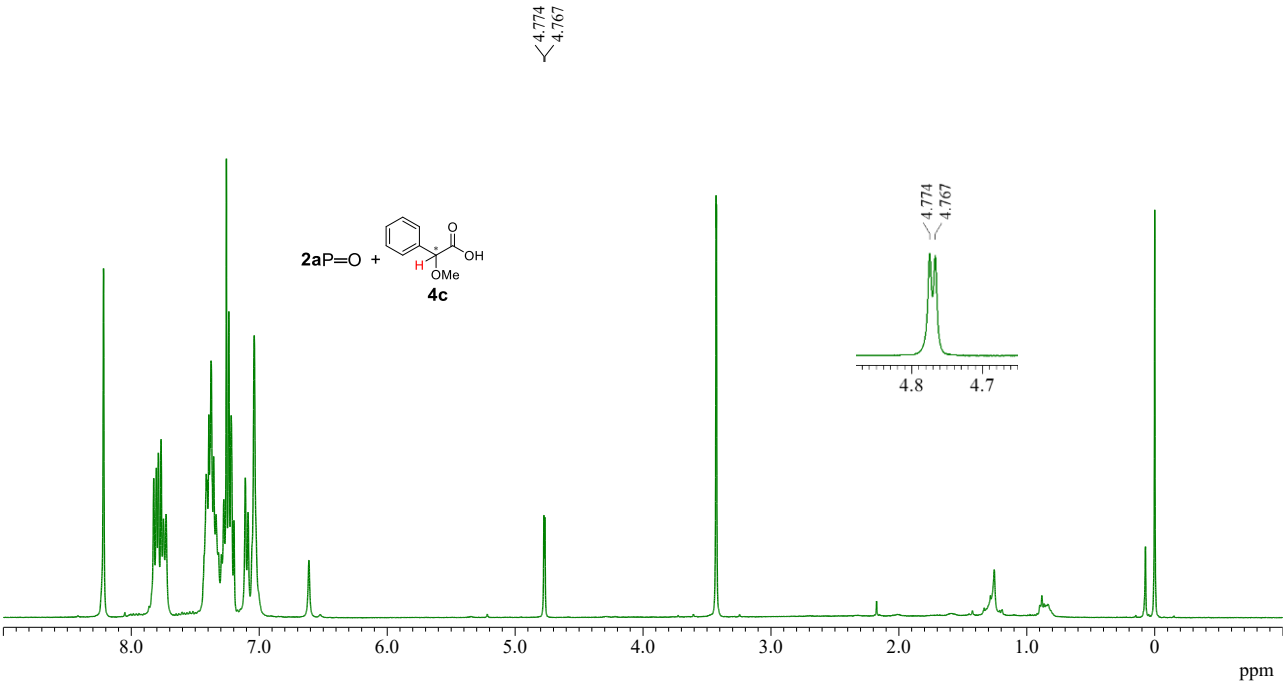

^{1}H NMR (400 MHz, $CDCl_3$)

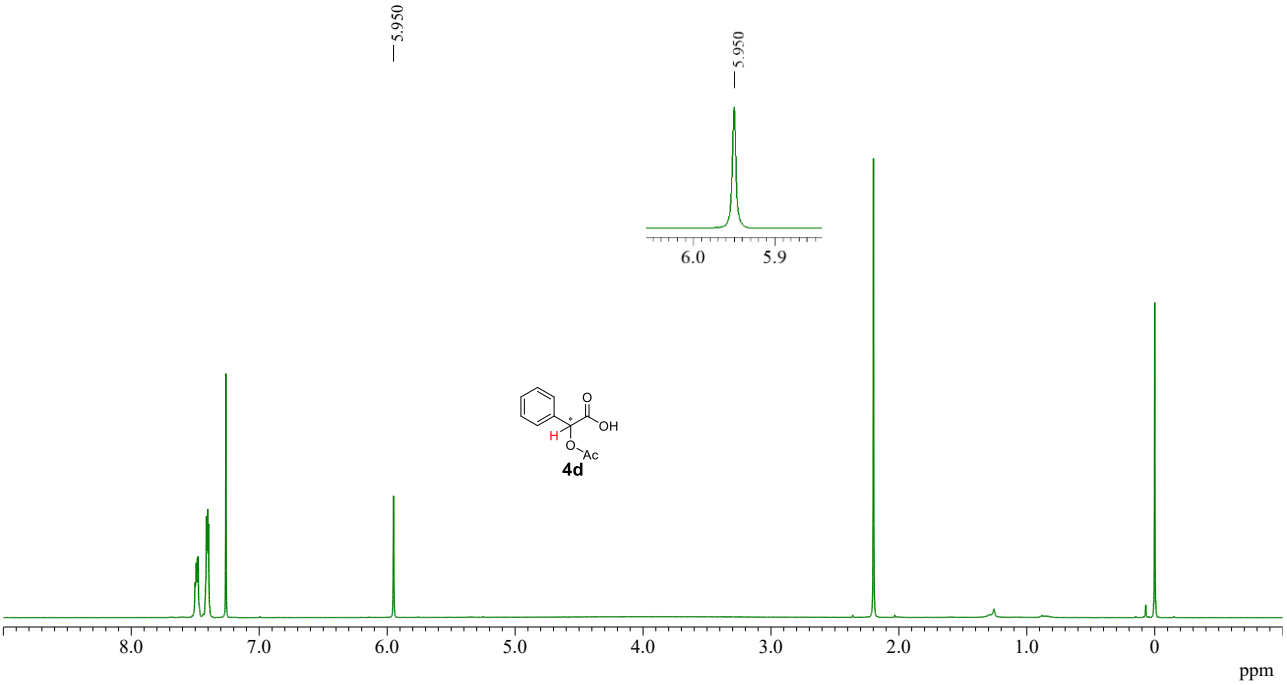

^{1}H NMR (400 MHz, $CDCl_3$)

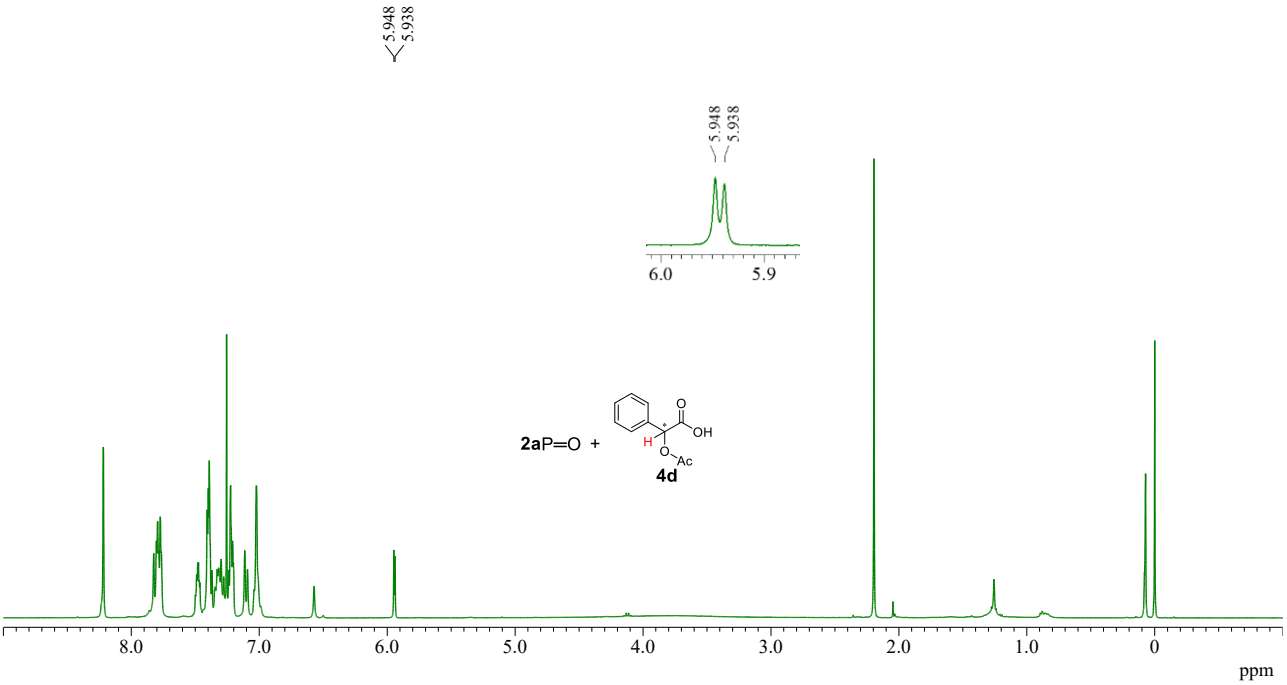

^{1}H NMR (400 MHz, $CDCl_3$)

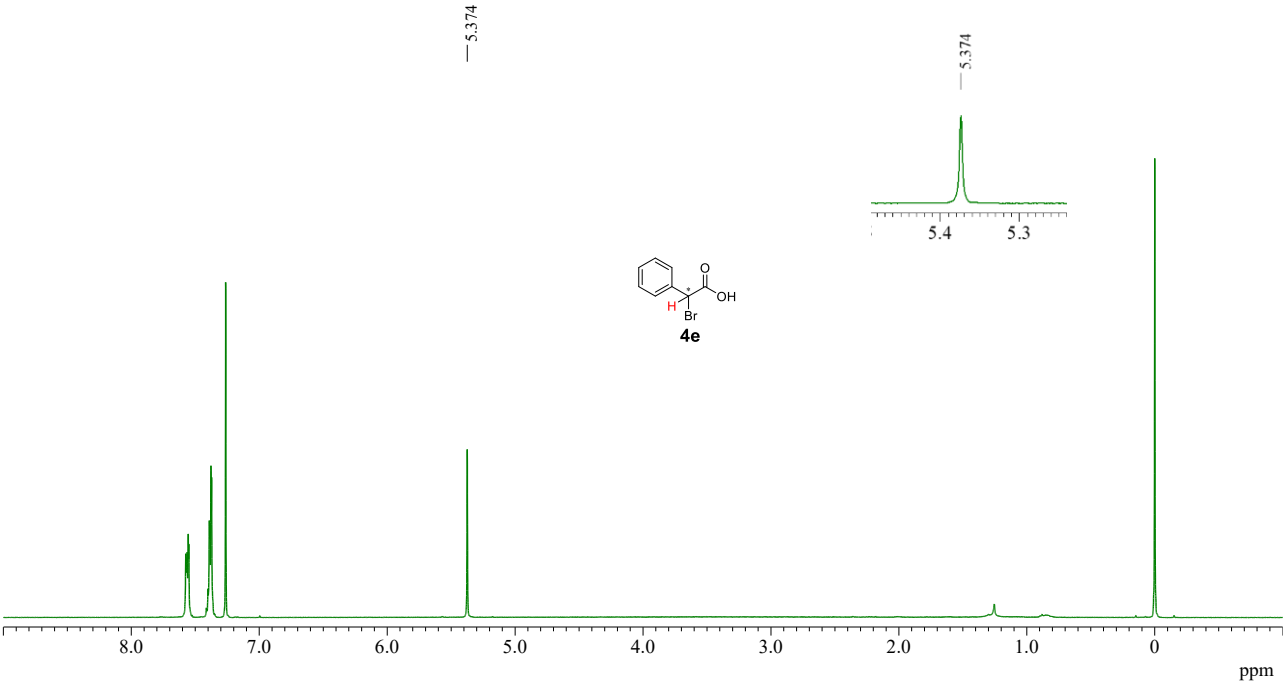

^{1}H NMR (400 MHz, $CDCl_3$)

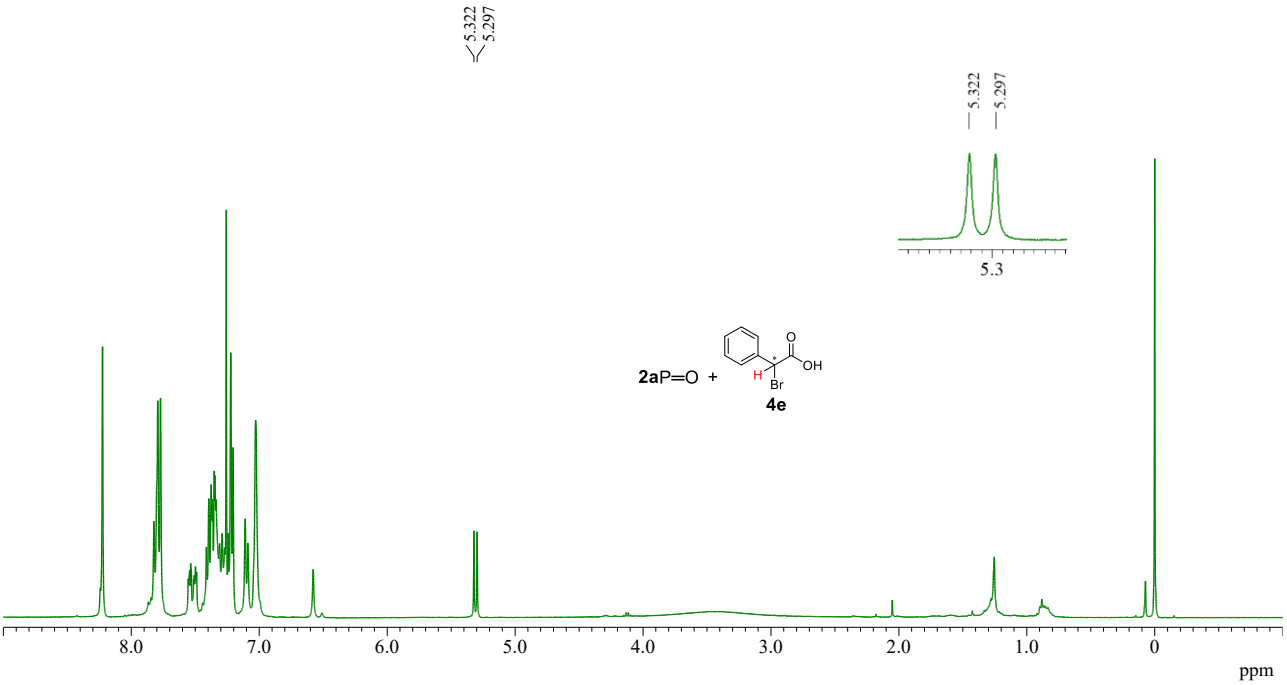

^{1}H NMR (400 MHz, $CDCl_3$)

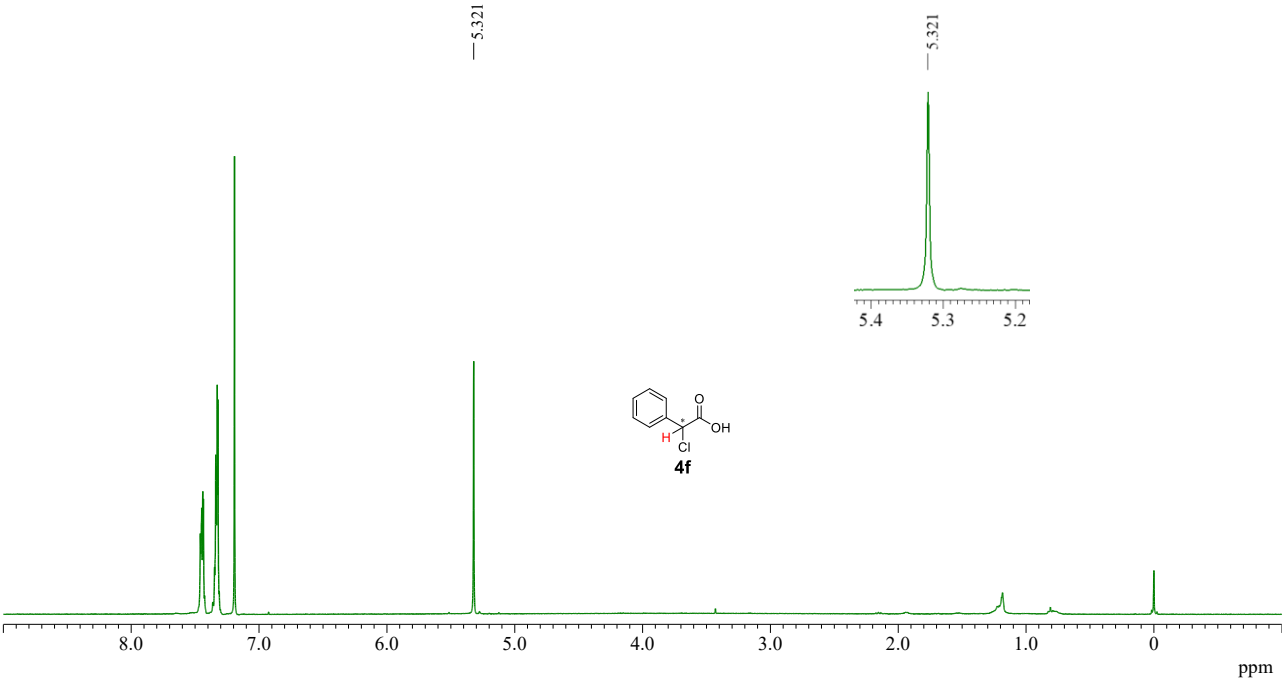

^{1}H NMR (400 MHz, $CDCl_3$)

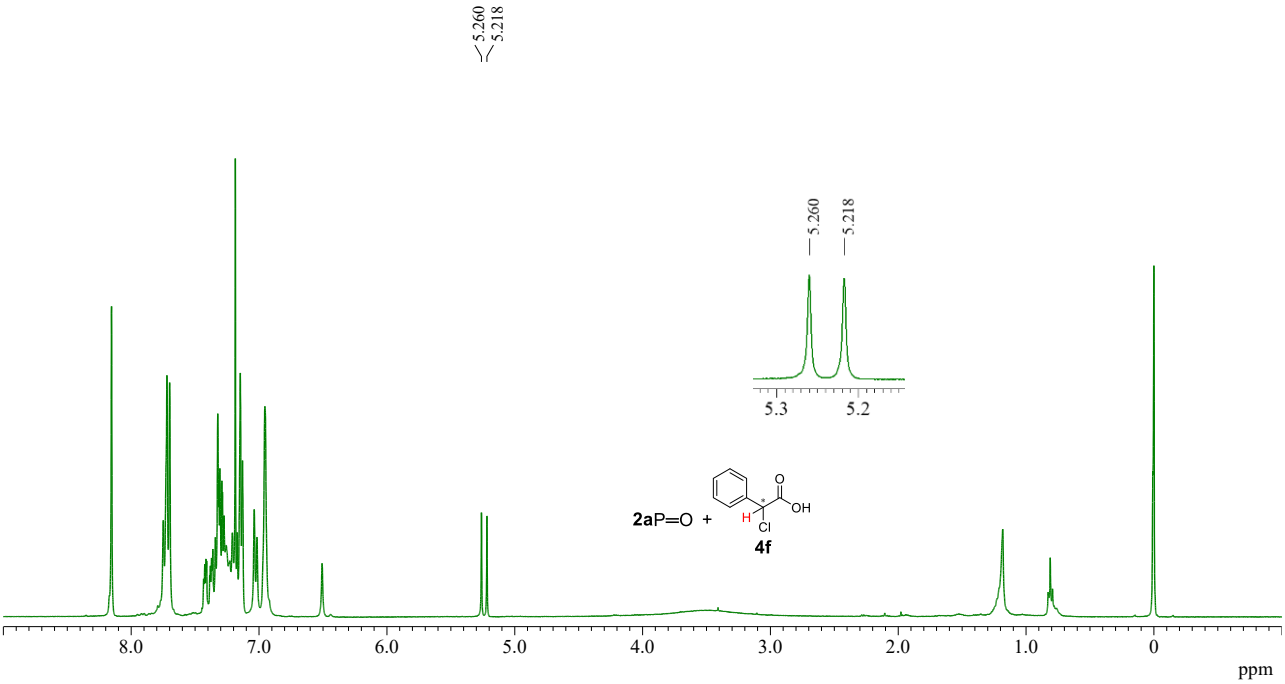

^{1}H NMR (400 MHz, $CDCl_3$)

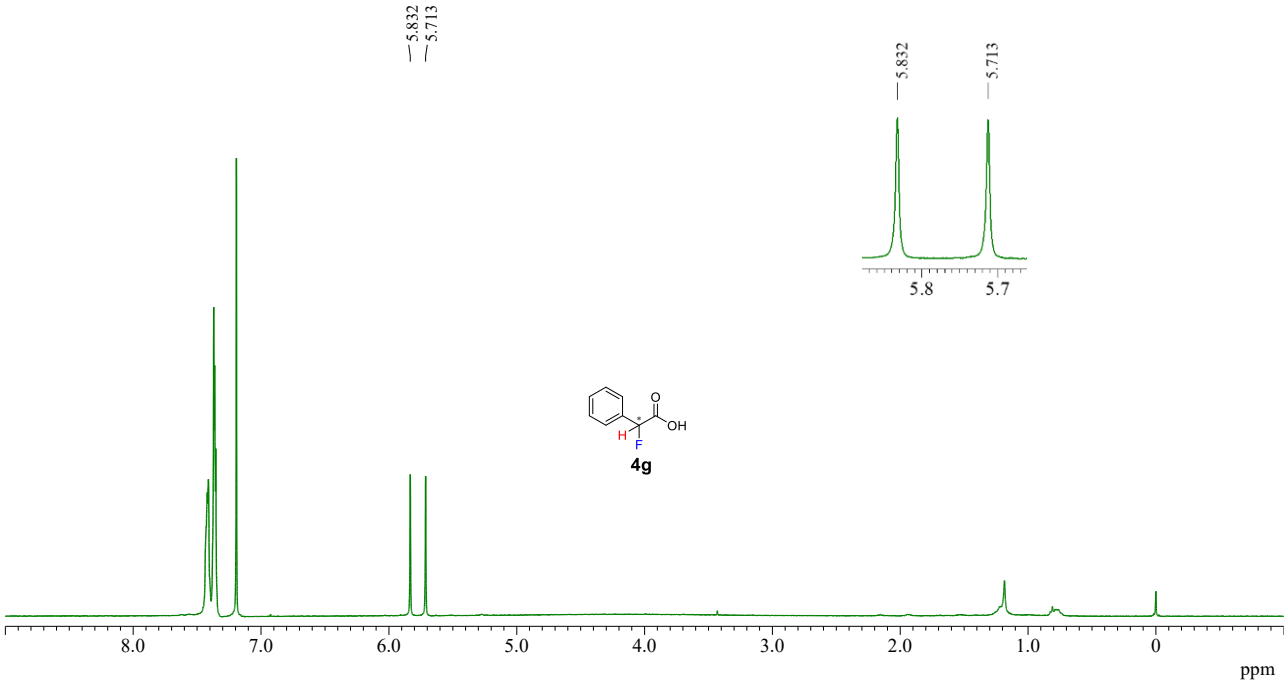

^{1}H NMR (400 MHz, $CDCl_3$)

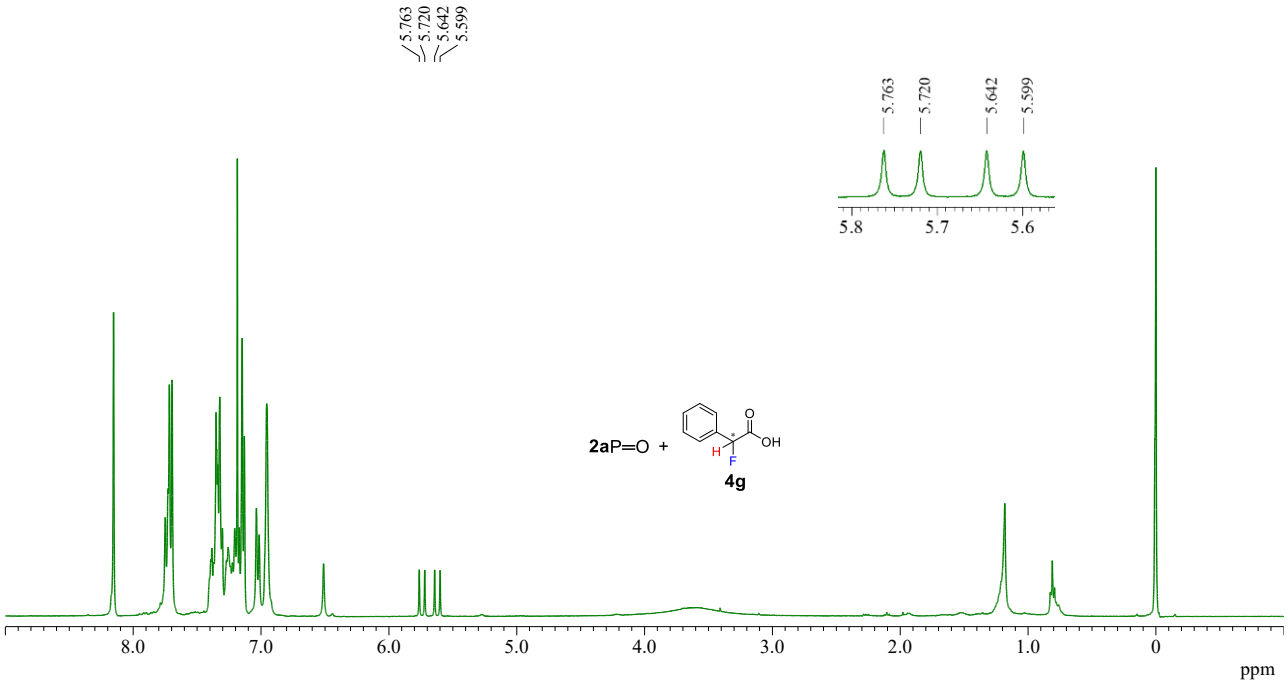

^{19}F NMR (376 MHz, $CDCl_3$, $BF_3{\cdot}OEt_2$ in $CDCl_3$ was employed as an external standard (–153.0 ppm).)

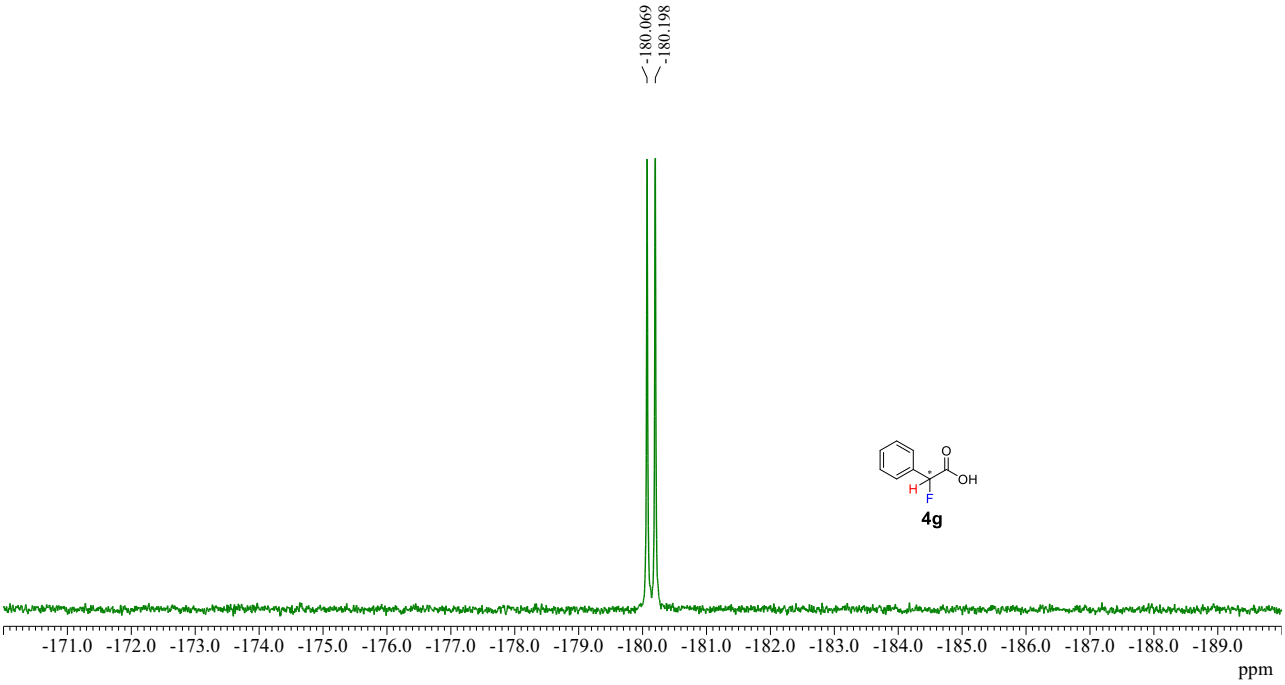

^{19}F NMR (376 MHz, $CDCl_3$, $BF_3{\cdot}OEt_2$ in $CDCl_3$ was employed as an external standard (–153.0 ppm).))

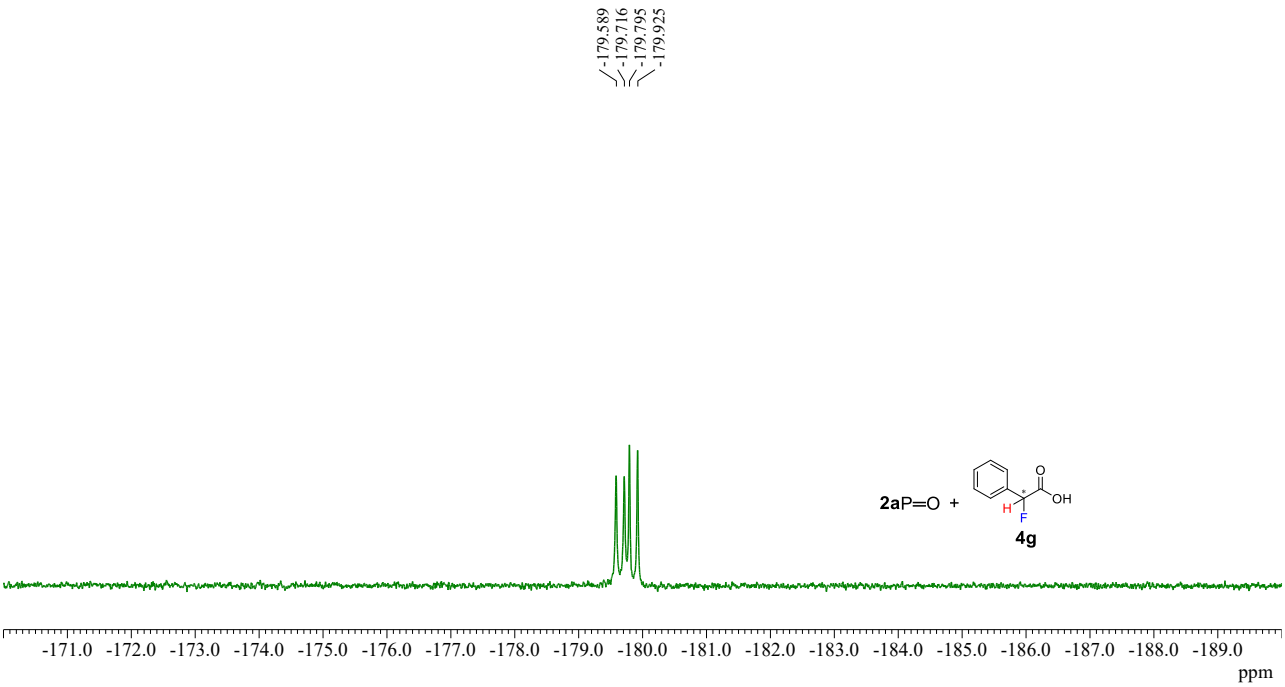

^{1}H NMR (400 MHz, $CDCl_3$)

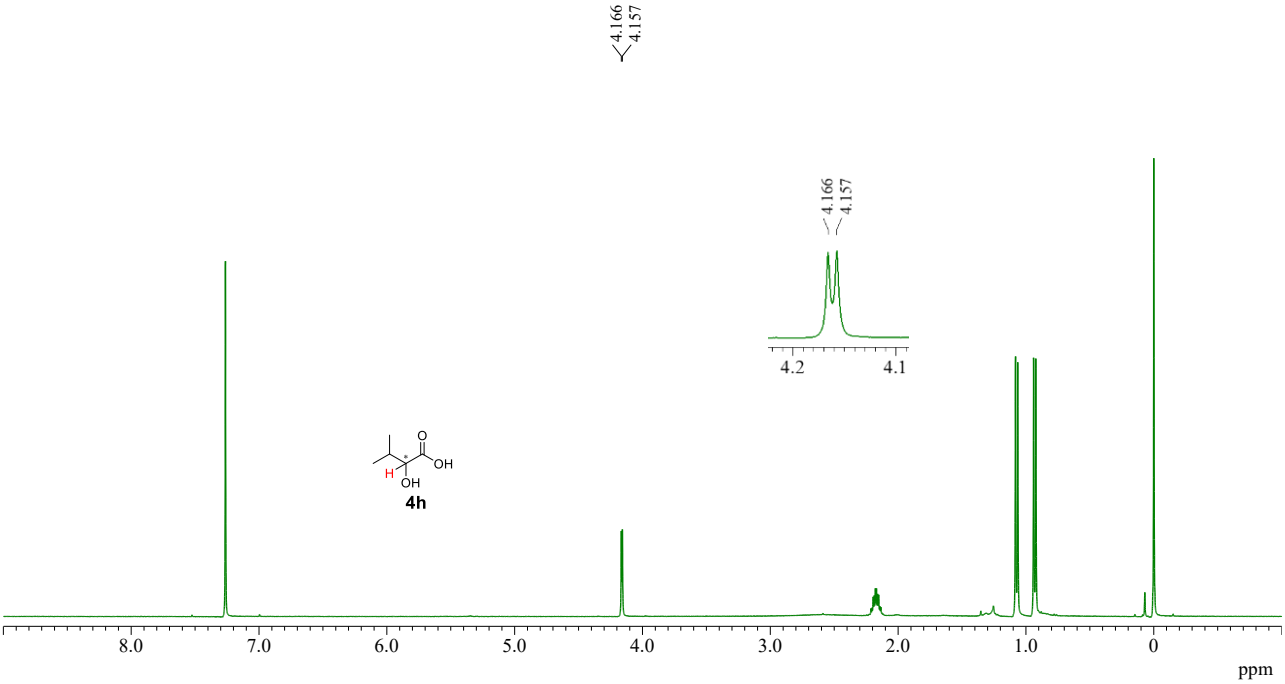

^{1}H NMR (400 MHz, $CDCl_3$)

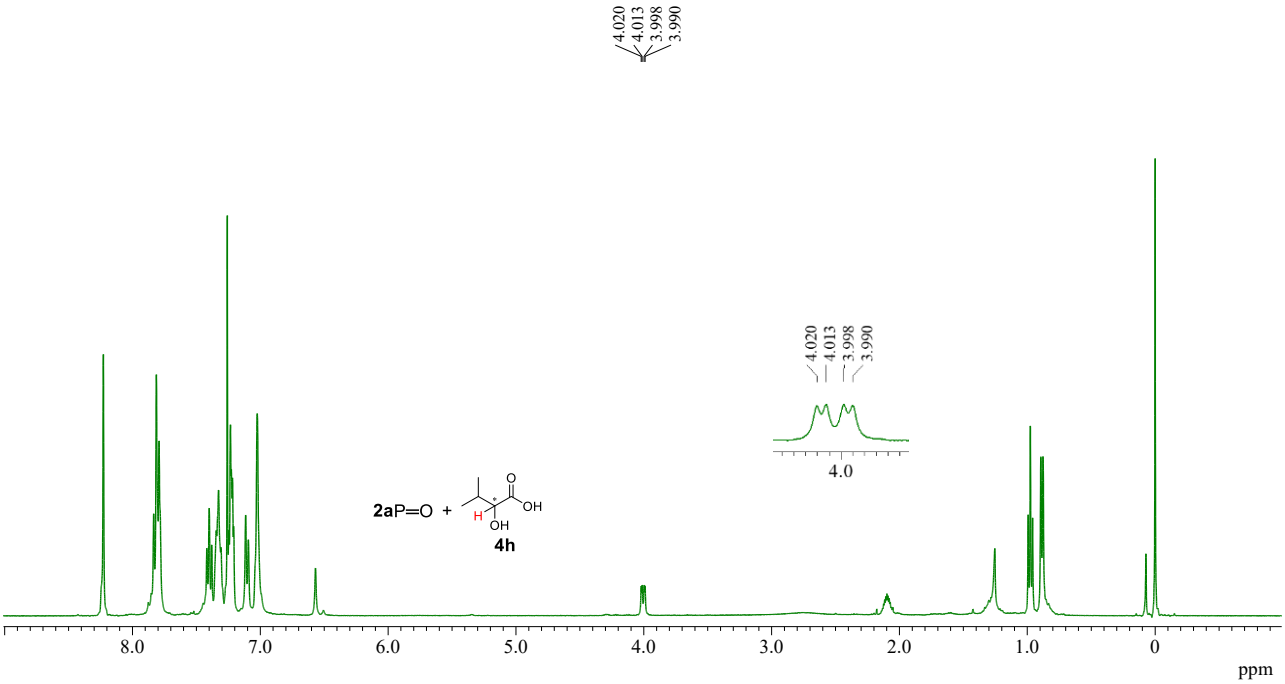

^{1}H NMR (400 MHz, $CDCl_3$)

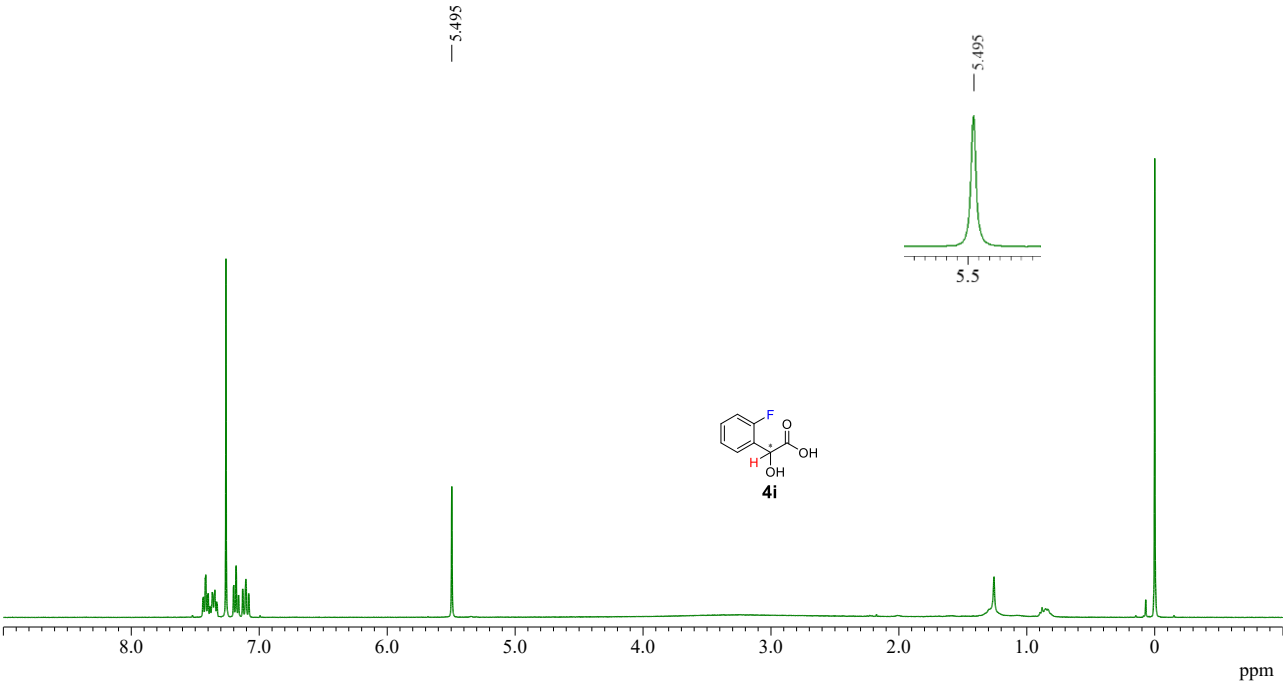

^{1}H NMR (400 MHz, $CDCl_3$)

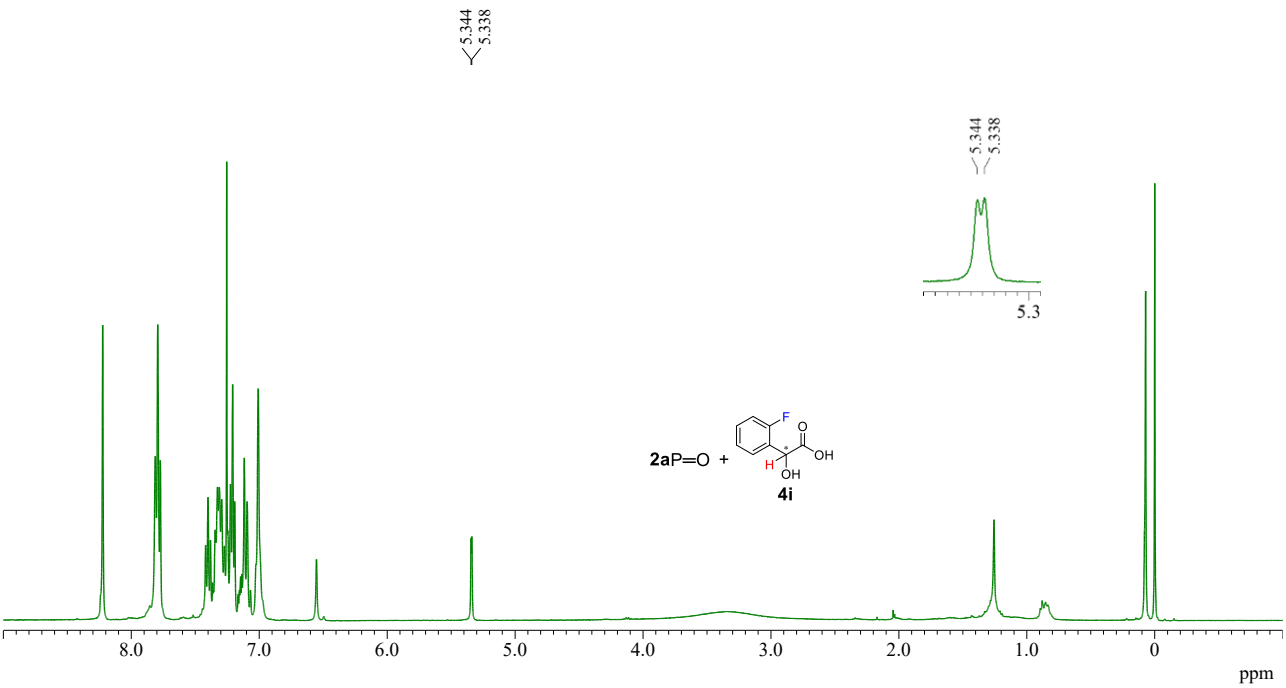

^{19}F NMR (376 MHz, $CDCl_3$, $CDCl_3$, $BF_3{\cdot}OEt_2$ in $CDCl_3$ was employed as an external standard (–153.0 ppm))

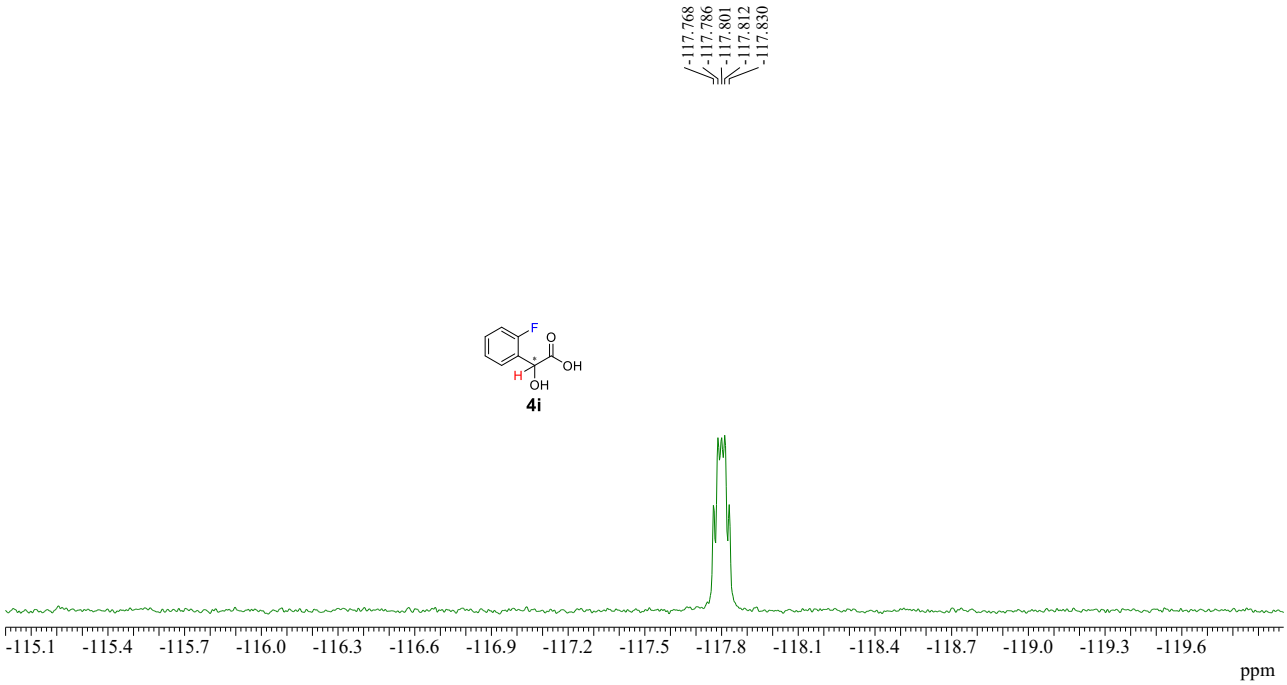

^{19}F NMR (376 MHz, $CDCl_3$, $CDCl_3$, $BF_3{\cdot}OEt_2$ in $CDCl_3$ was employed as an external standard (–153.0 ppm))

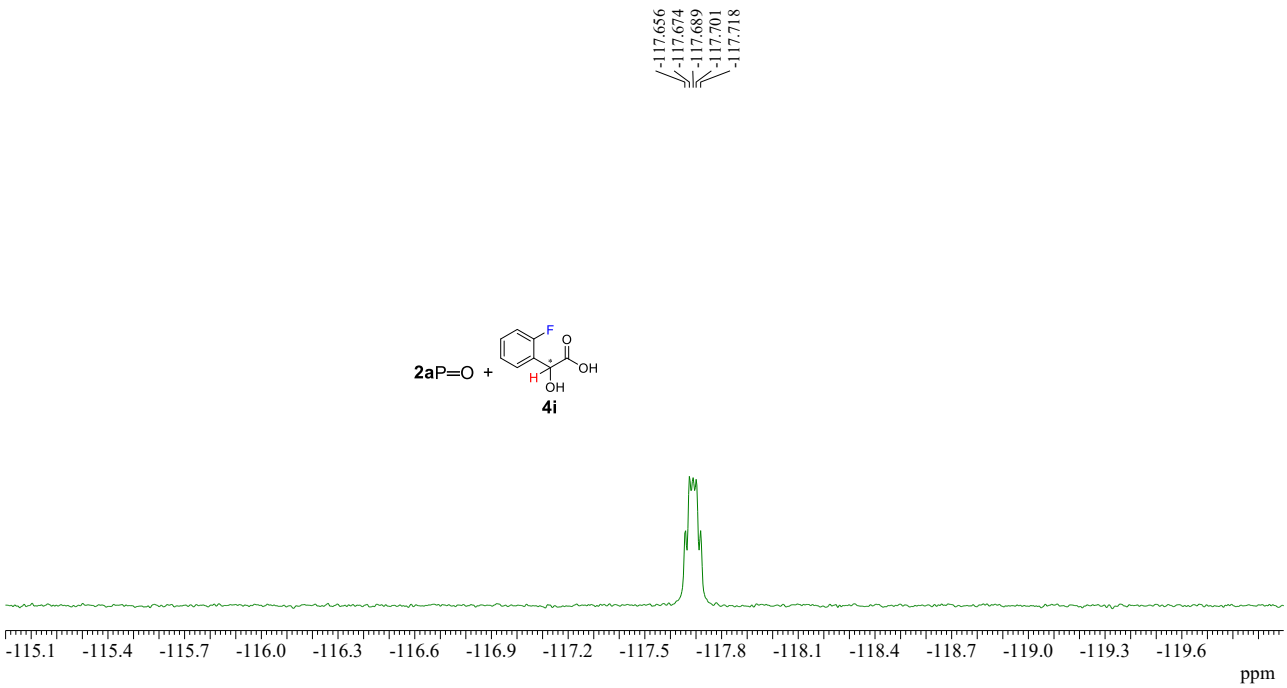

^{1}H NMR (400 MHz, $CDCl_3$)

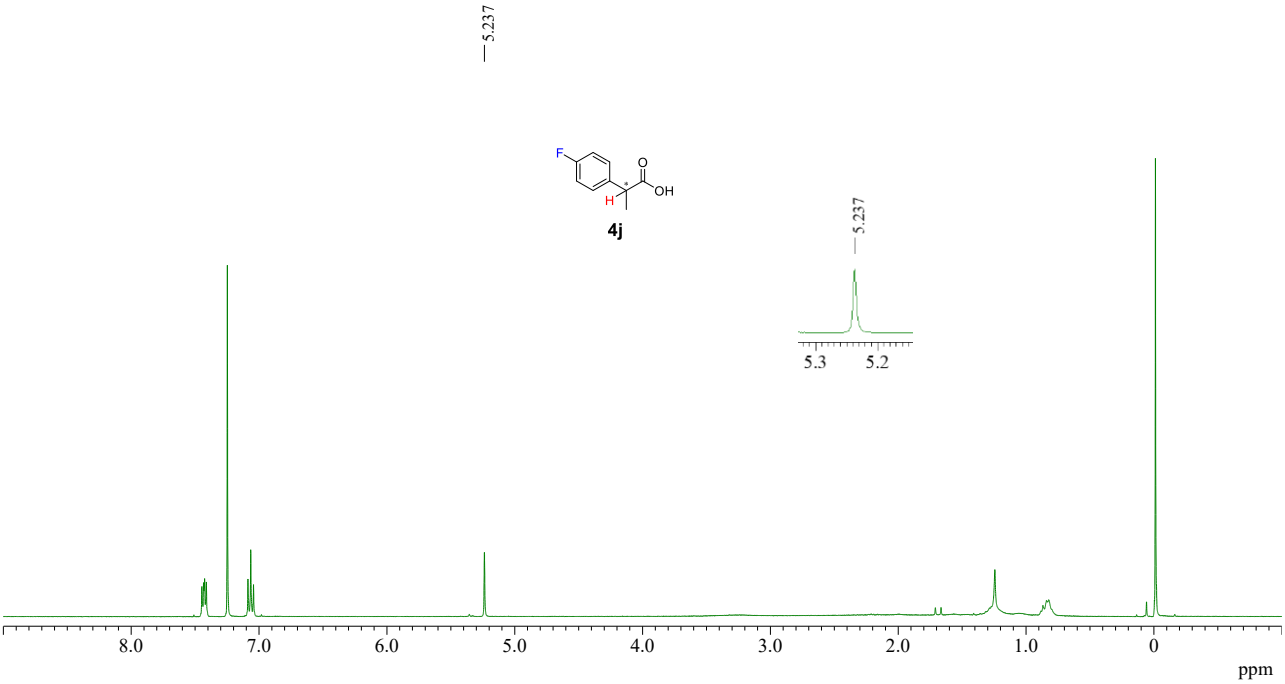

^{1}H NMR (400 MHz, $CDCl_3$)

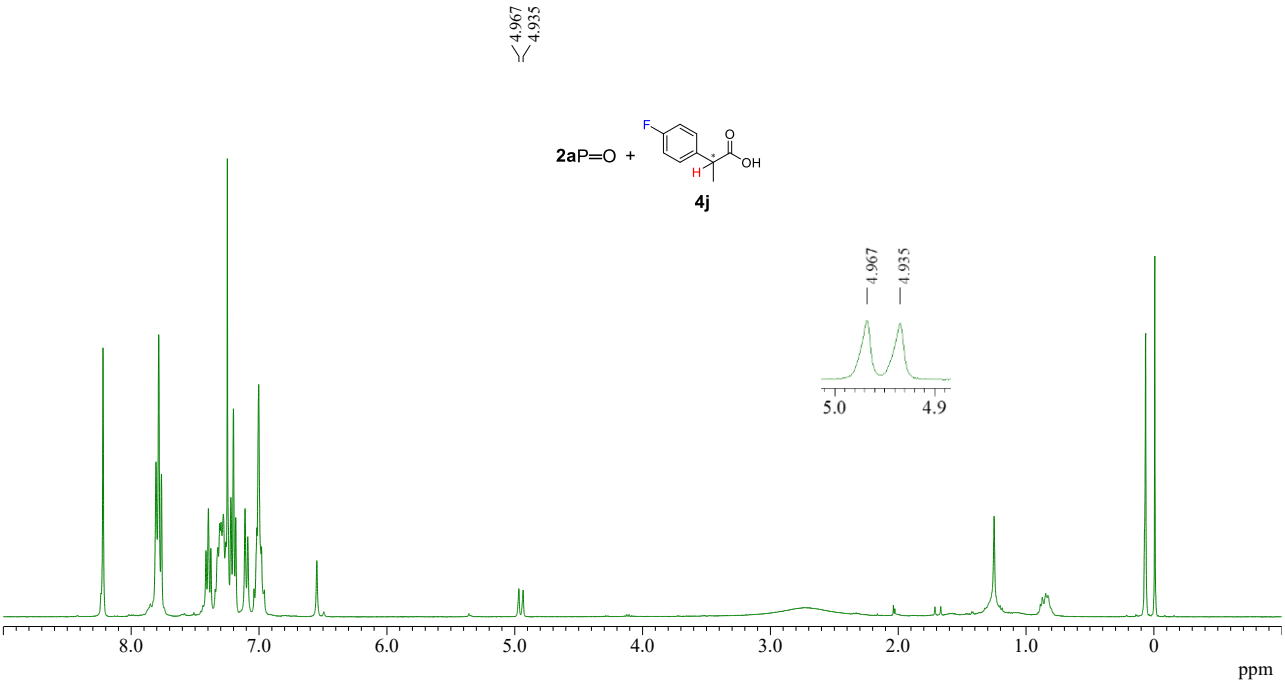

^{19}F NMR (376 MHz, $CDCl_3$, $BF_3{\cdot}OEt_2$ in $CDCl_3$ was employed as an external standard (–153.0 ppm))

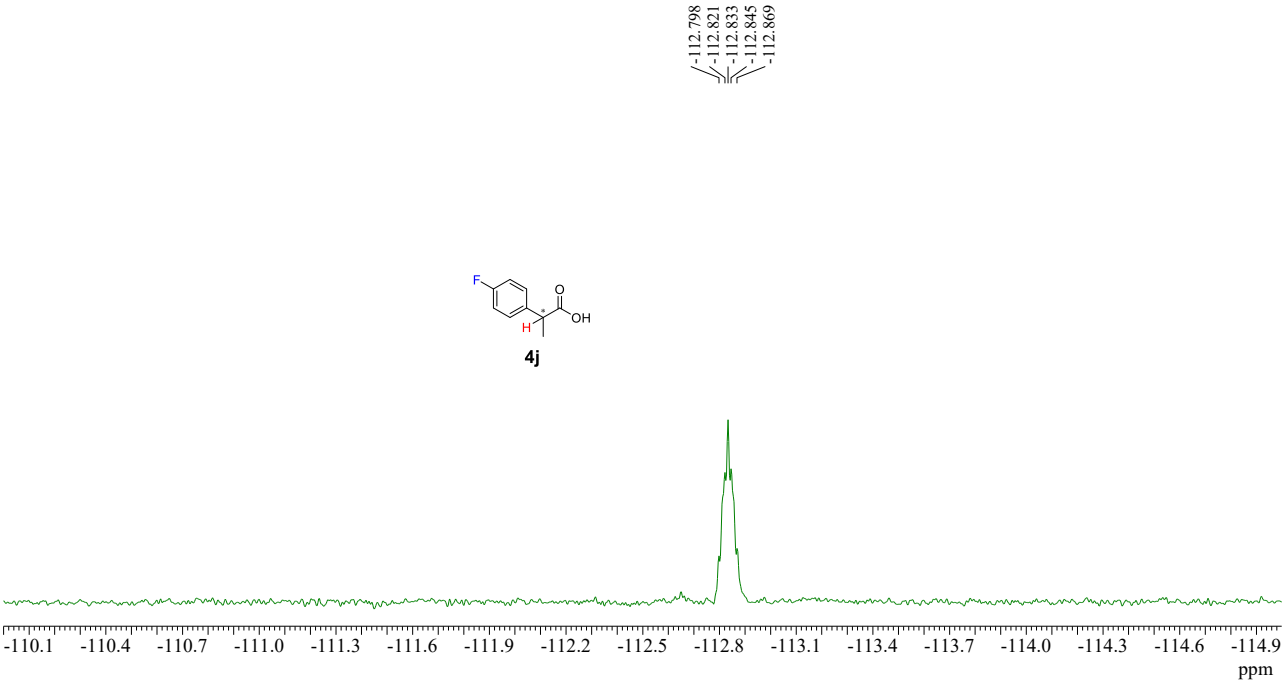

^{19}F NMR (376 MHz, $CDCl_3$, $BF_3{\cdot}OEt_2$ in $CDCl_3$ was employed as an external standard (–153.0 ppm))

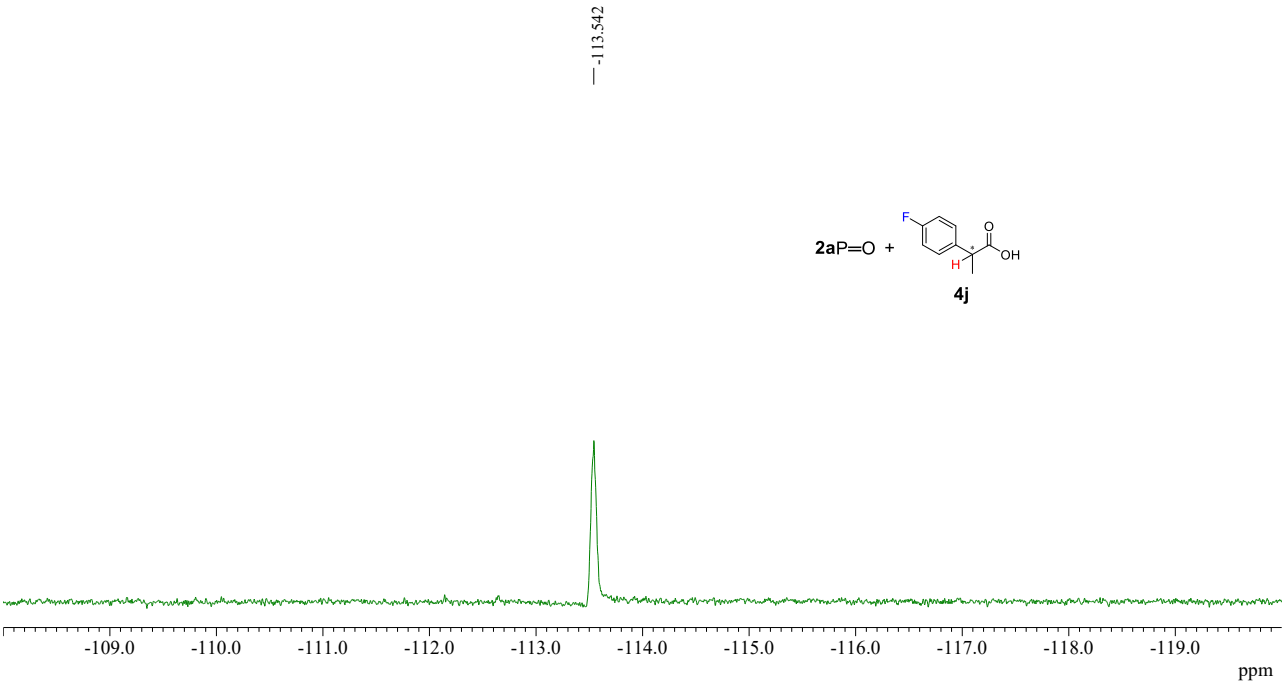

^{1}H NMR (400 MHz, $CDCl_3$)

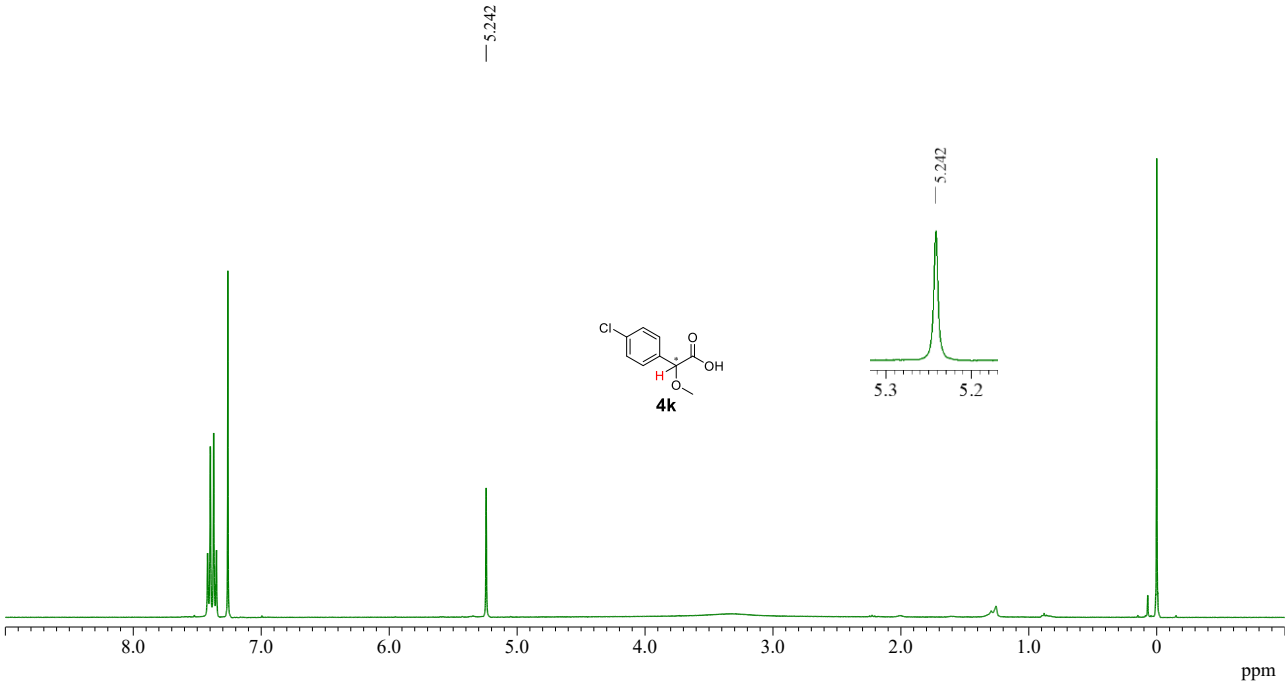

^{1}H NMR (400 MHz, $CDCl_3$)

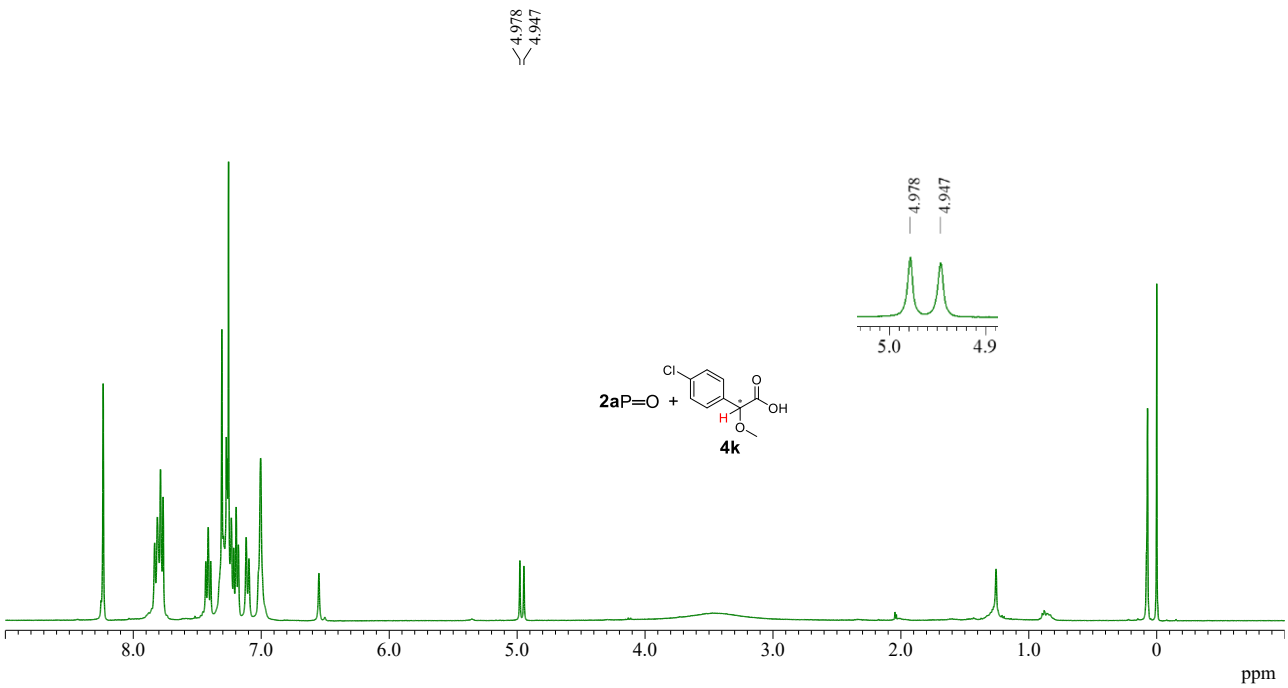

^{1}H NMR (400 MHz, $CDCl_3$)

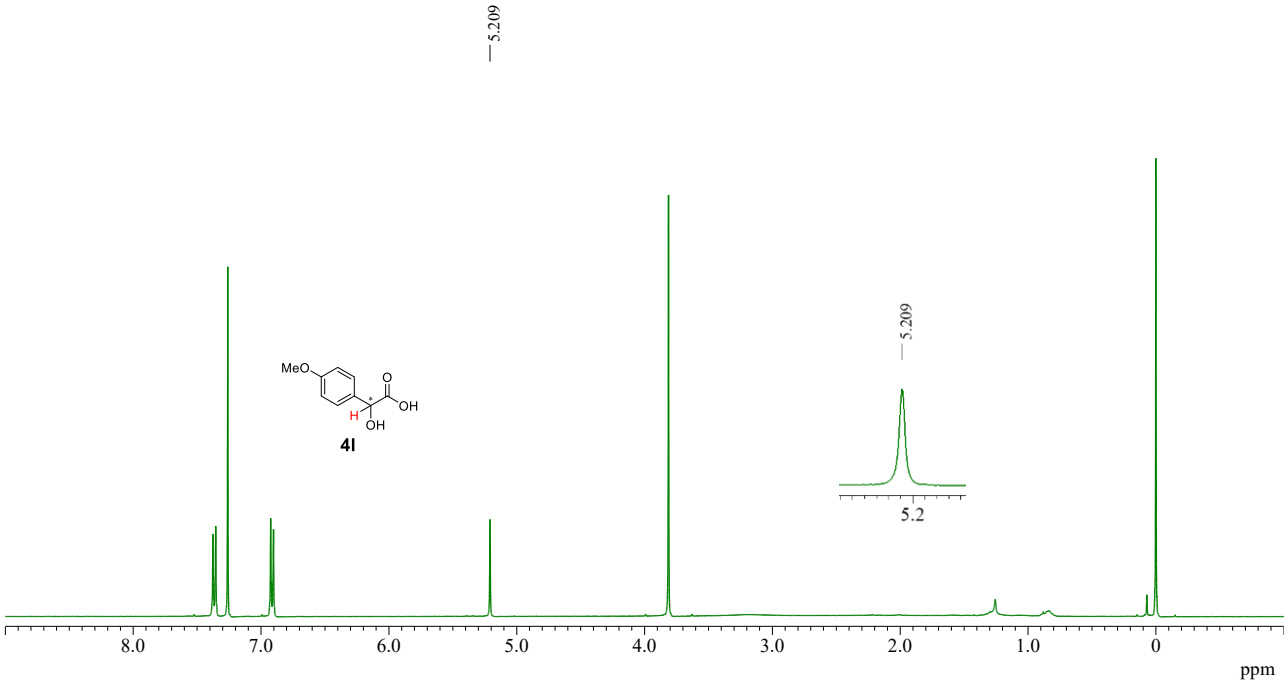

^{1}H NMR (400 MHz, $CDCl_3$)

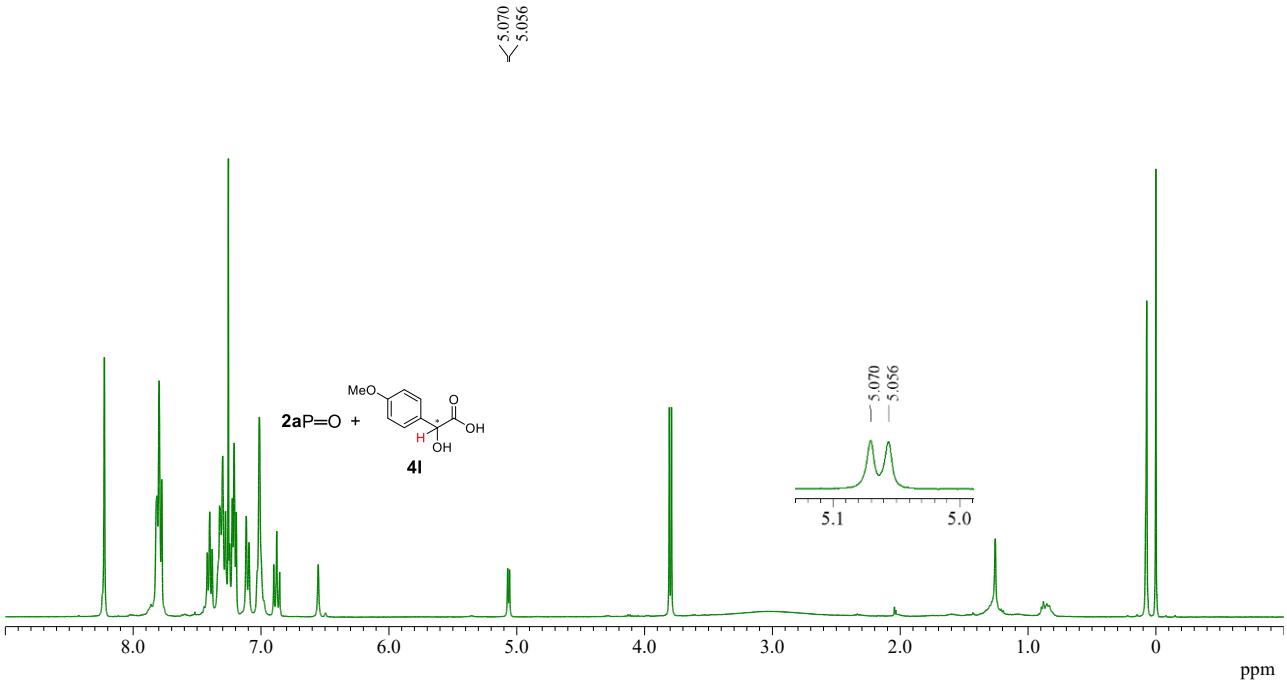

^{1}H NMR (400 MHz, $CDCl_3$)

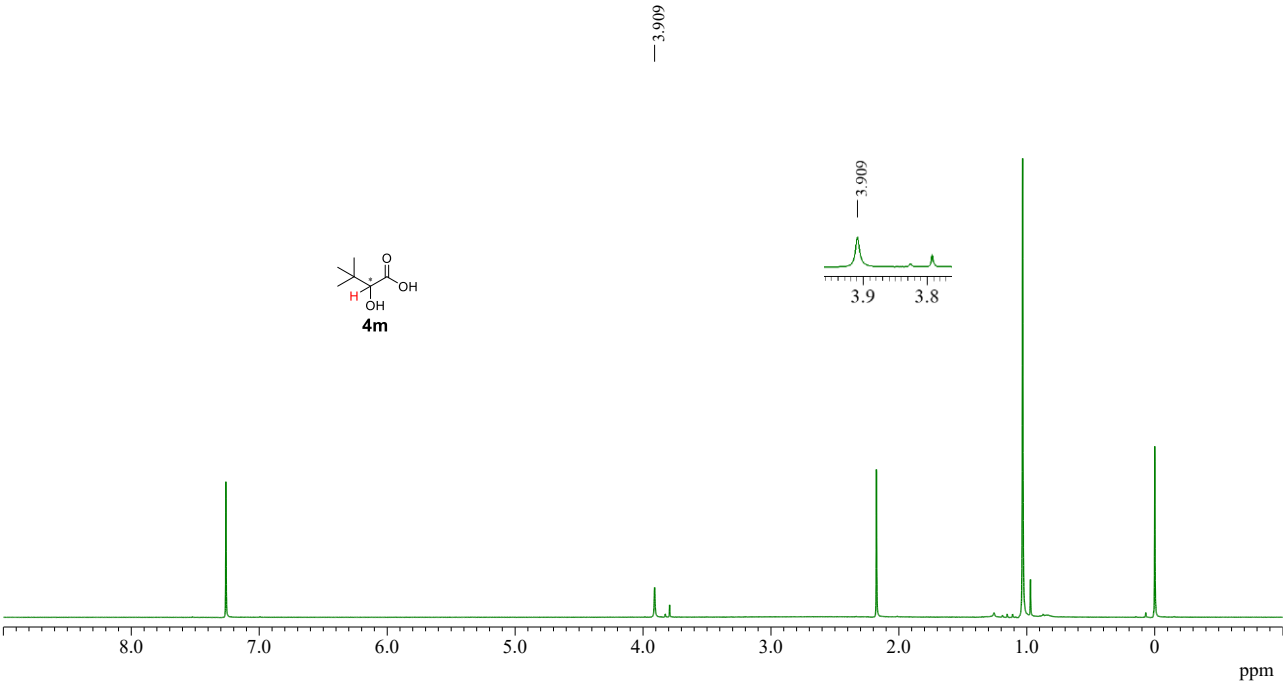

^{1}H NMR (400 MHz, $CDCl_3$)

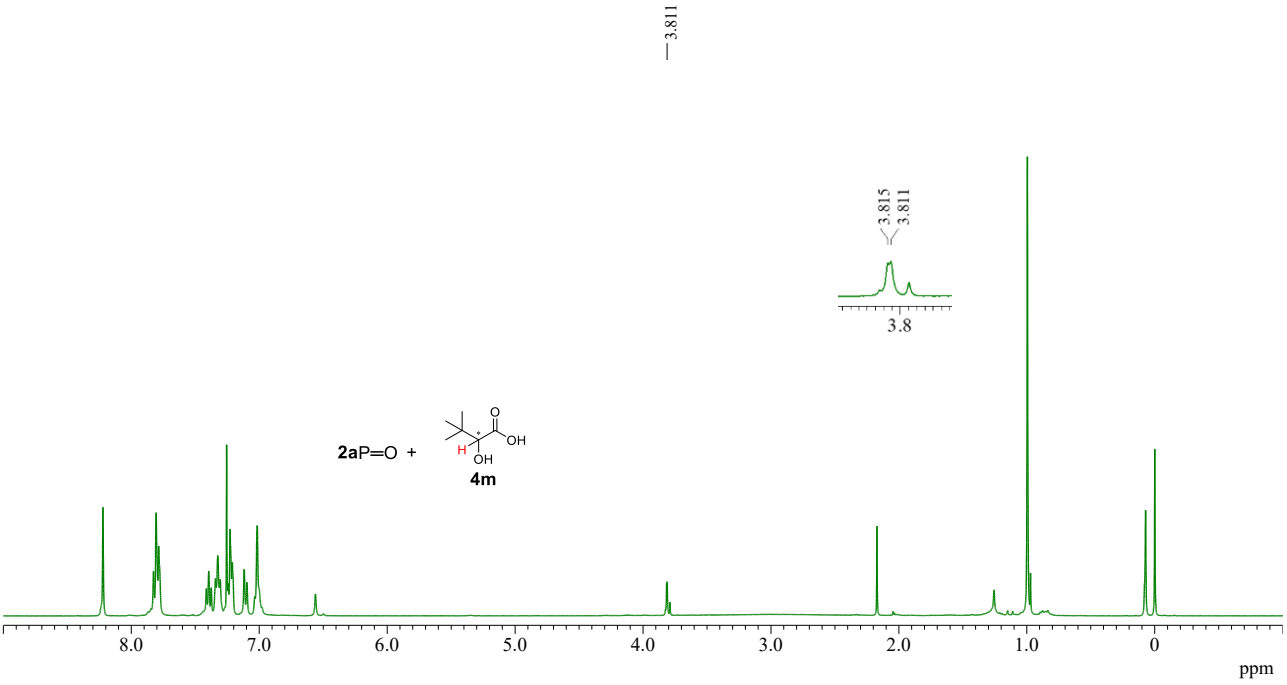

^{1}H NMR (400 MHz, $CDCl_3$)

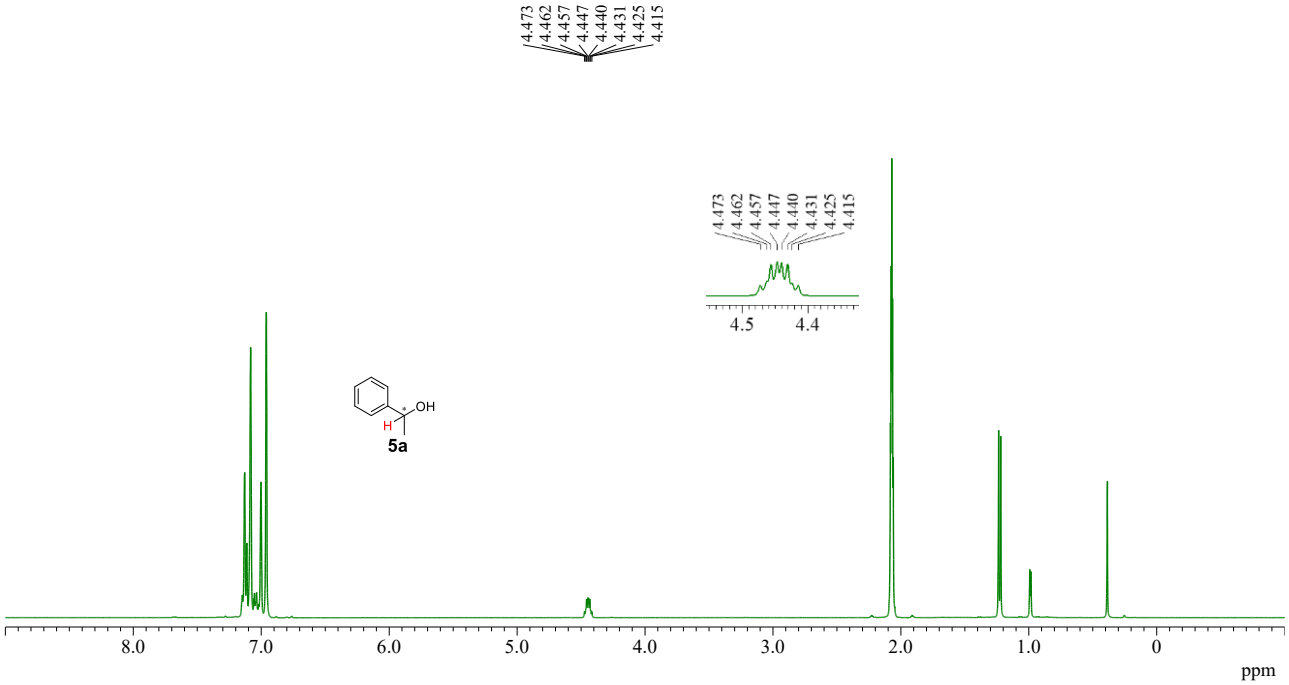

^{1}H NMR (400 MHz, $CDCl_3$)

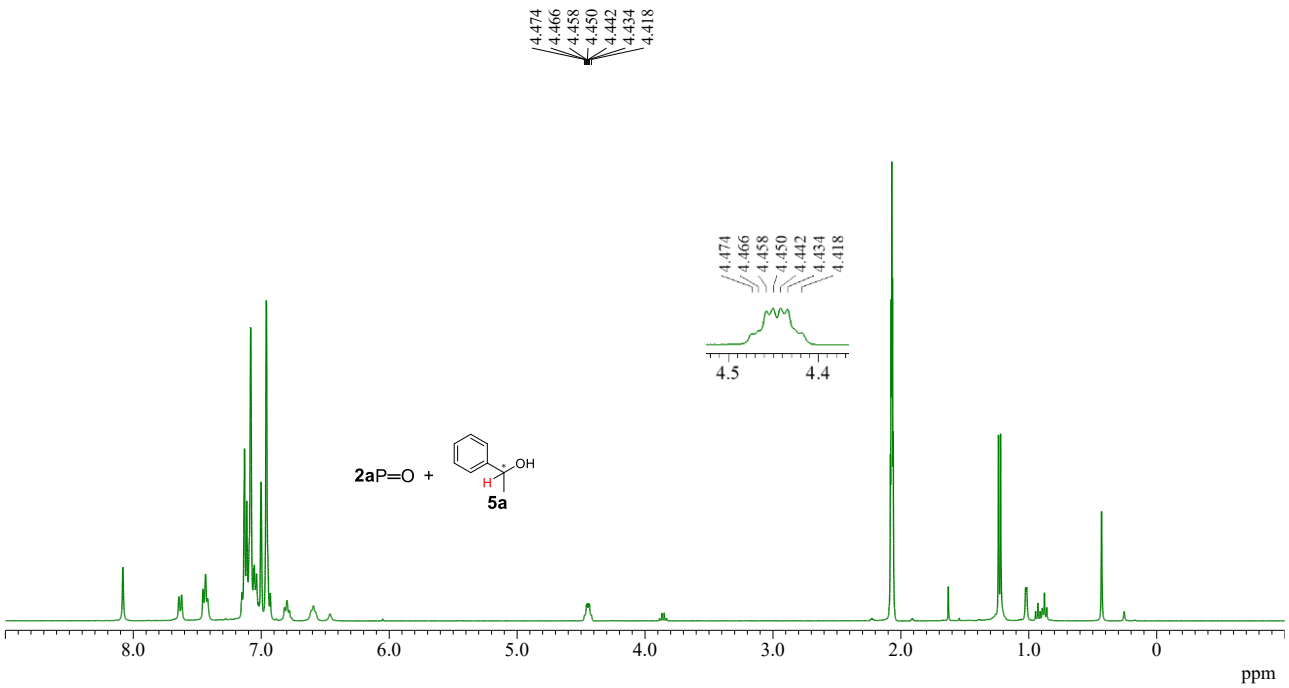

^{1}H NMR (400 MHz, $CDCl_3$)

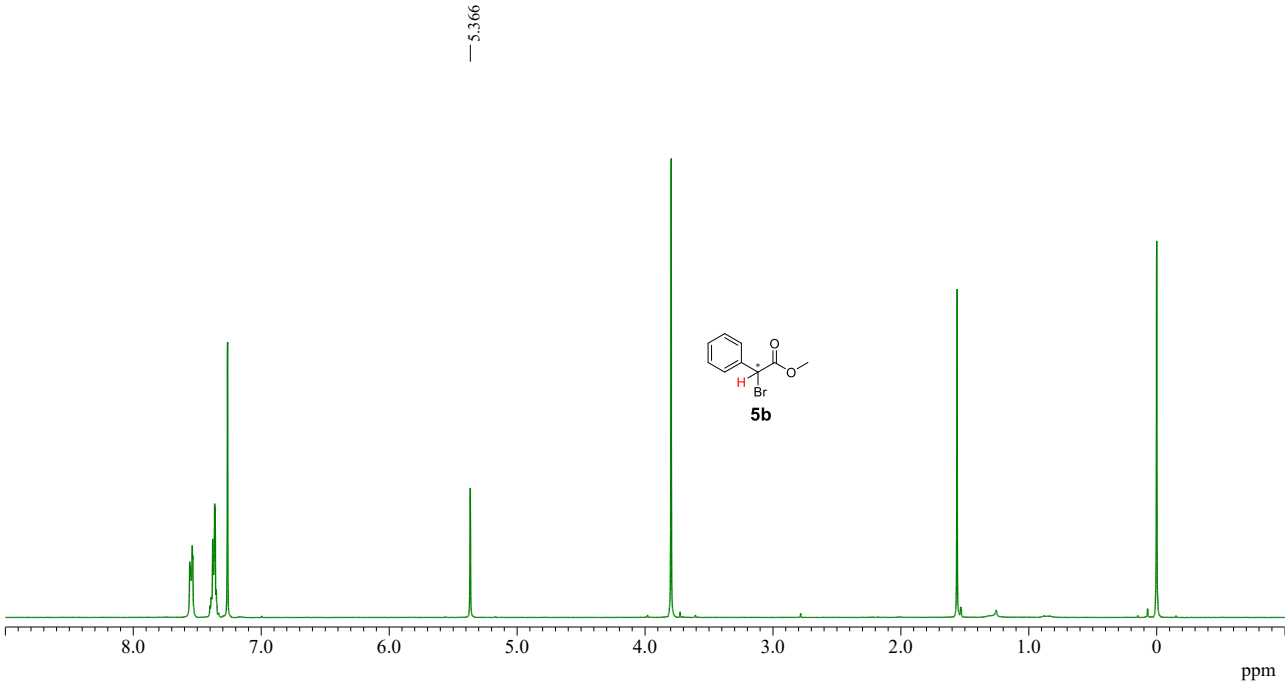

^{1}H NMR (400 MHz, $CDCl_3$)

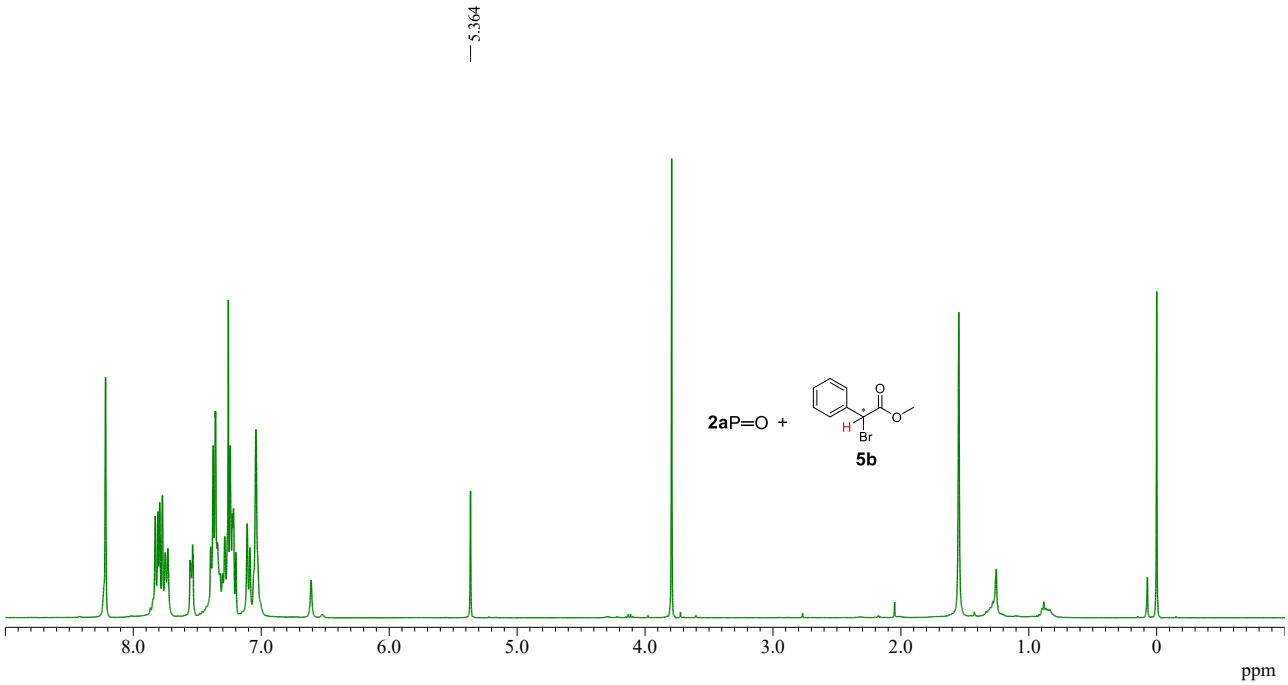

^{1}H NMR (400 MHz, $CDCl_3$)

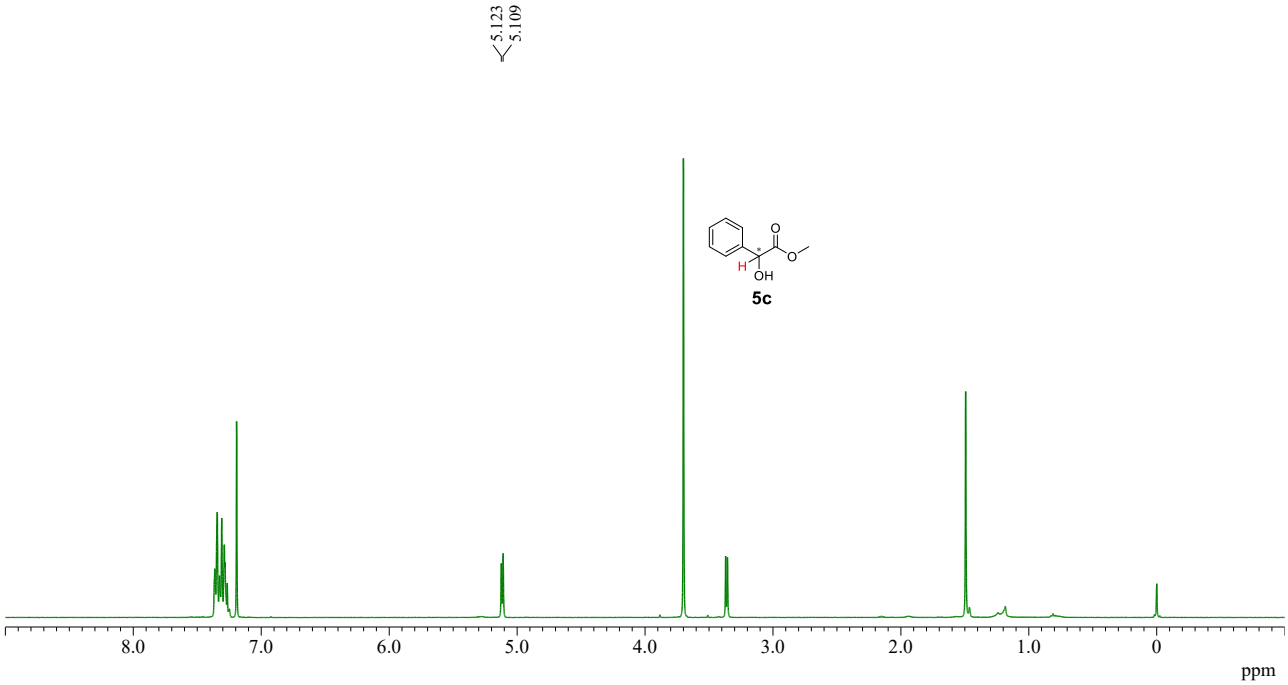

^{1}H NMR (400 MHz, $CDCl_3$)

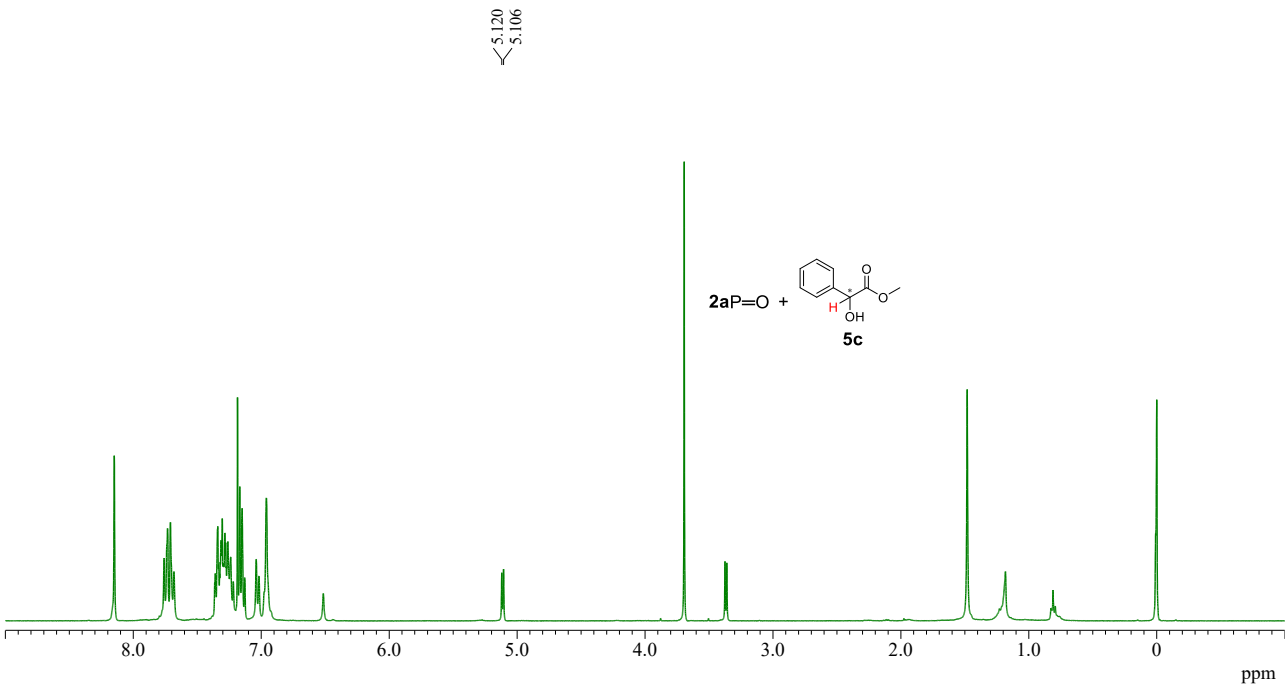

3-5. Reference

[1] D. E. Drayer, *Clin. Pharmacol. Ther.* **1986**, *40*, 125–133.

[2] P. Peluso, B. Chankvetadze, *Chem. Rev.* **2022**, *122*, 13235–13400.

[3] D. Parker, *Chem. Rev.* **1991**, *91*, 1441–1457.

[4] T. J. Wenzel, J. D. Wilcox, *Chirality* **2003**, *15*, 256–270.

[5] H. L. Goering, J. N. Eikenberry, G. S. Koermer, C. J. Lattimer, *J. Am. Chem. Soc.* **1974**, *96*, 1493–1501.

[6] G. R. Sullivan, in *Top. Stereochem.*, **1979**, pp. 287–329.

[7] T. J. Wenzel, in (Eds.: E.M. Carreira, H.B.T.-C.C. Yamamoto), Elsevier, Amsterdam, **2012**, pp. 545–570.

[8] G. Li, M. Ma, G. Wang, X. Wang, X. Lei, *Front. Chem.* **2020**, *Volume 8*-.

[9] D. Yang, X. Li, Y.-F. Fan, D.-W. Zhang, *J. Am. Chem. Soc.* **2005**, *127*, 7996–7997.

[10] T. Viswanathan, A. Toland, *J. Chem. Educ.* **1995**, *72*, 945.

[11] H. N. Naziroglu, M. Durmaz, S. Bozkurt, A. Sirit, *Chirality* **2011**, *23*, 463–471.

[12] C. Peña, J. González-Sabín, I. Alfonso, F. Rebolledo, V. Gotor, *Tetrahedron* **2008**, *64*, 7709–7717.

[13] F. Ma, L. Ai, X. Shen, C. Zhang, *Org. Lett.* **2007**, *9*, 125–127.

[14] X. X. Zhang, J. S. Bradshaw, R. M. Izatt, *Chem. Rev.* **1997**, *97*, 3313–3362.

[15] M.-S. Seo, H. Kim, *J. Am. Chem. Soc.* **2015**, *137*, 14190–14195.

[16] E. J. Kwahk, S. Jang, H. Kim, *Org. Lett.* **2021**, *23*, 7829–7833.

[17] A. E. Sheshenev, E. V Boltukhina, A. A. Grishina, I. Cisařova, I. M. Lyapkalo, K. K. (Mimi) Hii, *Chem. Eur. J.* **2013**, *19*, 8136–8143.

[18] H. Nakatsuji, Y. Sawamura, A. Sakakura, K. Ishihara, *Angew. Chem. Int. Ed.* **2014**, *53*, 6974–6977.

[19] S. E. Denmark, M. T. Burk, *Org. Lett.* **2012**, *14*, 256–259.

[20] T. Murai, H. Tsuji, S. Imaizumi, T. Maruyama, *Chem. Lett.* **2010**, *39*, 524–526.

[21] T. Murai, *Chem. Lett.* **2023**, *52*, 703–714.

[22] Y. Li, F. M. Raushel, *Tetrahedron: Asymmetry* **2007**, *18*, 1391–1397.

[23] M. Koller, H. Thiermann, F. Worek, *Toxicol. Lett.* **2020**, *320*, 28–36.

[24] M. Yasuda, S. Yoshioka, H. Nakajima, K. Chiba, A. Baba, *Org. Lett.* **2008**, *10*, 929–932.

[25] H. Nakajima, M. Yasuda, R. Takeda, A. Baba, *Angew. Chem. Int. Ed.* **2012**, *51*, 3867–3870.

[26] A. Konishi, K. Nakaoka, H. Maruyama, H. Nakajima, T. Eguchi, A. Baba, M. Yasuda, *Chem. Eur. J.* **2017**, *23*, 1273–1277.

[27] D. Tanaka, Y. Kadonaga, Y. Manabe, K. Fukase, S. Sasaya, H. Maruyama, S. Nishimura, M. Yanagihara, A. Konishi, M. Yasuda, *J. Am. Chem. Soc.* **2019**, *141*, 17466–17471.

[28] X. Liu, K. Tomita, A. Konishi, M. Yasuda, *Chem. Eur. J.* **2023**, *29*, e202302611.

[29] X. Liu, A. Konishi, M. Yasuda, *Asian J. Org. Chem.* **2025**, *14*, e202500299.

[30] K. A. Ahrendt, C. J. Borths, D. W. C. MacMillan, *J. Am. Chem. Soc.* **2000**, *122*, 4243–4244.

[31] X. Liu, K. Tomita, A. Konishi, M. Yasuda, *Chem. Eur. J.* **2023**, *29*, e202302611.

[32] O. V. Dolomanov, L. J. Bourhis, R. J. Gildea, J. A. K. Howard, H. Puschmann, *J. Appl. Crystallogr.*

2009, *42*, 339–341.

[33] D. F. Xiang, T. Narindoshvili, F. M. Raushel, *Biochemistry* **2020**, *59*, 4463–4469.

Conclusion

This thesis presents the synthesis and application of C_3-symmetric chiral cage-shaped phosphorus compounds. The C_3-symmetric chiral phosphite derivatives were employed as chiral ligands in transition metal-catalyzed asymmetric reactions, achieving excellent enantioselectivity. Furthermore, the cage-shaped phosphate compounds were found to function as chiral organocatalysts and promising chiral shift reagents for the enantiodiscrimination of chiral carboxylic acids.

In Chapter 1, synthetic methods for constructing two types of C_3-symmetric chiral cage-shaped phosphites bearing three homochiral binaphthyl units were established. Experimental and theoretical studies demonstrated that the Lewis basicity and C_3-symmetric chiral environment could be modulated by the tethered groups (C–H or Si–Me) within the cage-shaped framework. Variations in the chiral environment of each phosphite led to differences in reactivity and enantioselectivity in asymmetric Rh-catalyzed conjugate addition reactions. These C_3-symmetric phosphite ligands effectively promoted the reaction, achieving excellent enantioselectivity and enabling the synthesis of valuable chiral pharmaceutical intermediates.

In Chapter 2, two C_3-symmetric chiral cage-shaped phosphates were synthesized and employed as Lewis basic organocatalysts in asymmetric iodolactonization reactions. These catalysts exhibited complementary reactivity and enantioselectivity: the C–H tethered phosphate was more effective for the formation of five-membered lactones, whereas the Si–Me tethered analogue was better suited for six-membered lactones. This structural tuning enabled control over the chiral environment and contributed to broadening the substrate scope of asymmetric iodolactonization.

In Chapter 3, the development of a new chiral shift reagent for measuring the enantiopurity of chiral amino acids and carboxylic acids was accomplished using C_3-symmetric chiral cage-shaped phosphates. The NMR experimental results of acid substrates suggest the importance of π–π interactions and hydrogen bonding interactions with C–H tethered chiral cage-shaped phosphates. Further examination of other chiral phosphorus compounds as chiral shift reagents revealed that the ring current effect from the homochiral binaphthyl-containing cage-shaped molecule plays an important role in this system.

A knowledge obtained from Chapters 1 and 2 is that the steric properties of C_3-symmetric cage-shaped phosphorus compounds can be finely controlled by modifying the tethered groups, enabling precise control over catalytic reactivity and enantioselectivity in asymmetric transformations. Chapter 3 provides an important understanding that the cage-shaped architecture not only contributes to chiral discrimination through π–π and hydrogen bonding interactions, but also that the ring current effect of robust homochiral binaphthyl units plays a crucial role in chiral recognition ability.

This study highlights the promising utility of C_3-symmetric chiral cage-shaped architectures in the development of asymmetric catalytic systems and chiral recognition technologies.

List of Publications

1) Cage-Shaped Phosphites Having C_3-Symmetric Chiral Environment: Steric Control of Lewis Basicity and Application as Chiral Ligands in Rhodium-Catalyzed Conjugate Additions
   X. Liu, K. Tomita, A. Konishi, M. Yasuda
   Chem. Eur. J. **2023**, *29*, e202302611.

2) C_3-Symmetric ChiralCage-Shaped Phosphates: Synthesis and Application as Organocatalysts in Asymmetric Iodolactonizations
   X. Liu, A. Konishi, M. Yasuda
   Asian J. Org. Chem. **2025***,14*, e202500299.

3) Recognition of Carboxylic Acids and Amino Acids Using C_3-Symmetric Cage-Shaped Phosphates as Chiral-Shift Reagents
   X. Liu, A. Konishi, M. Yasuda
   Chem. Lett. Accepted